

UNIVERSITÉ DU QUÉBEC À CHICOUTIMI

**MÉMOIRE PRÉSENTÉ À
L'UNIVERSITÉ DU QUÉBEC À CHICOUTIMI
COMME EXIGENCE PARTIELLE
DE LA MAÎTRISE EN INGÉNIERIE**

PAR

JAMSHID SHIRANDASHT

**ÉVALUATION DE LA TECHNIQUE LIMCA II POUR LA MESURE
D'INCLUSIONS DANS L'ALUMINIUM PUR ET L'ALLIAGE BINAIRE
Al-6%Si : RÔLE DE LA TEMPÉRATURE DE COULÉE**

HIVER 2005



Mise en garde/Advice

Afin de rendre accessible au plus grand nombre le résultat des travaux de recherche menés par ses étudiants gradués et dans l'esprit des règles qui régissent le dépôt et la diffusion des mémoires et thèses produits dans cette Institution, **l'Université du Québec à Chicoutimi (UQAC)** est fière de rendre accessible une version complète et gratuite de cette œuvre.

Motivated by a desire to make the results of its graduate students' research accessible to all, and in accordance with the rules governing the acceptance and diffusion of dissertations and theses in this Institution, the **Université du Québec à Chicoutimi (UQAC)** is proud to make a complete version of this work available at no cost to the reader.

L'auteur conserve néanmoins la propriété du droit d'auteur qui protège ce mémoire ou cette thèse. Ni le mémoire ou la thèse ni des extraits substantiels de ceux-ci ne peuvent être imprimés ou autrement reproduits sans son autorisation.

The author retains ownership of the copyright of this dissertation or thesis. Neither the dissertation or thesis, nor substantial extracts from it, may be printed or otherwise reproduced without the author's permission.

Dedicated to my parents

RÉSUMÉ

Les alliages aluminium-silicium (Al-Si) constituent la majorité de moulages en aluminium, ceci est dû à la fluidité élevée fournie par la présence d'un volume relativement grand de la phase eutectique du silicium. La demande des pièces coulées en aluminium de plus haute qualité, en particulier dans les industries de l'automobile et de l'aérospatiale, a concentré beaucoup d'attention sur la qualité de l'aluminium fondu. La propreté du métal, une caractéristique importante qui affecte la qualité et la performance du produit final, est déterminée par la quantité des éléments de trace, de gaz, d'oxydes, d'impuretés et d'inclusions actuelles dans le métal liquide. Les inclusions dans les alliages coulés d'aluminium ont été un problème important dans le processus et contrôle de qualité.

Le contrôle de la propreté du métal dans les alliages Al-Si fondus exige des moyens de surveiller et réduire au minimum la présence des impuretés, des inclusions et des gaz. Beaucoup de techniques ont été présentées pour mesurer le contenu d'inclusion dans les fontes en aluminium. Parmi elles, la technique de LiMCA (analyseur liquide de propreté en métal) est une technique non destructive qui est capable d'effectuer des mesures in situ des concentrations d'inclusion et de les distinguer selon la dimension particulière.

La présente étude a été entreprise pour étudier les possibilités de la technique de LiMCA pour mesurer différents types d'inclusions en alliages purs commerciaux d'aluminium et d'Al-6%Si, en utilisant deux températures différentes (680 et 750 °C). Le but principal de l'étude était d'évaluer la technique dans le cas des alliages de fonderie, où les niveaux d'inclusion sont considérablement plus élevés que ceux trouvés dans les alliages d'aluminium corroyés pour lesquels la technique de LiMCA a été généralement employée jusqu'à maintenant.

Les types d'inclusions étudiés qui sont Al_2O_3 , Al_4C_3 , MgO, CaO, TiB_2 et $TiAl_3$, représentant des inclusions typiquement trouvées dans les alliages d'aluminium de fonderie. Les additions d'inclusion ont été faites en utilisant la poudre, l'alliage mère, métal pur et de matrice composite de métaux. Dans le cas des inclusions de poudre, les inclusions ont été injectées dans la fonte d'alliage en utilisant une technique d'injection de poudre pour préparer un contenu d'inclusions dans les lingots qui seront plus tard employés pour l'addition d'inclusion aux fontes fraîches d'alliage pour effectuer les essais de LiMCA. Les données de LiMCA ont été obtenues sous forme de parcelles qui ont fourni toute la concentration en nombre et en volume de concentration des inclusions, en fonction du temps et de la dimension particulière. L'examen microstructural des échantillons solidifiés obtenus à partir du tube de sonde de LiMCA utilisé pour les mesures et à partir des prélèvements de la fonte a été également effectué, en utilisant la microscopie et la microanalyse optique de sonde d'électron (EPMA).

Une analyse des données de LiMCA obtenues et des microstructures correspondantes a montré qu'après les procédures semblables d'addition d'inclusion, le

nombre maximum des inclusions dans les fontes en aluminium pures commerciales à 750 °C que est donné par des inclusions d' Al_2O_3 , suivies des inclusions d' Al_4C_3 , alors que les inclusions de CaO montrent les plus basses concentrations. La plupart des inclusions sont détectées dans la gamme de grandeur de 20 à 25 μm . Dans le cas des inclusions de MgO, les plus grandes additions du MgO augmentent la distribution d'inclusion dans les gammes plus étendues de dimension particulaire, montrant la tendance des inclusions de MgO à l'accumulé. Les natures semblables des courbes pour des inclusions de MgO obtenues à partir des essais effectués à la température de 680 °C indiquent la répétitivité des prélèvements de LiMCA pris du même métal liquide.

La comparaison du nombre total et la moyenne des inclusions TiB_2 montrent leur tendance de disperser dans la fonte plutôt qu'accumulé. Même avec une plus grande addition des inclusions TiB_2 à la fonte, la technique de LiMCA peut correctement détecter l'augmentation correspondante de la concentration dans la gamme de dimension particulaire de 20 à 25 μm . Les concentrations en volume pour les inclusions TiAl_3 dans les fontes pures d'Al à 680 °C restent hautes pour toutes les gammes de dimension particulaire, tandis que pour d'autres inclusions, les dimensions particulières plus élevées montrent de bas volumes.

Dans les alliages Al-6%Si coulés à 750 °C, il y a une première période de 15-20 minutes avant que les lectures d'inclusion commencent à être détectées correctement par le LiMCA. Les inclusions Al_2O_3 et TiB_2 montrent les concentrations les plus élevées dans les gammes inférieures de dimension particulaire, où TiB_2 montre cette tendance pour presque toute la gamme de dimension particulaire. Les inclusions Al_4C_3 montrent des concentrations près de celles d' Al_2O_3 , alors que les CaO et les MgO montrent les plus basses concentrations. Les effets de l'agglomération et de la sédimentation de particules sont également reflétés par les caractéristiques de distribution de dimension particulaire. Bien que les inclusions de CaO montrent les plus basses concentrations dues à leur basse mouillabilité, leur présence est encore différenciée par le LiMCA en ce qui concerne les niveaux bas d'inclusion d'alliage (sans aucune addition). Les inclusions CaO, MgO et TiB_2 montrent des concentrations en volume élevées.

Le LiMCA est sensible à la taille et à la concentration d'inclusion. Sa sensibilité augmente pendant que la température de fonte diminue. Les concentrations plus élevées d'inclusion de LiMCA II à des températures plus basses de 680 °C pour tous les types d'inclusion ont été étudié. Cet effet est le plus prononcé pour des inclusions de la poudre TiB_2 et Al_4C_3 . Les types d'inclusion suivants montrent les concentrations les plus élevées : TiB_2 (poudre) > MgO + Mg > TiB_2 (alliage mère) > Al_4C_3 (poudre) dans cet ordre.

Les inclusions de TiB_2 (poudre) et de MgO (métal) sont associées à l'excédent de volumes élevés de toutes les gammes de dimension particulaire, indiquant la présence des inclusions de toutes les tailles dans la fonte et des effets délétères relatifs des inclusions. Les niveaux beaucoup plus élevés d'inclusion de MgO obtenus avec l'addition du métal de

magnésium (plus la surchauffe de la fonte) montre que cela l'addition directe du métal est une source bien meilleure de ces inclusions qu'en utilisant la poudre de MgO elle-même (20.000 contre. ppb 5.000). Ceci démontre la sensibilité et la fiabilité de la technique de LiMCA à la présence et la source des inclusions supplémentaires à la fonte.

En ce qui concerne des additions d'inclusion en utilisant des alliages mères, les nombres de la concentration de TiB_2 sont beaucoup plus hauts que ceux de $TiAl_3$. Cependant, dans les deux cas, la plupart des inclusions sont trouvées dans la gamme de dimension particulière allant de 20 à 25 μm . Du point de vue de fournir des noyaux hétérogènes à la fonte par l'utilisation des alliages mères de raffinage de grain, les mesures de LiMCA prouvent clairement que Al-5%Ti-1%B est beaucoup plus efficace que l'alliage Al-10%Ti.

Dans la présente étude, l'évidence microstructurale de l'accumulation d'une vaste quantité d'inclusions de TiB_2 comme capturée par le tube de sonde de LiMCA prouve que LiMCA est la seule technique qui peut capturer de tels agglomérés en ligne, sans n'importe quel problème, car d'autres techniques telles que le PoDFA et le Prefil ne peuvent pas mesurer de tels agglomérés TiB_2 sans leurs systèmes de filtre obtenant obstrués et interrompant les mesures. C'est une conclusion significative, et démontre un aspect très important de la technique de LiMCA, en particulier en raison du fait que des alliages mères de type d'Al-Ti-B sont régulièrement utilisés pour l'affinage des grains.

ABSTRACT

Aluminum-silicon (Al-Si) based casting alloys constitute the majority of aluminum castings, due to the high fluidity provided by the presence of a relatively large volume of the Al-Si eutectic. The demand for higher quality aluminum cast products, particularly in the automotive and aerospace industries, has focused much attention on the quality of molten aluminum. Metal cleanliness, an important characteristic that affects the quality and performance of the final product, is determined by the amount of trace elements, gases, oxides, impurities and inclusions present in the melt. Inclusions in aluminum alloy castings have been a major problem in process and quality control.

Control of metal cleanliness in molten Al-Si alloys requires the means to monitor and minimize the presence of impurities, inclusions and gases. Many techniques have been introduced to measure the inclusion content in aluminum melts. Among them, the LiMCA (Liquid Metal Cleanliness Analyzer) technique is a non-destructive technique that is capable of carrying out *in situ* measurements of the inclusion concentrations and distinguishing them according to the particle size.

The present study was undertaken to investigate the capability of the LiMCA technique for measuring different types of inclusions in commercial pure aluminum and Al-6%Si casting alloys, under low (680 °C) and high (750 °C) melt temperature conditions. The main purpose of the study was to evaluate the technique in the case of casting alloys, where the inclusion levels are considerably higher than those found in wrought aluminum alloys for which the LiMCA has generally been used to date.

The inclusion types studied included Al_2O_3 , Al_4C_3 , MgO, CaO, TiB_2 and TiAl_3 , representing inclusions typically found in aluminum casting alloys. The inclusion additions were made using powder, master alloy, pure metal and metal matrix composite sources. In the case of powder inclusions, the inclusions were injected into the alloy melt using a powder injection technique to prepare inclusion-containing ingots which were subsequently used for inclusion addition to fresh alloy melts to conduct the LiMCA tests.

The LiMCA data was obtained in the form of plots which provided the total concentration number and volume concentration of inclusions, as a function of time and particle size. Microstructural examination of solidified samples obtained from the LiMCA probe tube used for the measurements and from samplings of the melt was also carried out, using optical microscopy and electron probe microanalysis (EPMA).

An analysis of the LiMCA data obtained and the corresponding microstructures showed that following similar inclusion addition procedures, the maximum number of inclusions in commercial pure aluminum melts at 750 °C is exhibited by Al_2O_3 inclusions, followed by Al_4C_3 inclusions, while CaO inclusions show the lowest concentrations. Most inclusions are detected in the 20-25 μm size range. In the case of MgO inclusions,

increased additions of MgO increase the inclusion distribution in the larger particle size ranges, showing the tendency of MgO inclusions to agglomerate. Similar natures of curves for MgO inclusions obtained from tests carried out at 680 °C melt temperature indicate the repeatability of LiMCA samplings taken from the same melt.

Comparison of average and total number of TiB₂ inclusions show their tendency to disperse in the melt rather than agglomerate. Even with an increased addition of TiB₂ inclusions to the melt, the LiMCA can properly detect the corresponding increase in concentration in the 20-25 μm particle size range. Volume concentrations for TiAl₃ inclusions in pure Al melts at 680 °C remain high for all particle size ranges, whereas for other inclusions, the higher particle sizes show low volumes.

In Al-6%Si alloy melts at 750 °C, there is an initial period of 15-20 min before the inclusion readings begin to be detected properly by the LiMCA. The Al₂O₃ and TiB₂ inclusions display the highest concentrations in the lower particle size ranges, where TiB₂ shows this tendency for almost all particle size ranges. The Al₄C₃ inclusions show concentrations close to Al₂O₃, while CaO and MgO show the lowest concentrations, close to the base alloy levels for particle sizes > 35 μm. The effects of particle agglomeration and sedimentation are also reflected by the particle size distribution characteristics. Although the CaO inclusions show the lowest concentrations due to their low wettability, their presence is still differentiated by the LiMCA with respect to the base alloy inclusion levels (without any additions). The CaO, MgO and TiB₂ inclusions show high volumic concentrations.

The LiMCA is sensitive to both inclusion size and concentration. Its sensitivity is found to increase as the melt temperature decreases. The LiMCA II records higher inclusion concentrations at the lower 680 °C melt temperature for all inclusion types studied. This effect is most pronounced for the TiB₂ and Al₄C₃ powder inclusions. The following inclusion types show the highest concentrations: TiB₂ (powder) > MgO+Mg > TiB₂ (master alloy) > Al₄C₃ (powder) in that order.

The TiB₂ (powder) and MgO (metal) inclusions are associated with high volumes over all the particle size ranges, indicating the presence of inclusions of all sizes in the melt and the relative deleterious effects of the larger sized inclusions that could be expected as a result. The much higher MgO inclusion levels obtained with addition of Mg metal (plus superheating of the melt) shows that direct addition of the metal is a much better source of these inclusions than using MgO powder itself (*cf.* 20,000 vs. 5,000 ppb). This demonstrates the sensitivity and reliability of the LiMCA technique to the presence and source of inclusions added to the melt.

With respect to inclusion additions using master alloys, TiB₂ concentration numbers are much higher than those of TiAl₃. However, in both cases, most of the inclusions are found in the 20-25 μm particle size range. From the point of view of

providing heterogeneous nuclei to the melt through the use of grain refining master alloys, the LiMCA measurements clearly show that Al-5%Ti-1%B is much more effective than Al-10%Ti.

In the present work, microstructural evidence of the agglomeration of a vast amount of TiB_2 inclusions as captured by the LiMCA probe tube shows that LiMCA is the only technique that is able to capture such agglomerates in-line, without any problem, as other techniques such as the PoDFA and Prefil cannot measure such TiB_2 agglomerates without their filter systems getting clogged and interrupting the measurements. This is a significant finding, and demonstrates a very important aspect of the LiMCA technique, particularly in view of the fact that Al-Ti-B master alloys are regularly employed for grain refining aluminum casting alloys.

ACKNOWLEDGEMENTS

I would like to sincerely acknowledge the guidance of my supervisors Professors F. H. Samuel and A. M. Samuel, who gave me the opportunity to undertake this research study. I wish to convey my appreciation to all members of the TAMLA group for their assistance during various stages of my research work, in particular, Dr. Agnes Samuel for her critical review of the manuscript, Mr Alain Bérubé, technician, TAMLA-UQAC, for his cooperation and assistance with the castings, sample preparation and maintenance of the powder injection and LiMCA apparatus.

Financial support in the form of scholarships received from the Natural Sciences and Engineering Research Council of Canada (NSERC), the Fondation de l'Université du Québec à Chicoutimi (FUQAC), and General Motors Powertrain Group (GMPT, U.S.A) for donation of LiMCA II is gratefully acknowledged. The invaluable in-kind support received from GMPT through their loan of the LiMCA II apparatus and that of ABB Bomem Inc. in providing the necessary accessories for, and training in the use of the LiMCA is greatly appreciated.

Finally, I would like to record my gratitude to the members of my family, specially my parents for their continuous encouragement and support during my work.

TABLE OF CONTENTS

RÉSUMÉ.....	II
ABSTRACT.....	V
ACKNOWLEDGEMENTS.....	VIII
TABLE OF CONTENTS.....	IX
LIST OF FIGURES.....	XIII
LIST OF TABLES.....	XXIII
CHAPTER 1 DEFINITION OF THE PROBLEM.....	1
1.1 INTRODUCTION.....	2
1.2 OBJECTIVES.....	5
CHAPTER 2 LITERATURE SURVEY.....	6
2.1 INTRODUCTION.....	7
2.2 CLASSIFICATION OF ALUMINUM ALLOYS.....	8
2.2.1 Aluminum Casting Alloys.....	9
2.3 INCLUSIONS IN ALUMINUM ALLOYS.....	10
2.3.1 Sources of Inclusions.....	10
2.3.2 Classification of Inclusions.....	11
2.3.3 Effect of Inclusions on Casting Quality.....	13
2.4 TYPES OF INCLUSIONS.....	15
2.4.1 Oxide Inclusions.....	15
2.4.2 Salts.....	19
2.4.3 Carbides.....	19
2.4.4 Borides.....	20
2.4.5 Nitride.....	21
2.4.6 Fluorides.....	21
2.4.7 Intermetallic Compounds.....	22
2.4.8 Calcium Compounds.....	23

2.5	POROSITY.....	24
2.6	INCLUSION REMOVAL TECHNIQUES.....	27
2.6.1	Gravity Sedimentation.....	28
2.6.2	Electromagnetic Separation.....	29
2.6.3	Flotation.....	30
2.6.3.1	Stirring.....	31
2.6.4	Filtration.....	31
2.6.5	Degassing.....	32
2.6.5.1	Oxide Removal.....	34
2.6.6	Flux Treatment.....	35
2.7	INCLUSION MEASUREMENT TECHNIQUES.....	35
2.7.1	PoDFA Technique.....	38
2.7.2	Prefil Technique.....	39
2.7.3	LAIS Technique.....	40
2.7.4	Ultrasonic Technique.....	42
2.7.5	Reduced Pressure Test.....	43
2.7.6	Other Detection Methods.....	44
2.8	THE LiMCA TECHNIQUE.....	45
2.8.1	Description of LiMCA.....	45
2.8.2	LiMCA Operating Principles.....	48
2.8.3	Metallurgical Application of the LiMCA System.....	53
2.8.4	Particle Discrimination in the LiMCA System.....	53
2.8.5	Error Analysis of LiMCA Data.....	58
2.8.6	Advantages of LiMCA.....	59
CHAPTER 3 EXPERIMENTAL PROCEDURES.....		60
3.1	MATERIALS AND ALLOY PREPARATION.....	61
3.1.1	Preparation of Experimental Al-6%Si Alloy.....	62
3.1.2	Preparation of Inclusion-Containing Ingots of Al and Al-6%Si Alloys.....	64
3.2	INCLUSION ADDITION.....	65
3.2.1	Injection Technique.....	65
3.2.2	Injection Procedure.....	66
3.3	MELTING PROCEDURES FOR CONDUCTING LiMCA TEST.....	69
3.4	LiMCA TESTING.....	70

3.4.1	Start-Up Procedures.....	70
3.4.2	Operation of LiMCA II.....	73
3.5	METALLOGRAPHY.....	78
3.6	ANALYSIS OF LiMCA DATA.....	80
CHAPTER 4 EVALUATION OF INCLUSIONS IN PURE ALUMINUM MEASURED BY LiMCA.....81		
4.1	INTRODUCTION.....	82
4.2	EVALUATION OF INCLUSIONS IN PURE ALUMINUM AT 750 °C.....	83
4.2.1	Evaluation of Al ₂ O ₃ Inclusions.....	85
4.2.2	Evaluation of Al ₄ C ₃ Inclusions.....	92
4.2.3	Evaluation of CaO Inclusions.....	98
4.2.4	Evaluation of MgO Inclusions.....	104
4.2.5	Evaluation of TiB ₂ Inclusions.....	110
4.3	COMPARISON OF DIFFERENT INCLUSION ADDITIONS.....	118
4.4	EVALUATION OF INCLUSIONS IN PURE ALUMINUM AT 680 °C.....	120
4.4.1	Evaluation of CaO Inclusions.....	120
4.4.2	Evaluation of MgO Inclusions.....	124
4.4.3	Evaluation of TiAl ₃ Inclusions.....	127
CHAPTER 5 EVALUATION OF INCLUSIONS IN Al-6%Si ALLOY MEASURED BY LiMCA AT 750 °C.....131		
5.1	INTRODUCTION.....	132
5.2	EVALUATION OF INCLUSIONS IN Al-6%Si ALLOY AT 750°C.....	133
5.2.1	Evaluation of Al ₂ O ₃ Inclusions.....	135
5.2.2	Evaluation of Al ₄ C ₃ Inclusions.....	142
5.2.3	Evaluation of CaO Inclusions.....	147
5.2.4	Evaluation of MgO Inclusions.....	152
5.2.5	Evaluation of TiB ₂ Inclusions.....	155
5.3	COMPARISON OF DIFFERENT INCLUSION ADDITIONS.....	160

CHAPTER 6 EVALUATION OF INCLUSIONS IN Al-6%Si ALLOY MEASURED BY LiMCA AT 680 °C.....	161
6.1 INTRODUCTION.....	162
6.2 EVALUATION OF INCLUSIONS IN Al-6%Si ALLOY AT 680°C.....	163
6.2.1 Evaluation of TiB ₂ Inclusions (added as powder).....	164
6.2.2 Evaluation of TiB ₂ Inclusions (added as Al-5%Ti-1%B master alloy).....	171
6.2.3 Evaluation of Al ₄ C ₃ Inclusions (added as powder).....	178
6.2.4 Evaluation of Al ₂ O ₃ Inclusions (added as MMC).....	181
6.2.5 Evaluation of CaO Inclusions (added as powder).....	185
6.2.6 Evaluation of MgO Inclusions (added as powder and Mg metal).....	190
6.2.7 Evaluation of TiAl ₃ Inclusions (added as Al-Ti 10% master alloy).....	195
6.3 COMPARISON OF DIFFERENT INCLUSION ADDITIONS.....	199
6.3.1 Effect of Melt Temperature on Inclusion Concentration Recorded by LiMCA.....	204
CHAPTER 7 EXAMPLES OF INCLUSIONS IN PURE Al AND Al-6%Si ALLOY.....	206
7.1 INTRODUCTION.....	207
7.2 MICROSTRUCTURES OF INCLUSIONS.....	209
7.2.1 Microstructures of Inclusions Added to Pure Aluminum Melts...209	
7.2.2 Microstructures of Inclusion-Containing Al-6%Si Alloy Ingots...216	
7.2.3 Microstructures of Inclusions Added to Al-6%Si Alloy Melts.....218	
CHAPTER 8 CONCLUSIONS.....	240
RECOMMENDATIONS.....	246
REFFRENCES.....	247

LIST OF FIGURES

CHAPTER 2

Figure 2.1	Typical aluminum oxide inclusions observed in Al-Si alloys.....	17
Figure 2.2	Examples of magnesium oxide inclusions.....	18
Figure 2.3	Examples of (a) Al_4C_3 , (b) TiB_2 inclusions.....	21
Figure 2.4	Examples of (a) AlN films and Al_2MgO_4 particles in an Al-10% Mg alloy.....	22
Figure 2.5	Light grey Al_3Zr rods in an AlZnMgZr alloy.....	24
Figure 2.6	Solubility of hydrogen in solid and liquid aluminum.....	25
Figure 2.7	Morphologies of (a) gas pores, and (b) shrinkage pores observed in aluminum castings.....	26
Figure 2.8	Schematic representation of gravity sedimentation.....	29
Figure 2.9	Schematic representation of inclusion removal by gas bubbles.....	31
Figure 2.10	Schematic representation of the inclusion size with respect to filter pore diameter.....	32
Figure 2.11	(a) Degassing mechanism, (b) mechanism of inclusion removal.....	33
Figure 2.12	Impellers used for (a) stirring, and (b) degassing.....	34
Figure 2.13	Schematic of the elements of the flux injection process.....	35
Figure 2.14	Principle of the PoDFA Technique.....	38
Figure 2.15	(a) Schematic diagram showing filtration behavior of aluminum alloy containing different types of inclusions; (b) the Prefil apparatus.....	40
Figure 2.16	Close-up of the LAIS during operation.....	41
Figure 2.17	Schematic diagram of the ultrasonic technique with auxiliary equipment.....	43
Figure 2.18	Schematic diagram of the LiMCA operation.....	46
Figure 2.19	The complete LiMCA system.....	47
Figure 2.20	Schematic representation of the ESZ principle for particle size measurement.....	50
Figure 2.21	Computer screen showing evolution of metal cleanliness as a function of time during a LiMCA operation.....	52
Figure 2.22	Histogram display of inclusion measurement in terms of inclusion particle size distribution.....	52

Figure 2.23	(a) Schematic configuration of the DSP-based LiMCA system, and (b) the seven peak parameters generated by DSP.....	55
Figure 2.24	(a) The voltage pulse as a function of particle diameter, and (b) ESZ resistance change with the position of non-conducting particles of various diameters in molten aluminum in the LiMCA system.....	57
CHAPTER 3		
Figure 3.1	(a) Binary phase diagram of the Al-Si system, and (b) cooling curve of experimental Al-6%Si alloy used in the present work.....	63
Figure 3.2	Schematic of the powder injection system.....	66
Figure 3.3	The powder injection apparatus during operation.....	67
Figure 3.4	Cooling system inside the main body of the LiMCA.....	68
Figure 3.5	The LiMCA system connected to the microcomputer during a LiMCA sampling.....	71
Figure 3.6	(a) The main menu, and (b) configuration page displays for a typical LiMCA test.....	72
Figure 3.7	(a) Permanent status, and (b) graphical display of hole resistance.....	73
Figure 3.8	Example showing the plot of total number of inclusions versus time obtained in real time on the microcomputer screen of LiMCA.....	76
Figure 3.9	The LiMCA probe tube after use (left) and before testing (right).....	77
Figure 3.10	The LiMCA system during operation.....	77
Figure 3.11	Close-up view of the LiMCA system during operation: (a) under vacuum, and (b) under pressure conditions.....	78
Figure 3.12	The optical microscope-image analysis system used for microstructural analysis.....	79
Figure 3.13	Electron probe microanalyzer used in the present work.....	80
CHAPTER 4		
Figure 4.1	Schematic representation of inclusion addition procedure.....	85
Figure 4.2	Concentration number of Al ₂ O ₃ inclusions in commercial pure aluminum as a function of time.....	86
Figure 4.3	Average number of Al ₂ O ₃ inclusions in commercial pure aluminum as a function of particle size.....	88
Figure 4.4	Total number of Al ₂ O ₃ inclusions in commercial pure aluminum as a function of particle size.....	88

Figure 4.5	Volumic concentration of Al_2O_3 inclusions in commercial pure aluminum as a function of time.....	89
Figure 4.6	Average volume of Al_2O_3 inclusions in commercial pure aluminum as a function of particle size.....	91
Figure 4.7	Total volume of Al_2O_3 inclusions in commercial pure aluminum as a function of particle size.....	91
Figure 4.8	Concentration number of Al_4C_3 inclusions in commercial pure aluminum as a function of time.....	93
Figure 4.9	Average number of Al_4C_3 inclusions in commercial pure aluminum as a function of particle size.....	94
Figure 4.10	Total number of Al_4C_3 inclusions in commercial pure aluminum as a function of particle size.....	94
Figure 4.11	Volumic concentration of Al_4C_3 inclusions in commercial pure aluminum as a function of time.....	95
Figure 4.12	Average volume of Al_4C_3 inclusions in commercial pure aluminum as a function of particle size.....	97
Figure 4.13	Total volume of Al_4C_3 inclusions in commercial pure aluminum as a function of particle size.....	97
Figure 4.14	Concentration number of CaO inclusions in commercial pure aluminum as a function of time.....	99
Figure 4.15	Average number of CaO inclusions in commercial pure aluminum as a function of particle size.....	101
Figure 4.16	Total number of CaO inclusions in commercial pure aluminum as a function of particle size.....	101
Figure 4.17	Volumic concentration of CaO inclusions in commercial pure aluminum as a function of time.....	102
Figure 4.18	Average volume of CaO inclusions in commercial pure aluminum as a function of time.....	103
Figure 4.19	Total volume of CaO inclusions in commercial pure aluminum as a function of time.	103
Figure 4.20	Concentration number of MgO inclusions in commercial pure aluminum as a function of time.....	105
Figure 4.21	Average number of MgO inclusions in commercial pure aluminum as a function of particle size.....	106
Figure 4.22	Total number of MgO inclusions in commercial pure aluminum as a function of particle size.....	106

Figure 4.23	Volumic concentration of MgO inclusions in commercial pure aluminum as a function of time.....	108
Figure 4.24	Average volume of MgO inclusions in commercial pure aluminum as a function of particle size.....	109
Figure 4.25	Total volume of MgO inclusions in commercial pure aluminum as a function of particle size.....	109
Figure 4.26	Concentration number of TiB ₂ inclusions in commercial pure aluminum as a function of time.....	112
Figure 4.27	Modified version of Figure 4.26 after elimination of erroneous readings.....	112
Figure 4.28	Average number of TiB ₂ inclusions in commercial pure aluminum as a function of particle size.....	114
Figure 4.29	Total number of TiB ₂ inclusions in commercial pure aluminum as a function of particle size.....	114
Figure 4.30	Volumic concentration of TiB ₂ inclusions in commercial pure aluminum as a function of time.....	116
Figure 4.31	Modified version of Figure 4.30 after elimination of erroneous readings.....	116
Figure 4.32	Average volume of TiB ₂ inclusions in commercial pure aluminum as a function of particle size.	117
Figure 4.33	Total volume of TiB ₂ inclusions in commercial pure aluminum as a function of particle size.....	117
Figure 4.34	Comparison of different inclusions added to commercial pure aluminum as a function of time.....	119
Figure 4.35	Comparison of different inclusions added to commercial pure aluminum as a function of particle size.....	119
Figure 4.36	Concentration number of CaO inclusions in commercial pure aluminum as a function of time.....	122
Figure 4.37	Total number of CaO inclusions in commercial pure aluminum as a function of particle size.....	122
Figure 4.38	Volumic concentration of CaO inclusions in commercial pure aluminum as a function of time.....	123
Figure 4.39	Total volume of CaO inclusions in commercial pure aluminum as a function of particle size.....	124
Figure 4.40	Concentration number of MgO inclusions in commercial pure aluminum as a function of time.....	125

Figure 4.41	Total number of MgO inclusions in commercial pure aluminum as a function of particle size.....	126
Figure 4.42	Volumic concentration of MgO inclusions in commercial pure aluminum as a function of time.....	126
Figure 4.43	Total volume of MgO inclusions in commercial pure aluminum as a function of particle size.....	127
Figure 4.44	Concentration number of $TiAl_3$ inclusions in commercial pure aluminum as a function of time.....	128
Figure 4.45	Total number of $TiAl_3$ inclusions in commercial pure aluminum as a function of particle size.....	129
Figure 4.46	Volumic concentration of $TiAl_3$ inclusions in commercial pure aluminum as a function of time.....	130
Figure 4.47	Total volume of $TiAl_3$ inclusions in commercial pure aluminum as a function of particle size.....	130
CHAPTER 5		
Figure 5.1	Schematic of inclusion addition to the Al-6%Si alloy melt.....	135
Figure 5.2	(a) Concentration number of Al_2O_3 inclusions in Al-6%Si alloy as a function of time.....	136
Figure 5.2	(b) Corrected version of the plot shown in Figure 5.2 (a).....	137
Figure 5.3	Average number of Al_2O_3 inclusions in Al-6%Si alloy as a function of particle size.....	139
Figure 5.4	Total number of Al_2O_3 inclusions in Al-6%Si alloy as a function of particle size.....	139
Figure 5.5	(a) Volumic concentration of Al_2O_3 inclusions in Al-6%Si alloy as a function of time (b) Corrected version of the plot shown in Figure (a).....	141
Figure 5.6	Average volume of Al_2O_3 inclusions in Al-6% alloy as a function of particle size.....	142
Figure 5.7	Total volume of Al_2O_3 inclusions in Al-6%Si alloy as a function of particle size.....	142
Figure 5.8	Concentration number of Al_4C_3 inclusions in Al-6%Si alloy as a function of time.....	144
Figure 5.9	Total number of Al_4C_3 inclusions in Al-6%Si alloy as a function of particle size.....	145
Figure 5.10	Volumic concentration of Al_4C_3 inclusions in Al-6%Si alloy as a function of time.....	146

Figure 5.11	Total volume of Al_4C_3 inclusions in Al-6%Si alloy as a function of particle size.....	147
Figure 5.12	Concentration number of CaO inclusions in Al-6%Si alloy as a function of time.....	149
Figure 5.13	Total number of CaO inclusions in Al-6%Si alloy as a Function of particle size.....	150
Figure 5.14	Volumic concentration of CaO inclusions in Al-6%Si alloy as a function of time.....	151
Figure 5.15	Total volume of CaO inclusions in Al-6%Si alloy as a function of particle size.....	151
Figure 5.16	Concentration number of MgO inclusions in Al-6%Si alloy as a function of time.....	153
Figure 5.17	Total number of MgO inclusions in Al-6%Si alloy as a function of particle size.....	153
Figure 5.18	Volumic concentration of MgO inclusions in Al-6%Si alloy as a function of time.....	154
Figure 5.19	Total volume of MgO inclusions in Al-6%Si alloy as a function of particle size.....	155
Figure 5.20	Concentration number of TiB_2 inclusions in Al-6%Si alloy as a function of time.....	157
Figure 5.21	Total number of TiB_2 inclusions in Al-6%Si alloy as a function of time.....	157
Figure 5.22	Volumic concentration of TiB_2 inclusions in Al-6%Si alloy as a function of time.....	159
Figure 5.23	Total volume of TiB_2 inclusions in Al-6%Si alloy as a function of time.....	159
Figure 5.24	Comparison of concentration number of different inclusions in Al-6%Si alloy as a function of particle size.....	160
CHAPTER 6		
Figure 6.1	Schematic of inclusion addition to the Al-6%Si alloy melt at 680 °C.....	164
Figure 6.2	Concentration number of TiB_2 inclusions (powder source) in Al-6%Si alloy as a function of time.....	166
Figure 6.3	Total number of TiB_2 inclusions (powder source) in Al-6%Si alloy as a function of particle size.....	166
Figure 6.4	Volumic concentration of TiB_2 inclusions (powder source) in	

	Al-6%Si alloy as a function of time.....	169
Figure 6.5	Total volume of TiB ₂ inclusions (powder source) in Al-6%Si alloy as a function of particle size.....	169
Figure 6.6	Microstructures of Al-6%Si alloy after addition of TiB ₂ (powder source) before the start of the LiMCA test.....	170
Figure 6.7	Microstructures of Al-6%Si alloy after addition of TiB ₂ (powder source) at the end of the LiMCA test.....	170
Figure 6.8	Concentration number of TiB ₂ inclusions (master alloy source) in Al-6%Si alloy as a function of time.....	172
Figure 6.9	Total number of TiB ₂ inclusions (master alloy source) in Al-6%Si alloy as a function of particle size.....	172
Figure 6.10	Volumic concentration of TiB ₂ inclusions (master alloy source) in Al-6%Si alloy as a function of time.....	176
Figure 6.11	Total volume of TiB ₂ inclusions (master alloy source) in Al-6%Si alloy as a function of particle size.....	176
Figure 6.12	Microstructures of Al-6%Si alloy after addition of TiB ₂ (as Al-5%Ti-1%B master alloy) before the start of the LiMCA test.....	177
Figure 6.13	Microstructures of Al-6%Si alloy after addition of TiB ₂ (as Al-5%Ti-1%B master alloy) at the end of the LiMCA test.....	177
Figure 6.14	Concentration number of Al ₄ C ₃ inclusions (powder source) in Al-6%Si alloy as a function of time.....	179
Figure 6.15	Total number of Al ₄ C ₃ inclusions (powder source) in Al-6%Si alloy as a function of particle size.....	179
Figure 6.16	Volumic concentration of Al ₄ C ₃ inclusions (powder source) in Al-6%Si alloy as a function of time.....	180
Figure 6.17	Total volume of Al ₄ C ₃ inclusions (powder source) in Al-6%Si alloy as a function of particle size.....	180
Figure 6.18	Concentration number of Al ₂ O ₃ inclusions (MMC source) in Al-6%Si alloy as a function of tim.....	182
Figure 6.19	Total number of Al ₂ O ₃ inclusions (MMC source) in Al-6%Si alloy as a function of particle size.....	182
Figure 6.20	Volumic concentration of Al ₂ O ₃ inclusions (MMC source) in Al-6%Si alloy as a function of time.....	184
Figure 6.21	Total volume of Al ₂ O ₃ inclusions (MMC source) in Al-6%Si alloy as a function of particle size.....	184
Figure 6.22	Concentration number of CaO inclusions (powder source) in	

	Al-6%Si alloy as a function of time.....	186
Figure 6.23	Total number of CaO inclusions (powder source) in Al-6%Si alloy as a function of particle size.....	186
Figure 6.24	Volumic concentration of CaO inclusions (powder source) in Al-6%Si alloy as a function of time.....	189
Figure 6.25	Total volume of CaO inclusions (powder source) in Al-6%Si alloy as a function of particle size.....	189
Figure 6.26	Concentration number of MgO inclusions (powder+metal source) in Al-6%Si alloy as a function of time.....	191
Figure 6.27	Total number of MgO inclusions (powder+metal source) in Al-6%Si alloy as a function of particle size.....	192
Figure 6.28	(a) Volumic concentration of MgO inclusions in Al-6%Si alloy as a function of time (MgO powder addition).....	193
Figure 6.28	(b) Comparison of volumic concentration of MgO inclusions in Al-6%Si alloy as a function of time: MgO powder vs. Mg metal addition.....	193
Figure 6.29	Total volume of MgO inclusions (powder + metal source) in Al-6%Si alloy as a function of particle size.....	194
Figure 6.30	Concentration number of TiAl ₃ inclusions (master alloy source) in Al-6%Si alloy as a function of time.....	196
Figure 6.31	Total number of TiAl ₃ inclusions (master alloy source) in Al-6%Si alloy as a function of particle size.....	196
Figure 6.32	Volumic concentration of TiAl ₃ inclusions (master alloy source) in Al-6%Si alloy as a function of time.....	198
Figure 6.33	Total volume of TiAl ₃ inclusions (master alloy source) in Al-6%Si alloy as a function of particle size.....	198
Figure 6.34	Comparison of different inclusions added to Al-6%Si alloy melts (at 680 °C) as a function of time.....	200
Figure 6.35	Comparison of concentration numbers of different inclusions in Al-6%Si alloy as a function of particle size.....	201
Figure 6.36	Comparison of volumic concentrations of different inclusions in Al-6%Si alloy (at 680 °C) as a function of time.....	203
Figure 6.37	Comparison of volumic concentrations of different inclusions in Al-6%Si alloy as a function of particle size.....	203
Figure 6.38	Comparison inclusion concentrations for different inclusion types in Al-6%Si alloy at 750 °C and 680 °C melt temperature.....	205

CHAPTER 7

Figure 7.1	(a) LiMCA tube before and after sampling, (b) close-up of the actual solidified metal block obtained from probe tube, (c) the sectioned and mounted sample.....	208
Figure 7.2	(a, b) Backscattered images of CaO inclusions and (c, d) corresponding X-ray images of Ca obtained from a LiMCA probe tube sample at the start of a LiMCA test.....	211
Figure 7.3	(a) Backscattered image of two MgO inclusions in a commercial pure Al matrix obtained from a LiMCA probe tube sample at the start of a LiMCA test, (b, c, d) corresponding X-ray images of Mg, O and Al.....	212
Figure 7.4	Backscattered images showing examples of MgO films in commercial pure Al, obtained from a LiMCA probe tube sample at the start of LiMCA test; (c, d) corresponding X-ray images of oxygen.....	213
Figure 7.5	(a, b) Backscattered images of TiAl ₃ inclusions, and (c, d) corresponding X-ray images of Ti obtained from a LiMCA probe tube sample at the start of a LiMCA test.....	215
Figure 7.6	Optical micrographs showing inclusions observed in various inclusion-containing Al-6%Si alloy ingots: (a) Al ₄ C ₃ , (b) CaO, (c) MgO, and (d) TiB ₂	217
Figure 7.7	Backscattered images of TiAl ₃ inclusions in Al-6%Si alloy, and corresponding X-ray images of Ti obtained from LiMCA probe tube samples: (a), (c) at the start, and (b), (d) at the end of the LiMCA test. (BS: backscattered image).....	219
Figure 7.8	Backscattered images (a, d) showing long and short TiAl ₃ plates and corresponding image of Ti (b, e), Si (c) and Fe (f). Samples obtained from LiMCA probe tube at start (a, b, c) and end (d, e, f) of the LiMCA test.....	220
Figure 7.9	Optical micrographs showing the sizes and acicular nature of TiAl ₃ inclusion particles (arrowed) in a LiMCA probe tube sample of Al-6%Si alloy melt to which Al-10%Ti master alloy was added.....	222
Figure 7.10	(a) Backscattered image of CaO inclusions and Ca-containing compounds in Al-6%Si alloy; (b, c) corresponding X-ray images of Ca and O; (d) EDX spectrum corresponding to the light gray large Ca-compound particle shown in(a).....	224
Figure 7.11	Optical micrographs showing CaO inclusions in Al-6%Si alloy; (a) at the start, and (b) end of the LiMCA test.....	226

Figure 7.12	(a) Backscattered image of Al_4C_3 inclusions (arrowed) in Al-6%Si alloy, and, (b, c) corresponding X-ray images of O and C taken from a sampling cup casting before the start of the LiMCA test.....	227
Figure 7.13	Optical micrographs showing Al_4C_3 inclusions in Al-6%Si alloy samples before the start (a, c) and at the end (b, d) of a LiMCA test.....	229
Figure 7.14	Optical micrographs showing MgO inclusions in Al-6%Si alloy samples before the start (a, c) and at the end (b, d) of a LiMCA test.....	230
Figure 7.15	Optical micrographs showing MgO inclusions (Mg metal source) in Al-6%Si alloy samples.....	231
Figure 7.16	Optical micrographs showing Al_2O_3 inclusions (arrowed) in Al-6%Si base alloy, obtained from casting samples taken at the start (a, c), and end (b, d) of the LiMCA measurement.....	233
Figure 7.17	(a) Backscattered image of TiB_2 powder inclusion particles in Al-6%Si alloy taken from a casting sample obtained before the start of the LiMCA test; (b, c) corresponding X-ray images of Ti and B.....	234
Figure 7.18	Optical micrographs showing TiB_2 powder inclusion particles in Al-6%Si alloy in samples obtained at the start (a) and end (b) of the LiMCA test.....	235
Figure 7.19	(a) Backscattered image showing TiB_2 inclusions resulting from Al-5%Ti-1%B master alloy addition to Al-6%Si alloy; (b, c) corresponding X-ray images of Ti and B.....	236
Figure 7.20	Optical micrographs taken from the same sample shown in Figure 7.19, showing TiB_2 inclusions, oxides and undecomposed master alloy particles in the Al-6%Si alloy matrix.....	237
Figure 7.21	(a) Backscattered image showing a large agglomerate of TiB_2 inclusions resulting from Al-5%Ti-1%B master alloy addition to Al-6% alloy, obtained from a sample taken from the LiMCA sampling probe at the start of the LiMCA test; (b, c) corresponding X-ray images of Ti and B.....	239

LIST OF TABLES

CHAPTER 2

Table 2.1	Classification of inclusions observed in aluminum melts according to their sources.....	12
Table 2.2	Summary of different types of inclusions observed in molten aluminum.....	14
Table 2.3	Inclusion removal methods.....	28
Table 2.4	Inclusion detection methods.....	37

CHAPTER 4

Table 4.1	Calculated average and total and number of MgO inclusions during 30 min of LiMCA sampling.....	107
-----------	--	-----

CHAPTER 6

Table 6.1	Inclusion concentration vs. particle size in base and TiB ₂ -containing Al-6%Si alloy melts (powder addition).....	167
Table 6.2	Comparison of inclusion readings of TiB ₂ -inclusion-containing (Test 3) and base Al-6%Si alloy melts reported in Table 6.1.....	168
Table 6.3	Inclusion concentration vs. particle size in base and TiB ₂ -containing Al-6%Si alloy melts (master alloy addition).....	173
Table 6.4	Comparison of inclusion readings of TiB ₂ -inclusion-containing (Test 3) and base Al-6%Si alloy melts reported in Table 6.3.....	174
Table 6.5	Inclusion concentration vs. particle size in base and CaO-containing Al-6%Si alloy melts (master alloy addition).....	187
Table 6.6	Comparison of inclusion readings of CaO-inclusion-containing (Test 1) and base Al-6%Si alloy melts reported in Table 6.5.....	187
Table 6.7	Comparison of concentrations of different inclusions in Al-6%Si alloy (at 680 °C) as a function of particle size.....	201
Table 6.8	Comparison of volumic concentrations of different inclusions in Al-6%Si alloy (at 680 °C) as a function of particle size.....	202

CHAPTER 1

DEFINITION OF THE PROBLEM

CHAPTER 1

DEFINITION OF THE PROBLEM

1.1 INTRODUCTION

Aluminum is the second most widely used metal and the third most abundant element in the world. Its alloys have properties such as good resistance to corrosion, high strength-to-weight ratio, good electrical and thermal conductivity and good workability, which explains why the consumption of aluminum and its products has rapidly increased over the years. Aluminum alloys are classified into two groups: casting alloys and wrought alloys. Premium quality aluminum casting alloys are extensively used in various applications in the aerospace industry, and their usage has greatly spread into commercial casting and automotive applications.

Aluminum-silicon (Al-Si) based casting alloys of the heat-treatable casting alloys series constitute the majority of aluminum castings, due to the high fluidity provided by the presence of a relatively large volume of the Al-Si eutectic. These alloys are widely used in the automotive industry for a variety of manufacturing applications *i.e.*, in the casting of pistons, pumps, inner turbo frames, gearbox casings, rear-axle housings, cast wheels and other automotive components. Silicon, as the major alloying element, offers excellent castability and resistance to hot tearing. Also, the presence of silicon during solidification reduces the casting's susceptibility to shrinkage. The silicon content in Al-Si alloys can

range from 2% to 21%. Depending upon the silicon content, Al-Si alloys are classified as hypoeutectic (2-12 % Si), eutectic (12 % Si) and hypereutectic (13-21% Si) alloys. Among these alloys, those containing 6-7% Si, such as A356, A319, 380, *etc.* are extensively used in industry.¹

The demand for higher quality aluminum cast products, particularly in the automotive and aerospace industries, has focused much attention on the quality of molten aluminum. Metal cleanliness is one of the most important characteristics affecting the quality and, hence, the performance of the final product. It is determined by different factors such as the amount of trace elements, gases, oxides, impurities and inclusions present in the melt. Inclusions in aluminum alloy castings have been a major problem in process and quality control, as their presence not only impairs the mechanical properties but also causes harmful effects, including poor machinability, increased porosity and reduced corrosion resistance. Dissolved gases, mainly hydrogen, are another source of problems as they lead to the formation of porosity in the casting. The formation of porosity in the presence of impurities such as inclusions is accelerated, since “dirty” metal containing inclusions absorbs more hydrogen. In fact, inclusions have been observed to act as nucleation sites for porosity formation.²

Thus, the control of metal cleanliness in molten Al-Si alloys requires the means to a) monitor and b) minimize the presence of impurities, inclusions and gases. This can be done through the use of degassing and inclusion removal techniques. The most common methods employed include filtration for inclusion removal, degassing to reduce the hydrogen content of the melt (and hence gas-induced porosity), and fluxing for the removal

of trace elements and to prevent gassing of the melt. However, as the results of the analysis of grab samples are time consuming and obtained off-line after significant delays, neither the information required to take corrective measures, nor the information on the inclusion size distribution are available on site.

From the monitoring point of view, many techniques have been introduced to measure the inclusion content in aluminum melts. These include vacuum filtration techniques such as the PoDFA (Porous Disc Filtration Apparatus), LAIS (Liquid Aluminum Inclusion Sampling) and Prefil (Pressure Filtration) techniques, the Qualiflash technique, as also nondestructive techniques such as the LiMCA (Liquid Metal Cleanliness Analyzer) and ultrasonic techniques.²

The present study was undertaken to investigate the capability of the LiMCA II technique for measuring different types of inclusions in commercial pure aluminum and Al-6%Si casting alloys under low (680 °C) and high (750 °C) melt temperature conditions. The main propose was to evaluate the technique in the case of casting alloys, where the inclusion levels are considerably higher than those found in wrought aluminum alloys for which the LiMCA has generally been used to date.

1.2 OBJECTIVES

An assessment of the melt cleanliness of commercial pure aluminum and an experimental Al-6% Si casting alloy was made using the LiMCA II technique, where various inclusions were introduced to the alloy melt using powder injection or master alloys in various concentrations.

The objectives of the present research work were as follows.

- 1) Investigate the sensitivity of the LiMCA II technique in measuring the concentration of carbide (Al_4C_3), boride (TiB_2), aluminide (TiAl_3) and oxide (CaO , MgO , Al_2O_3) inclusions in commercial pure aluminum and experimental Al-6%Si alloys.
- 2) Determine the effect of melt temperature on the capacity of the LiMCA II technique in the measurement of these inclusions.
- 3) Carry out a microstructural examination of inclusion-containing samples obtained from the corresponding LiMCA tests for qualitative analysis of the LiMCA data.

CHAPTER 2
LITERATURE SURVEY

CHAPTER 2

LITERATURE SURVEY

2.1 INTRODUCTION

Aluminum, the second most plentiful metallic element on earth, became an economic competitor in engineering applications as recently as the end of the 19th century. Development of industrial components that demanded material characteristics consistent with the unique qualities of aluminum and its alloys has resulted in the growth in production and use of aluminum. Nowadays, aluminum has virtually replaced iron and steel in many applications.

In 1888, Charles Martin Hall, an American, and Paul T. Heroult, a Frenchman, worked independently and discovered almost simultaneously an economical process of producing aluminum by electrolysis from a fused salt bath. In the Hall-Héroult process, refined alumina is dissolved in a cryolite bath, with various fluoride salt additions made to control the bath temperature, resistivity, density and alumina solubility. The passage of an electrical current through the bath electrolyzes the dissolved alumina, with oxygen forming at and reacting with the carbon anode, and aluminum collecting as a metal pad at the cathode. The separated metal is periodically removed by siphoning or vacuum methods into crucibles, which are then transferred to casting facilities where ingots are produced.

The major impurities of smelted aluminum are iron and silicon, while zinc, gallium, titanium and vanadium are typically present as minor contaminants. Refining or purification techniques can be used to attain much higher levels of purity (99.99%) for highly specialized applications.^{3,4}

Aluminum has numerous characteristics that cannot be found in other metals. It is a light metal with a density only about one-third that of steel. It is resistant to weather and a large number of liquids and gases present in the environment. Its high reflectivity provides aluminum with decorative properties suitable for interior architectural applications. Aluminum is a good conductor of heat and electricity. Aluminum alloys can equal or even exceed the strength of normal structural steel. However, while the high elasticity of aluminum is a useful property in certain constructions exposed to shock loading, its toughness is reduced significantly at low temperature, as is the case with most commercial steels.³

2.2 CLASSIFICATION OF ALUMINUM ALLOYS

Aluminum alloys are used to alter the characteristics of aluminum to fit with the requirement of the end application. The most common alloying elements for aluminum are magnesium, silicon, manganese, zinc and copper. Optimum combination of required properties for a specified application can be found with the correct aluminum alloy and temper (heat treatment).

Aluminum alloys are divided into two main categories: casting alloys and wrought alloys. Based on the primary mechanism by which their properties are improved, the alloys

can be further classified as heat-treatable or work hardening alloys. Alloys which respond to thermal treatment based on phase solubility are described as heat-treatable. The heat treatments include solution heat treatment, quenching, and precipitation or age hardening. Many wrought alloys depend on work hardening through mechanical reduction, together with various annealing procedures, to improve their properties. Such alloys are termed work hardening alloys.

The Aluminum Association system of classification is the most widely used system in America and employs different nomenclatures for wrought and cast alloys.³ For wrought alloys, a four-digit system is used, ranging from the 1xxx series representing the controlled unalloyed (pure) composition to the 8xxx series alloys containing tin and lithium, to 9xxx series reserved for future use. Casting alloys are described by a three-digit system followed by a decimal value. In this case also, the series range from 1xx.x to 9xx.x (un-used).

2.2.1 Aluminum Casting Alloys

Aluminum casting alloys have many characteristics in common with foundry alloys and generally have the highest castability ratings. As casting materials, they have favorable characteristics such as good fluidity for filling thin sections, low melting points compared to many other metals, and rapid heat transfer from the molten aluminum to the mold, providing shorter casting cycles. Many aluminum alloys are relatively free from hot-short cracking and tearing tendencies. They are also chemically stable and provide a good as-cast surface finish with little or no blemishes.³

2.3 INCLUSIONS IN ALUMINUM ALLOYS

Natural impurities in aluminum alloys include metallic and non-metallic constituents. These impurities or inclusions are observed in the form of gases, elements and particles, and include hydrogen, oxides, carbides, nitrides and borides. The term “inclusion” represents any foreign substances such as solid or liquid isolated particles or agglomerates of different phases, which are present above the liquidus temperature of the alloy.⁵ Inclusion concentrations in aluminum melts range from 0.005 to 0.02% (volume fraction) and have been observed in a variety of morphologies. Inclusion particle sizes range from dispersoids of a few microns in size to films and clusters that extend over several millimeters.

2.3.1 Sources of Inclusions

Melt treatments are sources of inclusions. Modification and grain refinement are two melt treatments commonly applied to Al-Si alloys. Modification is usually carried out by the addition of chemical modifiers such as sodium or strontium. Grain refinement is carried out by the addition of grain refiners. In the present work, TiB_2 , one of the most common grain refiners added to Al-Si alloys, was used. Other sources such as carbides, nitrides and borides may enter into the melt along with the grain refiners.

Refractory lining of the melting furnace and transfer devices are other sources of inclusions. Lubricants, core materials and other extraneous debris generated from remelt operations may also become trapped in the casting as inclusions.⁶ Poor separation of fluxing reaction products is another source of inclusions, where the inclusions appear as

halides or salts. Oxidation reaction with air is the most prevalent source of oxide inclusions. An excessive temperature during melting accelerates the oxidation of aluminum.^{7, 8} Electrolytic cells are another source of oxide inclusions. Primary ingots and the reaction of paints, oil and other carbon-containing compounds with aluminum are typical sources of carbide inclusions.⁹

2.3.2 Classification of Inclusions

Inclusions are generally classified as exogenous or indigenous. They can be further classified into different categories depending on their composition, size, phase (solid or liquid), morphology and source. Exogenous inclusions are imported to the molten metal from external sources such as refractory particles (including alumina, silica, silicon carbide and aluminum carbide), remelted ingots, and from refractory/metal reactions. They can be present in several physical forms as discrete particles. An example of this type of inclusion is aluminum carbide, Al_4C_3 . Indigenous inclusions, which are the most common inclusions, are produced either from chemical reactions within the melt itself by oxidation, or else from deliberate melt treatments such as fluxing, modification or grain refinement, and can be either solid or liquid. Oxides such as MgO , Al_2O_3 and $MgAl_2O_4$ are examples of this category of inclusions. Table 2.1 shows the classification of inclusions in aluminum melts according to their sources.⁶

Inclusions in aluminum are classified according to their shapes into two groups. The first group is massive inclusions with an irregular distribution in the microstructure. Such inclusions result in casting leaks and a reduction in density and ductility. The second

Table 2.1 Classification of inclusions observed in aluminum melts according to their sources.⁷

Classification	Inclusion Types Observed	Potential Sources
Non-metallic Exogenous	Various refractory particles, Al_4C_3 , <i>etc.</i>	Refractory degradation; potroom metal; refractory/metal reactions.
Non-metallic Indigenous	MgO, Al_2O_3 films, clusters and dispersoids; Al_2MgO_4 films and clusters.	Melting; alloying metal; metal transfer turbulence, chemical reaction between metal and oxygen in furnace.
Homogenous Halide/Salts	$MgCl_2$ -NaCl- $CaCl_2$, <i>etc.</i>	Poor separation of fluxing reaction products.
Particle/Salt	$MgCl_2$ -NaCl- $CaCl_2$ /MgO, <i>etc.</i>	Salt generated during chlorine fluxing of Mg-containing alloys; filter and metal handling system releases.

kind is dispersed inclusions, which cannot be seen with a low magnification microscope. Such inclusions increase the viscosity of the aluminum melt, reducing its fluidity and ability to fill the mold space during solidification.⁵

Phase-wise, inclusions are categorized into two groups: solid and liquid inclusions. Solid inclusions are isolated, rigid particles or agglomerates of different phases, textures and morphologies which may be introduced in the melt through extraneous sources (such as refractory brick, grain refiner, *etc.*) or during processing.⁶ Oxides, nitrides, carbides, borides constitute this group of inclusions. Liquid inclusions are particles which are

deformable and may coalesce into globules. Chlorides, fluorides, salts are part of this class. Chlorides and salts (CaCl_2 , NaCl , MgCl_2), and fluorides (cryolite) appear in the form of liquid droplets, while inclusions such as borides and carbides appear in the form of particle clusters.

The common types of inclusions in aluminum are: oxides, nitrides, carbides, fluorides and borides. Oxide films are also commonly observed and are generated during the melting process when the melt surface becomes oxidized due to its contact with the surrounding atmosphere. Such oxide films are located on the melt surface, and can become entrapped within the melt during stirring, alloying or other melt treatment processing. Table 2.2 lists the different types of inclusions observed in molten aluminum, their size and morphology.^{6, 10, 11}

2.3.3 Effect of Inclusions on Casting Quality

In general, inclusions exhibit a complex structure, and are hard and brittle. Inclusions with particle sizes greater than 10-20 μm have a severe effect on the quality of the casting and on its mechanical properties.² Inclusions in aluminum alloys affect the casting quality in different respects, such as reducing the mechanical properties (especially fatigue and ductility), damaging the surface finish, decreasing machinability (hard spots) and reducing the soundness of the casting. Inclusions act as nucleation sites for the formation of porosity, resulting in a poor surface finish and an increased tendency for corrosion. In fact, inclusions cause a lack of pressure tightness in a casting and make the surface finish unsuitable for anodizing, painting or varnishing purposes.⁸

Table 2.2 Summary of Different Types of Inclusions Observed in Molten Aluminum.^{6, 12}

Type	Morphology	Size Range, μm
OXIDES Al_2MgO_4 (Spinel) Al_2O_3 (Corundum) MgO SiO_2 CaO	Particles, skins, flakes Particles, skins, films Polygonal particles, skins Lumps Particles	1-6 10-1000 0.2-1 0.5-5 <5
CARBIDES SiC Al_4C_3	Particles Rectangular or hexagonal disc.	0.5-25 0.5-25
BORIDES TiB_2 AlB_2 VB_2 ZrB_2	Clusters of hexagonal or rectangular discs Particles, clusters Clusters Particles, discs	1-50 1-20 1-20 1-10
NITRIDES AlN	Particles, clusters	10-50
OTHER Chlorides and salts ($\text{CaCl}_2, \text{NaCl}, \text{MgCl}_2$) Flourites (cryolite) Sludge Al(FeMnCr)Si Calcium silicate Potassium silicate CaSO_4 Na_3AlF_6	Liquid droplets Lumps or sphere-like particles Lumps or sphere-like particles Rods Spheres	0.5-1 10-100 1-1000 1-5 2-60
ULTRAFINE GAS BUBBLES Argon bubbles N_2 bubbles		10-30
INTERMETALLICS $\text{TiAl}_3, \text{TiAl}, \text{NiAl}, \text{NiAl}, \text{Al}_3\text{Zr}$	Particles, clusters	10-100

Both tensile strength and elongation are reduced drastically due to the presence of inclusions. The yield strength, however, is relatively unaffected. The hardness of some inclusions measures about 9.5 on the Moh scale (of 10 for diamond). Thus, even a small amount of such inclusions in the casting can lead to extensive tool wear during machining. In foil products, inclusions as small as 5 μm can be harmful. Inclusions reduce the fluidity and feeding properties. Non-metallic inclusions act as stress raisers and can cause premature failure of a component.

2.4 TYPES OF INCLUSIONS

A wide variety of inclusions exist in molten metals and are characterized according to their composition, size, morphology, source and phase (solid or liquid). The common types of inclusions in aluminum are oxides, nitrides, carbides, fluorides and borides. These are discussed in more detail in the following sections.

2.4.1 Oxide Inclusions

Oxide particles and films are the most common inclusion defects observed in aluminum melts. Due to its strong affinity for oxygen, aluminum can form more than fifteen different types of oxides, ranging from 2.35 in density for gamma-aluminum oxide to 4 for alpha-aluminum oxide (corundum). Oxides may be formed at various stages of the melting process. They may originate from electrolytic cells and from reactions between the melt and atmosphere. Aluminum oxidation is practically unavoidable, and the character of the oxide formed is determined by the oxidation mechanism. It has been found that increasing the melt temperature also increases the oxidation rate exponentially.^{13, 14, 15}

Al_2O_3

The common type of oxide in aluminum is Al_2O_3 . An X-ray diffraction analysis of isolated particles reveals that aluminum oxides occur in the form of α - Al_2O_3 and γ - Al_2O_3 . Gamma or alpha alumina (Al_2O_3) inclusions are frequently found in magnesium-free alloys. Gamma alumina of a lacy film morphology often forms initially and calcines after prolonged melt holding periods to the alpha phase. Al_2O_3 inclusions also occur as dark grey films or groups of films. The films are normally less than 1 μm thick and 10-500 μm in cross section. In many instances, Al_2O_3 films may form near hydrogen pores.

Analyses of oxides from different stages in the melting process have revealed that they can be classified into three categories depending upon the source of formation, *i.e.*, oxides originating from the alumina in electrolysis cells, oxides formed by reaction between the air and the melt, and oxides originating from the brick linings in the furnace, *etc.*^{11, 13, 14, 15}

Oxides in material coming from aluminum cells are mostly thin films; sometimes thick oxide lumps may also be present. While impurities are not found in most oxides, traces of iron, silicon, potassium, sodium, calcium or magnesium have been observed in thick films. Thin films are oxide inclusions which are formed by reaction between the air and the melt. Hard aluminum oxide (Al_2O_3) particles are observed as hard spots within a casting. Hard spots have a harmful effect on machining operations and tool life.¹⁵ Figure 2.1 shows typical α - and γ - alumina inclusions observed in Al-Si alloys.

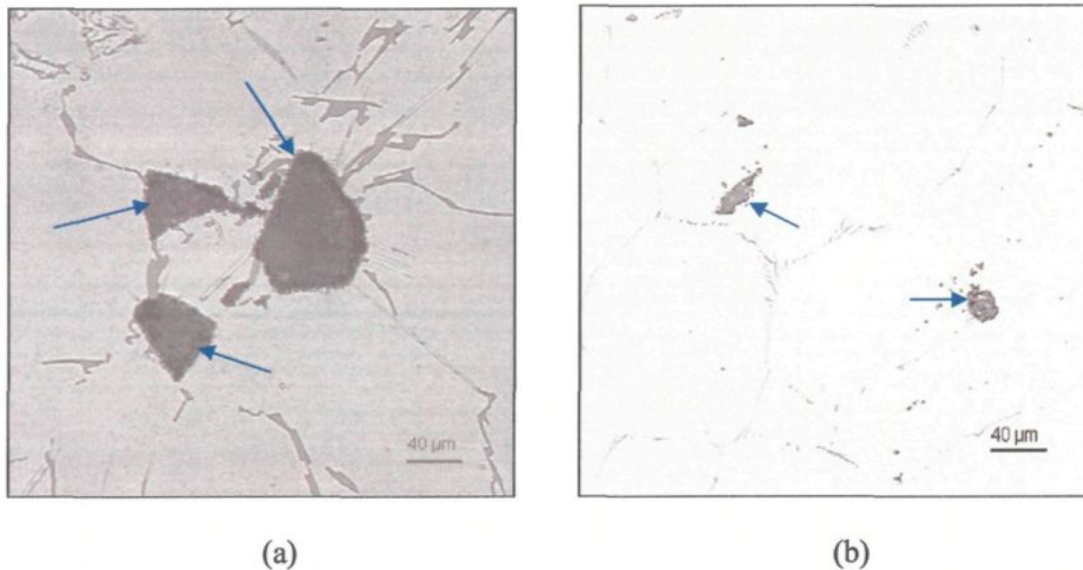
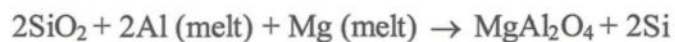


Figure 2.1 Typical aluminum oxide inclusions observed in Al-Si alloys: (a) α - Al_2O_3 , (b) γ - Al_2O_3 (arrowed).

MgAl_2O_4

Magnesium aluminates (spinel) usually form a thick film or cluster and are created by high melt surface temperatures from direct flame impingement. Spinel, MgAl_2O_4 , is formed by reaction between silicates or refractory materials and the melt, according to the following reaction:



Formation of spinels can also be accelerated in the presence of magnesia inclusions. Increased oxidation rates occur when the protective oxide layer breaks down during spinel formation. Spinel formation is reduced by additions of up to 0.1% of beryllium to the melt. Melts containing MgAl_2O_4 are often contaminated with impurities such as silicon, iron, potassium, sodium and calcium. These inclusions are black or brown,

thick films or elongated lumps consisting of adherent particles.^{12, 14} Figure 2.2(a) shows an example of MgAl_2O_4 particles.

MgO

Magnesia (MgO) inclusions are found in alloys containing magnesium and, like MgAl_2O_4 , MgO is the dominant oxide in Al-Mg alloys. The MgO inclusions can be black or brown, and occur in the form of thick films or elongated lumps consisting of loosely adherent particles.^{11, 13} The MgO and MgAl_2O_4 films are normally 10 to 500 μm in cross-section. However, morphological forms exist that include colonies of 1-5 μm dispersoids and clusters. Dispersoid colonies typically result from localized oxidation of magnesium due to improper submerging of the magnesium into the melt.³ Figure 2.2 shows typical magnesium oxide inclusions observed in aluminum-magnesium alloys.

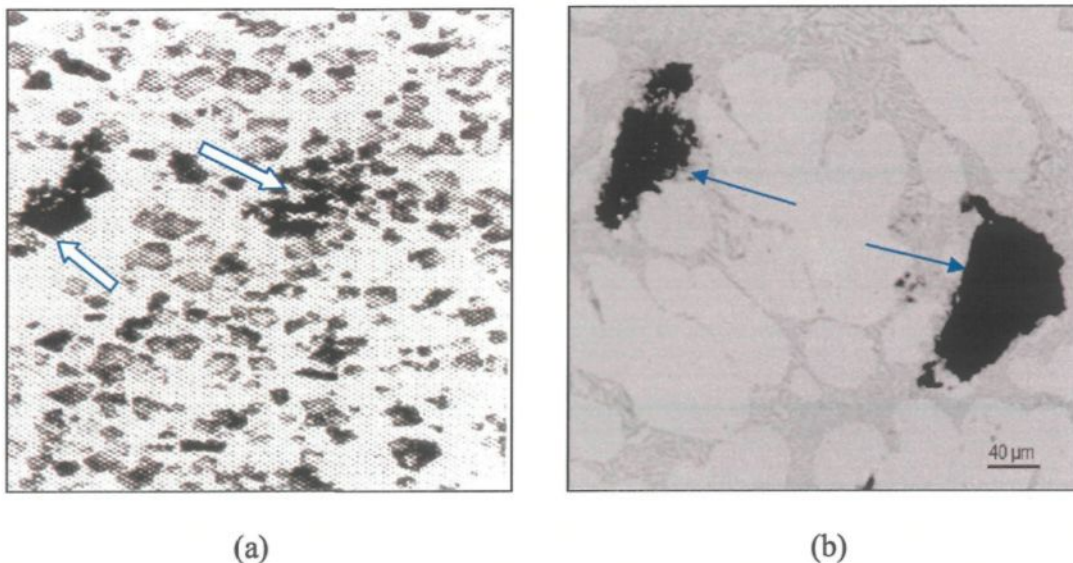
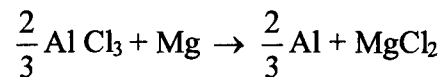
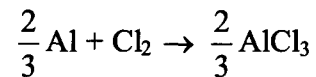


Figure 2.2 Examples of magnesium oxide inclusions: (a) MgAl_2O_4 ,¹¹ (b) MgO (arrowed).

2.4.2 Salts

Salt particles are inclusions soluble in water, and mostly contain Al, Na, Ca, K, Cl, F, and S originating from potroom metal (*e.g.* particles of pot flux), melt treatment salts, and products from the reaction of aluminum with active gases.¹³ These salts form when chlorine or argon/nitrogen-chlorine mixtures are used to remove hydrogen from the melt. If the melt contains magnesium, a molten salt, magnesium chloride (MgCl₂), is formed through the reactions:

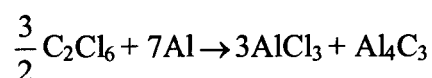


Since MgCl₂ melts at 708 °C, it can be present as a solid or as an immiscible liquid, depending on the melt temperature. Sodium and calcium may also form solid salts, and NaCl, MgCl₂, CaCl₂ are examples of inclusions of this type.⁹

2.4.3 Carbides

Carbides are hexagonal or rectangular grey discs, 0.1-10 μm in size, and normally found as isolated clusters or together with oxides and boride particles. They corrode in moist air and turn blue and brown. The main source of carbide formation is the reaction between the melt and the cathode or anode in the electrolytic cell. The refractory lining of the furnace, and the reaction of paints, oil and other carbon-containing compounds with aluminum are other sources of carbides. The common carbide in aluminum is aluminum carbide (Al₄C₃), which may be formed during the aluminum smelting process and

frequently results from poor quality ingot. These carbides are harmless due to their small size (1-10 μm). Aluminum carbide can also be formed through the use of certain solid degassing tablets consisting of hexachloroethane (C_2Cl_6) via the following reaction:



Aluminum carbide particles can also be as large as 50 μm , and most of them float to the surface along with the aluminum chloride vapor formed in the reaction. Microprobe analysis of aluminum carbide particles has revealed that several of them contain oxygen. Besides aluminum carbide, aluminum melts may contain carbon particles, graphite, $\text{Al}_4\text{O}_4\text{C}$, TiC , VC and CaC_2 .⁹ Figure 2.3(a) shows typical Al_4C_3 inclusions observed in Al-Si alloys

2.4.4 Borides

Ordinary aluminum contains less than 1 ppm borides, whereas grain-refined material can contain about 10 to 100 ppm borides. Common borides are TiB_2 and VB_2 , while ZrB_2 and CrB_2 are also detected in aluminum alloy melts. Boride particles are hexagonal or rectangular discs, ranging from 0.1 to 10 μm in diameter. These inclusions are normally found in clusters of 1 to 50 μm cross-section, along grain boundaries or near the center of the grain. It is difficult to distinguish between different types of borides, as TiB_2 , VB_2 , and ZrB_2 are all grey or brownish-grey in color. TiB_2 and VB_2 are the dominant inclusion types in grain-refined material.¹¹ Titanium boride clusters are formed as a result of too heavy grain refining, too long holding times, or as a reaction product in the boron

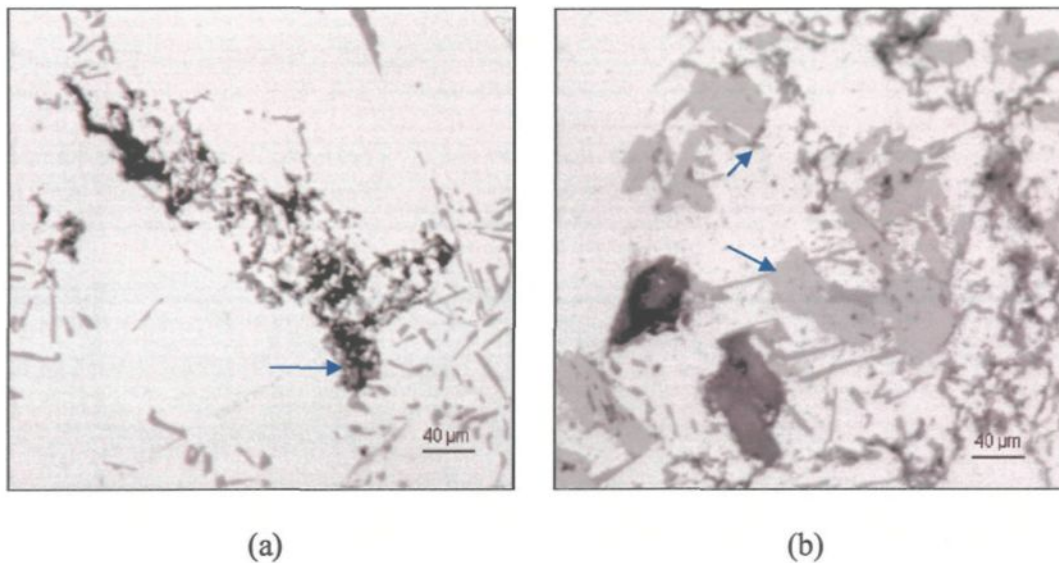


Figure 2.3 Examples of (a) Al_4C_3 , (b) TiB_2 inclusions (arrowed).

treatment of Al-melts. TiB_2 inclusions mostly appear together with other kinds of inclusions.¹⁶ Figure 2.3(b) shows an example of TiB_2 inclusions.

2.4.5 Nitrides

Commercial aluminum alloys contain 2 to 5 ppm nitrogen. Nitrides are present in aluminum as AlN and possibly as oxynitrides. They are commonly found in mixtures with oxides and are formed by reaction between the melt and the atmosphere. Figure 2.4(a) shows AlN -films with Al_2MgO_4 particles in an Al-10%Mg alloy.¹¹

2.4.6 Fluorides

Fluorides, in the form of CaF_2 , exist in cryolite inclusions in commercial aluminum alloys. Aluminum normally contains less than 1 ppm cryolite. The cryolite inclusions appear in the form of medium grey spherical particles that are transparent in polarized

light. These are 3 to 60 μm in diameter and contain particles of Al_2O_3 , CaF_2 and MgO . The source of cryolite particles is the alumina electrolyte. An analysis of these inclusions shows that NaF is also present in minor traces. Figure 2.4(b) shows an example of a spherical cryolite inclusion containing Al_2O_3 and CaF_2 impurities.¹¹

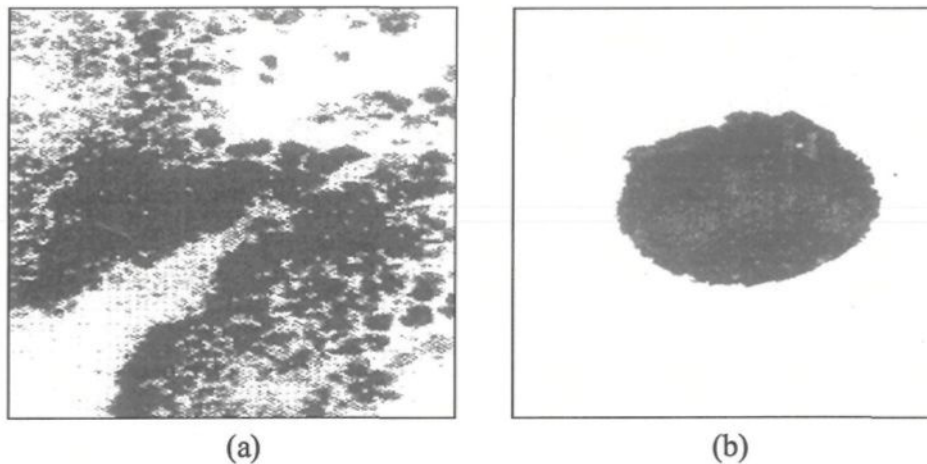


Figure 2.4 Examples of (a) AlN films and Al_2MgO_4 particles in an Al-10\%Mg alloy (mag: $\times 600$); (b) a spherical cryolite inclusion containing Al_2O_3 and CaF_2 impurities (mag: $\times 600$).¹¹

2.4.7 Intermetallic Compounds

According to common definition, intermetallics are compounds of metals whose crystal structures with ordered atom distributions are different from those of the constituent metals. They possess high density, high melting points and high hardness. In the form of inclusions, they can have a harmful effect. For example, large particles of titanium aluminide, TiAl_3 (greater than 10 μm), are generated due to poor quality grain-refining materials, and they give rise to inclusion defects, or intermetallic inclusions. On the other hand, TiAl_3 smaller than 5 μm are useful as grain-refining nuclei.^{13, 16}

Intermetallic phases originating from the solidification of a clean melt, are classified into two fundamental groups: Fe-rich and Cu-rich compounds. Depending on the morphology, the Fe-rich compounds may be divided into three distinct categories: plateletes (Al_5FeSi), Chinese script particles $\text{Al}_{15}(\text{Fe},\text{Mn})_3\text{Si}_2$ and polyhedral sludge crystals $\text{Al}_{15}(\text{Fe},\text{Mn},\text{Cr})_3\text{Si}_2$. Copper-rich particles of $\text{Al}_2\text{Cu}(\text{Si},\text{Fe},\text{Zn})_{0.2}$ are an example of Cu-rich compounds. Titanium aluminides, nickel aluminides and related phases are examples of other intermetallics.

2.4.8 Calcium Compounds

Calcium combines with aluminum and forms the intermetallic compounds Al_4Ca and Al_2Ca . Calcium also combines with silicon to form the intermetallic compounds CaSi_2 , Ca_3Si_4 , Ca_2Si , Ca_5Si_3 , and CaSi . In Al-Si casting alloys, the CaSi_2 intermetallic compound is insoluble in aluminum and has a deleterious effect on the mechanical properties and corrosion properties of the alloy. Calcium in aluminum alloys may also be present in the form of other calcium silicides, calcium phosphides and calcium nitrides. Calcium is also present in oxide films in traces, in the form of CaC_2 , CaSO_4 , CaS and CaF_2 .¹⁷

Chlorides are also present in traces and commonly found in oxides. Another important category of inclusions includes Al_3Zr and Al_3Ti particles. An example of Al_3Zr particles nucleated in the aluminum melt is shown in Figure 2.5. The Al_3Zr agglomerate is a bundle of rods most likely nucleated at one specific point in the melt. Iron-rich particles such as FeO or Fe_2O_3 may also form in the melt.

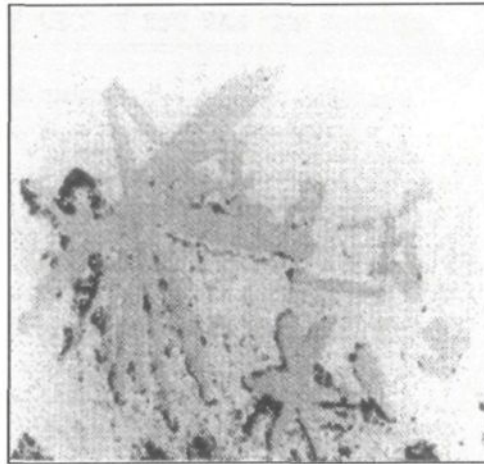


Figure 2.5 Light grey Al_3Zr rods in an AlZnMgZr alloy.¹¹

The classification of inclusions according to their sources in aluminum melts and the different types of inclusions observed in molten aluminum, their size and morphology⁶ have been provided in Tables 2.1 and 2.2 in section 2.3.2 previously.

2.5 POROSITY

Porosity is the most common defect found in cast metals and is the major cause of casting rejection. It is known that the quantity and the appearance of porosity are crucial to the mechanical properties of the casting, especially the fatigue properties, since micropores are a primary source of crack initiation, leading to final failure.¹⁸ The formation of porosity in the presence of impurities such as inclusions is accelerated, since “dirty” metal containing inclusions absorbs more hydrogen. The inclusions act as nucleation sites for pore formation. Thus, both porosity and inclusions are two important causes of casting rejection.

In general, two types of porosity can occur in cast aluminum: gas porosity and shrinkage porosity. Gas porosity, which is fairly spherical in shape, results either from the precipitation of hydrogen during solidification or from the occlusion of bubbles during the injection of metal in die-casting operations. Pores of this type are usually less irregular, with rather smooth outlines.¹⁹ Hydrogen, due to its significant solubility in liquid aluminum, is one of the main causes of gas porosity. As Figure 2.6 shows, there is considerable reduction of hydrogen solubility in the solid state. As molten aluminum solidifies, this excess hydrogen is rejected from the liquid and can manifest itself in the form of blowholes, porosity, or microporosity.^{20,21}

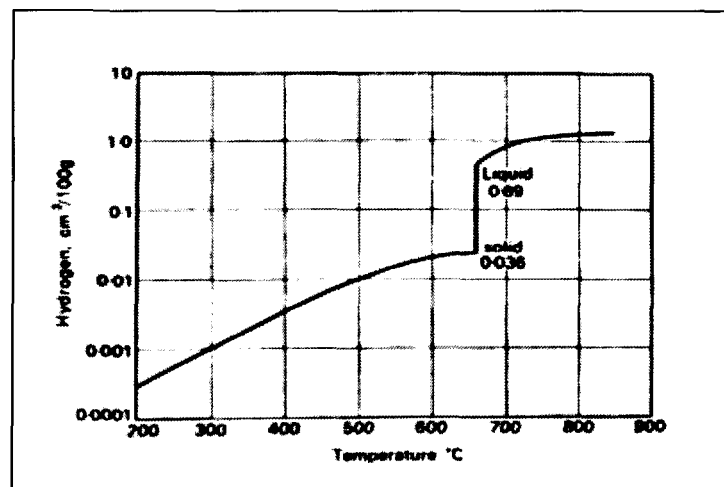


Figure 2.6 Solubility of hydrogen in solid and liquid aluminum.²⁰

Shrinkage porosity results from the decrease in volume accompanying solidification. In other words, it is caused by local insufficient liquid feeding in the later stages of solidification. Shrinkage porosity frequently takes the interdendritic form of void distributions, and is enlarged by an increase in the hydrogen content of the melt and a

lower solidification rate. This type of porosity is more likely to be seen in unmodified or not well-modified Al-Si alloys. Figure 2.7 shows the morphologies of gas and shrinkage pores observed in aluminum castings.

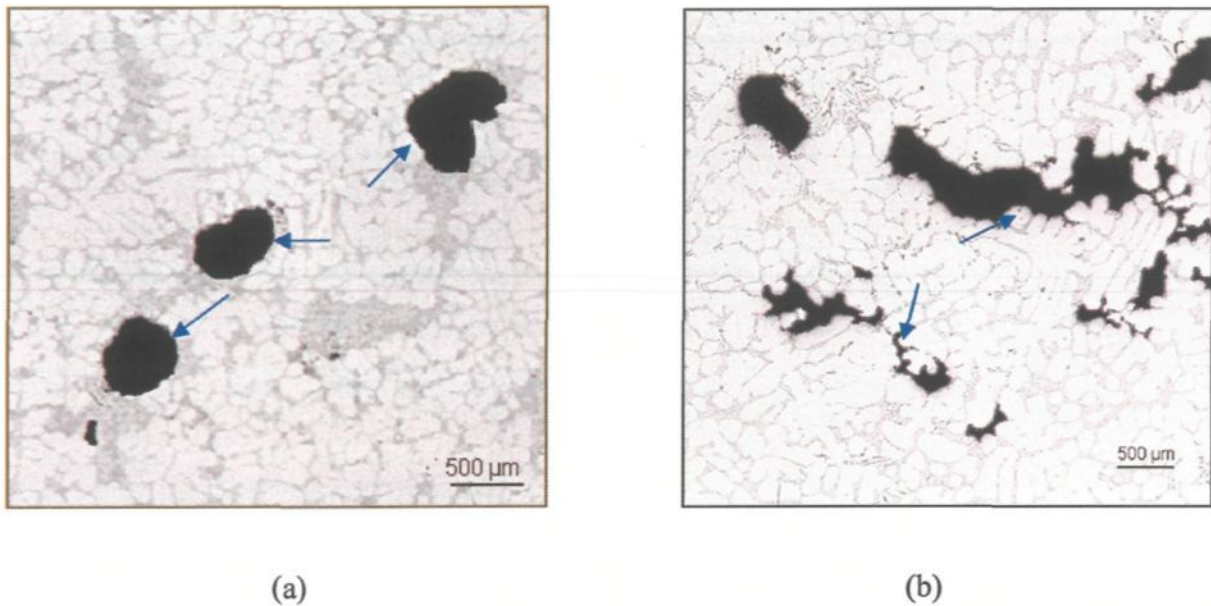


Figure 2.7 Morphologies of (a) gas pores, and (b) shrinkage pores observed in aluminum castings.

The formation of porosity during solidification can also be affected by several other factors such as cooling rate, alloying elements, modification and melt cleanliness. In aluminum casting, the formation of porosity is accelerated in “dirty” metal (*i.e.* melts containing more impurities or inclusions) compared to clean metal. In fact, dirty metal absorbs more hydrogen. Porosity formation in melts necessitates the nucleation of a gas bubble. The nucleation process and subsequent pore growth will control the amount of porosity in the final structure.

Whether due to an absence of nuclei or to a lower hydrogen content, it is found that cleaner melts are resistant to porosity formation in the final casting. Aluminum melts usually contain a wide variety of non-metallic particles, and because of their poor wettability, certain suspended particles represent potential nucleation points for pore formation. It is therefore reasonable to expect that with increasing inclusion concentration, pore formation becomes more feasible, resulting in higher porosity levels.^{21,22}

2.6 INCLUSION REMOVAL TECHNIQUES

The control of metal cleanliness in molten aluminum alloys is an integral part of quality control requirements in aluminum foundry alloys. As inclusions are unwanted by-products of molten aluminum, and have a harmful effect on the quality of a casting, an assessment of the inclusion level in the melt and their removal becomes essential.²³

Various melt treatment techniques are currently in use in the aluminum foundry industry, to remove inclusions from the melt, often in conjunction with hydrogen reduction. These include flux treatment, filtration, flotation, degassing and sedimentation.²⁴

In general, inclusion removal methods can be grouped into two broad categories: (i) volumetric force-driven separation methods like the sedimentation method, and (ii) externally assisted methods. In the latter case, applied external forces emphasize on the density difference between the inclusions and the melt and cause separation, or act as a device to transport the inclusions to the surface (gas bubbles), cause agglomeration of the inclusions and their separation through filtration, *etc.*^{24, 25} Inclusion removal methods classified under the two categories are shown in Table 2.3.

Table 2.3 Inclusion removal methods.¹²

Volumetric Separation	Particle size affected (μm)
Gravity sedimentation (metal settling) in holding furnaces	>90
Externally Assisted Methods	
Electromagnetic separation	>50
Flotation in degassing units	>1
Filtration	>1

2. 6. 1 Gravity Sedimentation

Settling (or sedimentation) usually refers to falling particles (*i.e.*, inclusions) in a liquid, and occurs as a result of the difference in density between the inclusions and liquid metal. Due to the density difference, the inclusions sink in the gravitational field, and are consequently removed by sedimentation. In sedimentation, an inclusion particle is subjected to the action of three forces, namely its weight, the local pressure gradient and the drag force.

These three forces are invariably taken into account in the inclusion removal process model.²⁶ A single particle in suspension in the liquid will sink with a velocity given by a balance between the buoyant (tendency for floating) and drag forces. Non-spherical particles or suspensions of particles will settle more slowly due to increased drag forces. Also, the settling velocity will be reduced close to surfaces due to wall effects.⁶ A schematic representation of gravity sedimentation¹² is shown in Figure 2.8.

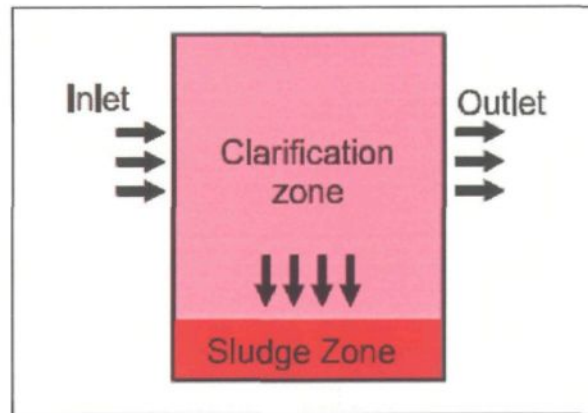


Figure 2.8 Schematic representation of gravity sedimentation.¹²

Common usage of the sedimentation technique is in the removal of sludges, simplified on account of their higher density. The main advantage of this method is that the particles in the liquid are collected in a small amount, so the subsequent analysis of particles is simplified. Also, this method is very rough and ready and involves no great capital investment. However, it is limited to inclusion sizes larger than $90\ \mu\text{m}$.²⁷

2.6.2 Electromagnetic Separation

In this technique, an external electromagnetic force acts upon the melt, and in reaction to this applied force, the inclusions move in the opposite direction and thus get separated. Electromagnetic separation methods are classified according to the manner in which the electric and magnetic fields in the melt are produced. Due to the complexity of producing strong, homogeneous magnetic fields, large force densities in large volume are difficult to achieve. Thus, the separation efficiency is quite low at inclusion sizes below $50\ \mu\text{m}$.¹²

2.6.3 Flotation

Flotation is another technique used in aluminum melts and involves purging a gas into the melt. A reactive or inert gas or a combination of both types is purged through a rotating impeller or a non-rotating lance into the liquid metal. Impeller rotation creates turbulence inside the melt, due to which randomly distributed solid inclusion particles collide, agglomerate and form larger clusters. These clusters either float up with the gas bubbles they encounter to the melt surface, or settle down due to density differences between them and the melt, and can thus be removed from the melt bulk. Chlorine and fluorine are the reactive gases, while argon and nitrogen are the inert gases generally used.

The efficiency of inclusion removal depends on the flow field inside the melt created by the flow of the bubbled clusters and by the impeller rotation. The size and number of gas bubbles limit the removal of solid inclusions. The agglomeration of the particles caused by turbulence in the flow field regulates the transport of inclusions to the surface of the gas bubbles. The addition of chlorine or other halogens is believed to affect the surface tension of the bubbles and make the oxides and inclusions adhere to the bubble surface more rapidly.^{12, 14, 26, 28, 29} A schematic representation of the removal of inclusions by gas bubbles is shown in Figure 2.9. Inclusions greater than 30-40 μm may be reliably separated from the melt by flotation.

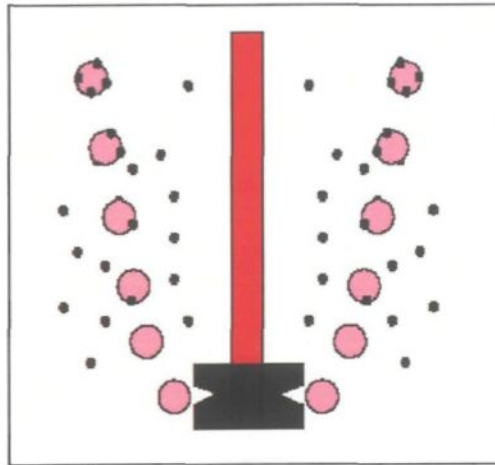


Figure 2.9 Schematic representation of inclusion removal by gas bubbles.¹²

2.6.3.1 Stirring

In this technique, convective forces within the melt carry the inclusions to the crucible wall or the dross at the surface, and thus remove them from the melt. Stirring is carried out by two mechanisms: the ascent of gas bubbles in the melt, and the rotation of the cylindrical impeller head. Both flotation and stirring have an excellent potential for inclusion removal. Flotation appears to be somewhat better than stirring for the removal of small inclusions, whereas larger inclusions are more easily removed by stirring.^{29,29}

2.6.4 Filtration

Filtration technology offers an effective way of removing inclusions in the size range of less than 30 μm . The two distinct modes of filtration widely used in industries are deep-bed and cake mode filtration.

Deep-bed filtration consists of a packed bed of refractory filters through which the molten aluminum flows. The inclusions deposit on to the grains of the filter medium due to diffusion, direct interception, gravity and/or surface forces.

In the case of cake mode filtration, inclusions are deposited at the upper surface of the filter. The latter aggregate of inclusions acts as a second filter above the original medium, rendering an additional resistance to flow, thus causing separation of the particulates from the melt. Bed filters, rigid media filters and ceramic foam filters are three major types of filters used for molten aluminum alloys.^{6, 30, 31, 32, 33, 34, 35} Figure 2.10 shows a schematic representation of the inclusion size with respect to the average filter pore size in pores per inch (ppi).

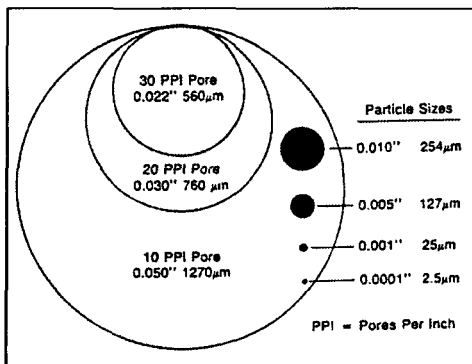


Figure 2.10 Schematic representation of the inclusion size with respect to filter pore diameter.³⁰

2.6.5 Degassing

Degassing is the most common method used for the removal of dissolved hydrogen from molten aluminum. It is carried out by injection of gas through a rotary impeller, producing fine gas bubbles and dispersing them throughout the metal. The design of the

impeller head affects determination of the bubble size. The graphite shaft and impeller head are submerged into the molten metal bath and small, well-dispersed bubbles produced. The reduction in size of the purging gas bubbles dramatically increases the available purge gas surface area. The tiny bubbles rise slowly to the surface, allowing a greater time to react with the hydrogen in the melt and facilitate its removal. The mechanism of hydrogen and inclusion removal is illustrated in Figure 2.11.

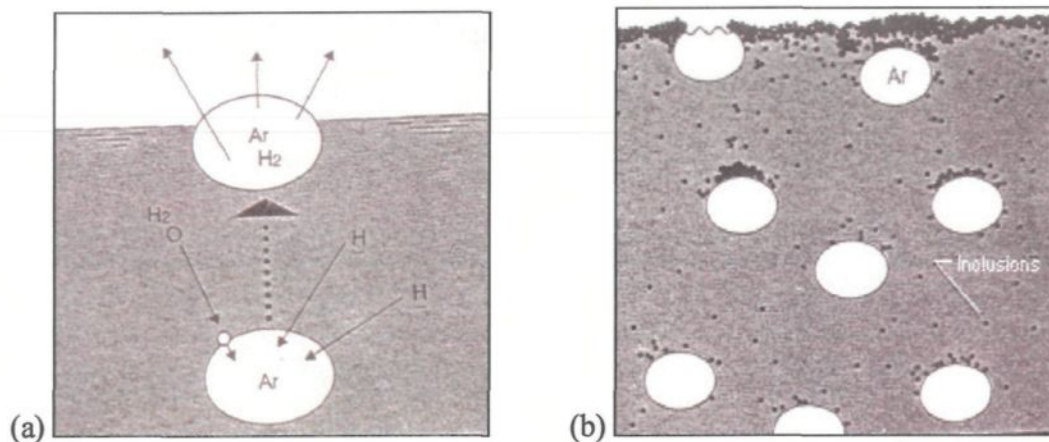


Figure 2.11 (a) Degassing mechanism, (b) mechanism of inclusion removal.³⁶

Degassing methods are grouped into purely physical methods (*e.g.*, inert gas treatment) and physico-chemical techniques (*e.g.*, inert gas mixture, chlorine treatment, *etc.*). The injection of dry nitrogen gas into the melt via a lance is one of the simplest and cheapest means of reducing the hydrogen gas level in molten aluminum. The efficiency of this operation is relatively low due to the large bubbles produced from the lance. Argon and some other reactive gases such as chlorine are also used for the removal of dissolved hydrogen from molten aluminum. Plunging chlorine-based tablets into the melt using a

perforated bell can be efficient in terms of reducing the hydrogen gas content. However, they are expensive and harmful for health.

The parameters that significantly affect the efficiency of a degassing procedure are the purging gas flow rate, the rotation speed of the impeller, the duration of gas purging and reversing the impeller rotation direction.^{36,37} Figure 2.12 shows an example of the type of impellers used for stirring and degassing.

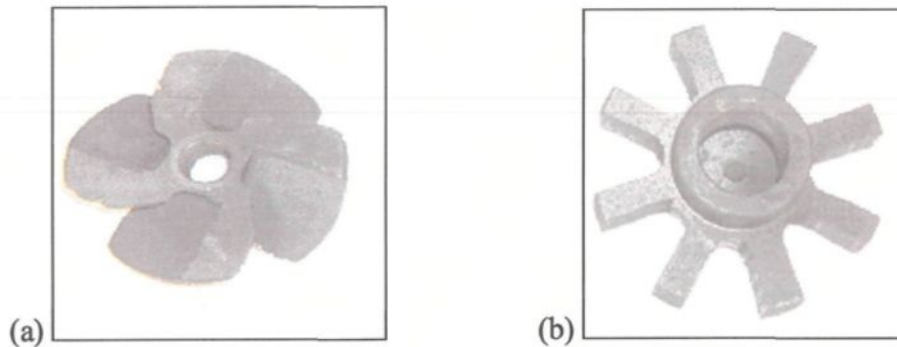


Figure 2.12 Impellers used for (a) stirring, and (b) degassing.

2.6.5.1 Oxide Removal

Studies have shown that the small purge gas bubbles of nitrogen or argon from the rotary degassing process can float oxides to the surface. The rate of oxide removal can be improved with a small percentage of chlorine present in the purge gas. The surface tension of the aluminum is changed by the chlorine and facilitates easy attachment of the oxides to the purging gas bubbles, and hence their removal.³⁷

2.6.6 Flux Treatment

Fluxing by injection is another method used for inclusion removal. The traditional method of flux addition includes equipment for blowing the flux through the melt surface and furnace walls. The most commonly used method is manually shoveling the flux into the melt, followed by manual stirring. These processes are operator dependent and labor intensive. A new method of flux injection is used in industry which offers less flux consumption, lower inclusion and hydrogen levels, less aluminum content in the dross and lower treatment time and costs.³⁷ Figure 2.13 shows the elements of the flux injection process.

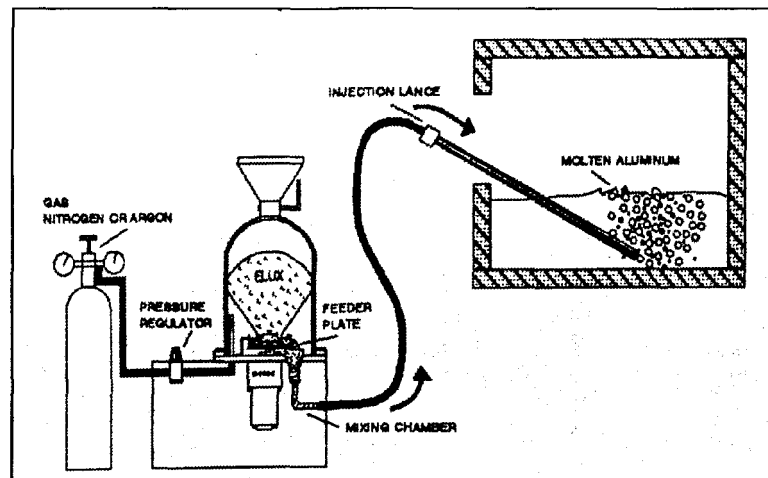


Fig 2.13 Schematic of the elements of the flux injection process.³⁷

2.7 INCLUSION MEASUREMENT TECHNIQUES

The control of metal cleanliness in molten aluminum alloys requires monitoring and minimizing the presence of impurities such as non-metallic inclusions and hydrogen to the lowest concentration levels. A number of techniques have been developed for the

determination of melt cleanliness. These range from qualitative to quantitative techniques, as well as analytical laboratory procedures. Due to the relatively low concentrations of inclusions normally present in the melt, a precise estimate of the inclusion levels is a rather complicated task. Furthermore, because of the non-uniform distribution of the inclusion particle sizes, additional complexities are introduced.^{10,38}

Several qualitative and semi-qualitative techniques are being used to estimate and control the inclusion concentrations in aluminum castings. These are classified into four categories based on their principle of operation: chemical analysis, quantitative metallography, non-destructive techniques and shop floor tests. While these methods provide useful process information, they are time consuming, not sufficiently quantitative, and expensive to use in terms of capital investment.

Included among these techniques are some very sophisticated (and expensive) electronic devices that characterize the volume, size and distribution of inclusions suspended in a melt (*e.g.* the LiMCA and the 4-M techniques), and on the other end of the scale, the simple shop floor reduced pressure test (RPT) which is the foundry standard often used for measuring the hydrogen level and, indirectly, the inclusion level in aluminum melts.

Vacuum pressure filtration methods such as the PoDFA, LAIS and PREFIL techniques determine the amount of inclusions present in the melt taking into consideration both the weight of the liquid metal filtered and subsequent metallographic examination of the filter section. Yet other methods involve complete solution of the sample material in

mixed acids or solvents, and collection of the insoluble inclusions.^{23, 38} Table 2.4 summarizes the different inclusion detection methods.

Table 2.4 Inclusion detection methods.¹²

Detection Methods	Sample Weight, g	Particle Size Affected, μm	Operation Type
Pressure Filter Tests PoDFA LAIS Prefil Qualiflash	≤ 2000 ≤ 1000	All sizes	Off-line Off-line Off-line
Electrical Resistivity Test LiMCA II	≤ 100 per min	> 15	On-line
Acoustic Detection Signal-noise technique Pulse-echo technique		> 10	On-line
Electrochemical Dissolution	≤ 100	All sizes	Off-line
Chemical Analysis Emission spectroscopy: Hot extraction; Combustion analysis; Neutron activation; Gas chromatography	0.5-30	All sizes	Off-line
Eddy Current Method	-	-	On-line
Capacitance Probe	-	-	On-line
X-Ray Detection	-	-	Off-line
Electromagnetic Detection	≤ 200 per min	> 10	On-line

2.7.1 PoDFA Technique

The PoDFA (Porous Disc Filtration Apparatus) technique is based on quantitative metallography in which direct examination of polished sections provides information on the type and morphology of inclusions. Figure 2.14 outlines the principle of the PoDFA.³⁸ Approximately 2 Kg of metal, taken directly from the melt that has to be analyzed, are passed through a filter. A balance located below the filtrate crucible enables the operator to precisely obtain the right amount of metal. The filters with the residue are then sectioned vertically along the central plane and prepared for metallographic examination. The inclusion concentration is reported in mm^2/Kg indicating the area of inclusions in the sectioned part.⁶ The technique can also distinguish inclusion type and differentiate, for instance, between the levels of borides, carbides and spinels present within an individual sample.

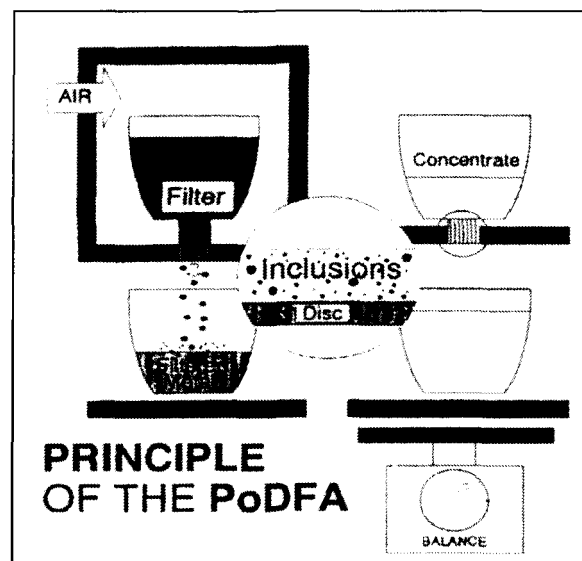


Figure 2.14 Principle of the PoDFA Technique.⁶

This technique may distinguish between very dirty metal (more than $1 \text{ mm}^2/\text{Kg}$) and relatively clean samples. However, it is not sensitive at inclusion concentrations less than $1 \text{ mm}^2/\text{Kg}$. The results can also be influenced by the presence of inclusion particles less than $10 \text{ }\mu\text{m}$ in size.^{6,23}

2.7.2 Prefil Technique

The Prefil (Pressure Filtration) technique is used to measure metal cleanliness and build up a database demonstrating the relationship between inclusion content and filtration rate behavior. It involves filtering a molten aluminum sample under pressure through an ultra-fine filter, resulting in a build up of solid inclusions on the filter surface. The inclusions are then metallographically examined, identified and counted. The inclusion levels are expressed in the form of units of inclusion area per kilogram of filtered melt (mm^2/Kg). Based on such quantitative analyses of inclusions, the corresponding filtration (or flow) curve can be characterized. The flow curves then provide the means for assessment of the melt cleanliness.

Figure 2.15 (a) depicts the schematic flow curves obtained for various melt conditions with the Prefil apparatus shown in Figure 2.15 (b). The machine consists of a two stage pressure cell (Prime and Run sequences), a refractory crucible containing the filter, and a digital balance to record filtrate weight against time. The machine is equipped with on-board data logging and software for footprint characterization. The crucible is made of a low-heat capacity, high-insulating fibrous material. Thus, no preheating prior to testing is required.

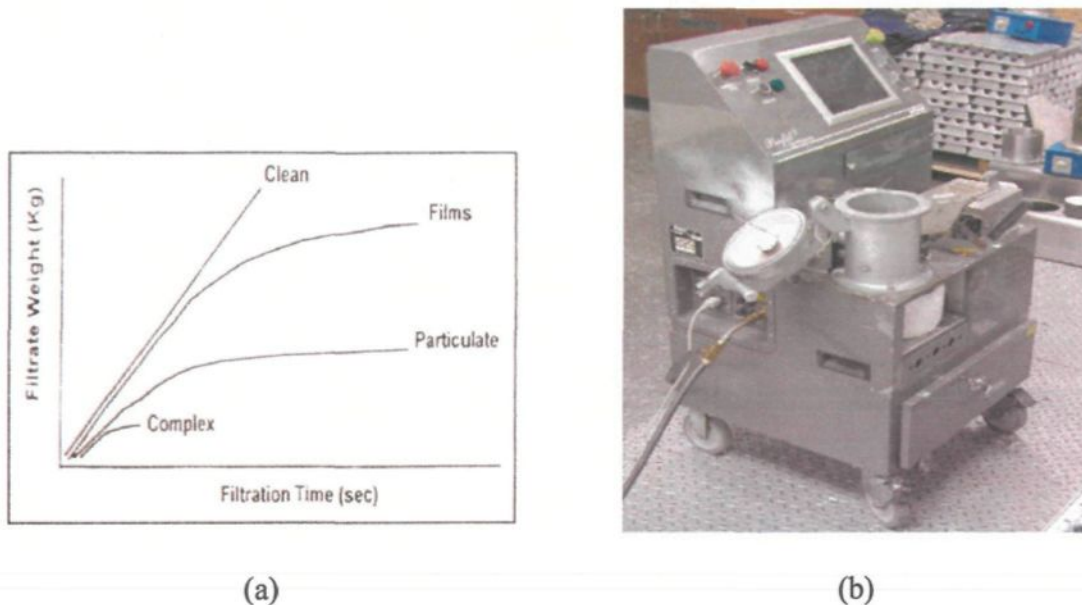


Figure 2.15 (a) Schematic diagram showing filtration behavior of aluminum alloy containing different types of inclusions;⁴⁰ (b) the Prefil apparatus.

The process concentrates the inclusions by about 5,000 to 10,000 times, which results in total inclusion contents between $0.005 \text{ mm}^2/\text{Kg}$ (very clean) and $50 \text{ mm}^2/\text{Kg}$ (very dirty). Quantitative metallography of pressure filtration residues is used in conjunction with existing in-house quality criteria to establish the relevant footprint. This correlation of inclusion contents with the shape of the filtration weight vs. time curves provides results that enable one to obtain immediate information on the quality of molten metal on a day-to-day basis without the need for continuous metallographic analysis.^{8, 40, 41, 42}

2.7.3 LAIS Technique

This is one of the pressure filtration techniques used for the measurement of inclusions. In the LAIS (Liquid Aluminum Inclusion Sampling) technique, the filtration rate is recorded during a standardized pressure filtration test, and it is compared with

preprogrammed information. Essentially, melts which are heavily contaminated will have a lower flow rate through the filter vs. a clean melt which will flow through the filter with much less resistance. LAIS is similar to PoDFA except that the sample is obtained inside the melt. After preheating the sampling device and using vacuum pressure, the resulting sample is metallographically analyzed. Figure 2.16 shows a schematic of the LAIS equipment during operation.

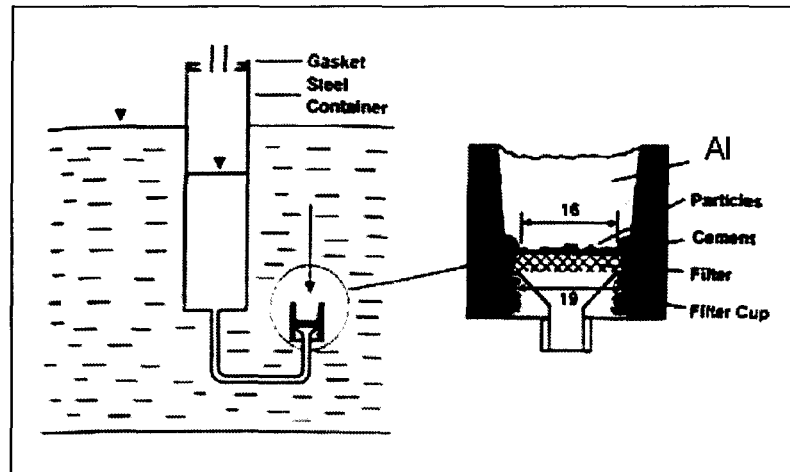


Figure 2.16 Close-up of the LAIS during operation.⁴¹

In this method, the metal is sucked through a filter and into a canister by means of low pressure or a vacuum behind the filter. Similar to the PoDFA, the inclusions are retained inside the filter or on the top of the filter, depending on the size and shape of the filter pores or openings and on the number and size distribution of inclusions. The entire sampler unit is immersed in the bulk melt, completely eliminating the need for ladling or remelting.⁴² The sampler is positioned inside the melt, so that the filter cup inlet is 20-25

cm below the melt surface. Upon immersion, a stopper rod placed in the tapered filter cup effectively prevents surface debris or dross from entering inside. After a few minutes of preheating, sampling is commenced by turning on the vacuum pump and removing the stopper rod. The liquid metal is sucked through the sintered stainless steel filter into the holding sample (up to 1.9 Kg of metal).

When the sample has cooled, the filter cup is cut off from the sampler and the contents are pressed out. The contents of the filter cup are then sectioned parallel to the flow direction and subsequently prepared for metallographic examination. The filtered metal in the canister is also removed and weighed.^{10, 41, 42, 43}

2.7.4 Ultrasonic Technique

This technique is based on the principle of sound pulse dissipation. For inclusion measurements, a transmitter sends a signal from a piezoelectric crystal through the molten metal. When the signal passes through the melt, some amount of its energy is reflected by inclusions. The reflection results in the reduction of the signal's energy. The reduced signals are collected by a receiver and displayed on an oscilloscope.

These signals give an indication of the content and size of inclusions. With the ultrasonic technique, both non-metallic and metallic inclusions can be detected. Figure 2.17 shows a schematic diagram of the ultrasonic technique with auxiliary equipment. This method is well suited to on-line inspection of running aluminum alloy strips over the whole length and width. However, the instrument uses a two-probe sender/receiver unit and requires external calibration before each use. Extensive sampling in conjunction with

the PoDFA technique showed that extremely clean metal could be distinguished from extremely dirty metal, but that the resolution at intermediate cleanliness levels was limited. This technique is unable to provide particle size distribution of inclusions and can only detect inclusions with sizes greater than $100\ \mu\text{m}$.^{10,23,45}

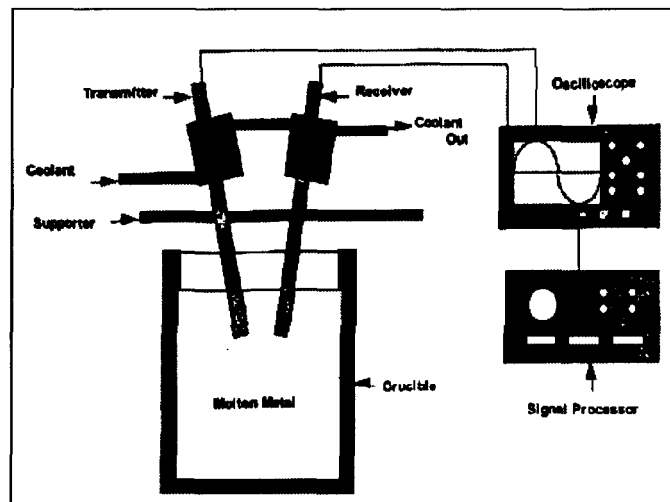


Figure 2.17 Schematic diagram of the ultrasonic technique with auxiliary equipment.⁴⁵

2.7.5 Reduced Pressure Test

The reduced pressure test is a common test, widely employed in foundries to evaluate the quality of molten aluminum alloys. The reduced pressure encourages pore and gas bubble formation during solidification, and the size of the porosity formed in the samples is magnified significantly, allowing the effects of pore nucleation and growth to be easily seen. Thus, the reduced pressure test is a useful tool in the investigation of pore formation and its related influences.

The formation of porosity during solidification is also affected by cleanliness of the melt. It has been demonstrated that, under the same casting conditions, *i.e.* the same hydrogen level and solidification rate, dirtier melts tend to generate more porosity than cleaner ones.⁴⁶

2.7.6 Other Detection Methods

Various other techniques exist for the detection of inclusions in molten metal. Acoustic techniques use transducers and receivers for molten metal applications based on signal-noise and pulse-echo principles.^{12, 47} Chemical methods include electrochemical dissolution involving the extraction of non-metallic inclusions by dissolving the aluminum matrix, and chemical analysis.¹² The eddy current method, electromagnetic detection and X-ray detection methods are example of electromagnetic-based methods.

In the eddy current method, the applied eddy current produces magnetic fields in the melt and makes it possible to determine the distribution and detection of slag in molten flows through insulating tubes.¹² The electromagnetic detection technique involves the use of the electromagnetic forces to move inclusions to an inspection location, followed by an optical image measurement to detect inclusions visually. While this technique has a better resolution performance compared to other on-line methods, it is expensive in its construction.¹²

In the X-ray detection technique, the metal sample is raised in an induction crucible. Due to the effect of the electromagnetic force, non-metallic inclusions move to

the outer periphery of the sample. The metal sample is cooled and moved to an analyzing position in an X-ray fluorescence analyzer to detect non-metallic inclusions.⁴⁷

2.8 THE LiMCA TECHNIQUE

The LiMCA (Liquid Metal Cleanliness Analyzer) is a non-destructive technique based on the electrical resistive pulse or electric sensing zone (ESZ) principle. This method allows for measurement of inclusions in terms of their number and volume fraction in the melt, together with their size distribution, where these measurements can be made available on-line very quickly, at time intervals on the order of one minute. This enables the LiMCA to monitor quasicontinuously and in real time the evolution of cleanliness along a cast, either as a function of process parameters or only as a function of time. Using this technique, inclusions as small as 20 μm can be detected. The LiMCA analyzer is simple to operate, compact and suited to on-line monitoring of molten aluminum alloys.

2.8.1 Description of LiMCA

The LiMCA system is designed to measure the concentration and size distribution of non-conductive particles suspended in molten aluminum. The LiMCA unit consists of a probe, a current source and a signal processing system as shown in the schematic diagram of Figure 2.18. The probe consists of two electrodes and a sampling tube made of non-conducting material (alumina silicate), having a small orifice (about 300 μm) near its bottom. The tube is immersed in liquid metal, and by applying vacuum or pressure, the liquid metal can be made to flow into or out of the tube through the orifice. A constant electric current is applied between the electrodes, which circulates through the orifice

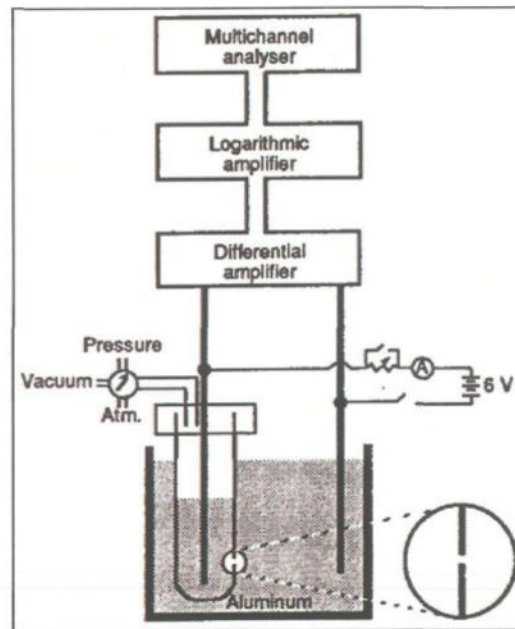


Figure 2.18 Schematic diagram of the LiMCA operation.⁴⁸

where it is carried by incoming liquid metal. The presence of particles in the liquid flow modifies the electrical resistance detected at the orifice. The change in resistance causes a voltage pulse of duration approximately equal to the transit time it takes the particles to appear across the orifice. The voltage drop across the orifice is monitored. The signal processing system translates the voltage fluctuations and the distribution of their amplitudes to particles, and the volume distribution of these particles is expressed in the form of histograms, showing the particle density per particle size interval.

Figure 2.19 shows the complete LiMCA system which consists of a head, a flexible hinged neck, and a main body. The main body interconnects to a microcomputer which serves as the control station.



Figure 2.19 The complete LiMCA system.⁴⁹

The LiMCA analyzer provides continuous on-line measurements of the number of inclusions (expressed in thousands per kilogram, “K/Kg”) in the 20 to 300 μm diameter range. This data can be analyzed as total counts combined with the size distribution of the inclusions comprised within the total. In addition, the qualitative information concerning the nature and species of the inclusions is very valuable in the study and understanding of their sources. The impact of furnace preparation, alloying practice, feed stock mix, settling time, and similar parameters on melt cleanliness can be determined, allowing the development of process practices and procedures to minimize or eliminate their occurrence.⁴⁹

The continuous, full batch analysis of the inclusion number density provided by the LiMCA, used together with data obtained from the PoDFA technique (which provides a qualitative assessment of inclusions) has yielded an in-depth understanding of the nature and behavior of the process dynamics of metal treatment, filtration and molten metal.^{49, 50}

2.8.2 LiMCA Operating Principles

The LiMCA technique is based on the electric sensing zone (ESZ) principle, in which a constant current is maintained between two immersed electrodes that are separated by an insulating sampling tube. The tube contains a small orifice through which the molten aluminum is drawn in. A pneumatic system creates a difference in pressure between the inside and the outside of the tube to force in liquid metal through the orifice, while measuring the electrical current between the electrodes. The sensitive electrode system measures the small voltage variation at the electrodes caused by the passage of suspended particles through the orifice in the tube. A constant current is maintained through the orifice with a DC power supply and two types of electrodes - one type situated inside and the other two outside the insulating tube in the surrounding melt.

The presence of a particle in the liquid flowing through the orifice affects the electrical resistance detected at the orifice. In fact, when a particle enters the orifice, it displaces the volume of the conducting fluid. This causes a temporary rise in the electrical resistance of the orifice. This resistance changes in the presence of an applied current, causing a voltage pulse of a duration approximately equal to the transit of the particle across the orifice.

The electrical potential produced by the constant current varies in relation to the change in resistance each time a particle goes through the orifice. The pulse magnitude detects a particle in suspension that is larger than a predetermined size (20 μm), and whose electrical current is different from that of the molten metal. A difference in voltage due to the passage of particles takes the form of pulses on the reference line. The reference line corresponds to the voltage created by the constant current going through the circuit (consisting of the electrodes and the liquid metal) when no inclusions are present.

The amplitude varies from only 10 μV up to 2000 μV , making highly-sensitive measuring equipment mandatory. A signal-processing program is used to calculate the inclusion particle density and size distribution from the number of pulses over a measured time and by measuring their amplitudes. The resulting inclusion measurement is expressed as a volumic concentration in parts per million (ppm) or parts per billion (ppb). A schematic representation of the ESZ principle is shown in Figure 2.20 for a spherical particle passing through the ESZ along the center axis of the orifice.⁵¹

The transient change in resistance, ΔR_{AB} , caused by the introduction of a small non-conducting particle into an orifice is represented as:

$$\Delta R_{AB} = \frac{4 \rho_e d^3}{\pi D^4} \quad (1)$$

where ρ_e is the electrical resistivity of the liquid, and d and D are the respective diameters of the particle and the orifice.

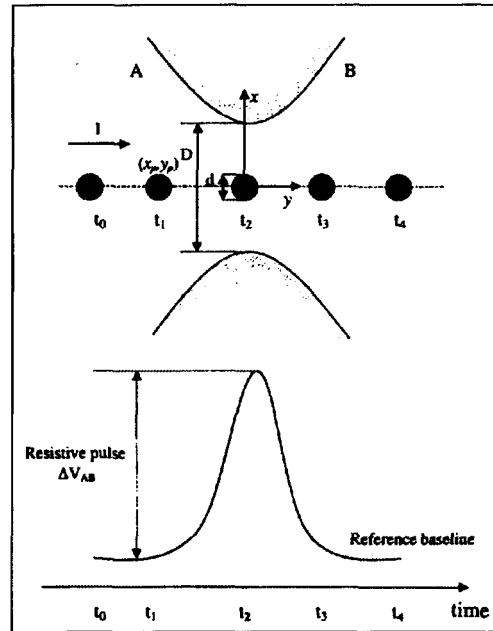


Figure 2.20 Schematic representation of the ESZ principle for particle size measurement.⁵¹

By applying an electric current I , the transient pulse voltage can be expressed as:

$$\Delta V_{AB} = \frac{4\rho_e I d^3}{\pi D^4} \quad (2)$$

If d is less than D , ΔR_{AB} is increased through the distortion of the electric field flowing around the spherical inclusion and needs to be modified by a factor $f(d/D)$, as shown in the following equation:

$$\Delta V_{AB} = \frac{4\rho_e I d^3}{\pi D^4} f(d/D) \quad (3)$$

where $f(d/D)$ is a correction factor obtained from an analysis of a sphere in a circular tube.

According to Equation (3), every particle registers a pulse when passing through the ESZ orifice and, depending upon its size, gives rise to a specific voltage pulse. The number of pulses observed over a period of time thus provides information on the density

of non-conductive inclusions in the metal. Consequently, an inclusion size distribution can be calculated from the amplitude distribution of successive pulses.⁵¹ Experimentally and theoretically, it has been proven that inclusions of different density could be discriminated on the basis of differently shaped voltage transients generated during their passage through the electric sensing zone.⁵²

LiMCA results are expressed as a number concentration N_{20} (number of inclusions larger than a selected diameter value) in thousands per kilogram of metal, *e.g.*, 5.0 k/kg, or as a volumetric concentration C_{20} (volume concentration of inclusions larger than a selected diameter value), *e.g.*, 0.05 ppm. Due to the complexity of the particle size distribution in aluminum melts, it has not been shown that these units can be generally converted from one to the other.^{48, 50}

The data is displayed on the computer screen in real time in the form of a graph plotting. Figure 2.21 shows an example of the total inclusion content as a function of time, while Figure 2.22 shows the total inclusions as a function of particle size.

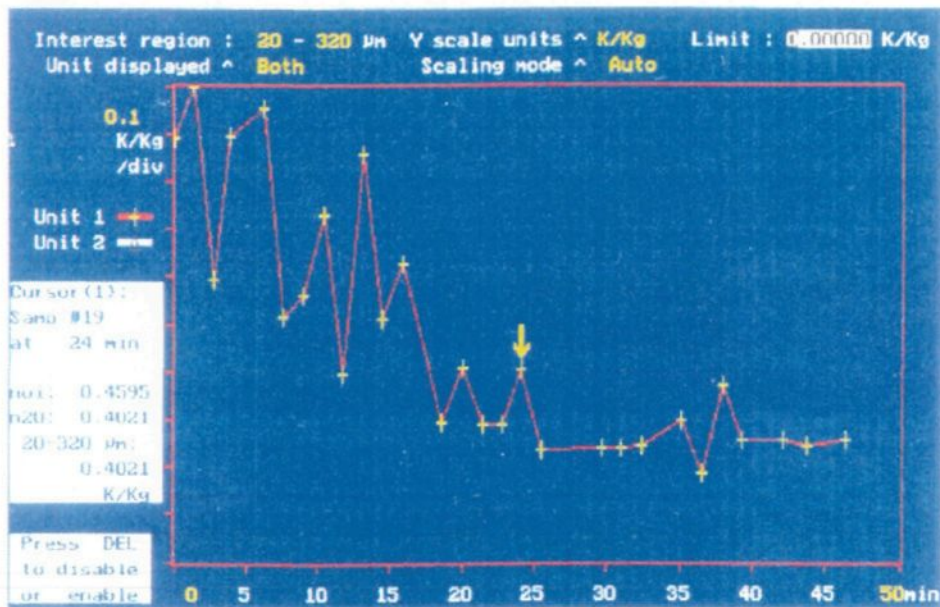


Figure 2.21 Computer screen showing evolution of metal cleanliness as a function of time during a LiMCA operation.⁴⁹

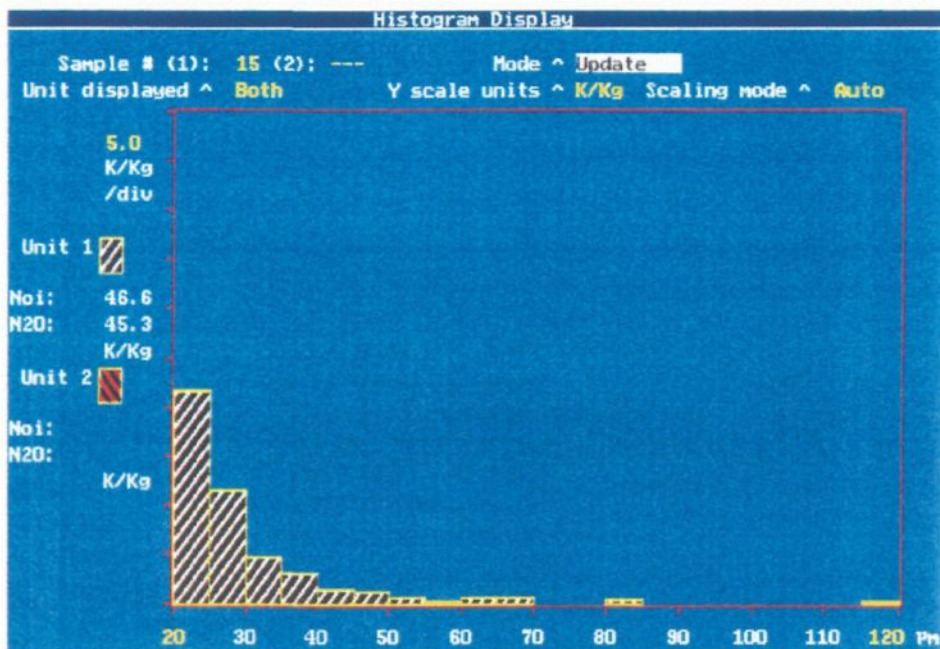


Figure 2.22 Histogram display of inclusion measurement in terms of inclusion particle size distribution.⁴⁹

2.8.3 Metallurgical Application of the LiMCA System

Over the last decade, the LiMCA system has been successfully applied in the aluminum industry in terms of process understanding, control and optimization, and has generated numerous results that were previously unattainable. Typical examples include evaluation of the impact of various alloying methods on metal cleanliness, optimization of settling times during furnace preparations for direct chill (DC) casting machines, and evaluation of inclusion removal performance of commercial filters and degassers.⁵³ Monitoring the inclusion level in liquid aluminum flowing through launders to direct chill casting operations following scrap recycling, melting, alloying, refining (chlorination), settling, degassing and metal filtration operations has demonstrated the critical need for proper metal flow control during casting operations.

In addition to liquid aluminum, LiMCA technology has been developed for molten magnesium, copper and steel.⁵³ Other metallurgical aspects of molten metal investigated using the LiMCA system include the study of settling phenomena in the holding furnace, analysis of the dynamic process of liquid metal filtration, studies on the grain refinement mechanism of TiB_2 , and melt cleanliness measurements in the tundish.⁵³

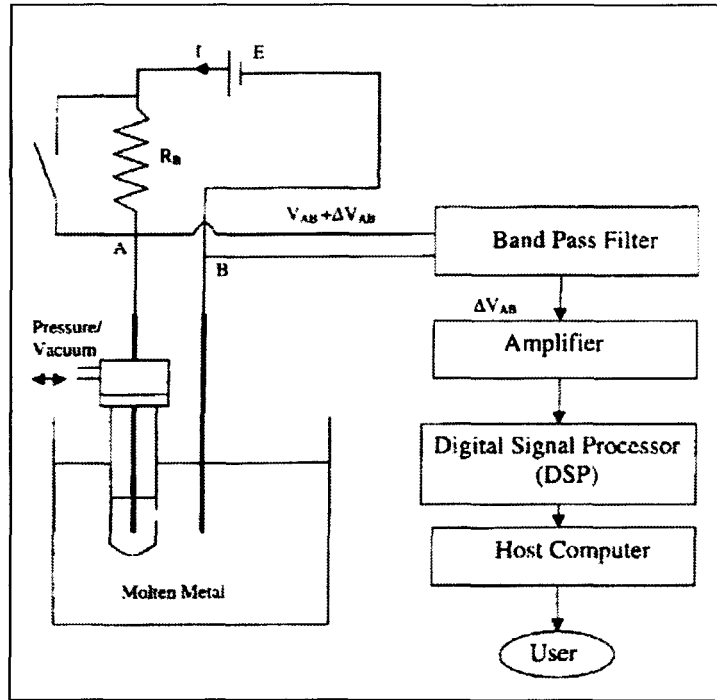
2.8.4 Particle Discrimination in the LiMCA System

Inclusion particles of different types affect the properties of materials differently. Therefore, the ability to discriminate particles is a valuable feature for an on-line inclusion detection system. According to the ESZ principle, every particle generates a voltage pulse when passing through an ESZ area, where non-conducting particles of the same size but

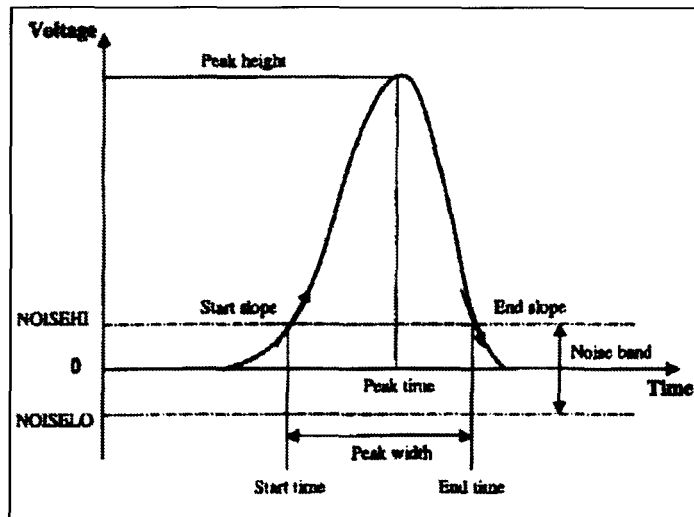
different types give rise to voltage pulses of the same magnitude. This would appear to preclude distinction between hard deleterious solid particles and harmless microbubbles or liquid droplets. For example, microbubbles and microdroplets of salt are often counted by the LiMCA system as inclusions, leading to an overestimation in the number of potentially harmful solid inclusions within the melt.

With the use of digital signal processing (DSP) technology, however, particle discrimination in the LiMCA system can be made feasible, as more information can be extracted from the particle signals measured besides the pulse height. Theoretically and experimentally, inclusions of different densities can be distinguished on the basis of differently shaped voltage transients generated during their passage through the electric sensing zone. Figure 2.23 (a) shows a schematic configuration of the DSP-based LiMCA system, while Figure 2.23 (b) shows how each pulse is characterized by seven parameters (*start slope, end slope, time to reach the maximum voltage, total signal duration, start time and end time of each pulse, and peak height*).^{51, 52, 54, 55}

All these parameters are dependent on the two noise thresholds NOISEHI (high) and NOISELO (low) which mark the margins of the signal's noise band. The noise band reflects the operational conditions and determines the minimum size of the particles that the system can detect under such conditions. From Figure 2.23 (b) it is observed that the particle transient time flowing through the ESZ in the LiMCA system is not the time the particle takes to traverse the physical length of the ESZ, but rather the time it takes to pass through the region where the pulse height generated by the particle is higher than the threshold value.



(a)

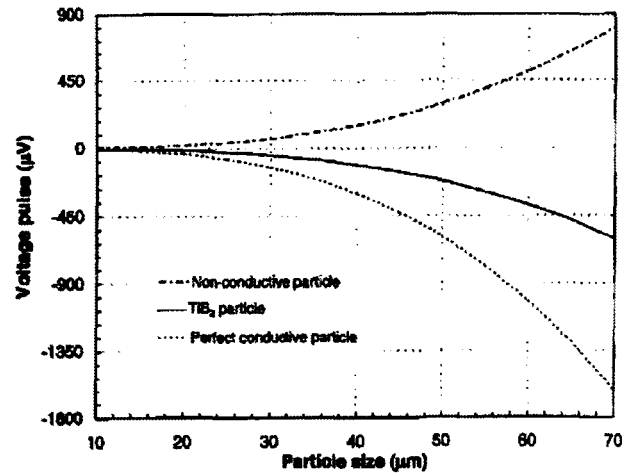


(b)

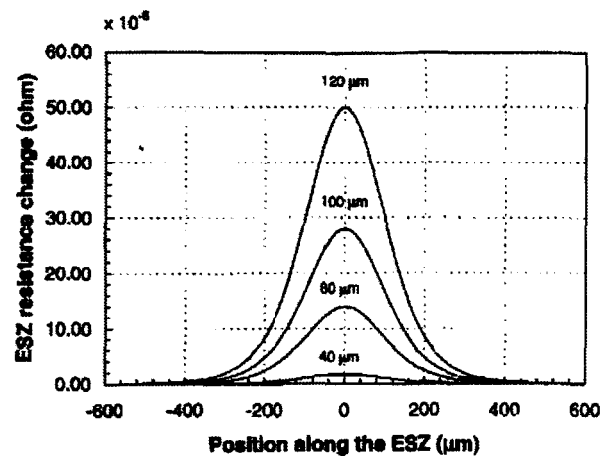
Figure 2.23 (a) Schematic configuration of the DSP-based LiMCA system, and (b) the seven peak parameters generated by DSP.⁵³

The LiMCA system can discriminate inclusions based on inclusion density and conductivity. Conducting and non-conducting inclusions can be readily discriminated from each other as they generate negative and positive peak signals, respectively. The magnitudes of the signals are different for particles of the same size but of different conductivity. Figure 2.24 (a) shows a plot of voltage pulse as a function of particle diameter obtained from LiMCA measurements in molten aluminum under typical operating conditions for non-conducting, perfectly conducting and equivalent-to-TiB₂ type conducting particles. It can be seen that the amplitude of the signals caused by perfectly conducting particles is twice that for non-conducting particles of the same size, while the amplitude for TiB₂ particles is only three fourths that of non-conducting particles of the same size.⁵³

Figure 2.24 (b) shows the variation in ESZ resistance as particles of different diameter pass through the orifice of 300 μm in molten aluminum under typical operating conditions. Large particles reach the noise threshold resistance farther away from the orifice center than do smaller particles. Thus, smaller particles travel shorter distances for transient times measured by the LiMCA system.



(a)



(b)

Figure 2.24 (a) The voltage pulse as a function of particle diameter, and (b) ESZ resistance change with the position of non-conducting particles of various diameters in molten aluminum in the LiMCA system.⁵²

Experimental data and mathematical calculations have shown that bubbles have shorter transient times than solid particles of the same size, which can be explained by the different relative velocities developed when they move through the ESZ. Bubbles created

by the fluid flow travel faster than the particles, which are slightly denser than the fluid, causing them to lag behind when traveling within the ESZ. Also, larger particles have longer transient times than smaller ones of the same density.

It is also found that the difference in transient times for bubbles and particles becomes more significant as particle size increases, improving the discrimination between particles of different densities. Besides the transient time, the pulse shape is also characteristic of different particles in the LiMCA system.^{53, 56}

2.8.5 Error Analysis of LiMCA Data

The efficiency of LiMCA measurements are often presented without any error estimates. In some cases, the choice of size classes (size distributions), voltage and current noise introduces uncertainties. During a LiMCA measurement, when the liquid metal is flowing through the probe orifice, all non-conducting particles between 20 and 300 μm are counted. This counting process may be described by a classical one-dimensional Poisson distribution process, if we assume that the occurrence of particles is independent.

Due to the Poisson distribution process for inclusion counting, the counted numbers themselves introduce uncertainties in the measurements, both for the number size distributions (N_{20} measurements) and the time variation of the volume fraction (C_{20}) measurements.

LiMCA measurements have been analyzed in terms of the variance in the particle size range distributions measured, the applied voltage and the signal noise of the apparatus to provide error estimates for the LiMCA data measured.⁵⁷

2.8.6 Advantages of LiMCA

The on-line monitoring capability of LiMCA for inclusion detection (*i.e.*, melt cleanliness) provides a technique that is rapid, quantitative and extremely sensitive. In comparison, other methods are off-line and thus time consuming and less effective. The LiMCA apparatus is simple to operate, tightly integrated and provides continued on-line measurement of the inclusion numbers and full analysis of the inclusion number density.

As mentioned previously, the LiMCA is useful in several metallurgical applications including optimization of settling times during furnace preparation for direct chill (DC) casting machines, evaluation of inclusion removal performance of commercial filters and degassers, and monitoring of inclusion levels in liquid aluminum. However, due to the size of the orifice, there is a limitation in detecting inclusions less than 20 μm . Also, in the case of very dirty metal, the orifice can become easily blocked by big particles, interrupting measurement and leading to false inclusion counts. In terms of cost as well, the LiMCA is an expensive instrument and requires careful maintenance.

CHAPTER 3
EXPERIMENTAL PROCEDURES

CHAPTER 3

EXPERIMENTAL PROCEDURES

In keeping with the objectives of this study, inclusions were added to commercially pure aluminum and Al-6%Si alloys in varying amounts, using both master alloys and powder injection to introduce the inclusion particles into the melt. LiMCA measurements were carried out for each melt condition using a LiMCA II machine, and corresponding samplings for chemical analysis and microstructural analysis (where about 100g of molten metal was solidified in a small metallic sampling cup) were also taken. Metallographic samples were prepared from the latter casting and from the solidified metal in the LiMCA test probe used for the measurement, to obtain a qualitative analysis of the inclusion types and levels corresponding to each melt condition. Details of the experimental procedures that were followed are provided in the following sections.

3.1 MATERIALS AND ALLOY PREPARATION

Commercial pure aluminum (99.78% purity) and experimental Al-6%Si alloy were used in the present work. Various inclusion additions were made to their melts as follows.

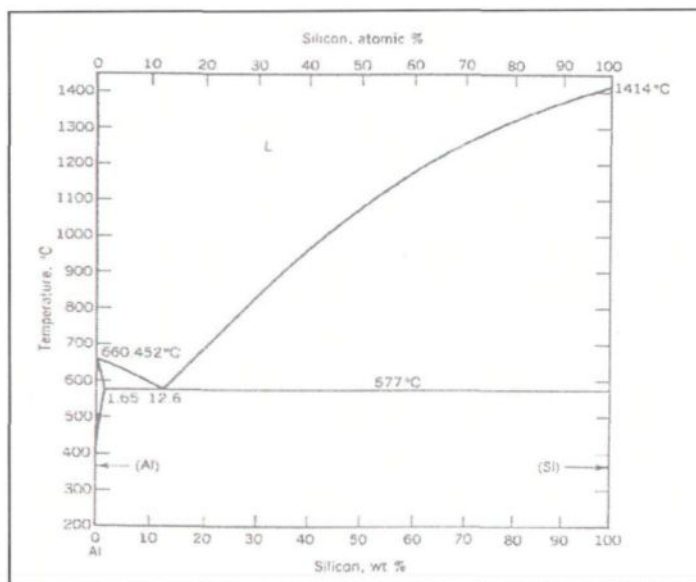
- Inclusions of Al_4C_3 , TiB_2 , CaO and MgO were added in the form of powder.

- Inclusions of Al_2O_3 were added in the form of an Al- Al_2O_3 metal matrix composite alloy.
- Magnesium was added as pure metal.
- Inclusions of TiAl_3 added in the form of Al-10%Ti master alloy.
- In addition to the powder form, TiB_2 was also added in the form of Al-5%Ti-1%B master alloy.

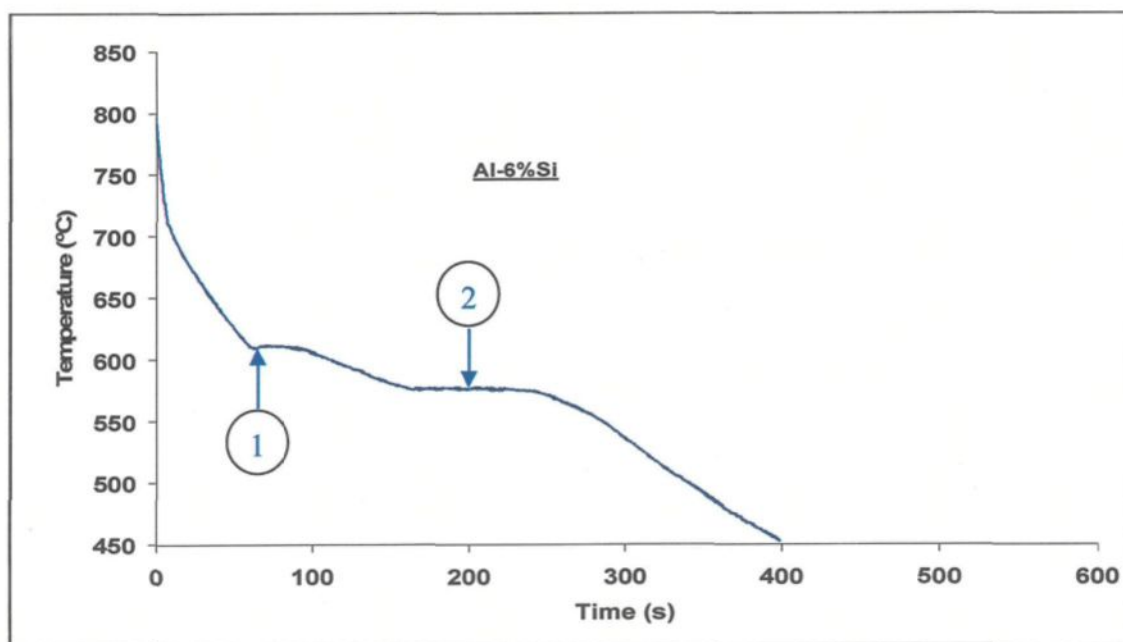
3.1.1 Preparation of Experimental Al-6%Si Alloy

Ingots of commercial pure aluminum were cut, cleaned, dried and melted in a 300 lb SiC crucible, using an electric resistance furnace. The temperature was kept at $750^\circ\text{C} \pm 5^\circ\text{C}$. A calculated amount of pure silicon was added to the melt to obtain an Al-6% Si alloy composition. The melt was held for two to three hours to ensure the complete mixing of silicon in the melt and then stirred for about 30 min. The melt was poured into ingot molds and a sampling for chemical analysis was also taken simultaneously. The Al-6%Si ingots thus prepared were kept aside for use in further experiments.

Figure 3.1 shows (a) the binary phase diagram of the Al-Si system and (b) the cooling curve of the experimental Al-6%Si alloy obtained from thermal analysis, showing the start of solidification of the α -Al dendritic network (1) and the Al-Si eutectic reaction plateau (2). Thermal analysis is a well-known technique for determining the reactions that take place during the solidification of an alloy. The first derivative of the cooling curve is also calculated from the obtained temperature-time data and provides peaks corresponding to (and hence precise information about) these reactions.



(a)



(b)

Figure 3.1 (a) Binary phase diagram of the Al-Si system,⁵⁸ and (b) cooling curve of experimental Al-6%Si alloy used in the present work.

3.1.2 Preparation of Inclusion-Containing Ingots of Al and Al-6%Si Alloys

In most cases, addition of inclusions to the two alloys was carried out using a powder injection technique.⁵⁹ The powder injection apparatus fabricated in-house at UQAC has been used successfully to introduce powder inclusion particles into aluminum alloys. In this technique, a sufficient quantity of solid particles (powder) is heated in an inert argon atmosphere for a sufficient amount of time and then blown in a continuous stream into the melt by means of the inert carrier gas.

The gas bubbles are continuously broken with the help of a rotating impeller. As the solid particles pass through the melt, buoyant forces slow down the gas bubbles without affecting the velocity of the particles. When the solid particles contact the gas-liquid interface, larger particles with sufficient kinetic energy are able to penetrate the interface and enter the melt, whereas smaller particles cannot penetrate the barriers and are carried to the surface of the melt.

After powder injection is completed, the melt is poured into ingot molds, and the ingots kept aside for use in subsequent experiments. In this manner, three ingots were prepared for each type of powder addition, for each of the two alloys used (pure Al and Al-6% Si). In the case of Al_2O_3 inclusions, addition of inclusions was carried out by direct addition of Al_2O_3 in the form of an Al- Al_2O_3 metal matrix composite alloy to the melt.

3.2 INCLUSION ADDITION

As mentioned previously, various inclusions were added to the two alloys used in this study. Those that were added in the form of powders were introduced into the alloy melts using the powder injection technique.⁵⁹ Details of this technique and the procedure employed are provided below.

3.2.1 Injection Technique

A schematic diagram of the powder injection system is shown in Figure 3.2, which comprises (a) a fluidizer tube, (b) a carrier tube and a quartz nozzle, (c) resistance heating coils, (d) an adjustable two-dimensional movable stand, (e) a melting unit with resistance heating, (f) an impeller (stirrer) with adjustable rotation speed, and (g) flow diversion baffles.

The fluidizer unit is a cylindrical quartz tube (45 mm diameter x 300 mm height), heated by means of electric resistance coils. It has a gas inlet system on one side and a conical outlet fitted to the carrier tube on the other side. The carrier tube, which is also heated by electric resistance coils to compensate for the heat loss during blowing, converges uniformly into an immersion nozzle of 2 mm diameter.

The impeller system is comprised of an alumina-coated stainless steel tube with three blades (60 mm diameter) inclined at an angle of 45° to the stock. The impeller system is fitted to the argon cylinder outlet so that it can be used as a degassing system before the injection stage. The injecting part of the system is mounted on a two-dimensional movable stand so that the nozzle position can be adjusted accordingly.

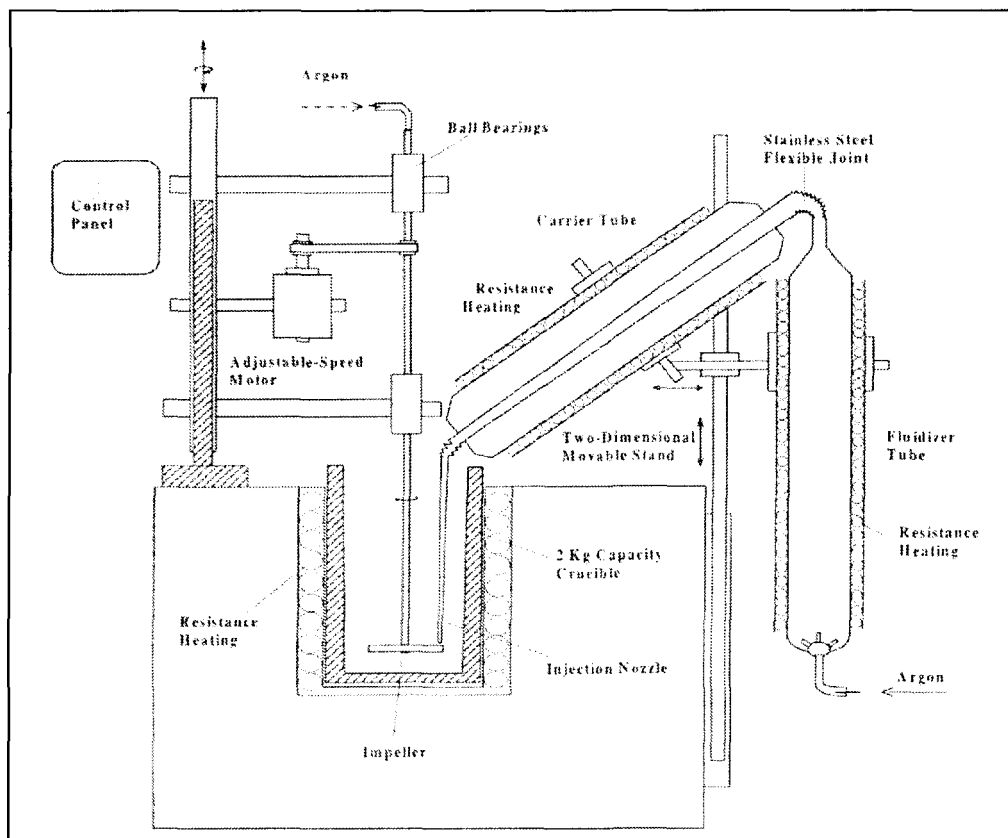


Figure 3.2 Schematic of the powder injection system.⁶⁰

3.2.2 Injection Procedure

Individual powder injections were made to 2-kg melts of pure aluminum (or Al-6% Si alloy), using the powder injection apparatus shown in Figure 3.3. A measured amount of powder, placed in the fluidizer tube (section A), was heated for about two hours at 400°C prior to injection, to remove any humidity. During preheating, a slow stream of argon was passed through the powder bed, at a flow rate that would not lift the powder out of the fluidizer tube. The argon flow also helps in breaking up any clustering or agglomeration of the powder particles.

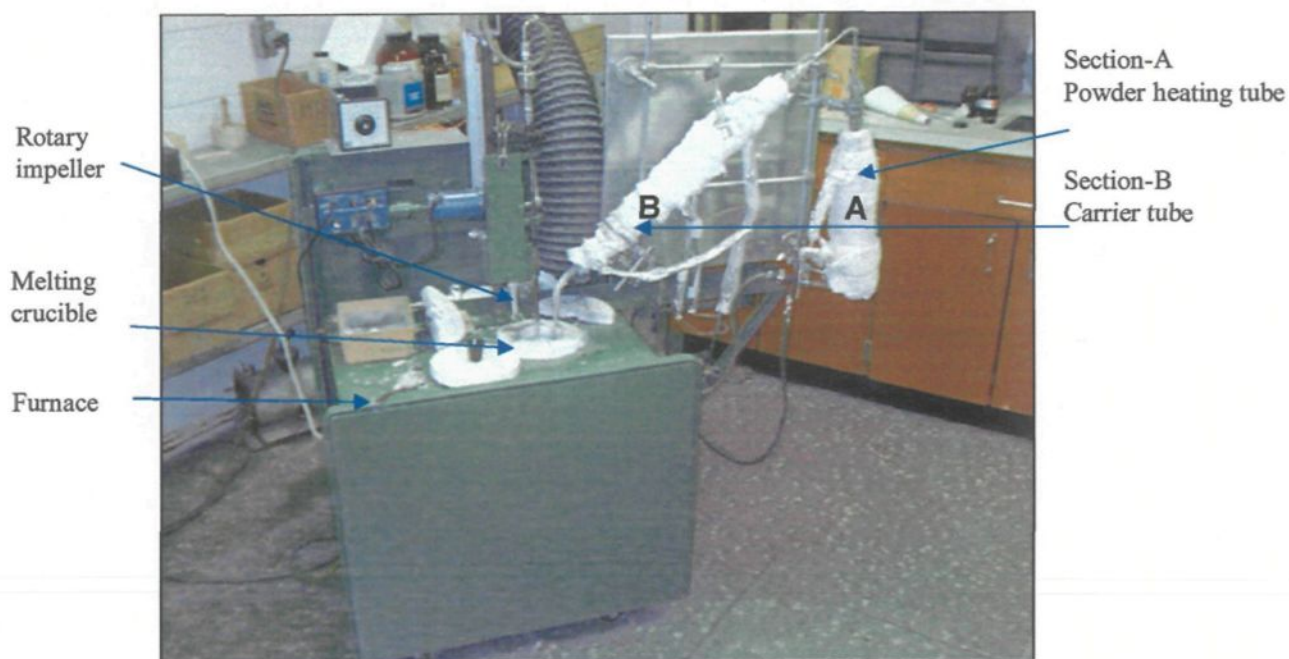


Figure 3.3 The powder injection apparatus during operation.

The melting (pure Al or Al-6%Si alloy) was carried out using an electric resistance furnace in 2-kg silicon carbide crucibles. The temperature of the melt was kept at about 750°C. Once the melt reached this temperature, the impeller was lowered into the melt and the flow of argon started. Degassing was carried out prior to injection by using pure, dry argon for about 15 min, following which skimming of the surface dross was done.

When the melt was ready, the flow of argon was disconnected from the impeller side and connected to the injection system side. The flow rate of argon gas was increased to 15-30 ft³/hr, depending on the type and size of the inclusion particles introduced. The nozzle was then immersed in the melt.

The position of the submerged nozzle in the melt is very crucial for efficient recovery of the particles: while blowing, gas bubbles carrying the inclusions must be

delivered directly onto the blades of the impeller. The direction of rotation is kept such that the impeller forces the metal down. The bubbles must remain as long as possible in the melt to increase the probability of powder transfer. In this regard, three factors must be taken into account:

- i) *The bubble size*: the smaller the bubble size the slower it travels through the melt before it escapes to the atmosphere. The impeller rotation speed has a large effect on reducing the size of bubbles liberated after breaking.
- ii) *The position of the nozzle in the melt*: the nozzle is placed in the middle between the wall and the center of the crucible in order to provide the bubbles with a long helical path to the melt surface and, consequently, increase their residence time in the melt.
- iii) *The direction of rotation of the impeller*: It is always kept such that the impeller pushes the metal down. As a result, the liquid streams carry the bubbles to levels lower than the nozzle position, lengthening their travel path to the atmosphere.

The injection is done using a flow of argon gas from the bottom of the fluidizer tube (section A) and through the carrier tube (section B), with a flow rate of 15-30 ft³/hr. During the injection, the impeller is rotated slowly, at a speed of 8 rpm, to stir the melt and allow the incorporation of more powder particles into the melt. Normally, injection is continued for approximately 2 h to ensure adequate introduction of the inclusion particles into the melt, while stirring is continued 5 min after the injection to ensure proper mixing.

3.3 MELTING PROCEDURES FOR CONDUCTING LiMCA TESTS

Ingots of pure aluminum (or Al-6%Si alloy) were melted in a 30-kg capacity SiC crucible in which the LiMCA tests were to be conducted. The melting temperature was kept at $700^{\circ}\text{C} \pm 5^{\circ}\text{C}$. Before inclusion addition, the melt was degassed for 15 min using pure, dry argon.

A specified powder-containing ingot resulting from the injection procedure was added to the pure Al (or Al-6%Si alloy) melt. It should be mentioned here that for the pure Al melts, the powder-containing ingots prepared from pure Al were used. Similarly, for the Al-6% Si melts, the powder-containing ingots prepared from Al-6% Si alloy were used. After each addition, once the melt temperature reached the specified value, the melt was stirred for 5 min using the rotary impeller (without argon flow), followed by a LiMCA test.

From the same melt, a sampling for microstructural analysis was also taken, before and after each LiMCA test, for qualitative inclusion analysis. In this manner, LiMCA tests were carried out for each of the Al_4C_3 , TiB_2 , CaO , MgO and Al_2O_3 inclusion additions (at three different concentrations of each) to the pure Al and Al-6%Si alloy melts, and the corresponding samples for microstructural analysis obtained.

As will be described in section 3.5, samples for metallographic examination were also obtained from the solidified metal in the LiMCA probe tube used for the corresponding LiMCA test/sampling.

3.4 LiMCA TESTING

The LiMCA measurements in the present study were carried out using a LiMCA II machine. The sections below provide information with respect to this version of the LiMCA.

3.4.1 Start-Up Procedures

Pure argon (at a pressure of 60-100 psi) is connected to the instrument, in order to keep the probe tube (made of alumina silicate material) in position within the rubber seal assembly inside the head section over the central electrode. The tube probe is just used once, and after each interruption in the test, is replaced. A flow of dry air is used to cool the LiMCA system, at a recommended pressure of 70-125 psi. The schematic diagram of Figure 3.4 shows the flow of air inside the main body of the LiMCA system during cooling.

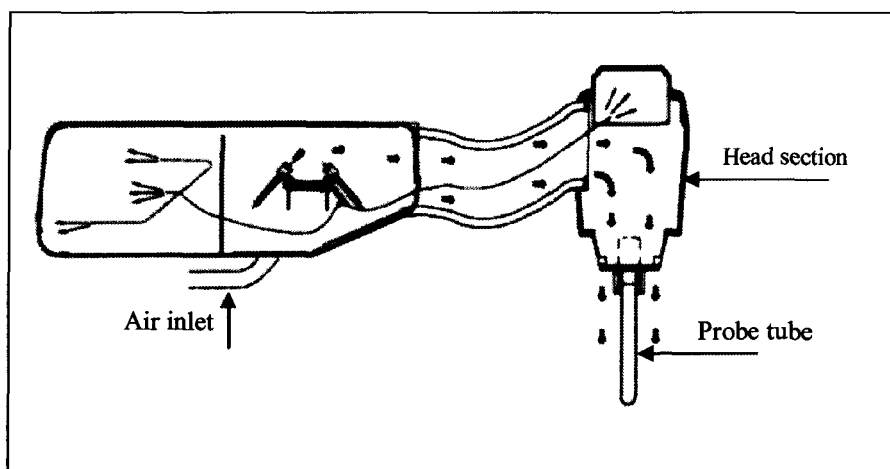
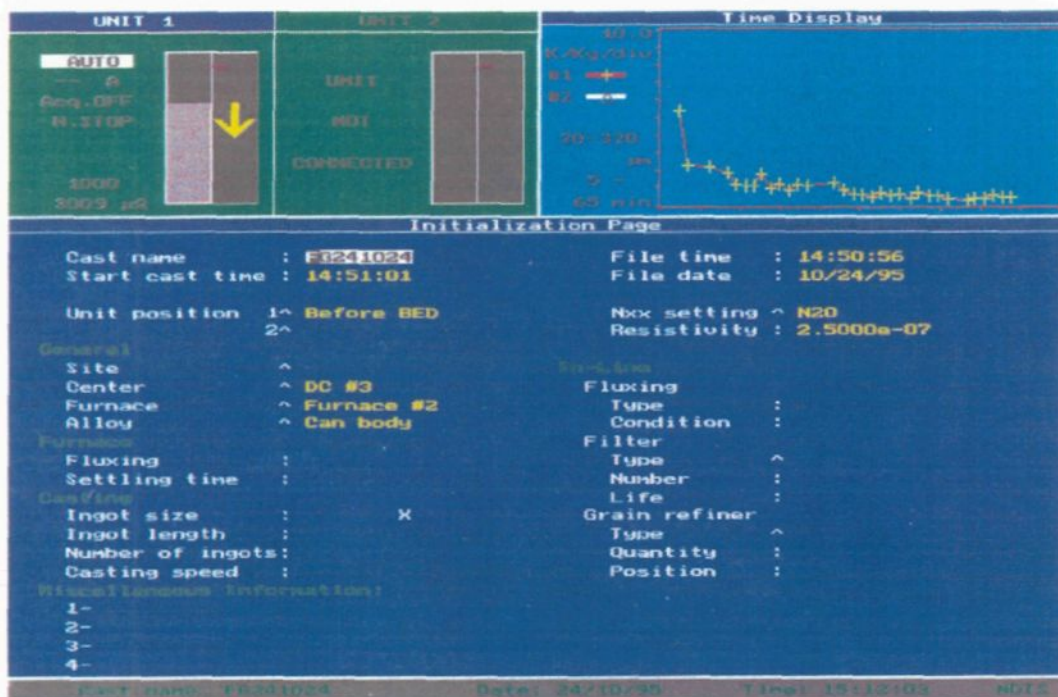


Figure 3.4 Cooling system inside the main body of the LiMCA.⁴⁹

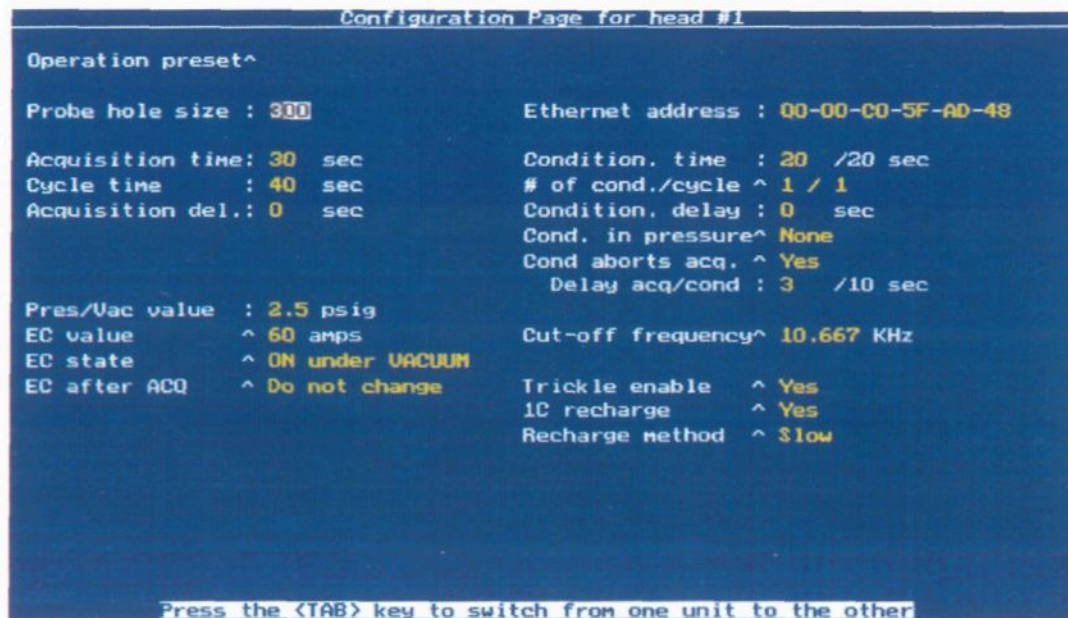
A microcomputer connected to the machine provides specifications including cast name and time, probe (tube) hole size, acquisition time, cycle time, pressure and vacuum values, and condition time on its main screen menu and initiation and configuration pages. Figure 3.5 exhibits the corresponding set-up, while Figure 3.6 shows an example of the main menu and the configuration pages displayed during a LiMCA test. In Figure 3.6 (a), the area in the top-left corner of the screen shows the *permanent status* of the estimated level of the liquid metal in the probe with time and, adjacent to it, the direction of the metal flow: an arrow pointing up indicates that the metal is entering the probe, and an arrow pointing down indicates that the metal is exiting the probe. The resistance of the hole (of the probe tube) during data acquisition is also provided.



Figure 3.5 The LiMCA system connected to the microcomputer during a LiMCA sampling.



(a)



(b)

Figure 3.6 (a) The main menu, and (b) configuration page displays for a typical LiMCA test.⁴⁹

An enlarged view of this is shown in Figure 3.7 (a), while Figure 3.7 (b) explains the corresponding values. These two plots display the hole resistance. The outer gray bar represents the current value of the hole resistance: if it is above the base value, this means that the current corresponding to the hole resistance is greater than the base value. The thinner yellow bar represents the maximum and minimum values for each point in time, and are reset at the start of a new acquisition.

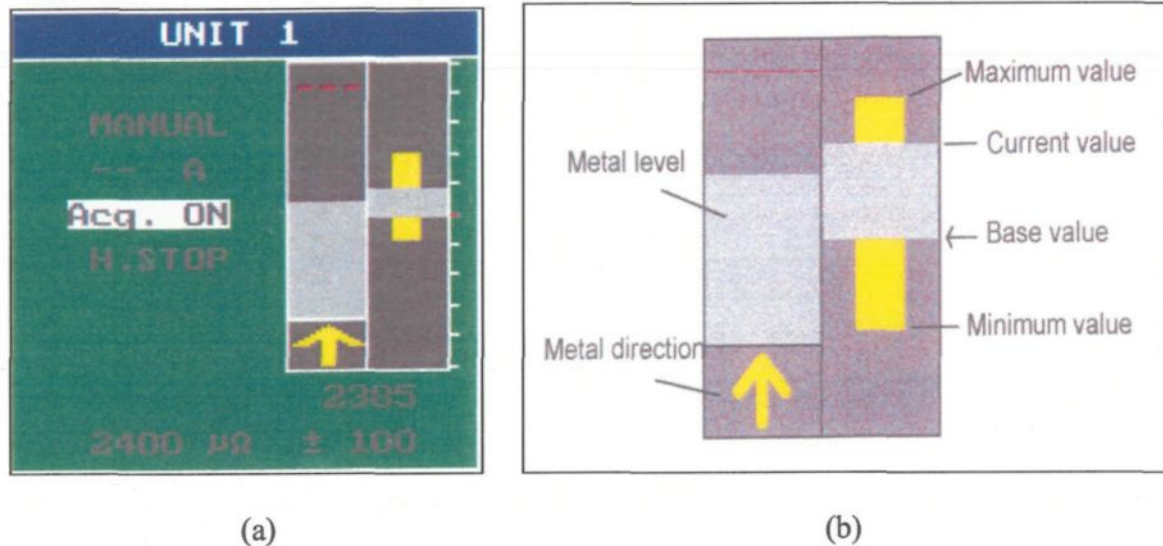


Figure 3.7 (a) Permanent status, and (b) graphical display of hole resistance.⁴⁹

3.4.2 Operation of LiMCA II

After connecting the LiMCA to the microcomputer, the argon and air flow valves are opened (at 50-60 psi and 75-80 psi pressures, respectively), following which the tube is inserted in the probe head section. The support pressure of the system appears on the system status page as 28.6 psi. The pressure in the probe tube is supposed to vary between

2.5 psi and -2.5 psi (vacuum). After the pressure/vacuum (Pres/Vac) value appears on the configuration page (see Figure 3.6 (b)), the calibration is carried out using the automatic control panel. After calibration, six bars appear in the form of a histogram (in the right corner of the main menu page). They must be of equal height with a noise level lower than six (6).

Following this, the melt surface is carefully skimmed to remove any dross and oxide layers. Then the LiMCA head is inserted 1 inch inside the melt and is kept as such till the temperature of the thermocouple reaches 200 °C in order to preheat the tube. The tube, made from alumina silicate, is sensitive to thermal shock. The pressure of the tube is set to 2.5 psig in manual setup mode in order to avoid the entering of the metal into the tube while the head is immersed in the melt. Later on, when the tube is inside the molten metal, the setup pressure mode is changed to automatic.

The pressure and vacuum conditions inside the tube are adjusted by the automatic setup of the LiMCA system. These parameters are related to the internal pressure of the probe during the test cycle. The system creates a vacuum inside the probe in order to force liquid metal into the probe through the small opening near the bottom of the tube. When the liquid metal reaches the thermocouple inside the probe, the system establishes a positive pressure inside the tube and the metal is forced out.

Pressure and vacuum readings are relative to atmospheric pressure and are expressed in psig: a zero psig reading corresponds to atmosphere pressure, and a negative value corresponds to vacuum conditions. The pressure and vacuum parameters can be

adjusted to lower or higher values when the probe hole is not of standard size (*i.e.*, 300 μm) or when the liquid metal is more or less viscous.

In normal conditions, acquisition is activated while the metal is going out of the tube under vacuum mode. Acquisition is a data collection process in which the passage of the inclusion particles in the “ESZ” region is detected and quantified in terms of the resistance of the particles and the corresponding deviation in the voltage/current, thus providing the means for calculating the number and volume fraction of the particles, respectively. The default acquisition time is set to 30 seconds in the normal mode (and also for calibration). There is an acquisition delay of a few seconds between the change from pressure to vacuum and start of acquisition.

The cycle time, which is the time during which the metal comes in and goes down the tube is typically set to 40 seconds. In each cycle, including vacuum, acquisition and pressure, the data corresponding to one sampling is displayed on the microcomputer screen in the form of an X-Y plot of the total number of inclusions as a function of time, as shown in Figure 3.8. The cycle time can be changed in the case of special materials. Sometimes, a progressive disturbance of the signal can be avoided by choosing a shorter acquisition time (the smaller the acquisition time, the less the acquisition of false data).

Sometimes, the hole of the tube is blocked by particles of bigger size. In such cases a boost current automatically or in manual mode pushes the particles out of the hole. As mentioned previously, after each experimental run, or for any reason resulting in interruption of a measurement, the tube is replaced.

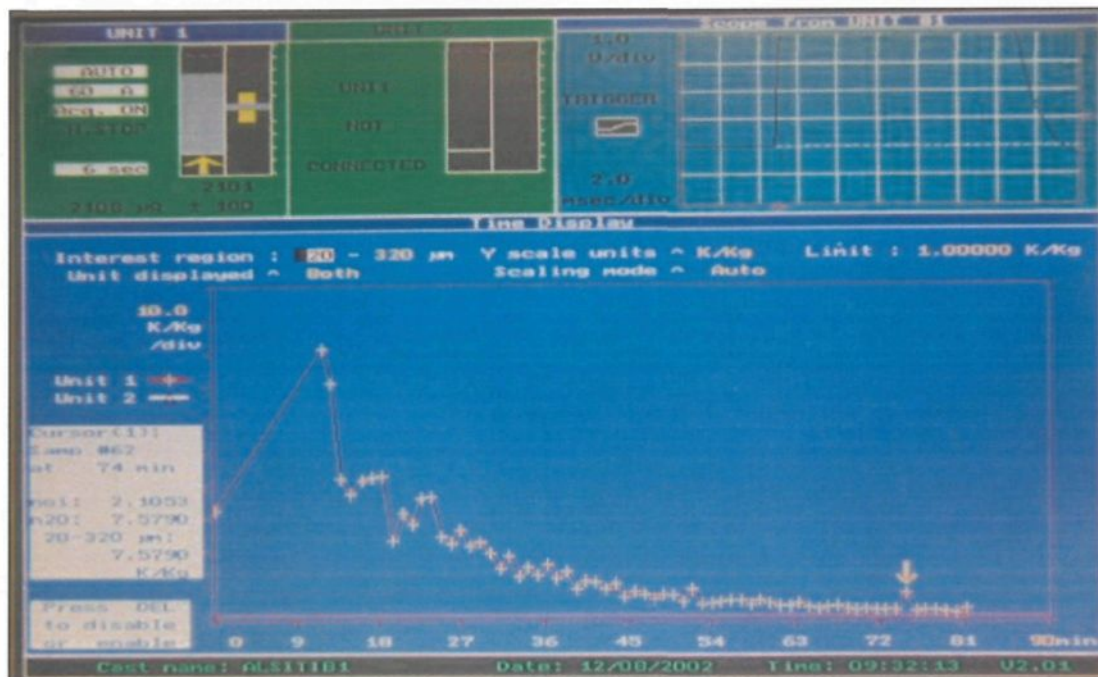


Figure 3.8 Example showing the plot of total number of inclusions versus time obtained in real time on the microcomputer screen of LiMCA.

Figure 3.9 shows the type of probe tube used in the LiMCA system. At the end of the test, the set-up is changed to manual and the machine is set to pressure mode in order to release the metal from the tube. Following this, the head section of the LiMCA machine is moved out of the melt.

Figures 3.10 and 3.11 show examples of the LiMCA during operation. For each addition of inclusions, four to five LiMCA tests were carried out. The target was to determine the sensitivity and reliability of the LiMCA for each inclusion type.

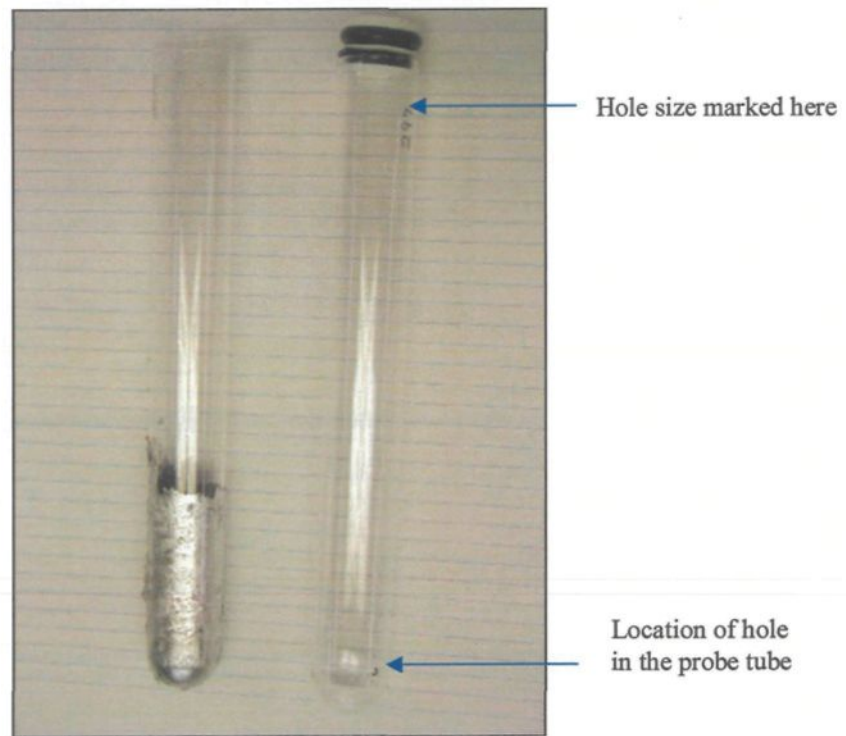


Figure 3.9 The LiMCA probe tube after use (left) and before testing (right).



Figure 3.10 The LiMCA system during operation.

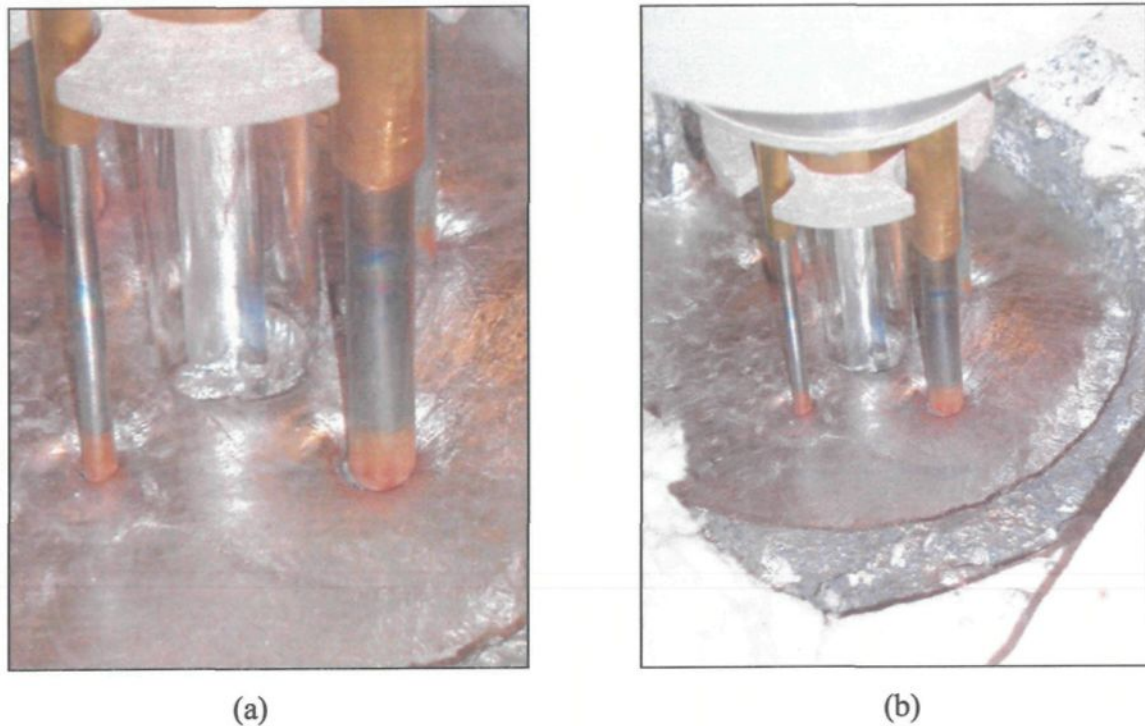


Figure 3.11 Close-up view of the LiMCA system during operation: (a) under vacuum, and (b) under pressure conditions.

3.5 METALLOGRAPHY

Samples for metallographic examination (2×2 cm) were sectioned from the metal solidified in the LiMCA probe tube after a LiMCA sampling and from the small castings (prepared for microstructural analysis), obtained from different melt compositions. The samples were mounted in bakelite and polished to a fine finish ($1\mu\text{m}$ diamond paste). The polished samples were then used for microstructural examination of the various inclusion types studied.

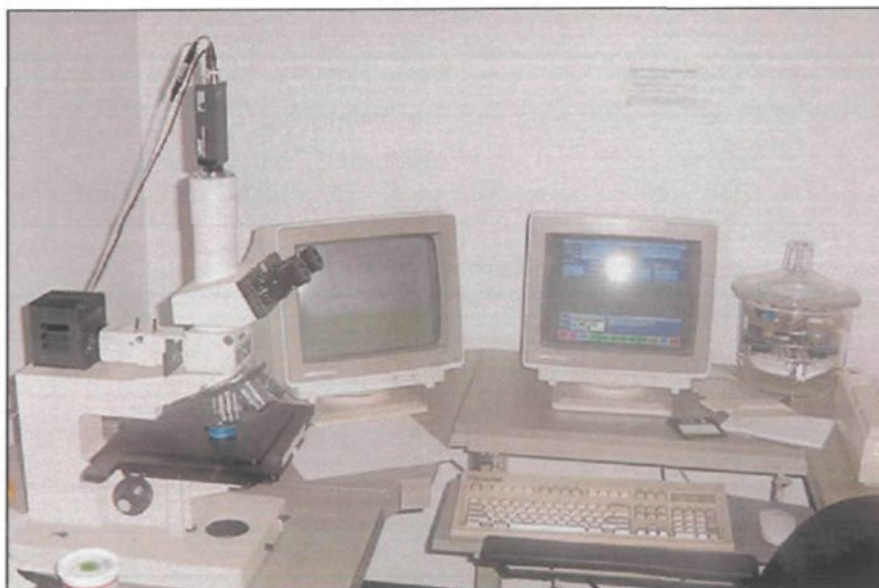


Figure 3.12 The optical microscope-image analysis system used for microstructural analysis.

The samples were examined using an Olympus BH2-UMA optical microscope-Leco 2001 image analyzer system for qualitative analysis of the inclusions. Figure 3.12 shows the optical microscope-image analysis set-up used for these measurements. In certain case, the sample were also examined using electron probe microanalysis (EPMA) to obtain further information on the inclusions observed under the optical microscope. Wavelength dispersion spectroscopy (WDS) and energy dispersive X-ray (EDX) analyses were also used to confirm the compositions of the captured inclusions and any possible reactions with the melt.

Figure 3.13 shows the Jeol WD/ED combined microanalyzer (McGill Microprobe Laboratory) that was employed for this purpose (model JXA-8900R, operating at 20 kV and 30 nA, with an electron beam size of $\sim 1 \mu\text{m}$).



Figure 3.13 Electron probe microanalyzer used in the present work.

3.6 ANALYSIS OF LiMCA DATA

The results of the LiMCA tests were plotted in terms of concentration number *vs.* time (N_{20} measurement data) and volume of inclusions *vs.* time (C_{20} measurement data), showing the inclusion size distribution with respect to the total concentration of inclusions in the melt.

CHAPTER 4

EVALUATION OF INCLUSIONS IN PURE ALUMINUM

MEASURED BY LIMCA

CHAPTER 4

EVALUATION OF INCLUSIONS IN PURE ALUMINUM MEASURED BY LIMCA

4.1 INTRODUCTION

Evaluation of different inclusions types by the LIMCA technique was undertaken in the present study. Two types of materials were used: commercial pure aluminum (99.78%) and Al-6%Si alloy, the first as a reference for aluminum alloys, and the second as representing the base alloy corresponding to the commercially popular 3xx series of aluminum foundry alloys such as 319, 356, *etc.* used in automotive applications.

Specified amounts of each inclusion type were added to a pre-heated melt of the alloy in the form of powder, master alloy or pure metal. In the case of powder inclusions, ingots containing the corresponding inclusions were first prepared using a powder injection technique to introduce the powder inclusion particles into the two types of alloy melts. These inclusion-containing ingots were then used to introduce the specified inclusion type into each alloy melt.

As mentioned above, certain inclusion types were also added in the form of master alloys (*e.g.*, TiB₂ as Al-5% Ti-1% B master alloy), pure metal (*i.e.* Mg) or, as in the case of

Al_2O_3 inclusions, in the form of metal matrix composite alloy (containing Al_2O_3 as the particulate reinforcement) in calculated amounts.

Two melt temperatures were used: 680 °C and 750 °C, corresponding to conditions of low and high superheat, in order to study the effect of superheat on the fluidity of the molten metal and, hence, the influence on sedimentation (settling) of the inclusion particles, as well as investigate the capacity of LiMCA to measure the inclusions under these conditions of superheat. In view of the fact that the main purpose of studying alloys (representing commercial 3XX alloys), only a few tests were carried out for pure aluminum melts at 680 °C, namely, for CaO, MgO and TiAl_3 inclusion additions.

This chapter presents the results for inclusions added to pure aluminum. These results will serve as a reference base for the LiMCA results obtained in the case of the Al- 6%Si alloy melts presented in Chapters 5 and 6.

The LiMCA technique to date has mainly been used to study inclusions in wrought aluminum alloys. Normally, aluminum casting or foundry alloys possess much higher levels of impurities and inclusions. In this study, therefore, the applicability of the LiMCA technique in the case of aluminum casting alloys was investigated, covering a wide range of inclusion types generally observed in such alloys.

4.2 EVALUATION OF INCLUSIONS IN PURE ALUMINUM AT 750 °C

A charge of 8.5 Kg pure aluminum was melted in a SiC crucible using an electric resistance furnace. The melt temperature was kept at 750 °C. Degassing was done for 15 min using pure, dry argon. Inclusion additions were carried out in three successive steps.

- (i) A measured amount (~ 500g) of a specific inclusion type was added to the melt, and the melt stirred to achieve a homogeneous dispersion of the inclusions. Following this a LiMCA sampling was taken.
- (ii) A second addition of the same inclusion type (~500 g) was added to the same melt, the melt was stirred, and a LiMCA sampling taken to measure the inclusion content corresponding to the increased addition.
- (iii) A third addition (500 g) was made to the same melt, and the same procedures followed.

The LiMCA data obtained from the three samplings were plotted in the form of graphs showing (i) the total number of inclusions and (ii) the volume concentration of inclusions as a function of time (*viz.*, N_{20} and C_{20} plots, respectively). LiMCA II results can be expressed as a number concentration (number of inclusions larger than a selectable diameter value) or as a volumic concentration (volume concentration of inclusions larger than a selectable diameter value).⁴⁸ Thus N_{20} and C_{20} measurements would correspond to measurements where the selected diameter is 20 μm . In using volumic concentrations to express inclusion concentrations, the relative weight of larger inclusions in the final value is effectively increased. Melt quality assessment based on such concentrations will more accurately reflect the relative harmful effects of different inclusion sizes.⁴⁸

A schematic representation of the inclusion addition and LiMCA sampling procedure is shown in Figure 4.1 for the addition of Al_2O_3 inclusions as an example. It is to be mentioned here that each LiMCA sampling was done over a period of 30 minutes, and readings were taken at every 1-2 min intervals. In some cases, the sampling line was

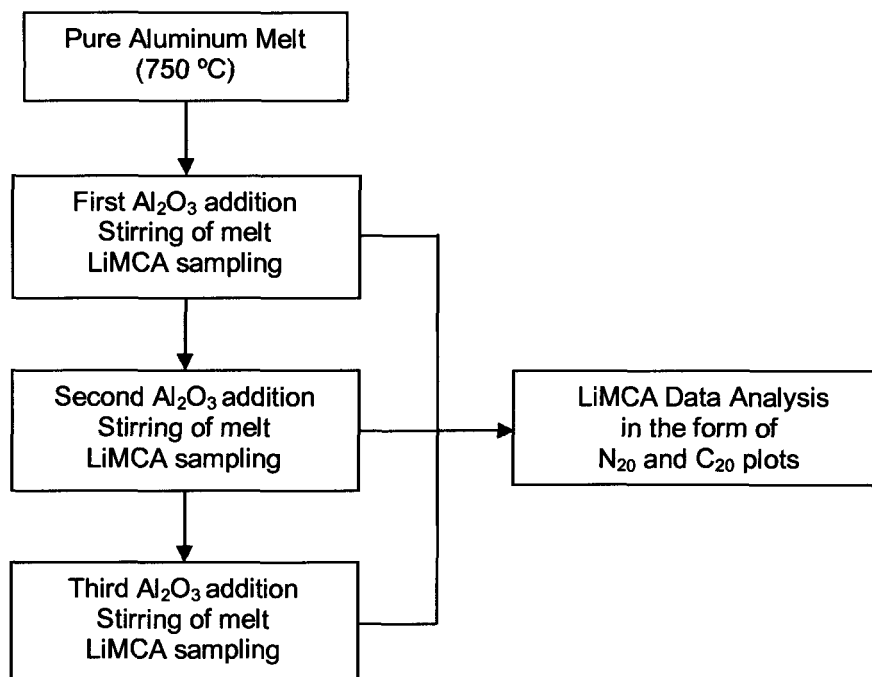


Figure 4.1 Schematic representation of inclusion addition procedure.

extended to 40 or 50 min to determine if any changes occurred in the stable level of the inclusion readings after the 30 min period.

4.2.1 Evaluation of Al₂O₃ Inclusions

As mentioned previously, the Al₂O₃ inclusions were added to the aluminum melt (maintained at 750 °C) in the form of an aluminum metal matrix composite containing Al₂O₃ as the particulate reinforcement. The average particle size of the Al₂O₃ inclusions was ~ 23 μm.⁶¹

N₂₀ Measurements: Total concentration number of inclusions (inclusions > 20μm)

Figure 4.2 shows the N₂₀ plot of the total number of inclusions as a function of time. As can be seen, the measured inclusion concentration drops to a minimum after 13 min and

remains the same for the rest of the 30 min time period. This indicates that the Al_2O_3 inclusions settled down to the bottom of the melt after about 13 min, so that the LiMCA probe tube (kept about 2 in below the melt surface) could not detect these inclusions any longer. The plot of inclusion levels for the pure aluminum melt is also shown in the figure to serve as a reference for comparison purposes. As expected, the inclusion levels in pure aluminum are minimal, the aluminum being of a commercial pure grade (99.78 % purity).

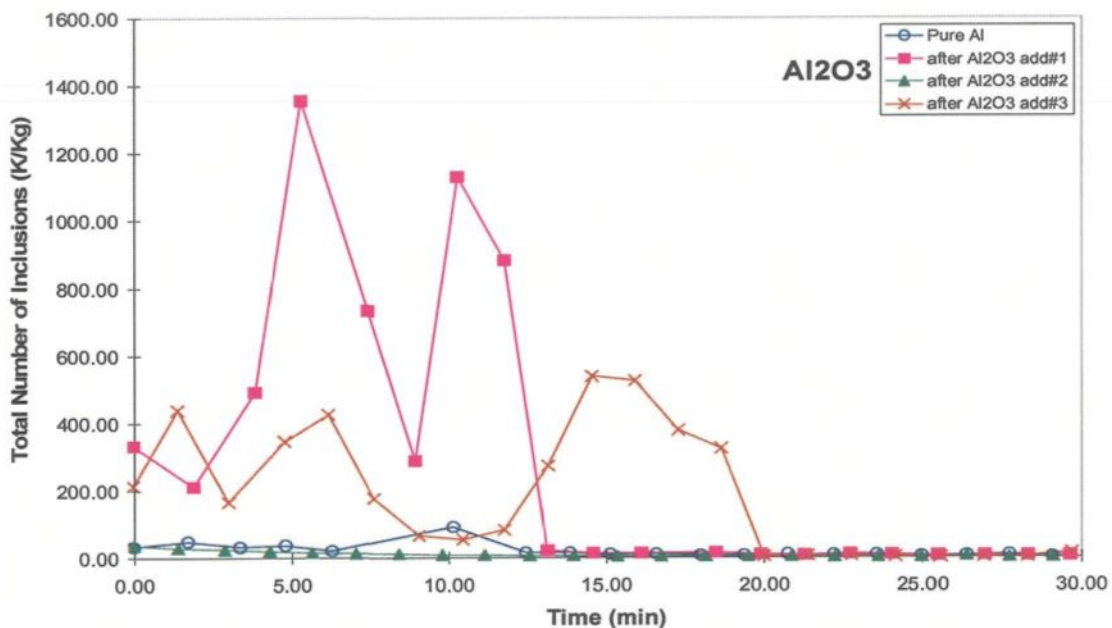


Figure 4.2 Concentration number of Al_2O_3 inclusions in commercial pure aluminum as a function of time.

The first addition of Al_2O_3 inclusions shows the highest inclusion concentrations among all additions, exhibiting two peaks at 5 and 10 min. In spite of the increase in the inclusion concentration following the second and third additions, the inclusion levels are lower as detected by the LiMCA. This may be accounted for by the sedimentation of the alumina particles due to their large particle size and higher density ($3.69\text{-}3.99\text{ g/cm}^3$)

compared to the aluminum melt (2.71 g/cm^3). Also, with the addition of more inclusions, the probability for their agglomeration would be increased, providing another reason for their rapid sedimentation. In fact, it was generally observed that after 30 min of testing, most of the inclusions studied settled down and no changes were observed for prolonged testing times. Thus, all plots shown have been drawn for a time period of 30 min.

In Figures 4.3 and 4.4, respectively, the average and total number of inclusions have been plotted as a function of particle size range.

The terms *average* and *total* are explained as follows: During the time period for which a LiMCA sampling is done (*e.g.*, 30 min), a certain number of readings are acquired at the preset time intervals (*e.g.*, 30 readings at time intervals of one min covering the 30 min LiMCA sampling period). The *average* of these (30) readings then represents the average number (or volume) concentration values plotted in Figure 4.3 for the different inclusion particle size ranges, whereas the *total* in each particle size range corresponds to the sum of these (30) readings.

As can be seen, maximum numbers of Al_2O_3 inclusions are observed in the 20-25 μm particle size range after the first and third additions and the distribution shows positive skewness. In contrast, the inclusion concentrations are considerably diminished after the second addition of the Al_2O_3 inclusions, showing a distribution close to that observed in the case of pure aluminum. With the third addition, while the distribution follows a pattern similar to that for the first addition, a larger number of inclusions are detected in the higher particle size ranges, from 50-55 μm onward. The number of inclusions in the larger particle size ranges is also found to increase with progressive inclusion additions.

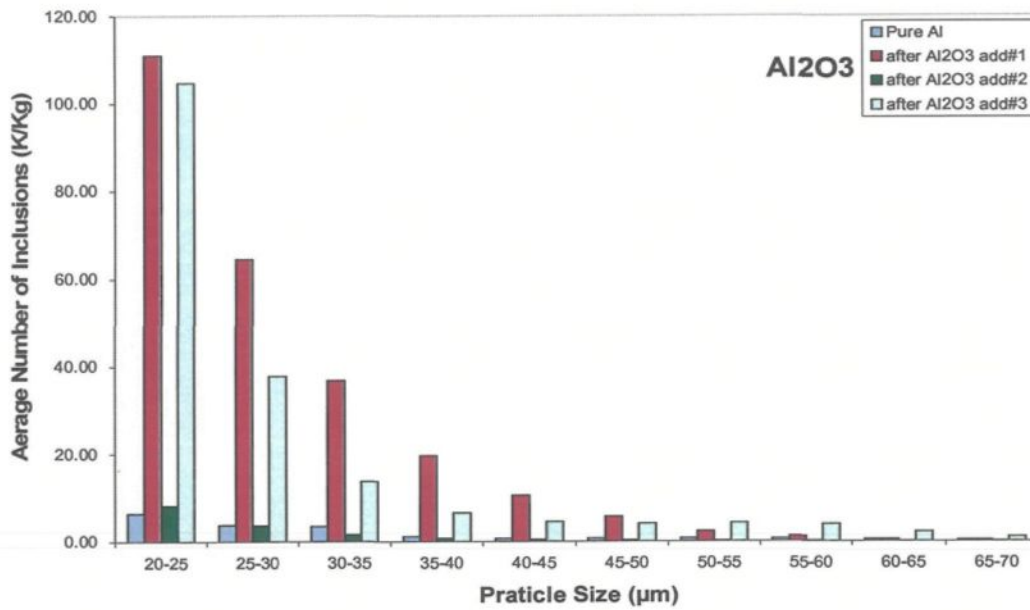


Figure 4.3 Average number of Al₂O₃ inclusions in commercial pure aluminum as a function of particle size.

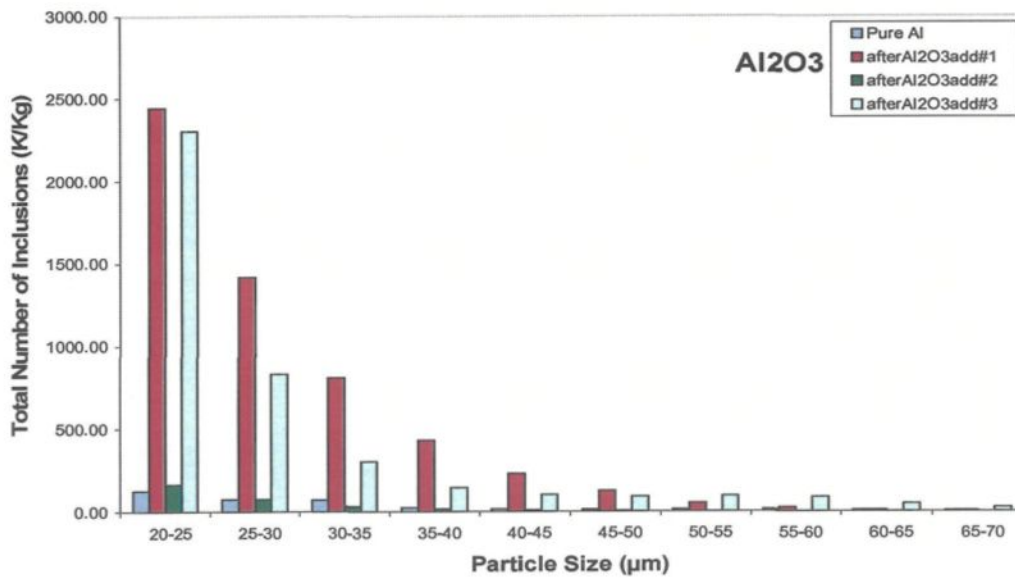


Figure 4.4 Total number of Al₂O₃ inclusions in commercial pure aluminum as a function of particle size.

Both this observation and the shape of the distribution curves indicate the feasibility of the agglomeration and sedimentation factors suggested earlier to explain the drop in inclusion levels in Figure 4.2.

C₂₀ Measurements: Volumic concentration of inclusions (inclusions >20 μ m)

The volumic concentration of Al₂O₃ inclusions is displayed in Figure 4.5. The highest volume of inclusions were detected by the LiMCA after the first addition. These values are higher than those obtained following the second and third additions, and much higher (about five times) than those measured for pure aluminum. Again, in this case also, the volume concentration drops after about 13 mins of testing, with no change thereafter.

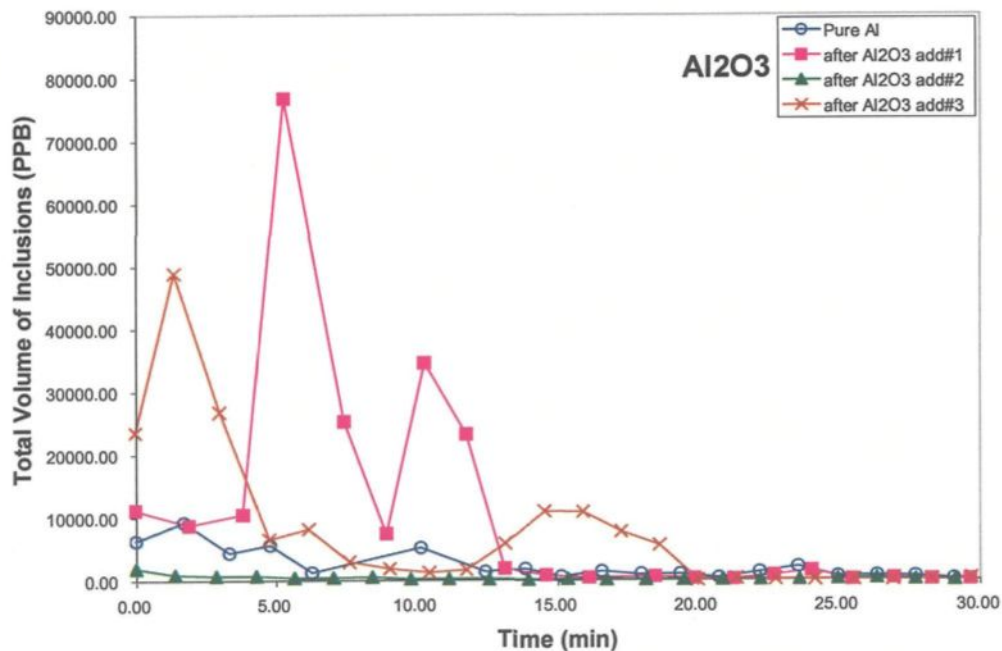


Figure 4.5 Volumic concentration of Al₂O₃ inclusions in commercial pure aluminum as a function of time.

Figures 4.6 and 4.7 show the corresponding plots of average and total volumic concentrations of Al_2O_3 inclusions as a function of the inclusion particle size. After the first addition, the particle distribution curve is more bell-shaped, and the maximum number of inclusions lie in the particle size range of 20 to 40 μm , extending also to the 40-45 μm and 45-50 μm ranges to a reasonable extent. As in the case of the N_{20} measurements (total number of inclusions), the volume concentrations are reduced considerably after the second addition.

In contrast, the third addition of Al_2O_3 inclusions results in a distribution which, although initially similar to that observed in the case of the N_{20} measurements, differs from the latter in that (i) the values decrease from one particle size range to the next but not drastically, and (ii) they increase again after crossing the 35-40 μm particle size range, showing a maximum at 55-60 μm and a gradual decrease thereafter. The maximum observed, however, is about two-thirds that observed in the 20-25 μm size range.

A comparison of the N_{20} and C_{20} particle distribution data (Figs 4.3-4.4 vs. Figs 4.6-4.7) reveals that the two measurements are not necessarily linked, *i.e.*, that they follow the same trend. This is particularly so at the first addition stage: the changes in volumic concentration are much more gradual on traversing the range of particle sizes (low to high), whereas those for the total concentration number of inclusions decrease rather sharply.

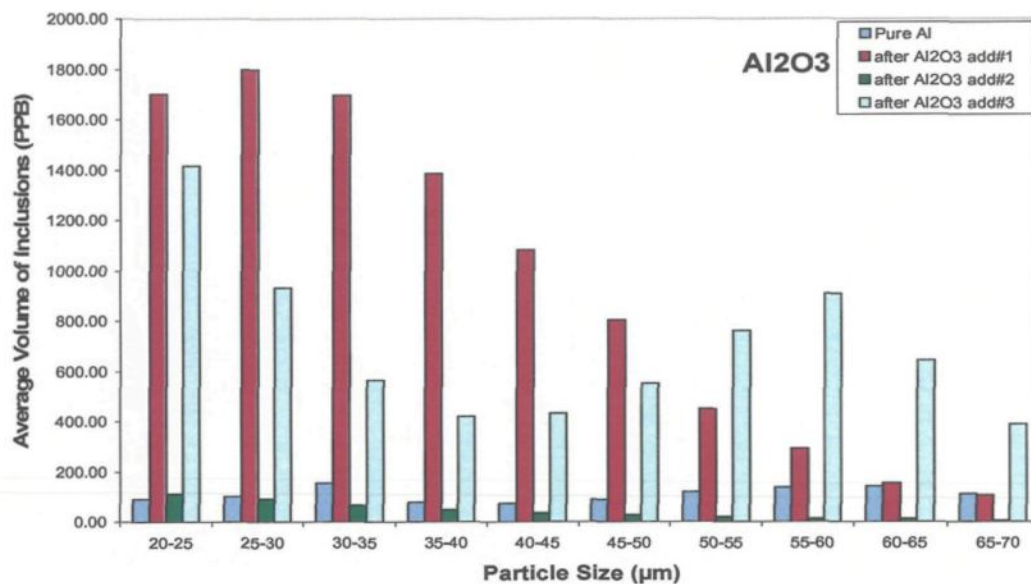


Figure 4.6 Average volume of Al₂O₃ inclusions in commercial pure aluminum as a function of particle size.

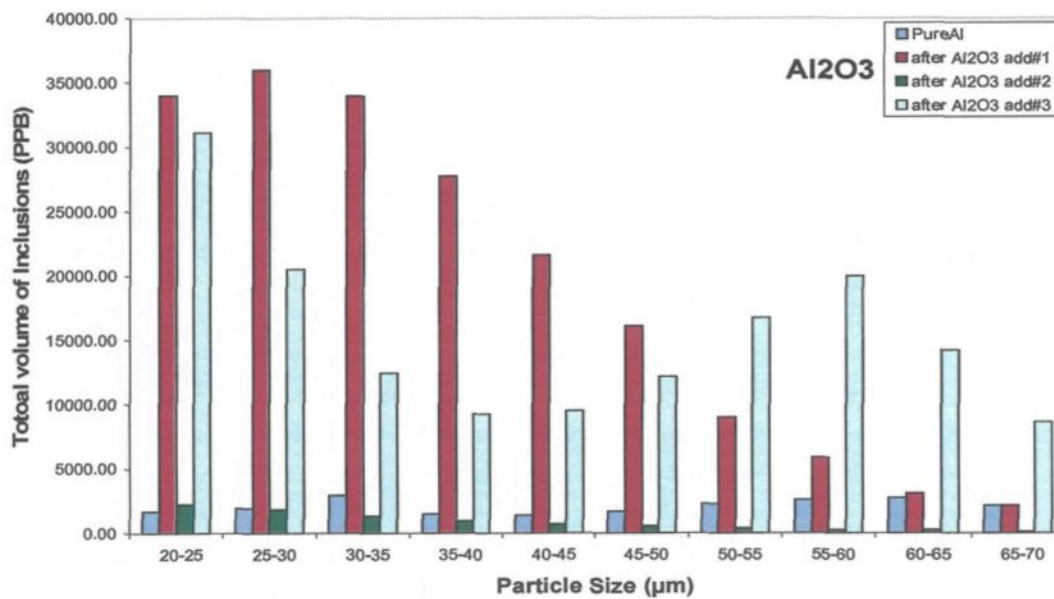


Figure 4.7 Total volume of Al₂O₃ inclusions in commercial pure aluminum as a function of particle size.

4.2.2 Evaluation of Al_4C_3 Inclusions

The addition of Al_4C_3 inclusions to a pure aluminum melt was carried out using prefabricated Al_4C_3 inclusion-containing aluminum ingots. The procedure for the preparation of such inclusion-containing ingots using the powder injection technique has already been described in Chapter 3, section 3.2.2.

Three inclusion-containing ingots were prepared for each powder inclusion type that was studied. These ingots were then used for carrying out the inclusion addition in three stages, where one ingot was added to the pure aluminum melt (8.5 Kg charge at 750 °C temperatures) in each stage.

After the first addition, the melt was stirred properly, followed by a LiMCA sampling that was continued without pause for about 30 min. The second Al_4C_3 inclusion-containing ingot was added and the same procedures repeated, followed by the third addition and the corresponding LiMCA sampling. The size of the Al_4C_3 powder particles used was less than 10 μm .

N_{20} Measurements: Total concentration number of inclusions (inclusions > 20 μm)

Figure 4.8 shows the plot of the number of inclusions as a function of time. As can be seen, the first and second additions show virtually no increase with respect to the pure Al base line. The third addition, however, shows much higher inclusion levels. On account of the lower density of Al_4C_3 (2.36 g/cm³) compared to aluminum (2.71 g/cm³), particle sedimentation does not take place until after 25 min of sampling. The smaller size

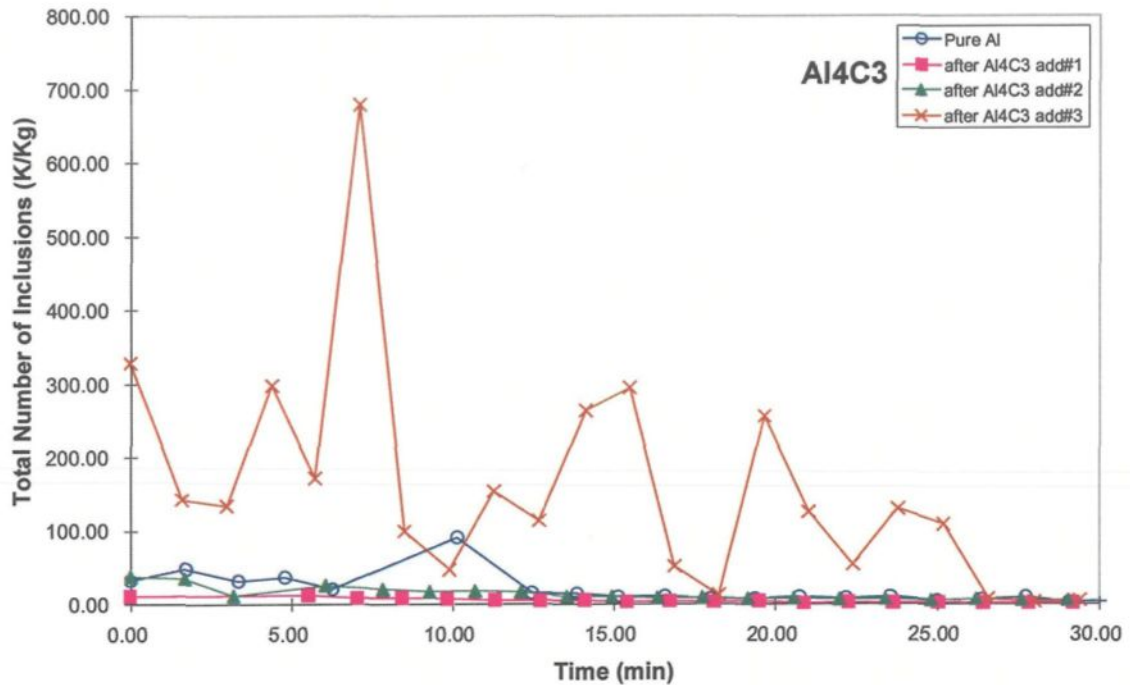


Figure 4.8 Concentration number of Al_4C_3 inclusions in commercial pure aluminum as a function of time.

(<10 μm) and low wettability of the Al_4C_3 particles does not facilitate clustering and formation of agglomerates.

Figures 4.9 and 4.10 show the plots of the average and total number of inclusions as a function of particle size range. Most of the inclusions lie in the 20-25 μm and 25-30 μm range, with almost negligible inclusions observed above 40 μm . As can be seen, the plots for both average and total number of inclusions show similar distributions.

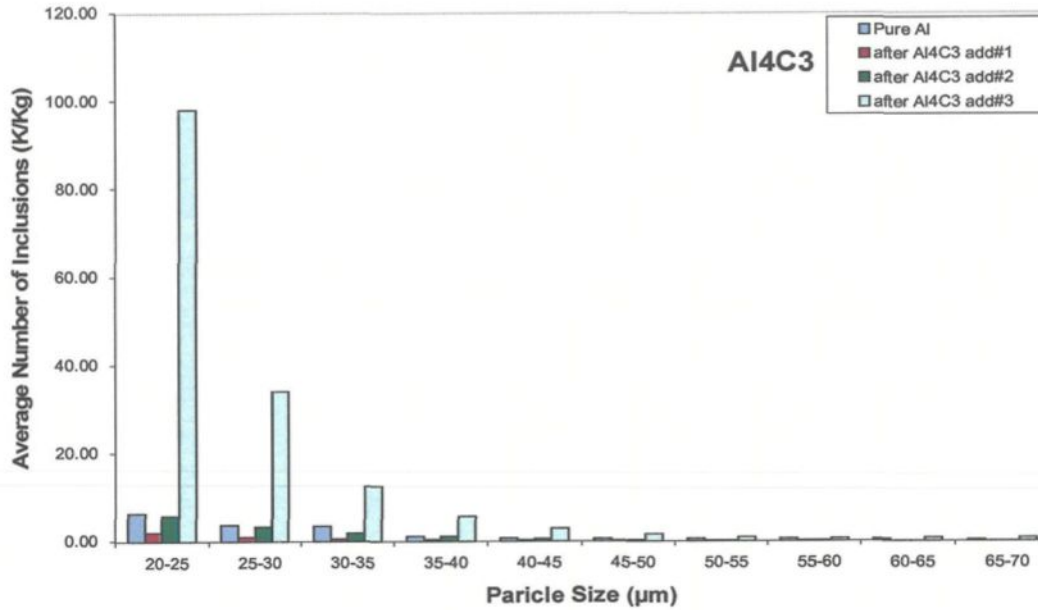


Figure 4.9 Average number of Al₄C₃ inclusions in commercial pure aluminum as a function of particle size.

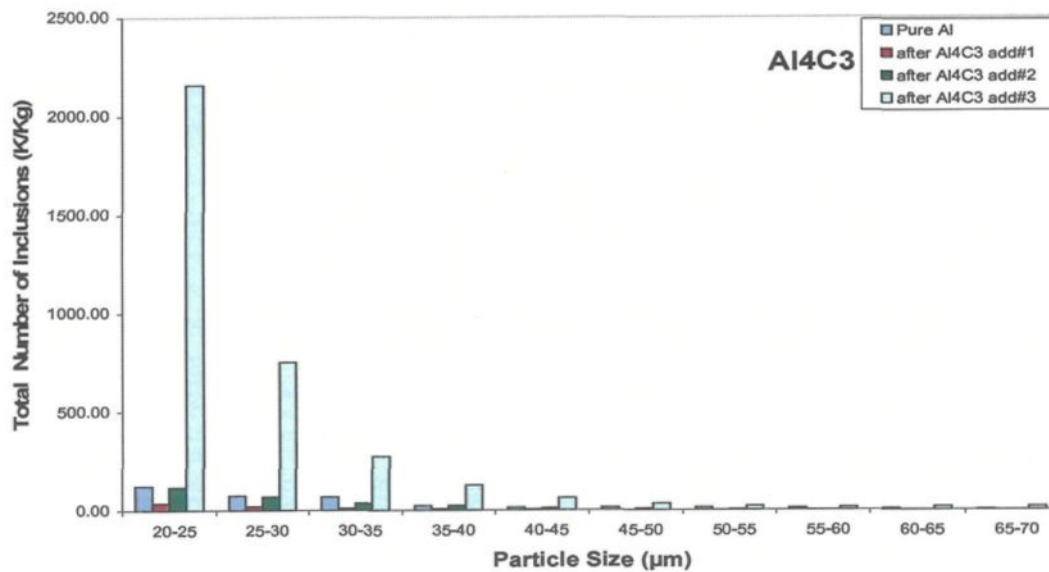


Figure 4.10 Total number of Al₄C₃ inclusions in commercial pure aluminum as a function of particle size.

C₂₀ Measurements: Volumic concentration of inclusions (inclusions >20 μ m)

Figure 4.11 displays the volumic concentration of Al_4C_3 inclusions, where the highest volumes of inclusions are observed after the third inclusion addition. As can be inferred from this graph, after about 13 min, the volume of inclusions drops down to very low values and remains stable thereafter.

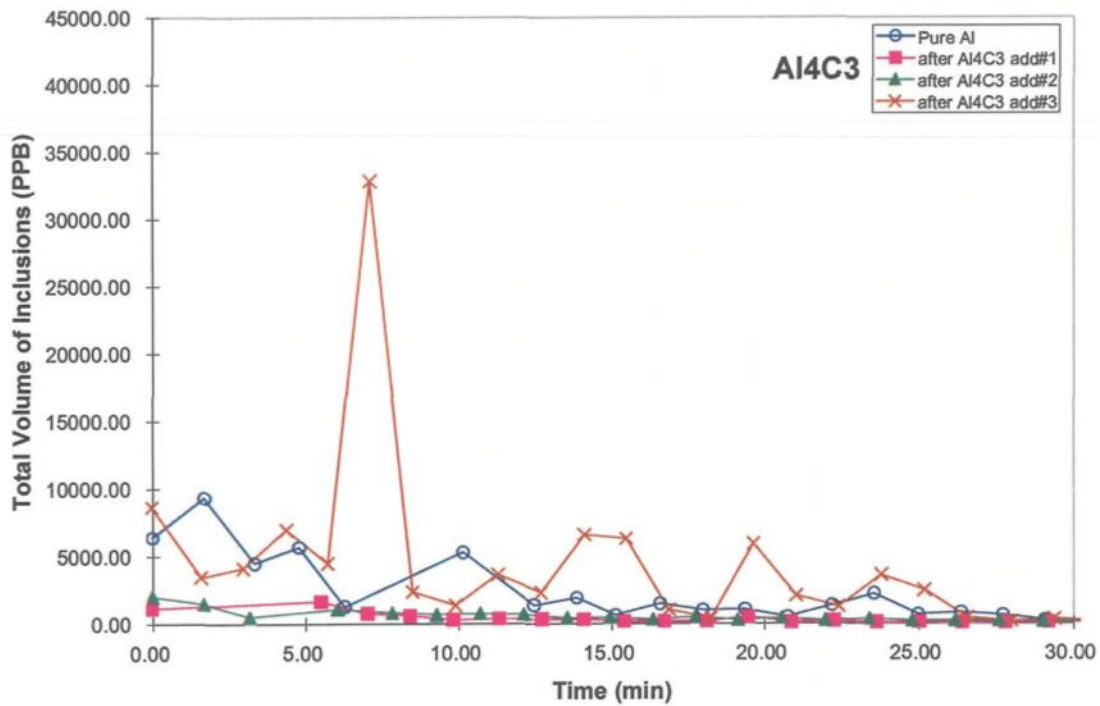


Figure 4.11 Volumic concentration of Al_4C_3 inclusions in commercial pure aluminum as a function of time.

Figures 4.12 and 4.13 show the average and total volume of inclusions as a function of particle size. The third addition of Al_4C_3 displays the highest volume of inclusions (in terms of average and total volume) among all additions. In the first addition, the calculated average and total volume inclusion readings after 30 min (for all particle size

ranges) were 10259.3 and 205185.9 ppb, respectively. These values were found to be higher than those obtained for subsequent additions of inclusions, and respectively five times higher than the volume of inclusions measured in pure aluminum.

In Figures 4.12 and 4.13, the highest amounts of inclusions lie in the 20-25 μm range, which is most likely expected to be the case due to the primary size of the Al_4C_3 inclusions. Other features of the distributions observed after the third inclusion addition (*viz.* the peaking in the 55-60 μm range in Figure 4.12 and the decreasing trend in Figure 4.13) can be attributed to particle agglomeration effects.

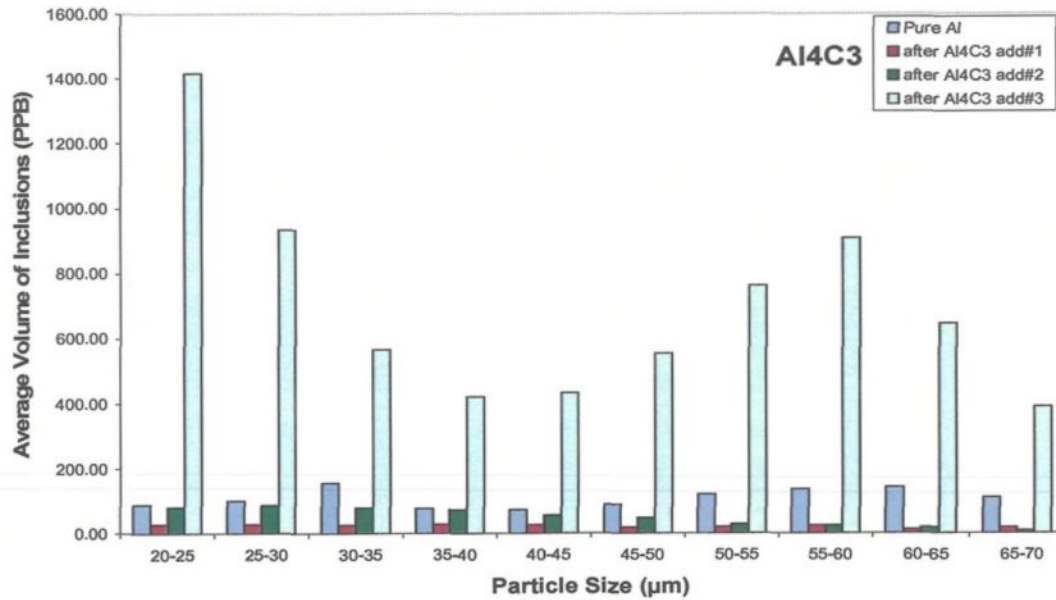


Figure 4.12 Average volume of Al₄C₃ inclusions in commercial pure aluminum as a function of particle size.

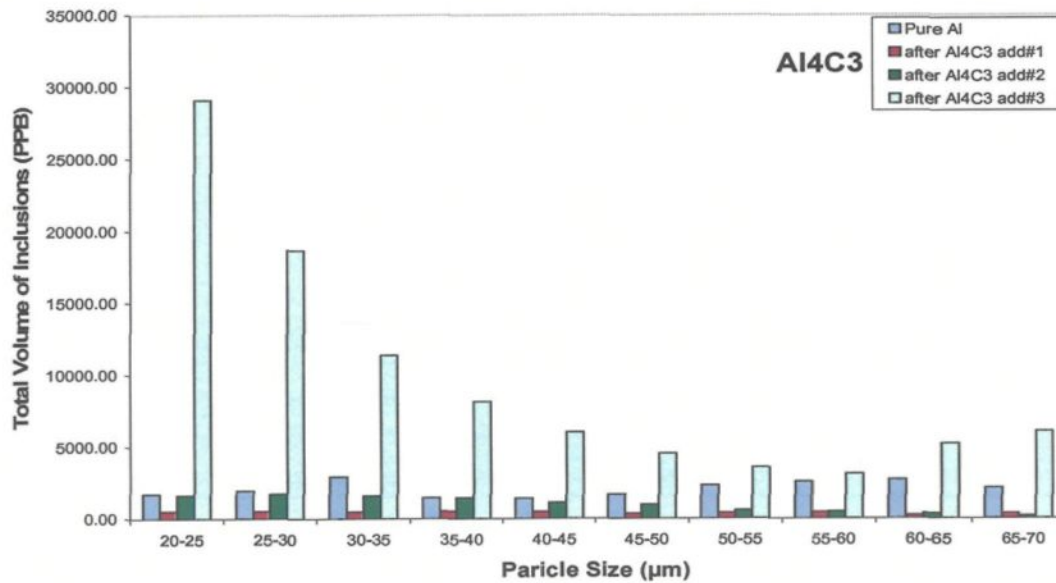


Figure 4.13 Total volume of Al₄C₃ inclusions in commercial pure aluminum as a function of particle size.

4.2.3 Evaluation of CaO Inclusions

As in the case of the Al_4C_3 inclusions, the addition of CaO inclusions to a pure aluminum melt was carried out using prefabricated CaO inclusion-containing aluminum ingots. The procedures for the preparation of the CaO inclusion-containing ingots and their injection into the aluminum melt for conducting LiMCA tests are the same as those described in section 4.2.2.

As before, the inclusion addition was carried out in three stages. After the first addition, the melt was stirred properly, followed by a LiMCA sampling that was continued without pause for about 30 min. The second CaO inclusion-containing ingot was added and the same procedure repeated, followed by the third addition and the corresponding LiMCA sampling. The primary size of the CaO powder particles used for injection was less than 10 μm .

N_{20} Measurements: Total concentration number of inclusions (inclusions > 20 μm)

The concentration number of inclusions (N_{20}) plotted as a function of time is shown in Figure 4.14. As can be seen, for the first addition of inclusions, the inclusion concentrations are similar to those observed in pure aluminum. The fact that only a slight change is observed with the second addition of CaO inclusions and that the inclusion level falls even further with the third addition may be attributed to the possible settling of the inclusions due to clustering and agglomeration, where, in the case of the third addition, the LiMCA probe (at its fixed position below the melt surface) may be unable to detect the inclusions that have settled to the bottom.

There is also the possibility that the inclusion-containing ingots did not contain sufficient amount of inclusions (*i.e.*, the injection process was not satisfactory in this case). In this respect, the physical properties of the individual inclusion particle types such as their wettability and density must be taken into consideration, as well, to understand the observed measurements.

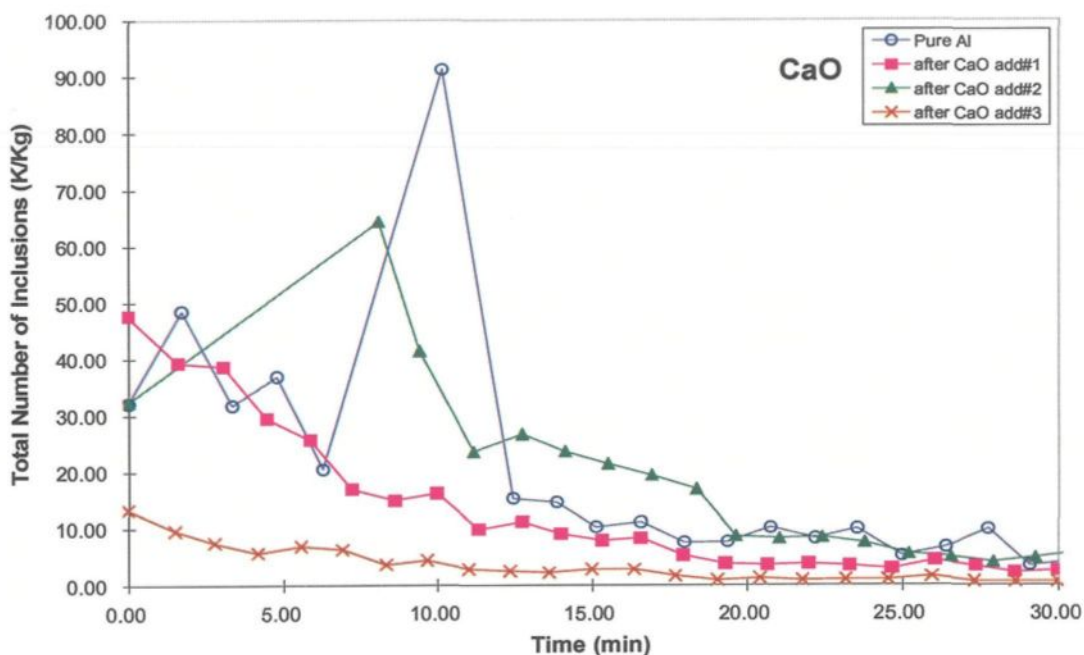


Figure 4.14 Concentration number of CaO inclusions in commercial pure aluminum as a function of time.

Figures 4.15 and 4.16 show the distributions of average and total number of inclusions (K/Kg) in terms of particle size during 30 min of testing. The highest amounts of inclusions for all additions were found in range of 20-25 μm . The overall average and total concentrations of inclusions are the highest among the three additions. It should be mentioned here that, due to the low wettability of the CaO particles, it was relatively

difficult to introduce them into the aluminum melt. Thus, the inclusion-containing ingots that were produced contained a low amount of CaO particles compared to the case of other inclusion types such as Al_2O_3 and Al_4C_3 . The low number of inclusions observed in the case of the third addition could be attributed to this fact.

C₂₀ Measurements: Volumic concentration of inclusions (inclusions >20 μm)

Figure 4.17 shows the volumic concentration of CaO inclusions. For up to ten minutes of the testing time, the volume concentration of inclusions corresponding to the second addition of CaO inclusions is observed to be higher than that for the first or the third additions. At this point in time, the inclusions begin to settle down rapidly and the volume concentrations are minimized to negligible values much before the end of the 30 min testing period. Compared to the fluctuations observed in the case of the pure aluminum melt, the CaO inclusion-containing melts show relatively stable concentrations.

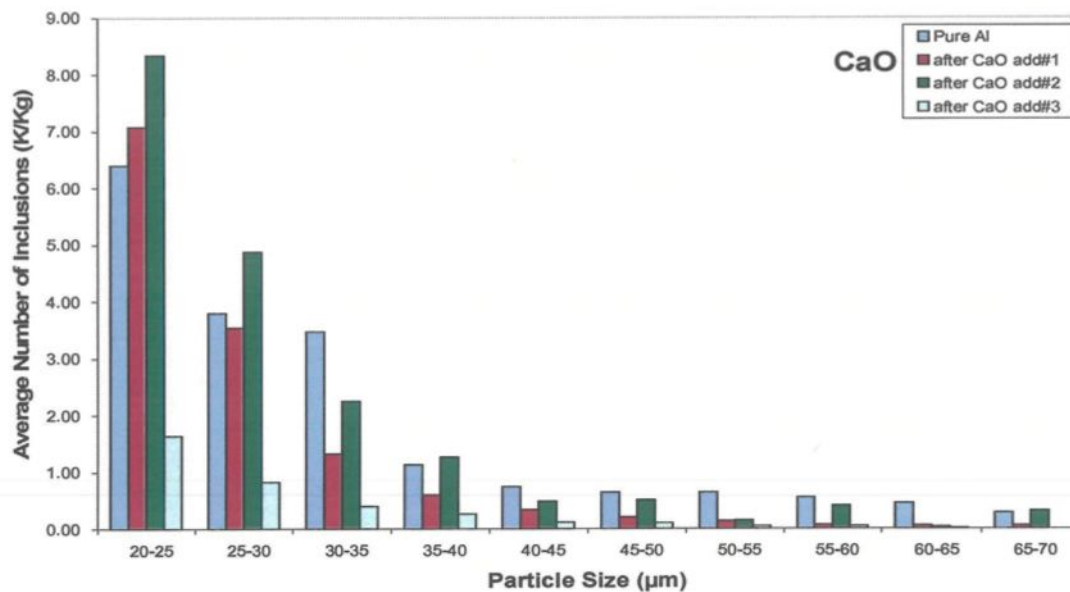


Figure 4.15 Average number of CaO inclusions in commercial pure aluminum as a function of particle size.

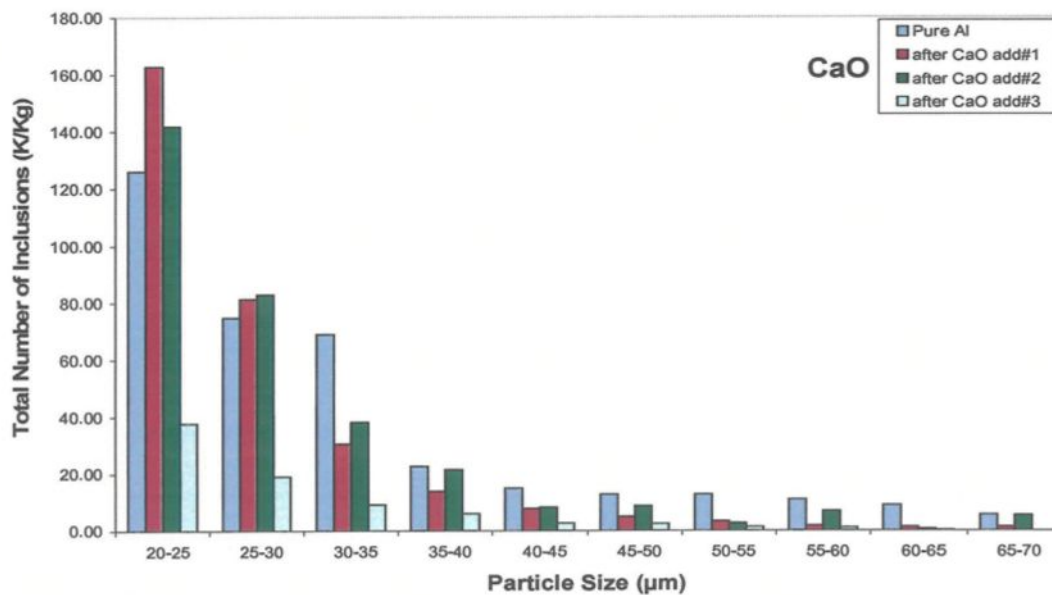


Figure 4.16 Total number of CaO inclusions in commercial pure aluminum as a function of particle size.

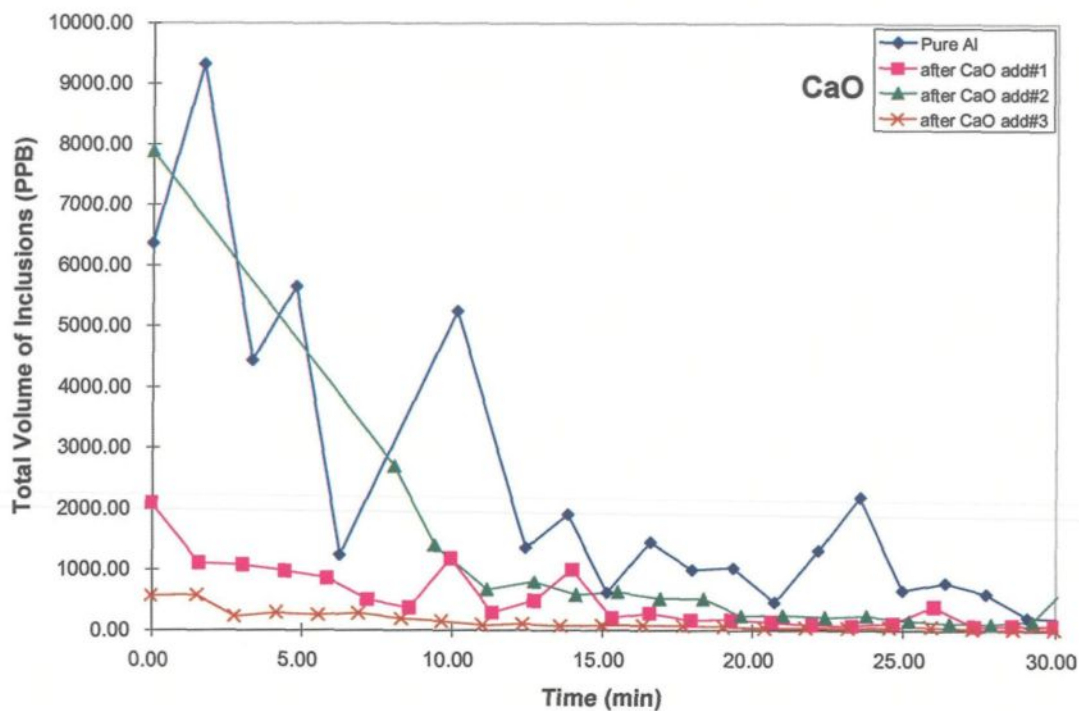


Figure 4.17 Volumic concentration of CaO inclusions in commercial pure aluminum as a function of time.

Figures 4.18 and 4.19 show the distribution of the average and total volumes of CaO inclusions as a function of particle size. The two figures show that, the more the inclusions added to the melt, the more the particles are clustered together, increasing the volume concentration readings for the second addition compared to the first. With the third addition, however, the inclusion clusters are apparently quite dense that they sink to the bottom of the melt. Consequently, volume concentrations read by the LiMCA system (with respect to its position near the melt surface) are reduced considerably.

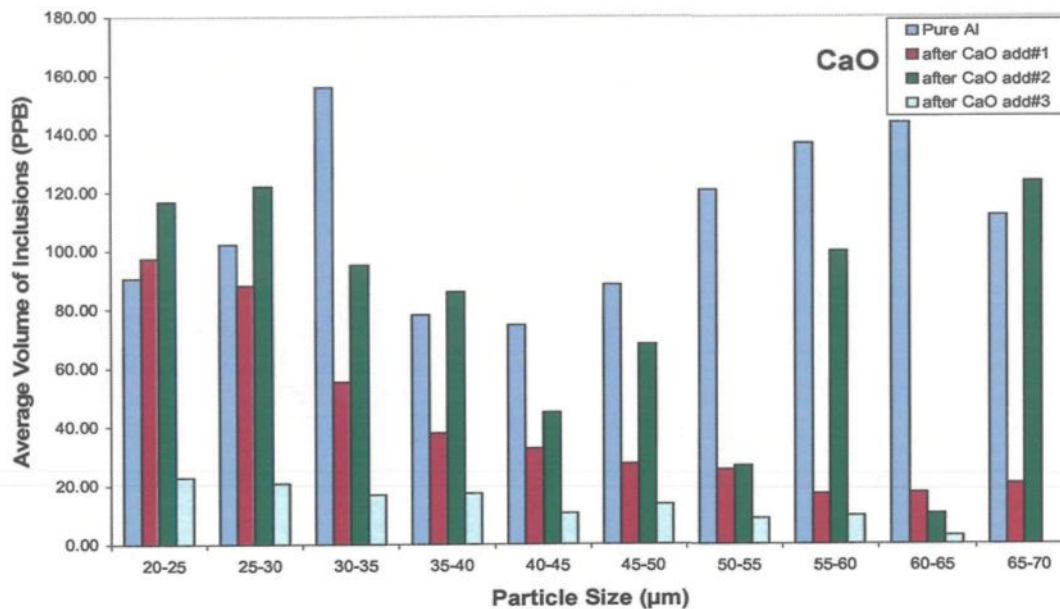


Figure 4.18 Average volume of CaO inclusions in commercial pure aluminum as a function of time.

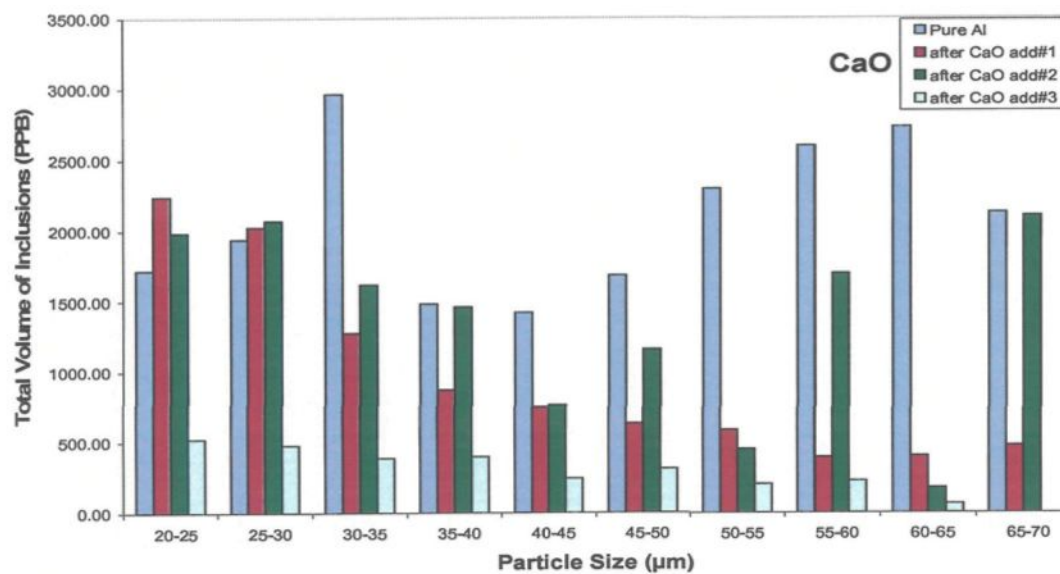


Figure 4.19 Total volume of CaO inclusions in commercial pure aluminum as a function of time.

4.2.4 Evaluation of MgO Inclusions

The addition of MgO inclusions to pure aluminum was carried out using the same procedures described in Chapter 3, section 3.2.2. As before, the inclusion addition was carried out in three stages to the pure aluminum melt (8.5 Kg charge at 750 °C temperature). After each addition, the melt was stirred properly, followed by a LiMCA sampling that was continued without pause for 30 min. The primary size of the MgO powder particles before injection was less than 70 μm .

N₂₀ Measurements: Total concentration number of inclusions (inclusions > 20 μm)

Figure 4.20 shows the concentration number of inclusions measured as a function of time. For the first addition of MgO inclusions, the counted number of inclusions is higher than that measured in pure aluminum. If we ignore the two peaks (at 20.1 and 24.5 min) in the first addition, the second and third additions lead to higher concentration numbers of inclusions. The difference between the number of inclusions in pure aluminum and in the melt containing MgO inclusions is not significant, and the slopes of the curves are moderate.

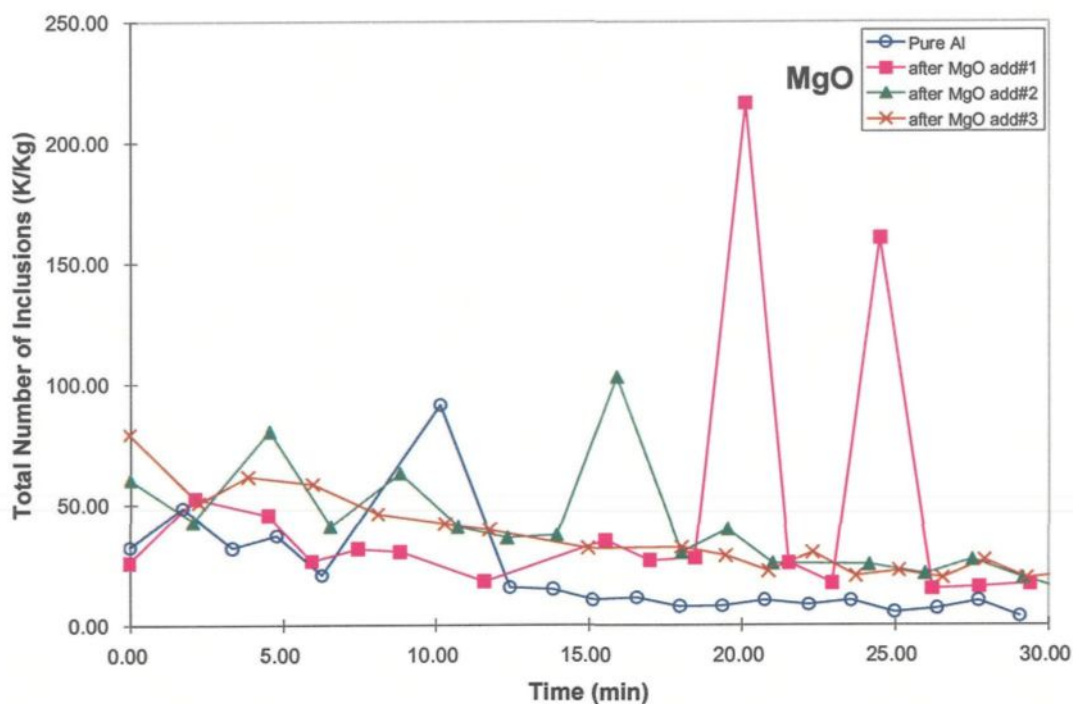


Figure 4.20 Concentration number of MgO inclusions in commercial pure aluminum as a function of time.

Figures 4.21 and 4.22 show the distribution of the average and total number of inclusions as a function of particle size. The highest amount of inclusions for the three additions were found to lie in the 20-25 μm , 25-30 μm and 30-35 μm particle size ranges, respectively. From a comparison of Figures 4.21 and 4.22, it can be seen that both plots show similar inclusion distributions. Also, the more the ingot-containing MgO inclusions added, the more the inclusions are distributed in the upper particle size ranges.

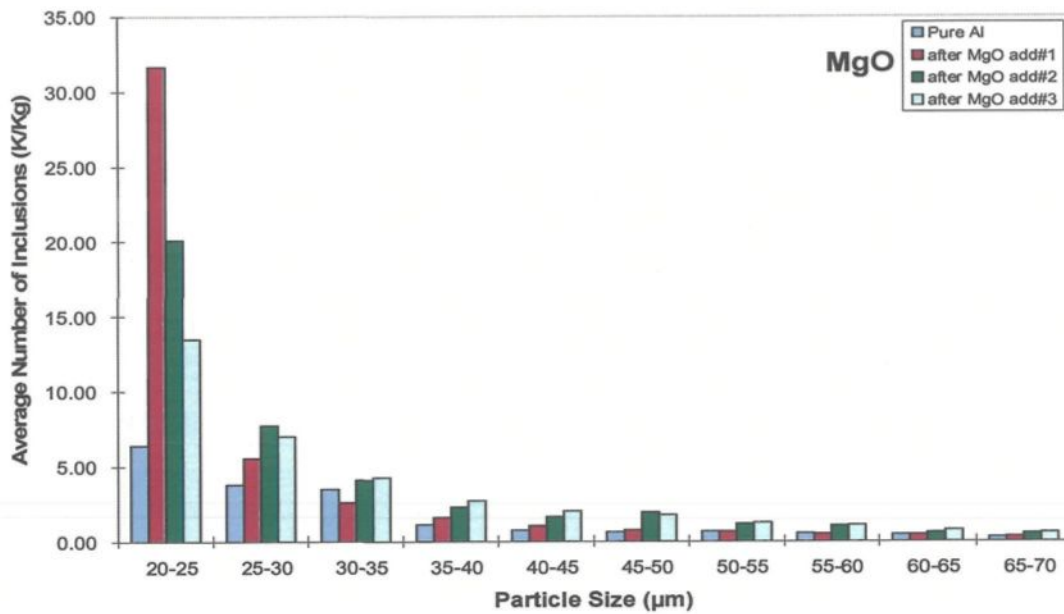


Figure 4.21 Average number of MgO inclusions in commercial pure aluminum as a function of particle size.

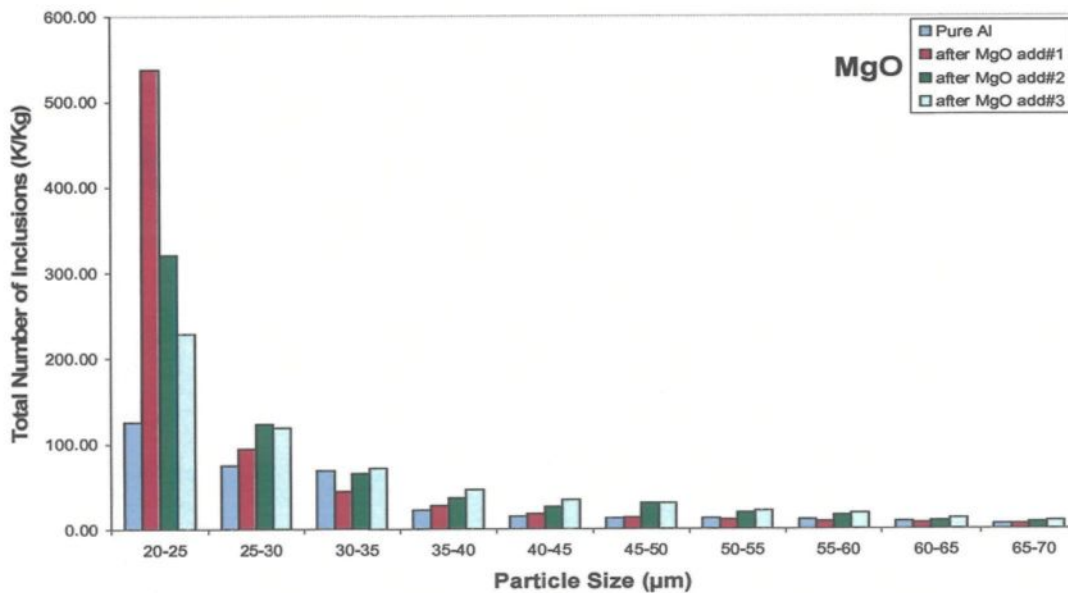


Figure 4.22 Total number of MgO inclusions in commercial pure aluminum as a function of particle size.

Table 4.1 lists the average and total number of inclusions obtained after the three additions of MgO inclusions during 30 min of testing. Due to the physical properties of MgO, after addition of more inclusions, these particles agglomerated together and resulted in larger numbers of inclusions in the larger particle size ranges. Also, the difference in inclusion levels between the pure aluminum melt and that after inclusion addition is small to almost negligible for the larger particle size ranges. These observations are again attributed to the same reasons as before.

Table 4.1 Calculated average and total and number of MgO inclusions during 30 min of LiMCA sampling

N ₂₀	Pure Aluminum	Addition of MgO inclusion-containing ingot		
		1 st addn	2 nd addn	3 rd addn
Average number of MgO particles (K/Kg)	20.1	46.3	41.4	37.0
Total number of MgO particles (K/Kg)	381.9	786.3	703.8	650.4

C₂₀ Measurements: Volumic concentration of inclusions (inclusions > 20 μm)

Figure 4.23 shows the volumic concentration of MgO inclusions as a function of time. In this case, the more the inclusions added to the melt, the greater the volumic concentrations of inclusions that were detected. The highest volumes of inclusions were detected for the third addition of MgO inclusions. From a volumic concentration of 12545 ppb at the start of sampling, the concentration dropped to 1718 ppb at the end of the 30 min time period.

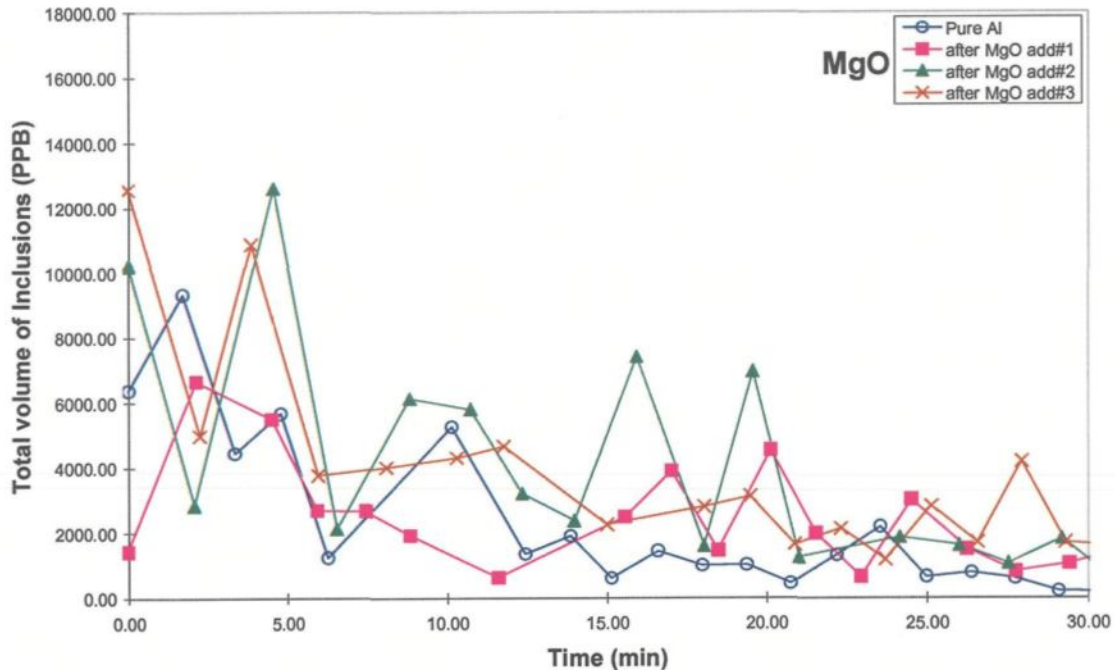


Figure 4.23 Volumic concentration of MgO inclusions in commercial pure aluminum as a function of time.

The density of MgO is 3.58 g/cm^3 compared to 2.71 g/cm^3 for aluminum. Thus it is expected that these inclusions will exhibit a large amount of sedimentation compared to those which have densities comparable to or less than that of aluminum (*e.g.*, Al_4C_3 which has a density of 2.36 g/cm^3).

Figures 4.24 and 4.25 show the distribution plots of the average and total volume of inclusions as a function of particle size. As can be seen, the highest volume of inclusions measured after the first addition lies in the 20-25 μm particle size range. Subsequent additions shift the highest volume concentrations to larger particle sizes. It could be inferred from these two plots that addition of more inclusions results in increasing the

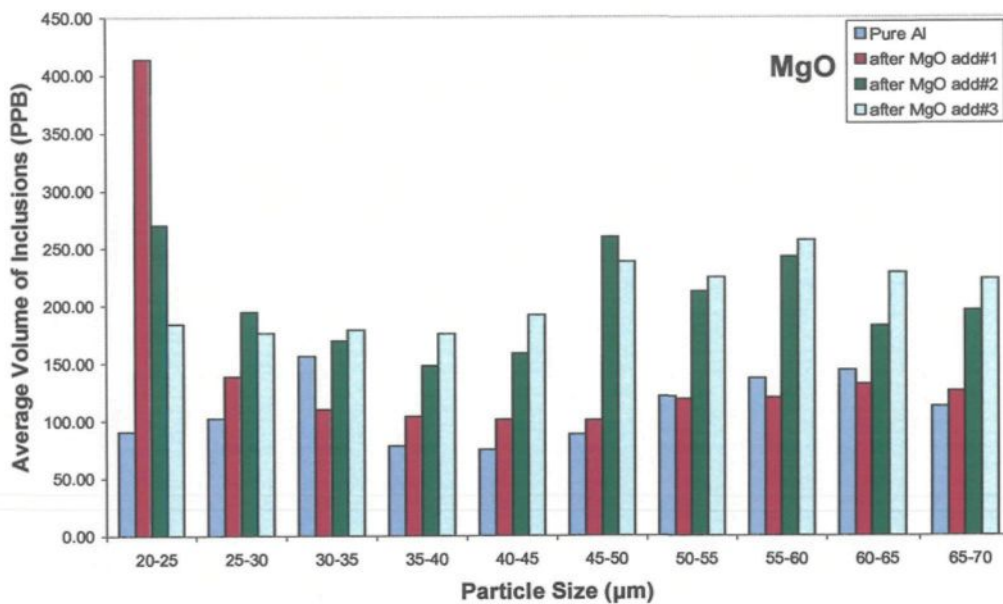


Figure 4.24 Average volume of MgO inclusions in commercial pure aluminum as a function of particle size.

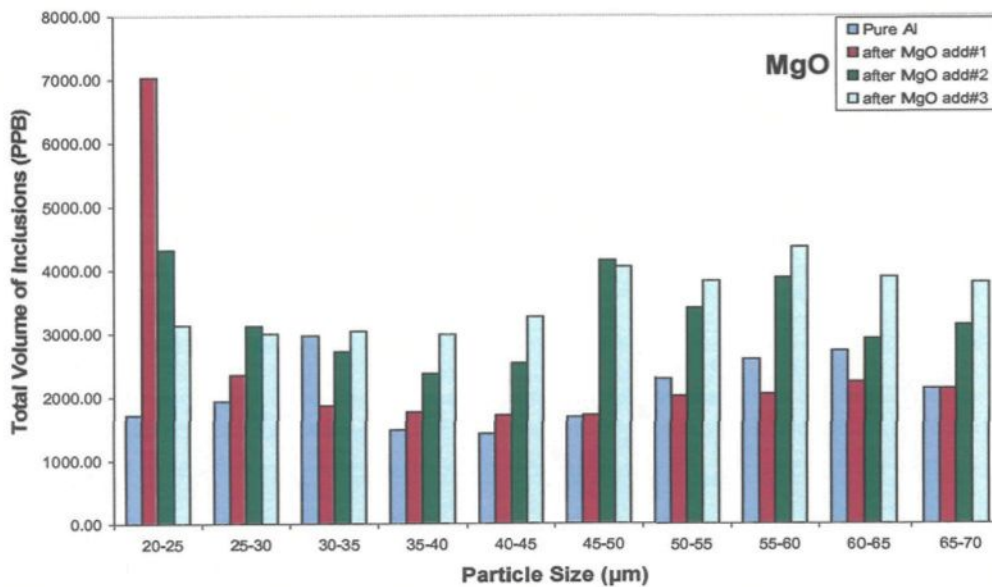


Figure 4.25 Total volume of MgO inclusions in commercial pure aluminum as a function of particle size.

volume of inclusions especially in the upper particle size ranges. In other words, this reflects the capability of the LiMCA to detect not only the changes in inclusion concentration levels in a melt, but also to distinguish between the different sizes of these inclusions.

4.2.5 Evaluation of TiB₂ Inclusions

The addition of TiB₂ inclusions to the pure aluminum melt was also carried out following the same procedures described in Chapter 3, section 3.2.2. The inclusion additions were made in three stages to the pure aluminum melt (8.5 Kg charge at 750 °C temperature). After the first addition, the melt was stirred properly, followed by a LiMCA sampling that was carried on for about 90 min. The second TiB₂ inclusion-containing ingot was added and the same procedure was repeated, followed by the third addition and the corresponding LiMCA sampling. The size of the TiB₂ powder particles used was less than 10 μm.

It ought to be mentioned here that the TiB₂ inclusion levels took a much longer time to reach stable minimum values (as will be shown on Figure 4.27 later on). For this reason, the LiMCA sampling period was extended to 90 min.

N₂₀ Measurements: Total concentration number of inclusions (inclusions > 20 μm)

Figure 4.26 show the distribution of the TiB₂ inclusion concentration during 90 min of LiMCA measurement. As can be seen, in the case of the first addition, the inclusion levels shoot up between ~19 and ~30 min, representing much higher numbers of inclusions than those observed on either side of this interval. These peaks are, in fact, erroneous readings that resulted from the accumulation of the particles and blocking of the probe tube hole during measurement as, while the inclusion concentrations showed high values at these points, the electrical resistance readings corresponding to these points were not changed in comparison to the electrical resistance readings before and after.

Thus, these peaks should not be taken into consideration when analyzing the results. It is suggested that in such cases, instead of referring directly to the N₂₀ plots (on-line results given by LiMCA), the collective data obtained (*i.e.* inclusion concentrations and the corresponding electrical resistance values) should be examined to analyze the results. For example, Figure 4.27 shows a modified version of Figure 4.26 after the erroneous points were eliminated. As can be seen, this facilitates interpretation of the results.

As Figure 4.27 shows, the number of inclusions in pure aluminum decreased after 30 min of testing, reaching a steady state condition thereafter, with no fluctuation in the inclusion level. The first addition of TiB₂ inclusions to the melt increased the number of inclusions detected and it took a longer time for the inclusion concentrations to reach the lowest level.

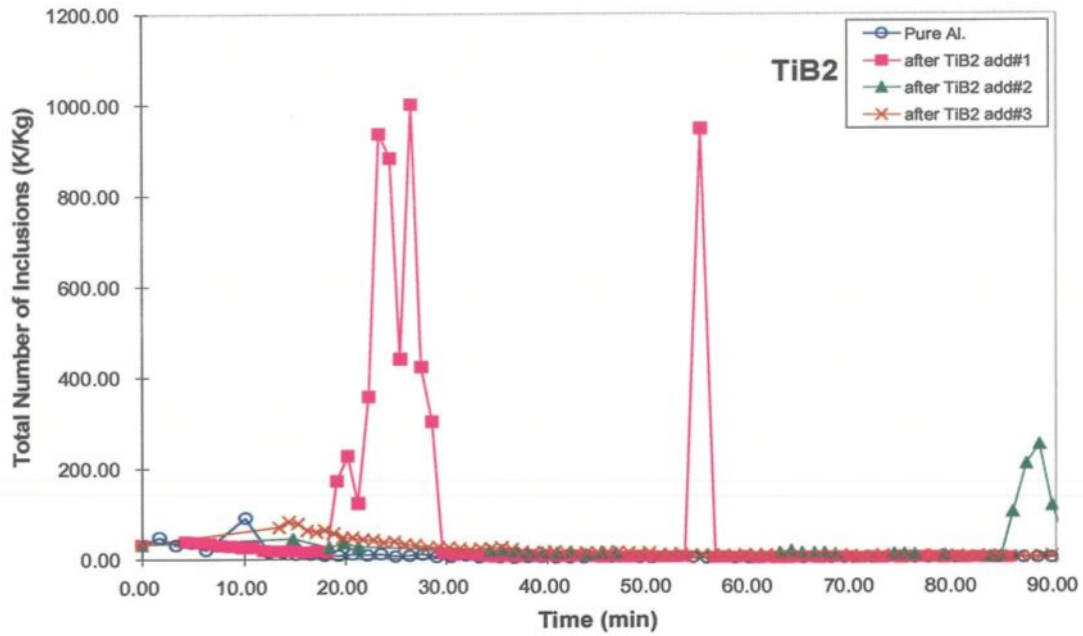


Figure 4.26 Concentration number of TiB_2 inclusions in commercial pure aluminum as a function of time.

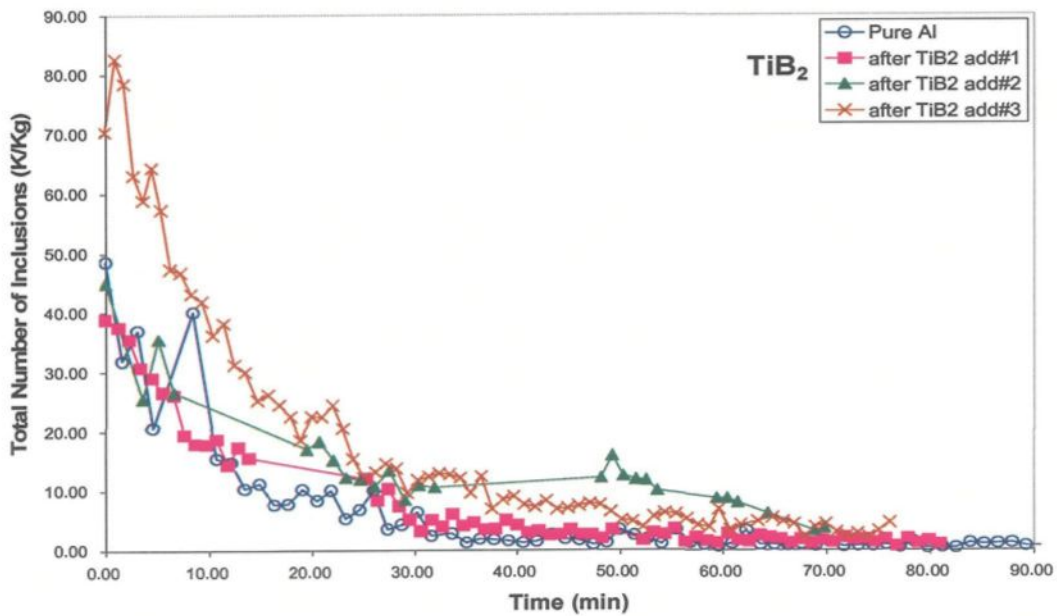


Figure 4.27 Modified version of Figure 4.26 after elimination of erroneous readings.

In the case of the second and third inclusion additions, the same trend was observed. However, some increase in inclusion levels was also observed after 60 min of testing, following which the levels dropped and reached their lowest values. The increase in TiB₂ concentration levels with the third inclusion addition stage is worth nothing.

Figures 4.28 and 4.29 show the average and total inclusion concentrations as a function of particle size (after eliminating the incorrect peak points of Figure 4.26). The highest numbers of inclusions were detected in the 20-25 μm range, in spite of the primary particle size of TiB₂ inclusions being less than 10 μm. Comparison of the average and total number of inclusions of pure aluminum with those of the three consecutive TiB₂ inclusion additions indicates that these inclusions disperse in the melt and have less tendency to agglomerate.

Secondly, even with the increase in the concentration of inclusions with the second and third addition of inclusions to the melt, the LiMCA can properly detect the corresponding higher number of inclusions observed in the 20-25 μm particle size range.

On the other hand, in the larger particle size range, the inclusion levels measured decrease with the third addition. This can properly be attributed to the settling of TiB₂ particles due to the large difference in their density (4.5-4.62 g/cm³) compared with aluminum (2.71 g/cm³).

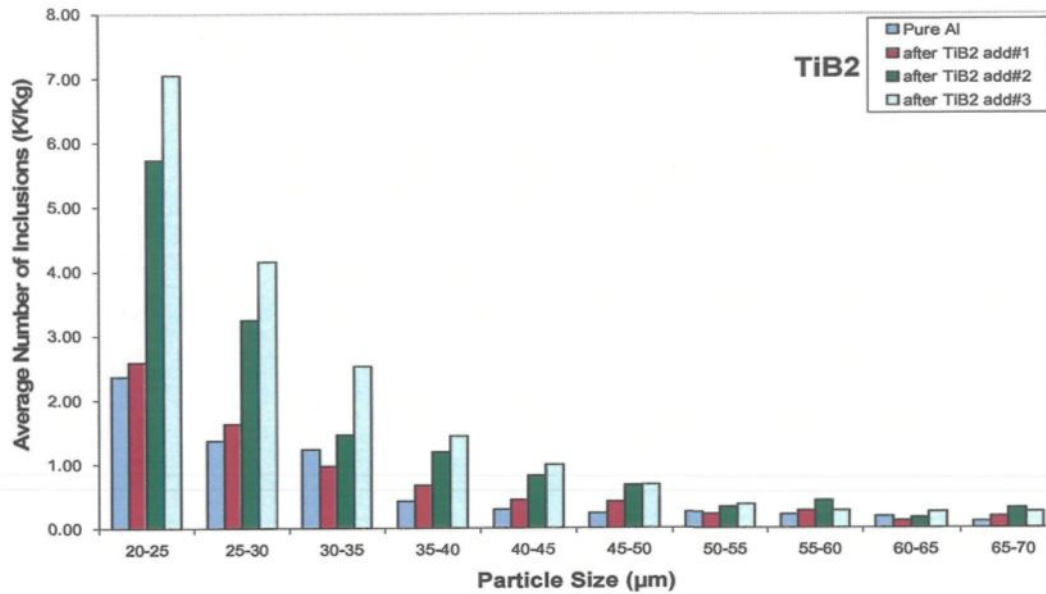


Figure 4.28 Average number of TiB₂ inclusions in commercial pure aluminum as a function of particle size.

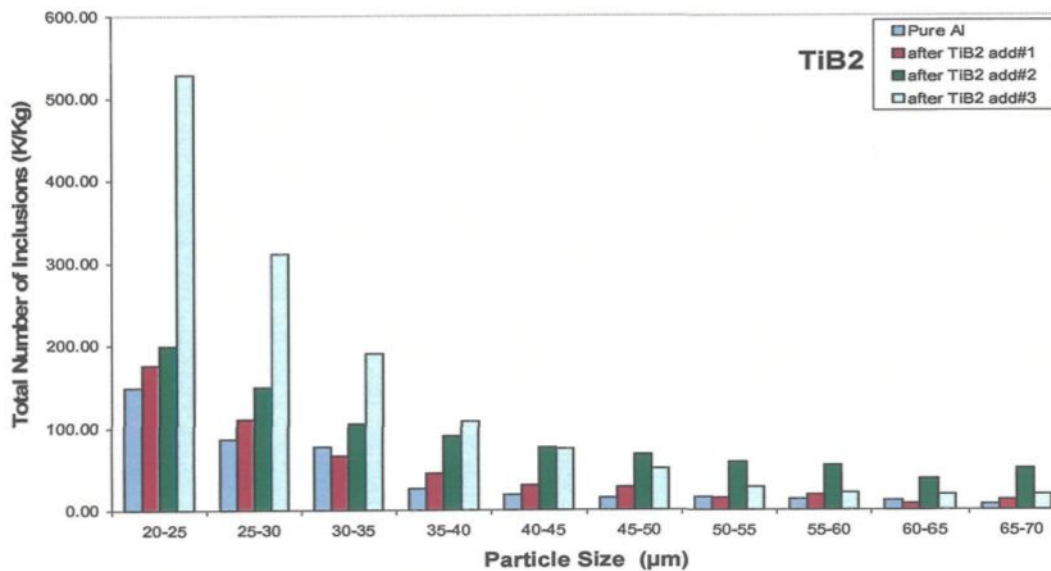


Figure 4.29 Total number of TiB₂ inclusions in commercial pure aluminum as a function of particle size.

C₂₀ Measurements: Volumic concentration of inclusions (inclusions >20 μ m)

Figure 4.30 shows the volumic concentration of TiB₂ inclusions as a function of time, over the 90 min period of the LiMCA test. Similar to the N₂₀ plot shown in Figure 4.26, a number of peaks are observed in the curve corresponding to the first TiB₂ addition, which are, infact, erroneous readings that resulted from the accumulation/blocking of particles in the probe tube hole during measurement. Analyzing the corresponding electrical resistance data, the data of Figure 4.30 was modified accordingly and correct representation is shown in Figure 4.31, after elimination of the erroneous points.

As Figure 4.30 shows, most of the inclusions settle down in the melt after about 40 min of sampling time. Also, the third TiB₂ inclusion addition displays higher volumic concentrations than the previous two additions during the first 30 min of testing.

Figures 4.32 and 4.33 show the distribution plots of the average and total volume of TiB₂ inclusions as a function of particle size. Figure 4.32 shows that, the more the inclusions added to the melt, the more the particles are clustered together, increasing the volume concentration readings for the third addition compared to the first. For the third addition, the highest volume concentrations are read by the LiMCA over all particle size ranges. In a way, this indicates that the TiB₂ inclusions are well dispersed within the melt and the LiMCA accordingly measures their increased concentrations in the melt.

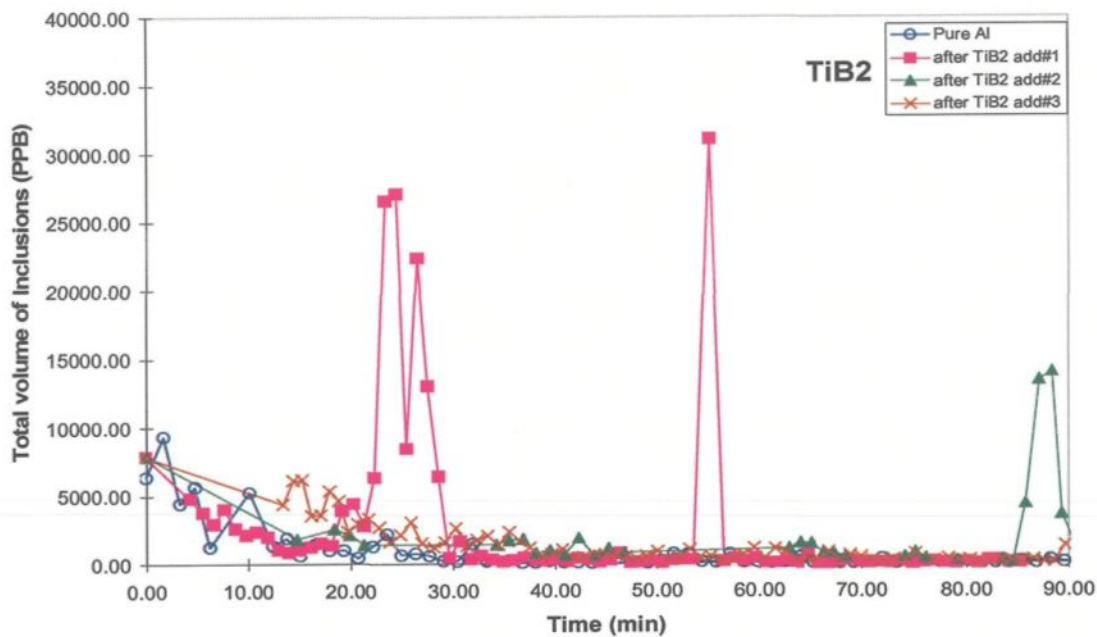


Figure 4.30 Volumic concentration of TiB_2 inclusions in commercial pure aluminum as a function of time.

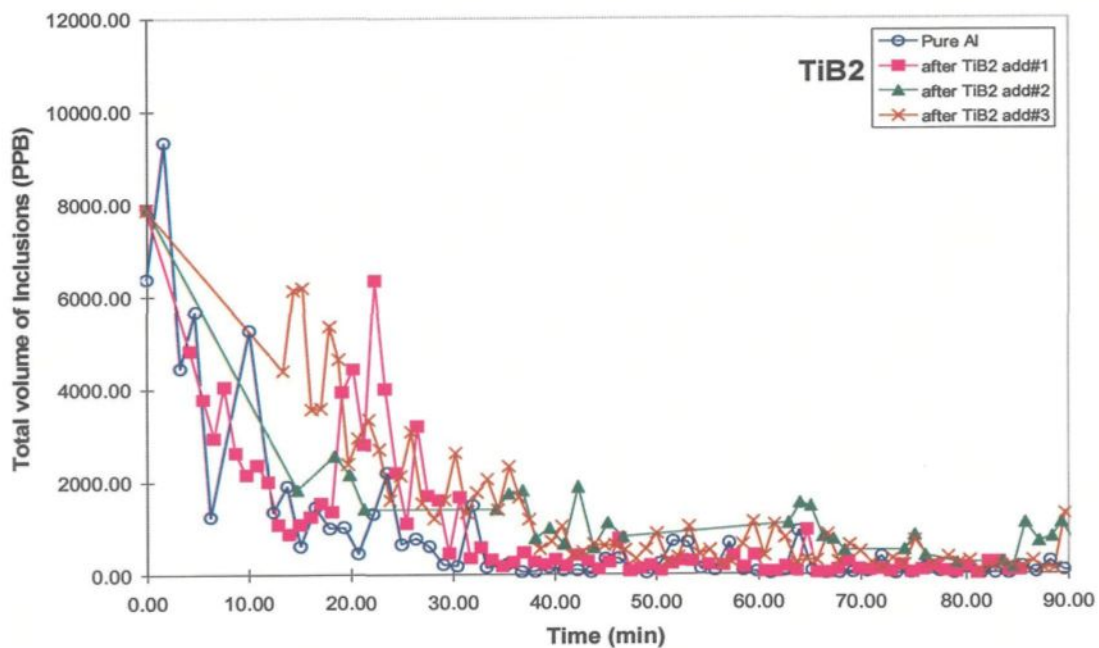


Figure 4.31 Modified version of Figure 4.30 after elimination of erroneous readings.

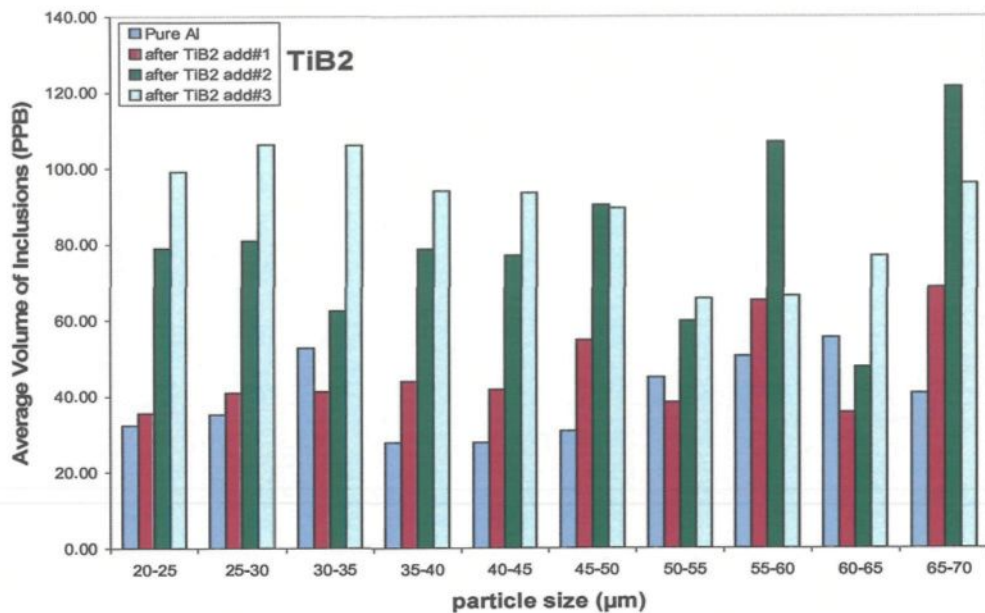


Figure 4.32 Average volume of TiB₂ inclusions in commercial pure aluminum as a function of particle size.

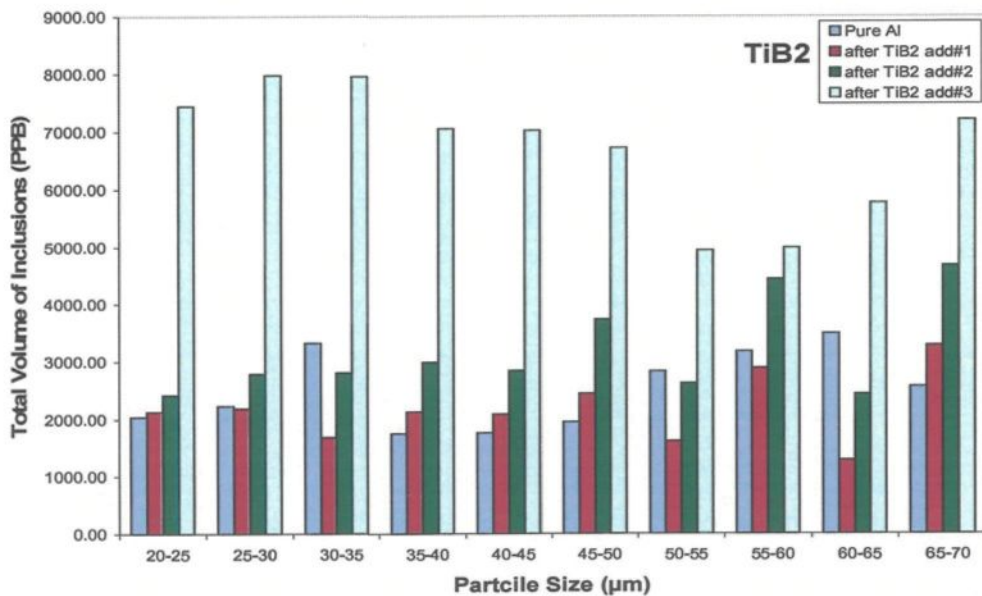


Figure 4.33 Total volume of TiB₂ inclusions in commercial pure aluminum as a function of particle size.

4.3 COMPARISON OF DIFFERENT INCLUSION ADDITIONS

A summary of the N_{20} plots (total number of inclusions vs. time) obtained for the various inclusion additions that were made to pure aluminum melts at 750 °C melt temperature is provided in Figure 4.34, while Figure 4.35 exhibits the same total concentration levels as a function of the particle size range.

As can be seen, the maximum number of inclusions are observed in the case of the Al_2O_3 inclusions, followed by the Al_4C_3 inclusions. Other inclusions show concentration levels close to the base level observed in the pure aluminum melt without any addition, with the CaO inclusions exhibiting the lowest values among them. The CaO particles are very fine and most of these particles were scattered in the air during the injection process. Thus, the ingots resulting from injection of CaO powder probably contained a small amount of inclusions; consequently, the LiMCA detected the lowest amount of these inclusions.

Most of the inclusions were detected in the lower available range of LiMCA, between 20-25 μm . On the other hand, the primary particle size of the powders used was, in most cases, less than 10 μm . This shows the detection accuracy of LiMCA with respect to small particle sizes.

The almost negligible values in the larger particle size ranges (50-55 μm and above) observed in Figure 4.35 can be variously explained by i) the effects of agglomeration of the particles, ii) their settling with the progress of time and thus their non-availability in the ESZ region of the LiMCA for detection, and iii) the difference in density between the inclusion type(s) and the pure aluminum melt.

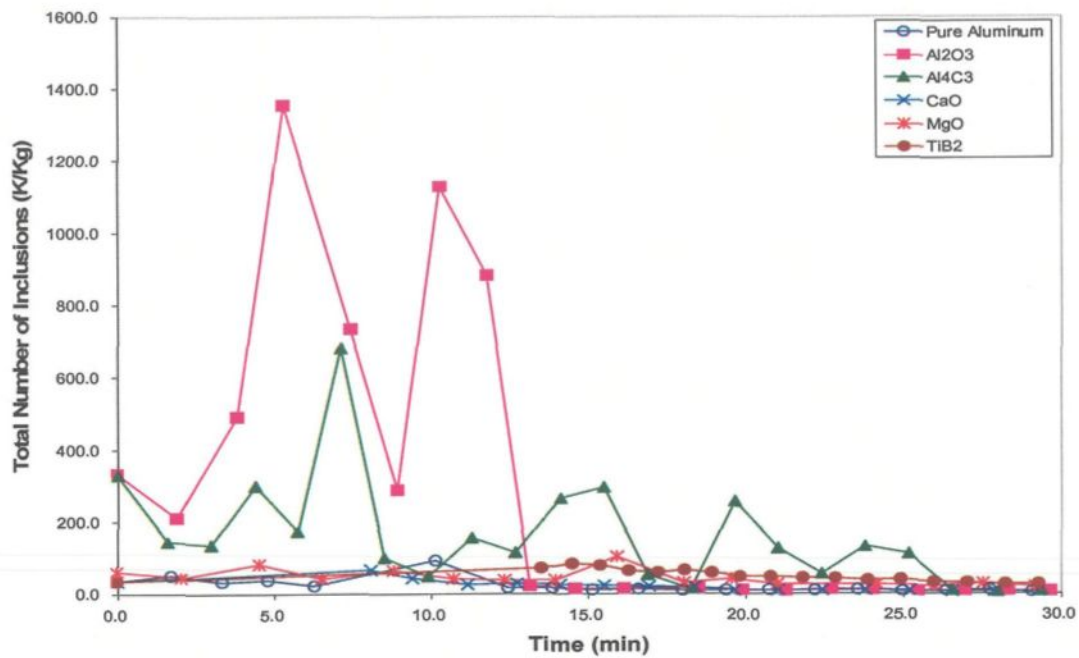


Figure 4.34 Comparison of different inclusions added to commercial pure aluminum as a function of time.

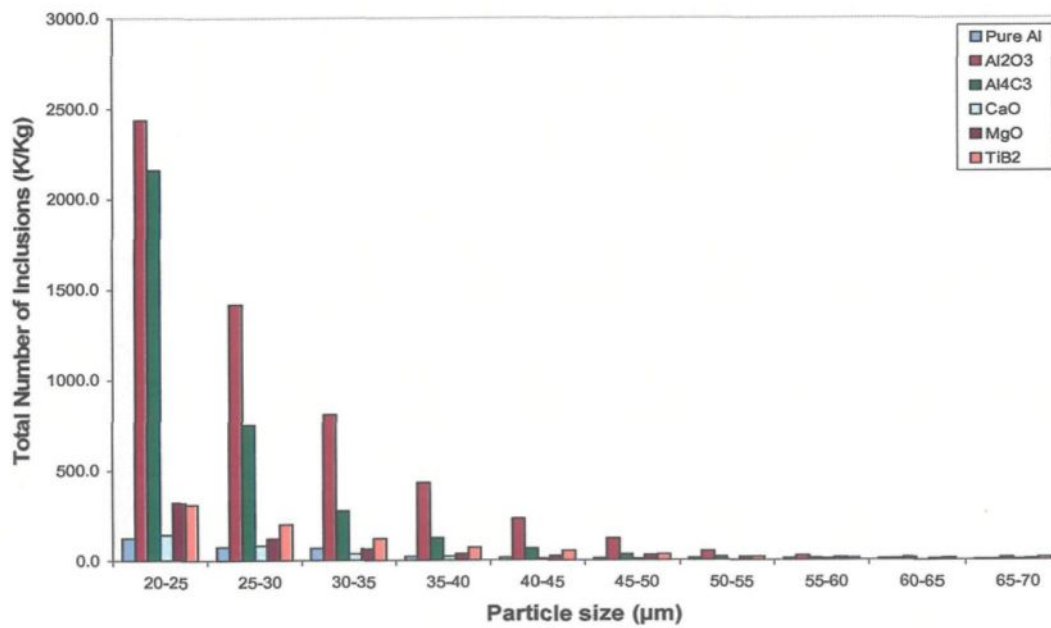


Figure 4.35 Comparison of different inclusions added to commercial pure aluminum as a function of particle size.

4.4 EVALUATION OF INCLUSIONS IN PURE ALUMINUM AT 680 °C

As in the previous cases, a charge of 8.5 Kg pure aluminum was melted in a SiC crucible using an electric resistance furnace. The melt temperature, however, was kept at 680 °C. Degassing was carried out for 15 min using pure, dry argon. Inclusion additions were carried out in one step.

A measured amount of the specific inclusion type was added to the melt, and the melt stirred to achieve homogeneous dispersion of the inclusions. Following this, a few (3-4) LiMCA samplings were taken for each inclusion added, to obtain a better average. Each LiMCA sampling was done for a period of 30 minutes, with readings taken at every 1-2 min intervals. The LiMCA data obtained from these samplings were plotted in the form of N_{20} and C_{20} graphs showing, respectively, the total number of inclusions and the volumic concentration of inclusions as a function of time. As mentioned in section 4.1, only three LiMCA tests were carried out for pure aluminum at 680 °C melt temperature: for CaO, MgO and $TiAl_3$ inclusion additions.

4.4.1 Evaluation of CaO Inclusions

The addition of CaO inclusions to the pure aluminum melt was carried out using prefabricated CaO inclusion-containing aluminum ingot. The procedure for the preparation of such inclusion-containing ingots using the powder injection technique has already been described in Chapter 3, section 3.2.2. For the experiments carried out at 680 °C melt temperature, one inclusion-containing ingot was prepared for each powder inclusion type that was studied. This ingot was added to the pure aluminum melt (8.5 Kg

charge at 680 °C temperature). The primary size of the CaO powder particles used was less than 10 μm .

N₂₀ Measurements: Total concentration number of inclusions (inclusions > 20 μm)

Figure 4.36 compares the concentration number of inclusions in pure aluminum with those in the CaO-containing melt at 680 °C, as a function of time. After 20 minutes of testing, most of the inclusions settle to the bottom of the crucible. The CaO inclusions decrease from their initial level of 147 K/Kg to 6.1 K/Kg, while in commercial pure aluminum the level of inclusions decreases from 54.5 to 2.8 K/Kg, reaching the minimum within 20 min only. As will be shown later on in Chapter 5, compared to the level of CaO inclusions obtained in the Al-Si base alloy, the commercial pure aluminum melt gives a lower level of inclusions. Figure 4.37 shows the inclusion distribution in the two cases, as a function of particle size.

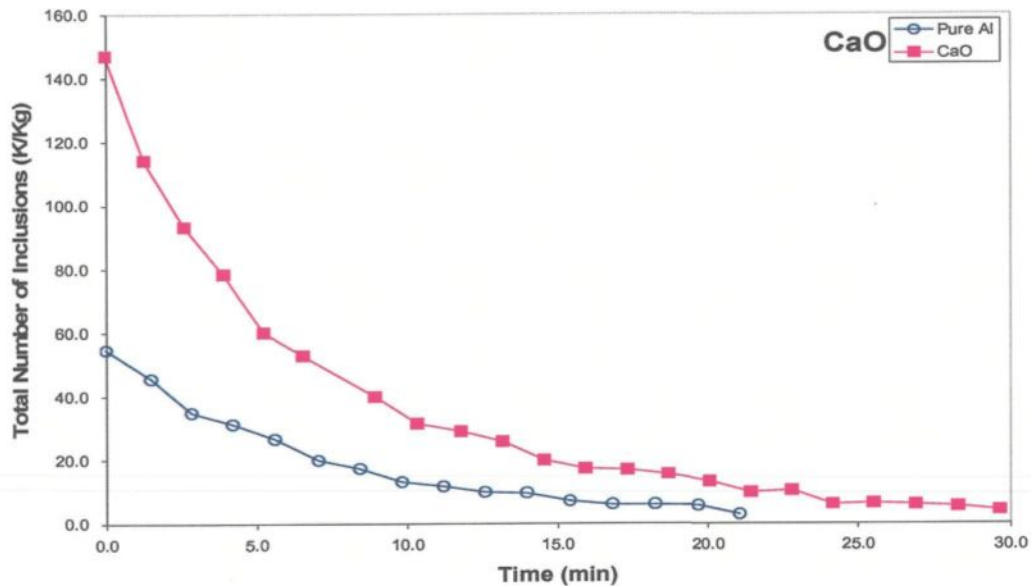


Figure 4.36 Concentration number of CaO inclusions in commercial pure aluminum as a function of time.

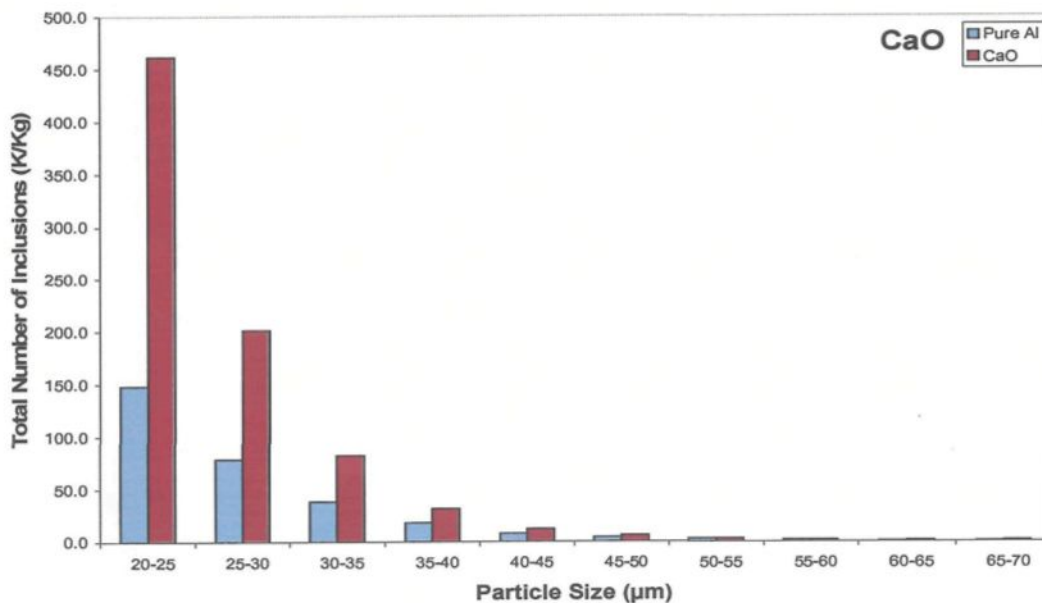


Figure 4.37 Total number of CaO inclusions in commercial pure aluminum as a function of particle size.

C₂₀ Measurements: Volumic concentration of inclusions (inclusions >20 μ m)

Figures 4.38 and 4.39 show the volumic concentration of inclusions vs. time and as a function of particle size, respectively. These two graphs are very similar to those for the concentration number of inclusions. The volumic concentration of inclusions drops to its lowest level after 20 min of testing, and the highest levels of inclusions are detected in the 20-25 μ m particle size range.

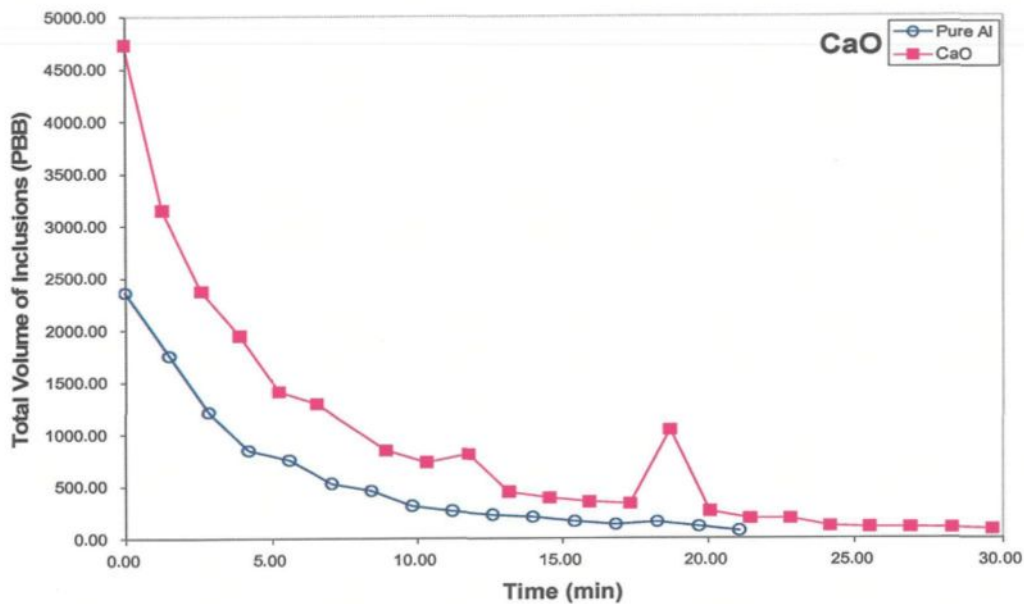


Figure 4.38 Volumic concentration of CaO inclusions in commercial pure aluminum as a function of time.

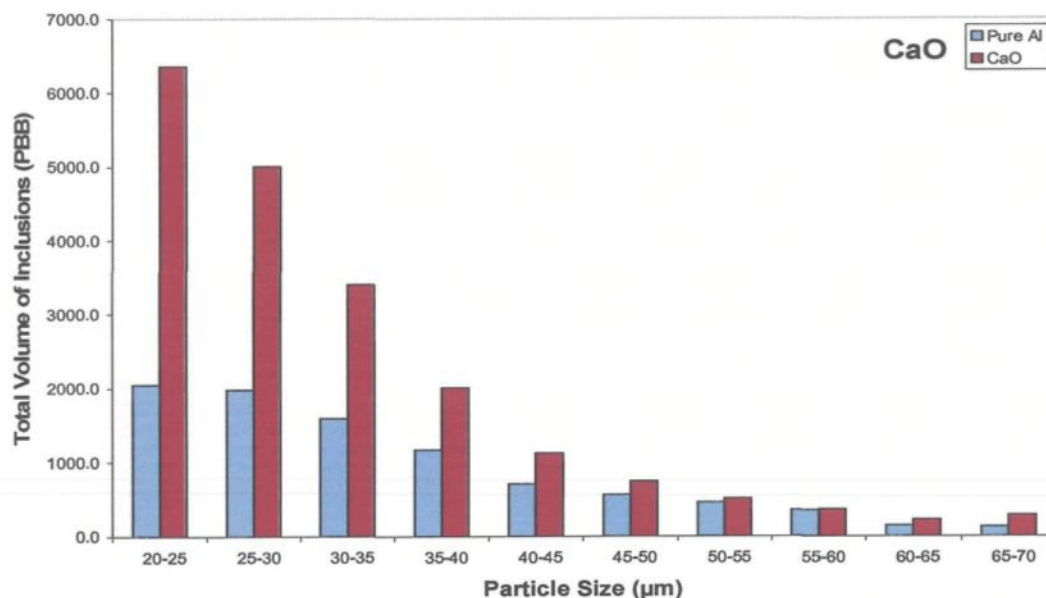


Figure 4.39 Total volume of CaO inclusions in commercial pure aluminum as a function of particle size.

4.4.2 Evaluation of MgO Inclusions

The addition of MgO inclusions to the pure aluminum melt was carried out using the prefabricated MgO inclusion-containing aluminum ingot. The procedure for preparing the latter was the same as that described in Chapter 3, section 3.2.2. As before, an 8.5 Kg charge of pure aluminum was melted at 680 °C; degassing was carried out for 15 min using pure, dry argon. A LiMCA sampling of the melt was done.

Next, the MgO inclusion-containing ingot was added to the melt, and the melt was stirred to incorporate the inclusions homogeneously within the melt. Four LiMCA samplings were taken, with the melt temperature maintained at 680 °C. The primary size of the MgO powder particles used was less than 70 μm.

N₂₀ Measurements: Total concentration number of inclusions (inclusions > 20 μ m)

Figures 4.40 and 4.41 show the plots of the concentration number of MgO inclusions vs. time and as a function of particle size. It is worth noting that the slope of the curves in Figure 4.40 are similar, with only a slight difference in their levels. This indicates the repeatability and reliability of the LiMCA samplings taken from the same melt.

C₂₀ Measurements: Volumic concentration of inclusions (inclusions > 20 μ m)

Figures 4.42 and 4.43 show the plots of volumic concentration of inclusions vs. time and vs. particle size, respectively. In each sampling, the volume concentration of inclusions dropped gradually after 20 min to its lowest level. Also the highest levels of inclusions were detected in the 20-25 μ m particle size range.

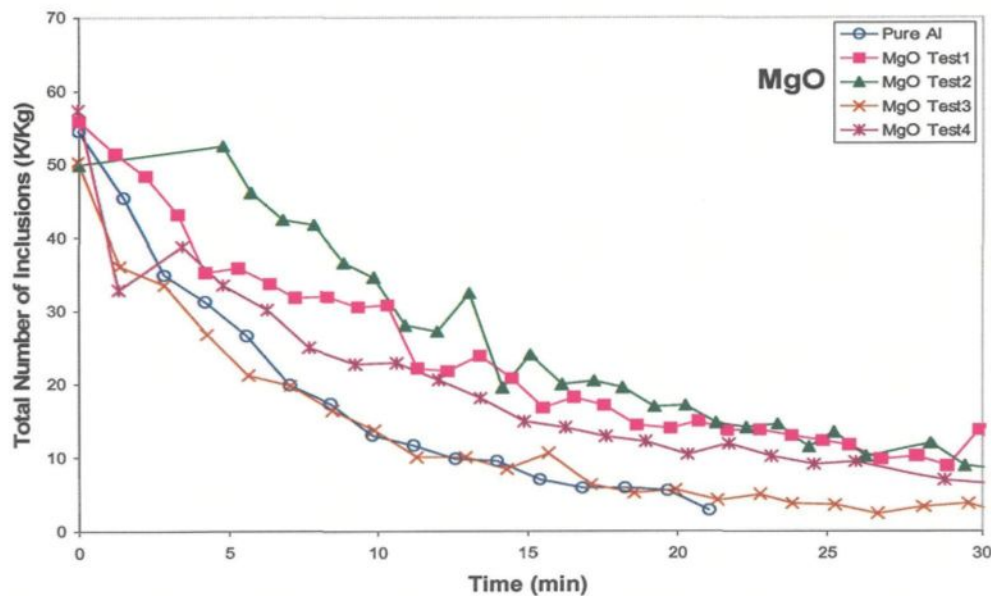


Figure 4.40 Concentration number of MgO inclusions in commercial pure aluminum as a function of time.

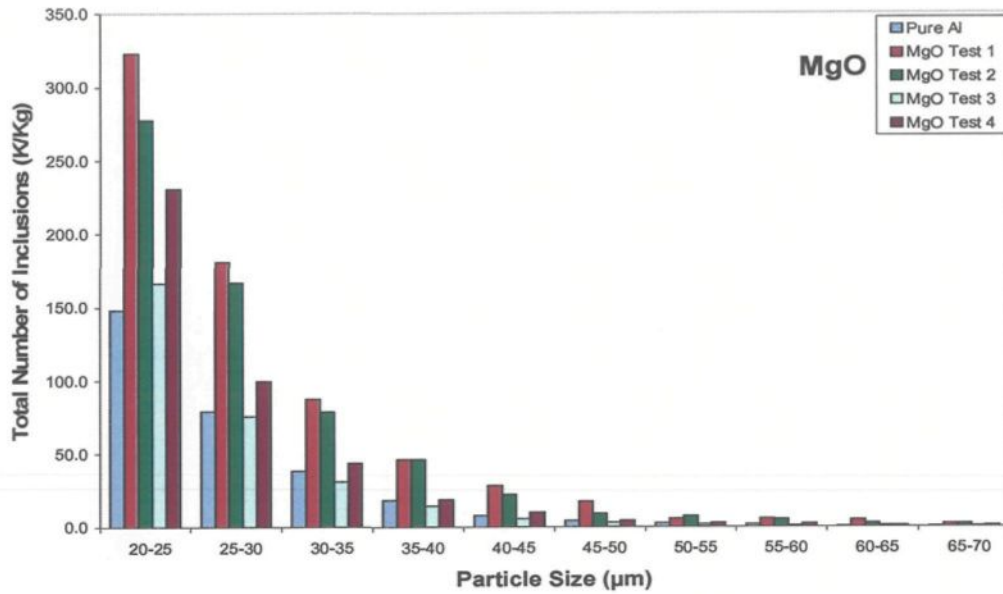


Figure 4.41 Total number of MgO inclusions in commercial pure aluminum as a function of particle size.

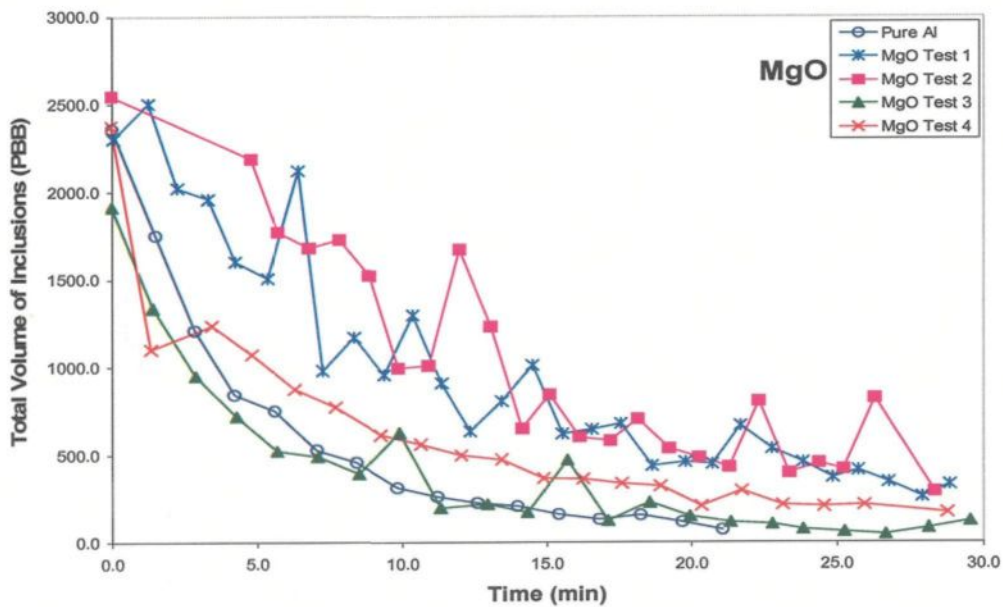


Figure 4.42 Volumic concentration of MgO inclusions in commercial pure aluminum as a function of time.

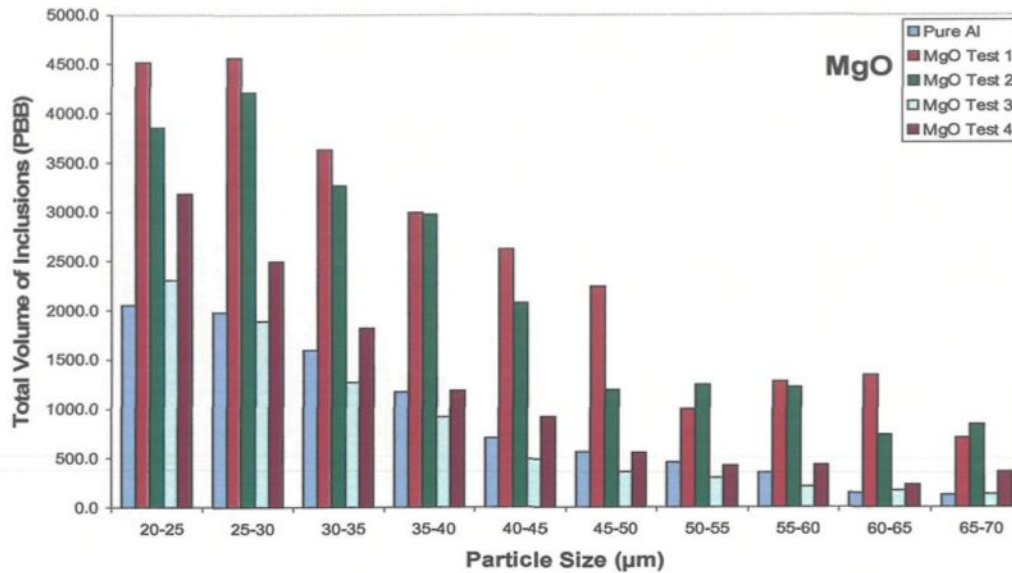


Figure 4.43 Total volume of MgO inclusions in commercial pure aluminum as a function of particle size.

4.4.3 Evaluation of $TiAl_3$ Inclusions

As in the previous cases, the crucible was charged with 8.5 Kg of commercial pure aluminum and melted. The melt temperature was kept at 680 °C and the melt was degassed for 15 minutes. A LiMCA sampling was done to obtain information about the inclusion levels in the commercial pure aluminum as a reference. A specified amount of Al-10% Ti master alloy (250 g) was then added to the melt. The temperature of the melt was maintained at 680 °C, and the melt was properly stirred. Following this, a LiMCA sampling was taken to obtain the concentration levels of the $TiAl_3$ inclusions in the melt.

N₂₀ Measurements: Total concentration number of inclusions (inclusions > 20 μ m)

Figures 4.44 and 4.45 show the two plots related to the concentration number of TiAl₃ inclusions as a function of time and of particle size. The level of TiAl₃ inclusions did not completely drop during 30 min: the level decreased moderately from 60.1 to 19.4 K/Kg after 30 min of testing (the latter value is not seen on the plot), while in case of commercial pure aluminum, after about 20 min, the level of impurities decreased from 54.5 to 2.8 K/Kg. Also, TiAl₃ inclusions were observed clearly in all particle size ranges.

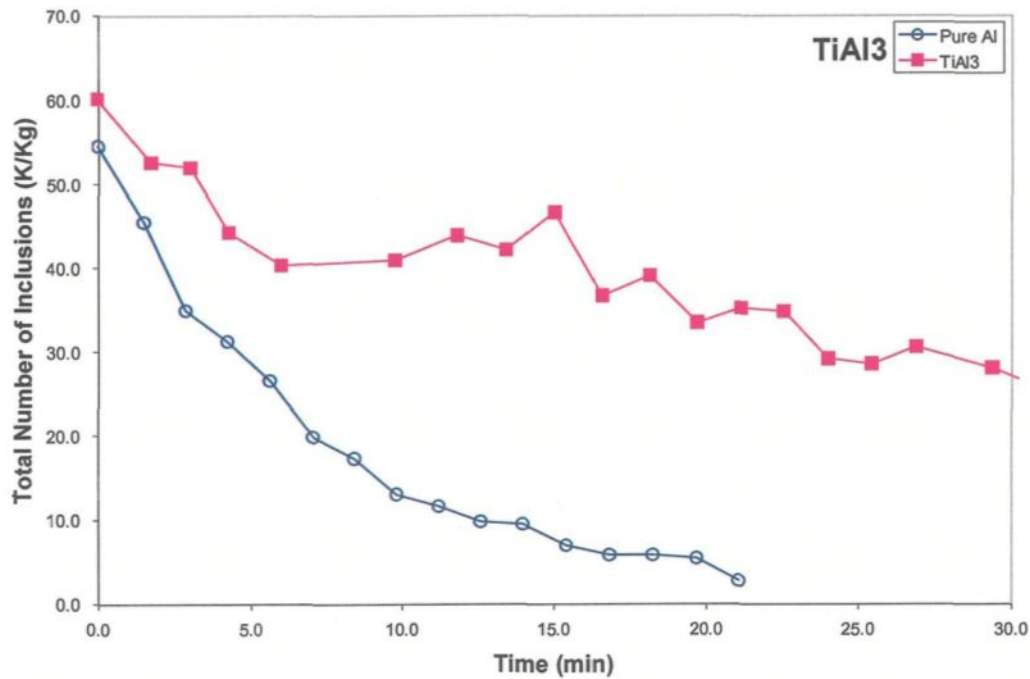


Figure 4.44 Concentration number of TiAl₃ inclusions in commercial pure aluminum as a function of time.

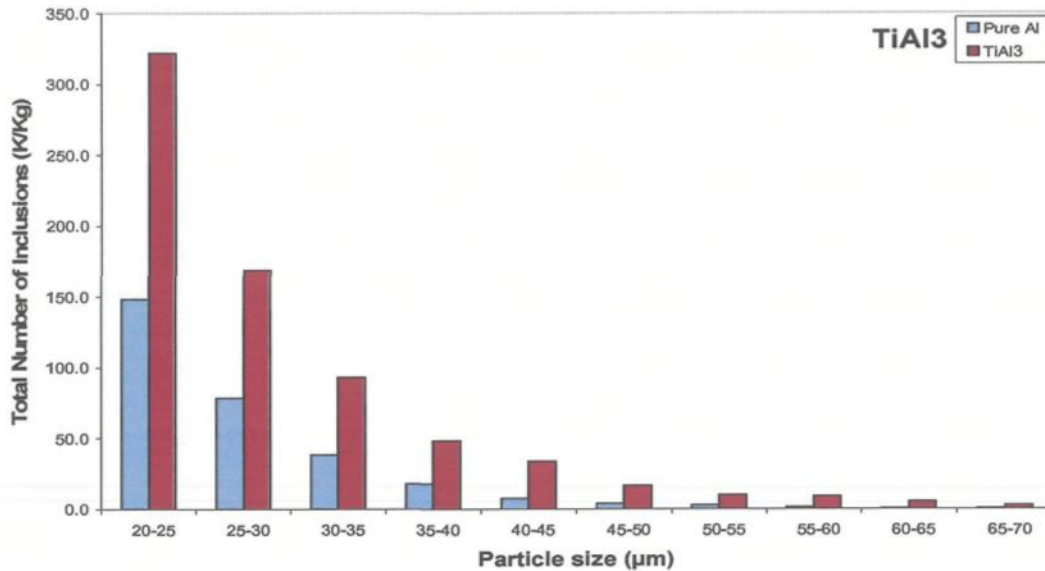


Figure 4.45 Total number of TiAl_3 inclusions in commercial pure aluminum as a function of particle size.

C₂₀ Measurements: Volumic concentration of inclusions (inclusions >20μm)

Figures 4.46 and 4.47 show the volumic concentrations of inclusions vs. time and as a function of particle size. The volume concentration of inclusions, Figure 4.46, like the concentration number of inclusions, shows no abrupt drop in level after 30 min. Figure 4.47 shows the volumic concentration of TiAl_3 inclusions for different particle sizes. It is worth noting that, in this case, the volume of TiAl_3 inclusions remains comparatively high in all particle size ranges, whereas in the case of other inclusions, the higher particle size ranges showed low volumes.

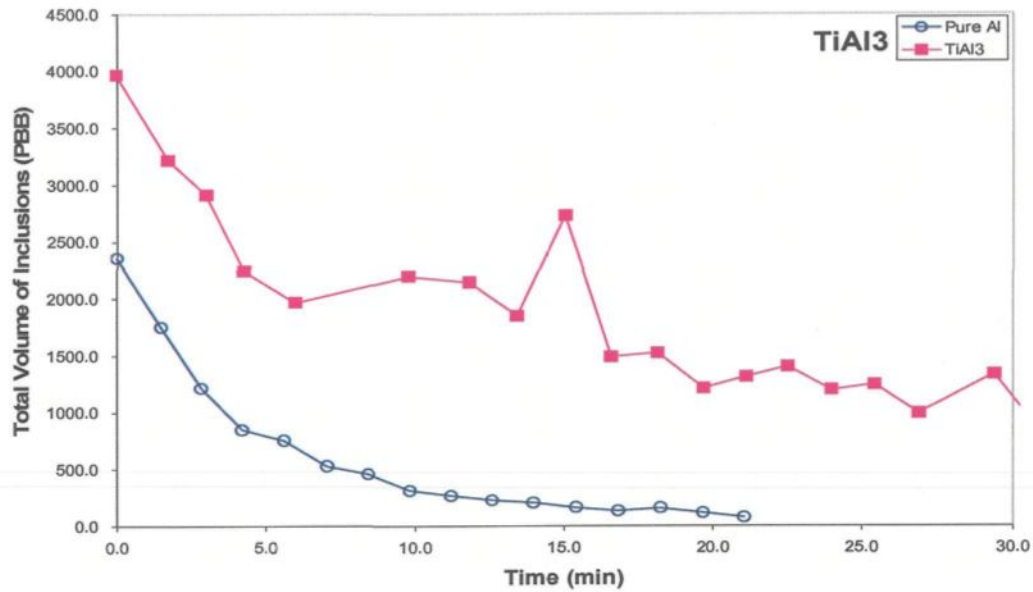


Figure 4.46 Volumic concentration of TiAl_3 inclusions in commercial pure aluminum as a function of time.

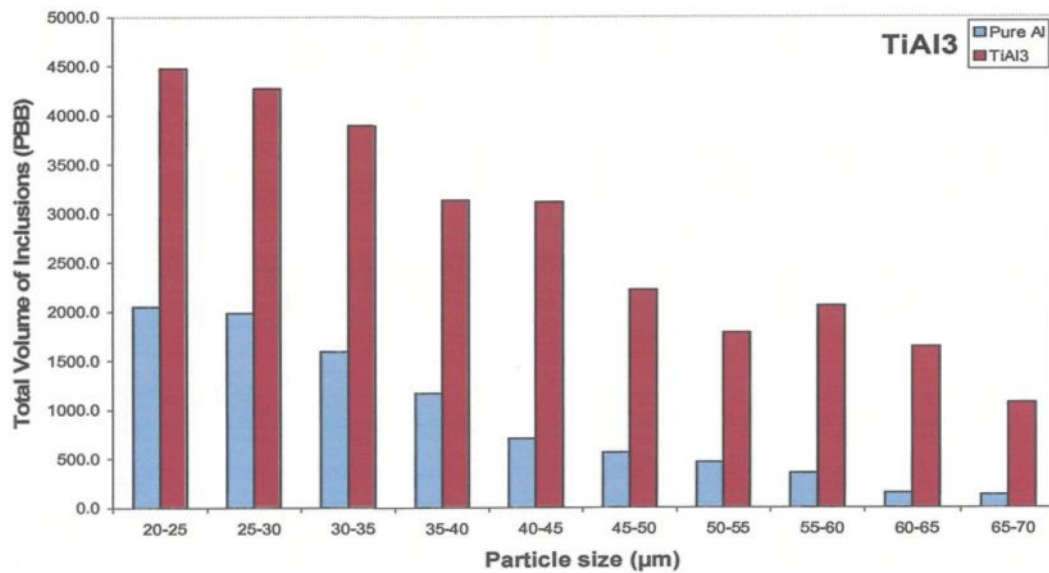


Figure 4.47 Total volume of TiAl_3 inclusions in commercial pure aluminum as a function of particle size.

CHAPTER 5

EVALUATION OF INCLUSIONS IN Al-6%Si ALLOY MEASURED

BY LiMCA AT 750 °C

CHAPTER 5

EVALUATION OF INCLUSIONS IN Al-6%Si ALLOY MEASURED BY LiMCA AT 750 °C

5.1 INTRODUCTION

This chapter presents the results on the evaluation of different inclusion types in Al-6%Si alloy melts, as measured by the LiMCA technique.

The Al-6%Si alloy used was prepared experimentally by adding pure silicon (99.987%) to commercially pure aluminum (99.78%). A 120 Kg charge of pure aluminum was melted in a 150 kg-capacity electric resistance furnace. The melt temperature was kept at 750 °C. The calculated amount of pure silicon was added to the melt. The melt was stirred using a rotary impeller, then held at the same temperature for about 2-3 hours to allow proper dissolution of the silicon into the melt.

Degassing was carried out using pure, dry argon for about 30 min, using the same rotary impeller. The Al-6%Si melt was poured into ingot molds. The ingots so prepared were kept aside for further use.

Specified amounts of each inclusion type were added to pre-heated melts of the Al-6%Si alloy, as described in Chapter 4. For this, inclusion-containing ingots of Al-6% alloy were first prepared for the various inclusion types that were studied, where the powder

injection technique was used in the case of powder inclusions, while those added in the form of master alloy or pure metal were added directly to the melt, in the calculated amounts. The inclusion-containing ingots were then used to introduce the specified inclusion type into a fresh Al-6%Si alloy melt for conducting the LiMCA tests.

Again, as in the case of the pure aluminum experiments, two melt temperatures were used, 750 °C and 680 °C, corresponding to high and low melt superheat conditions. After conducting all the LiMCA tests for the Al-6%Si alloy melts at the two melt temperatures, it was found that the experiments carried out at 680 °C provided far better results with respect to both repeatability and consistency of the measurements.

This is one of the important recommendations derived from the present study, that the LiMCA measurements in aluminum alloys should be conducted at melt temperatures of 680 °C or thereabouts (*i.e.*, up to 690°/695°C). In view of the importance of these results, they will be presented separately in Chapter 6. The LiMCA tests carried out at 750 °C are presented in this chapter.

5.2 EVALUATION OF INCLUSIONS IN Al-6%Si ALLOY AT 750 °C

A charge of 8.5 kg of Al-6%Si alloy was melted in a SiC crucible using an electric resistance furnace. The melt temperature was kept at 750 °C. Degassing was carried out for 15 min using a rotary impeller and pure, dry argon.

Inclusion additions were carried out in three successive steps as follows.

- (i) A measured amount of a specific inclusion type (~500 g) was added to the melt, and the melt stirred to achieve a homogeneous dispersion of the inclusions. Following this, a LiMCA sampling was taken.
- (ii) A second addition of the same inclusion type (~500 g) was added to the same melt and after stirring of the melt, a LiMCA sampling was taken to measure the inclusion content corresponding to the increased addition.
- (iii) A third addition (~500 g) was made to the same melt, and the same procedures were followed.

The LiMCA data obtained from the above three samplings were plotted in the form of graphs showing (i) the total number of inclusions and (ii) the volume concentration of inclusions as a function of time (*viz.*, N_{20} and C_{20} plots, respectively).

A schematic system of the inclusion additions and LiMCA sampling procedure is shown in Figure 5.1 for the addition of Al_4C_3 inclusions as an example. It is to be mentioned here that each LiMCA sampling was done over a period of 60 minutes, and readings were taken at every 1-2 min intervals.

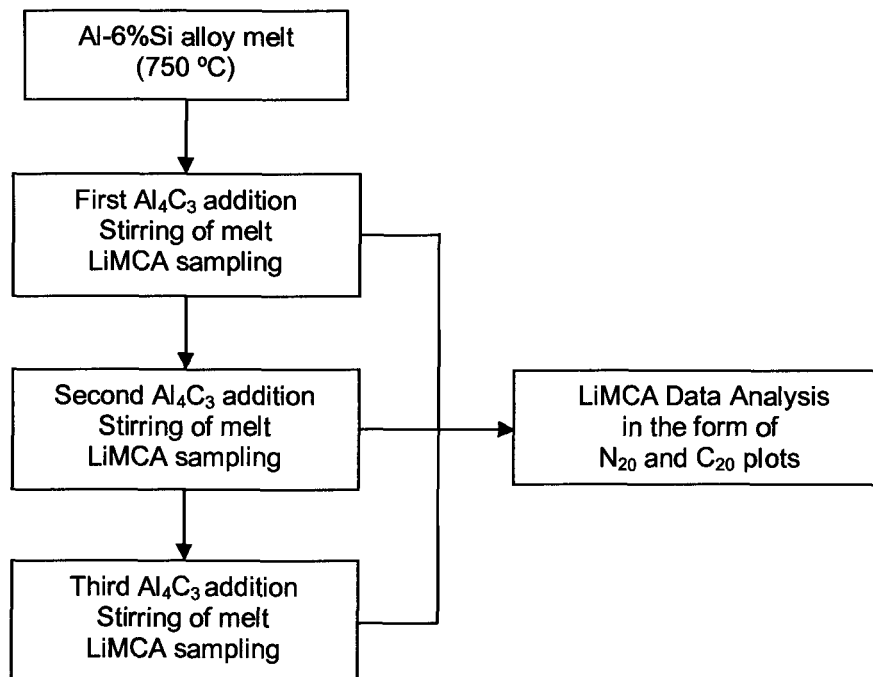


Figure 5.1 Schematic of inclusion addition to the Al-6%Si alloy melt.

5.2.1 Evaluation of Al_2O_3 Inclusions

Following the procedures outlined in the previous section, the Al_2O_3 inclusions were added to the Al-6%Si alloy melt (maintained at 750 °C) in the form of an aluminum metal matrix composite containing Al_2O_3 as the particulate reinforcement.

N_{20} Measurements: Total concentration number of inclusions (inclusions > 20 μm)

Figure 5.2(a) shows the N_{20} plot of the total number of inclusions as a function of time over 60 min of testing. It was found that, in the case of Al-6%Si alloy melts, there appeared to be an initial period of about 20 min before the inclusion levels began to be detected properly, compared to the N_{20} plots for the pure aluminum melts. Accordingly, in Figure 5.2(a), the Al-6%Si base alloy melt shows a low concentration of inclusions, following which the inclusion levels jump to much higher levels with the first addition of

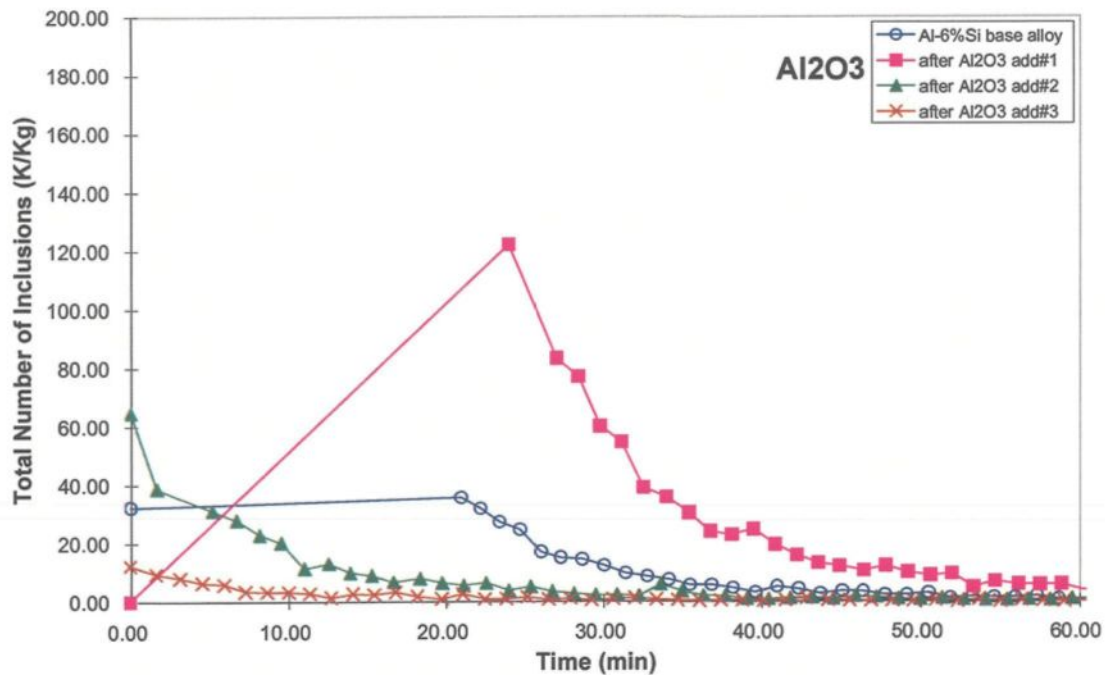


Figure 5.2 (a) Concentration number of Al₂O₃ inclusions in Al-6%Si alloy as a function of time.

Al₂O₃ inclusions. Stabilization is reached after about 40 min for the base alloy, while that for the first addition of Al₂O₃ inclusions is reached after about 55 min. In comparison, the second and third additions show extremely low to almost negligible inclusion concentrations over most of the testing period. This may be accounted for by the sedimentation of the alumina particles due to their high density (3.69-3.99 g/cm³) compared to that of the base alloy melt (2.67 g/cm³), accelerated as well by the increased probability for agglomeration of the inclusions with the increased additions.

The delay in reading by the LiMCA for the base alloy and the first addition could be related to the calibration of the machine with respect to the quantity and the random positioning of the inclusion particles in the ESZ region of the probe tube. In order to facilitate evaluation of the results, the first sampling point giving the highest reading is displaced to the starting point (*i.e.*, origin). Figure 5.2 (b) shows the corrected distribution of inclusions after displaying the starting points for the base alloy and the first addition to the left.

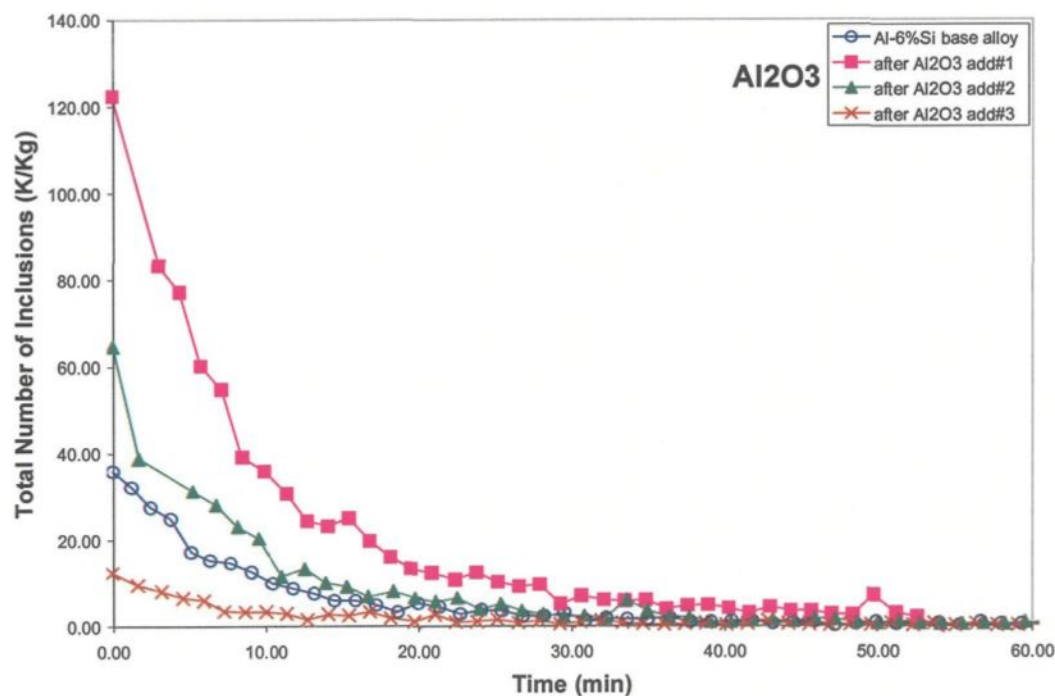


Figure 5.2 (b) Corrected version of the plot shown in Figure 5.2 (a).

Figures 5.3 and 5.4 show the average and total number of inclusions plotted as a function of particle size range. The terms *average* and *total* have been defined previously in Chapter 4, section 4.2.1, in relation to Figures 4.3 and 4.4. The same explanation applies in this case also, except that the time period of the LiMCA sampling is 60 min (instead of 30 min).

The highest number of inclusions are found in the 20-25 μm particle size range for the first addition of Al_2O_3 inclusions. The numbers decrease as the particle size range increases. After 20-25 μm , not many inclusions are detected by the LiMCA system, indicating that particle agglomeration and sedimentation take place somewhat faster in the Al-6% Si alloy melt. This is understandable taking into consideration the somewhat lower density of the alloy. The similarity of the distributions in Figures 5.3 and 5.4 indicates the approximate consistency of LiMCA measurements over the time period of the LiMCA sampling. It should be mentioned here that, having shown the similarity of the average and total concentration distributions and having discussed its significance, only the total concentration distributions will be shown in subsequent sections pertaining to other inclusion additions.

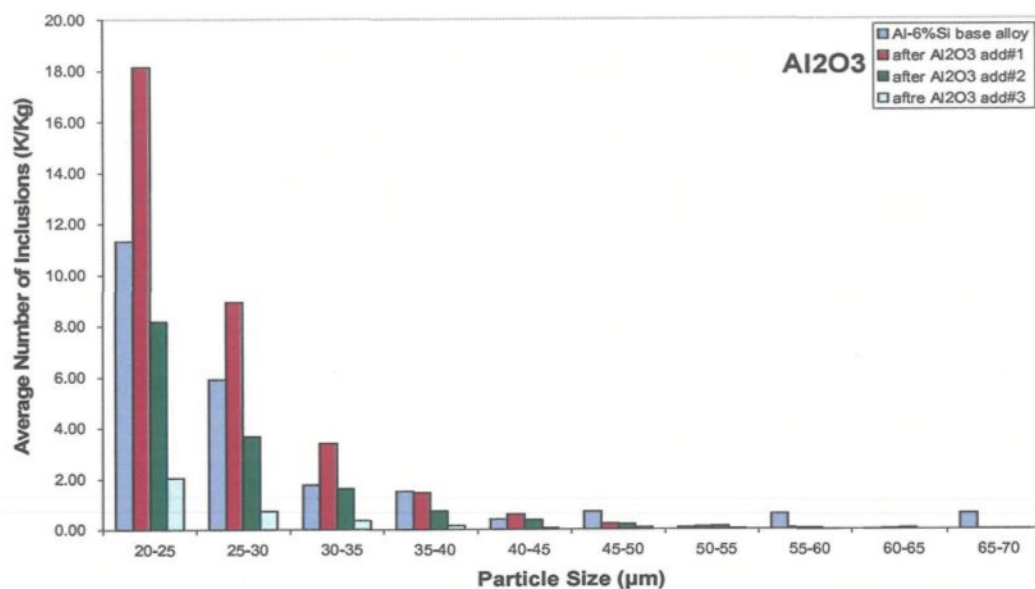


Figure 5.3 Average number of Al₂O₃ inclusions in Al-6%Si alloy as a function of particle size.

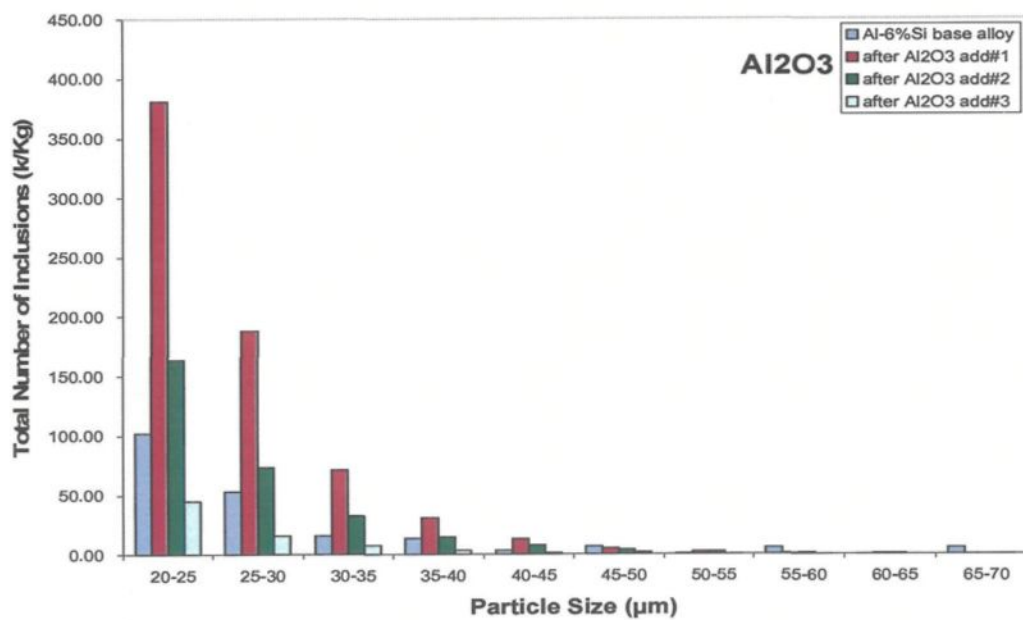


Figure 5.4 Total number of Al₂O₃ inclusions in Al-6%Si alloy as a function of particle size.

C₂₀ Measurements: Volumic concentration of inclusions (inclusions >20 μ m)

Figures 5.5 (a) and (b) display the actual and corrected volumic concentrations of Al₂O₃ inclusions as a function of time over the 60 min sampling period. The graphs are similar to those of Figure 5.2 for the total concentration of inclusions, and the highest volumic concentrations are observed after the first addition of Al₂O₃ inclusions.

The second and third additions register practically nil values over the 60 min sampling period. This does not signify an error in the LiMCA measurements, as can be seen from Figures 5.6 and 5.7, which display the corresponding plots of average and total volumic concentrations of Al₂O₃ inclusions as a function of the inclusion particle size. Although the volume concentrations decrease with subsequent additions of Al₂O₃ inclusions, the corresponding particle size distributions can still be clearly observed.

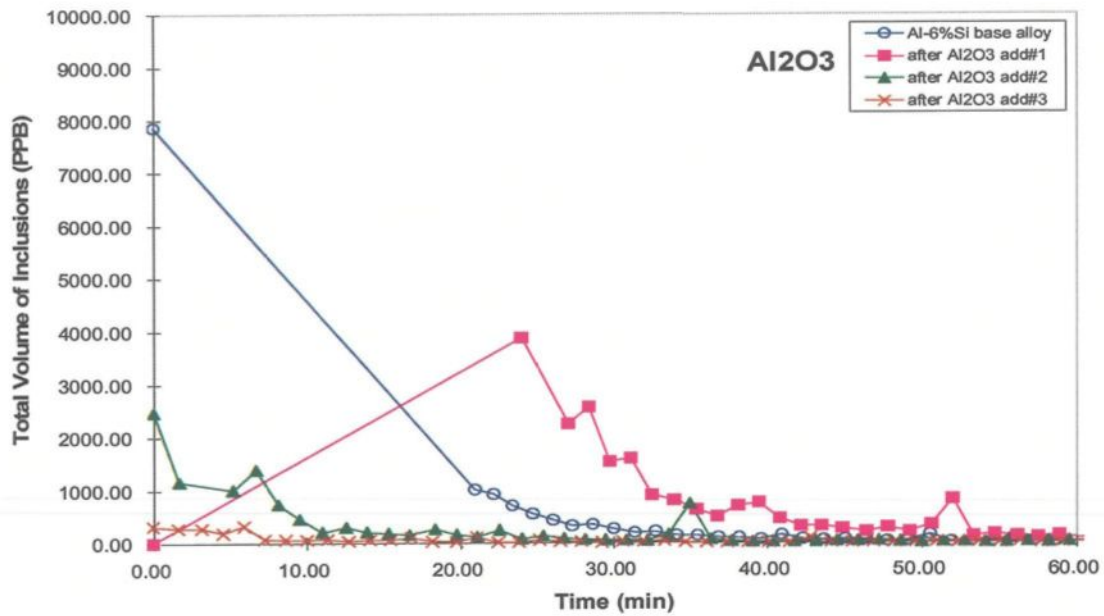


Figure 5.5(a) Volumic concentration of Al₂O₃ inclusions in Al-6%Si alloy as a function of time.

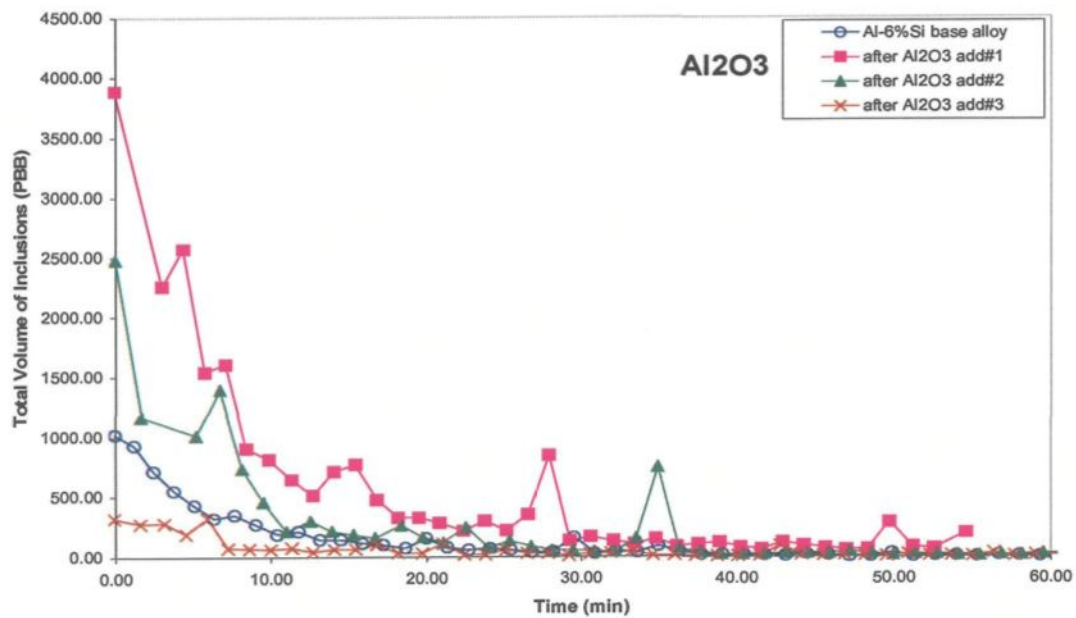


Figure 5.5(b) Corrected version of the plot shown in Figure 5.5(a).

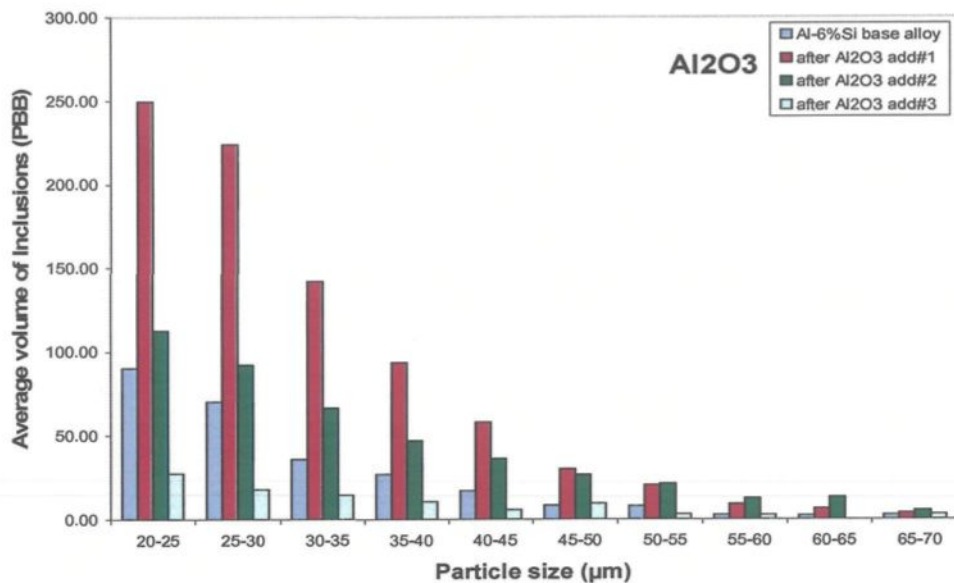


Figure 5.6 Average volume of Al₂O₃ inclusions in Al-6% alloy as a function of particle size.

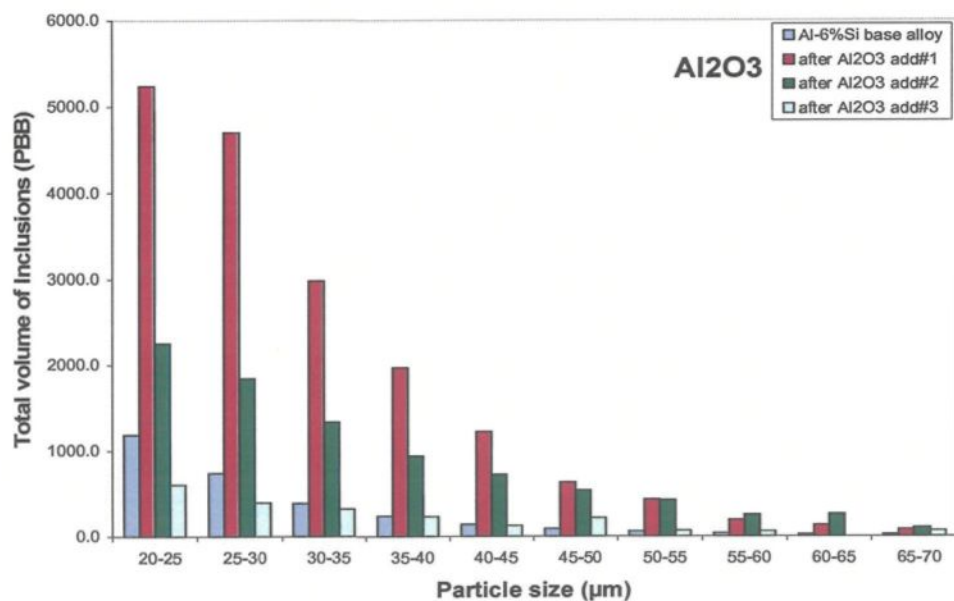


Figure 5.7 Total volume of Al₂O₃ inclusions in Al-6%Si alloy as a function of particle size.

5.2.2 Evaluation of Al_4C_3 Inclusions

The addition of Al_4C_3 inclusions to the Al-6%Si alloy melt was carried out using prefabricated Al_4C_3 inclusion-containing Al-6%Si alloy ingots, the preparation of which has been described in Chapter 3, section 3.2.2. Three inclusion-containing ingots were prepared for each powder inclusion type used.

Inclusion addition was carried out in three stages to an 8.5 Kg melt of Al-6%Si alloy, maintained at 750 °C. After each addition, the melt was stirred properly, followed by a LiMCA sampling that was continued without pause for 60 min. The size of the Al_4C_3 powder particles used was less than 10 μm .

N_{20} Measurements: Total concentration number of inclusions (inclusions > 20 μm)

As in the case of the Al_2O_3 inclusion additions, there was also an initial delay of about 18-20 min before the inclusions were properly detected in the base alloy melt and after the first addition of Al_4C_3 inclusions.

Figure 5.8 shows the corrected distribution of inclusions after displacing the starting points for the base alloy and the first addition to the left. The LiMCA measures the increase in inclusion concentrations with respect to the base alloy melt, and the levels become negligible after about 40 min of testing. As can be seen, the first and second additions show only a slight increase with respect to the base alloy melt readings. With the third Al_4C_3 inclusion addition, the inclusion levels were sufficiently high to allow detection from the start of the sampling period.

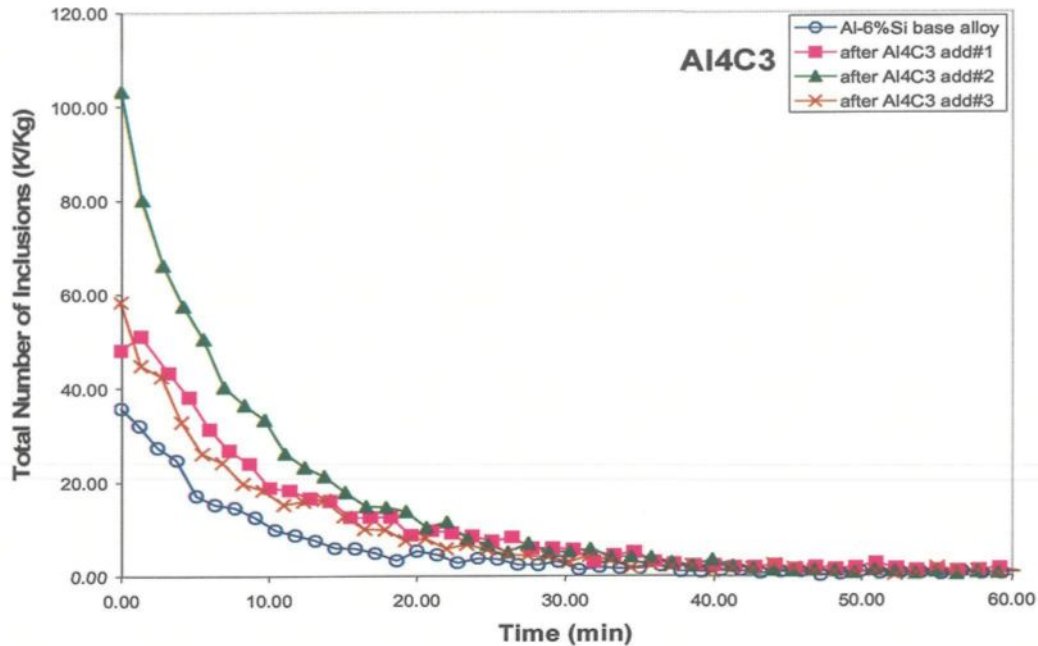


Figure 5.8 Concentration number of Al_4C_3 inclusions in Al-6%Si alloy as a function of time.

Due to the random location of inclusion particles in the sensing zone of the LiMCA probe, and due to differences in viscosity of the melt with different inclusion additions, the starting point of any LiMCA sampling (*i.e.*, when the level of liquid metal first touches the probe) will vary from sampling to sampling depending on the alloy melt, the inclusion type and the inclusion concentration.

The inclusion concentration distribution as a function of particle size range is shown in Figure 5.9. As can be seen, most of the particles lie in the lowest particle size ranges, from 20 to 35 μm . Of interest to note is that the highest number of inclusions are observed after the second addition of Al_4C_3 inclusions. Compared to the case of the Al_2O_3

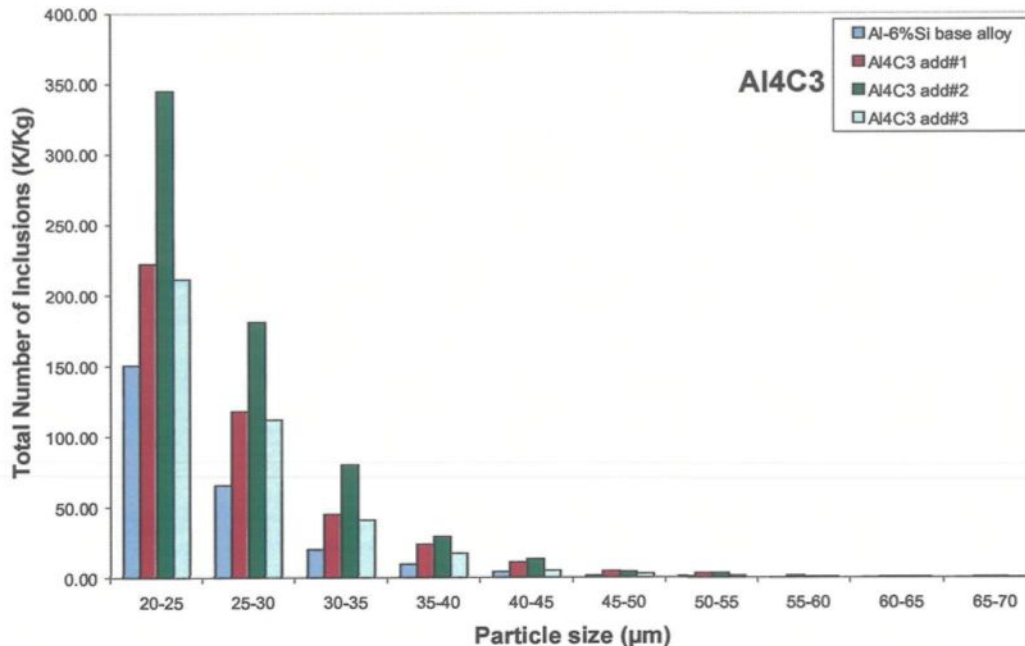


Figure 5.9 Total number of Al₄C₃ inclusions in Al-6%Si alloy as a function of particle size.

inclusions, agglomeration and sedimentation effects are not that significant. The similarity of the distributions for the base alloy and the three additions and the negligible levels in the higher particle size ranges provide an indication of the sensitivity of the LiMCA with respect to the size of the inclusion particles.

C₂₀ Measurements: Volumic concentration of inclusions (inclusions >20μm)

Figure 5.10 shows the corrected plot of the volumic concentration of inclusions obtained over a 60-min period of LiMCA sampling for the case of Al₄C₃ inclusion addition. As in the case of the N₂₀ plot, inclusion detection began after about 15-20 min of testing for the base alloy and first addition of Al₄C₃ inclusions.

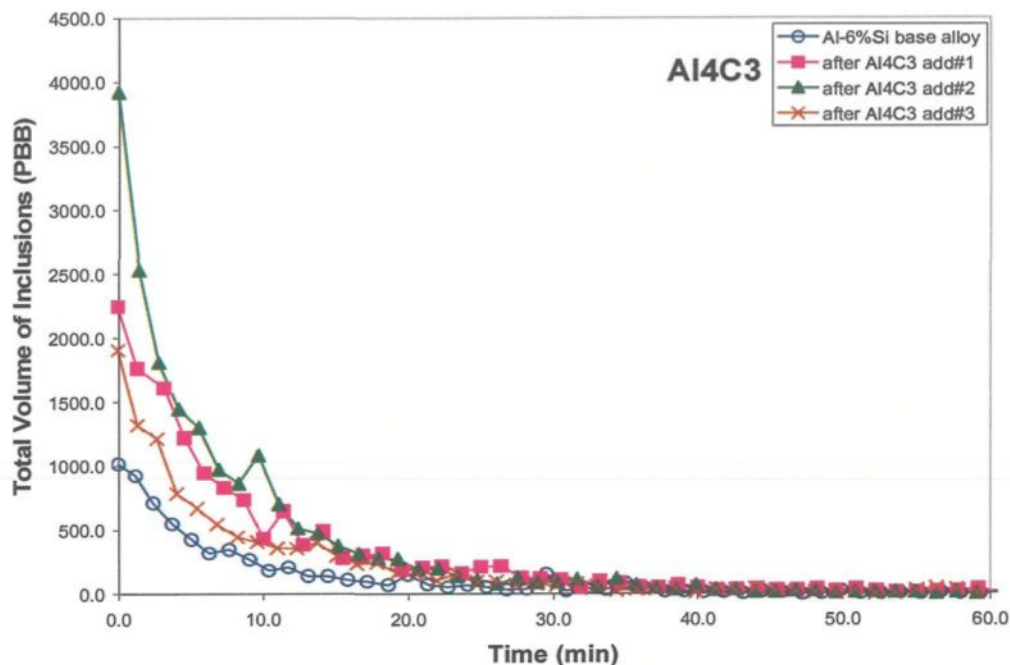


Figure 5.10 Volumic concentration of Al_4C_3 inclusions in Al-6%Si alloy as a function of time.

As Figure 5.10 shows, highest concentrations are obtained with the second addition of Al_4C_3 inclusions to the melt, but decrease to some extent with the third addition. In any case, compared to the base alloy, the increase in volumic concentrations with the increasing addition of Al_4C_3 inclusions was always detected.

Figure 5.11 displays the total volume of inclusions as a function of particle size. Similar to the total concentration vs. particle size range plot of Figure 5.9, the volumic concentrations show the same type of distribution. Highest volumic concentrations are obtained after the second addition of Al_4C_3 inclusions and the volumes decrease to comparable or smaller volumes than those obtained with the first addition.

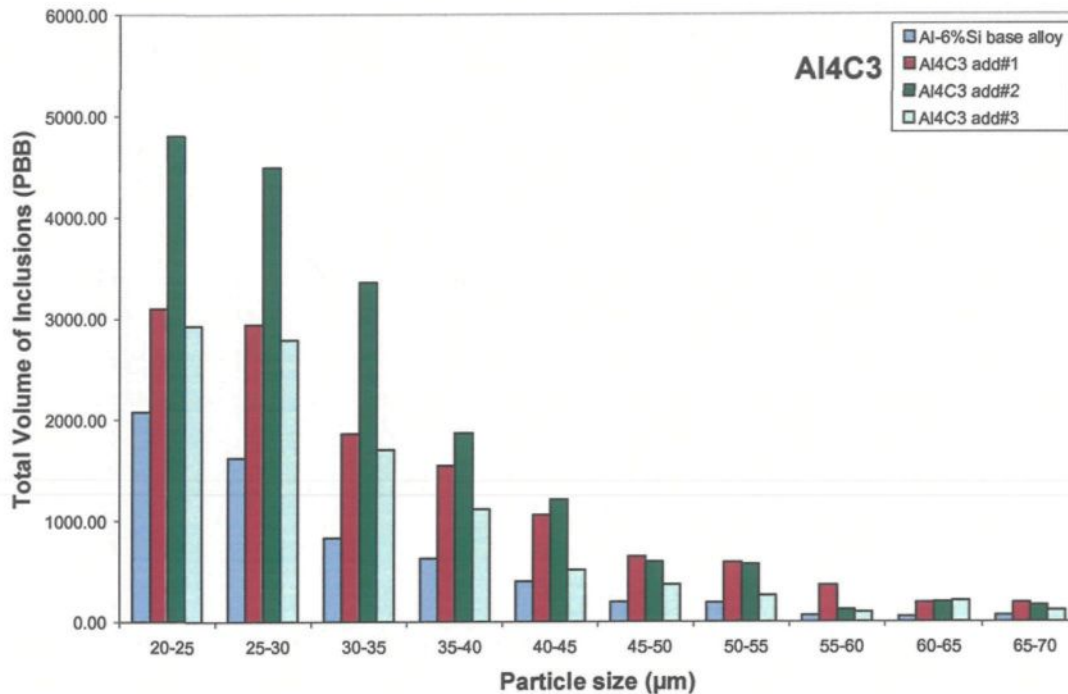


Figure 5.11 Total volume of Al_4C_3 inclusions in Al-6%Si alloy as a function of particle size.

The slight increase in the upper particle size ranges would indicate a certain degree of particle agglomeration. In comparison, the base alloy melt shows extremely low concentrations in the upper particle size range and, in general, much lower volumic concentrations compared to the melts containing the Al_4C_3 inclusions.

5.2.3 Evaluation of CaO Inclusions

Following the same procedures as before, the addition of CaO inclusions to the Al-6%Si alloy melt was carried out using prefabricated CaO inclusion-containing Al-6%Si alloy ingots. The inclusion addition was carried out in three stages. After each addition, the

melt was stirred properly, followed by a LiMCA sampling (for 60 min). The primary size of the CaO powder particles used for injection was less than 20 μm .

N₂₀ Measurements: Total concentration number of inclusions (inclusions > 20 μm)

Figure 5.12 shows the plot of the total number of inclusions measured over 60 min of LiMCA sampling. The graph has been corrected with respect to the starting points of the base alloy and first addition melts. As can be seen, the curves are similar in the four cases: the CaO inclusion-containing Al-6%Si melts display almost double the concentration of inclusions at the start of sampling; the concentrations decrease at similar rates until a steady state is reached after about 35-40 min of sampling time, when all four melt conditions (including the base alloy melt without CaO inclusion addition) show a very low level of inclusions, indicating that the inclusions have settled to the bottom of the melt crucible.

Figure 5.13 shows the total number of inclusions as a function of particle size for the CaO inclusion additions to the Al-6%Si alloy melt. The highest amount of inclusions are obtained for the first addition, with comparable to slightly lower levels for the third addition, both these being much higher than the inclusion levels displayed by the base alloy. It is surprising, therefore, to find that the inclusion levels for the second addition show levels lower than the base alloy in the lowest particle size range of 20-25 μm , and comparable levels at increased particle sizes.

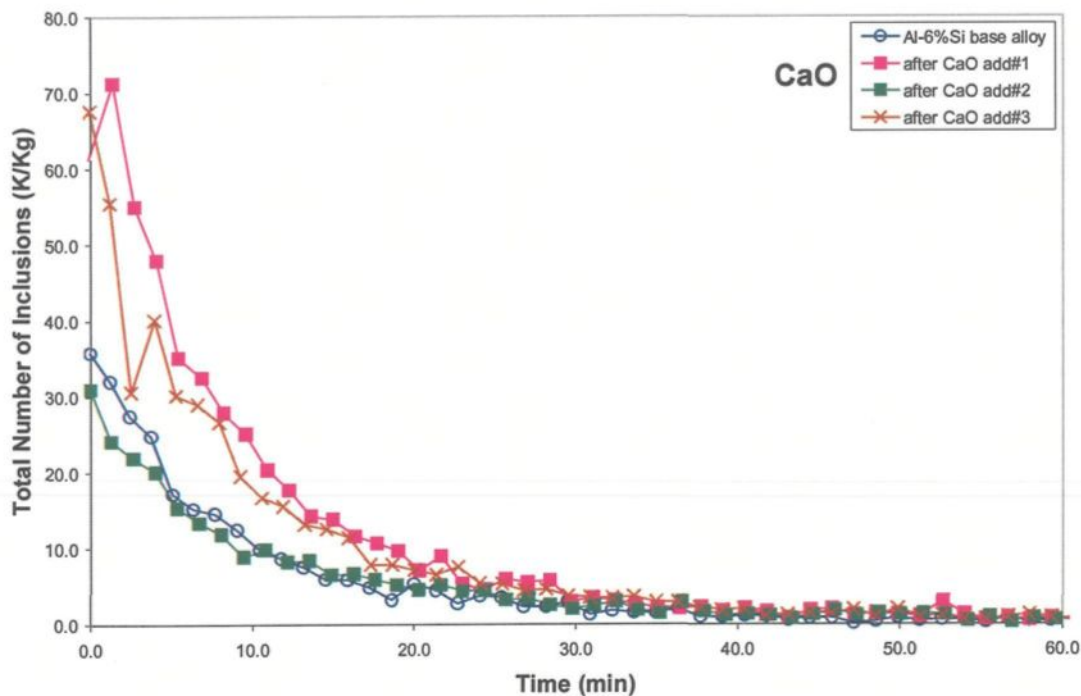


Figure 5.12 Concentration number of CaO inclusions in Al-6%Si alloy as a function of time.

As discussed previously in Chapter 4, section 4.2.3, the addition/injection of CaO powder particles to the pure aluminum or Al-6%Si alloy melts proved to be quite difficult. Thus it is quite probable that the CaO inclusion-containing ingot corresponding to the second addition in Figure 5.13 may have actually contained little or no CaO inclusions. This being the case, the inclusion levels would be lowered with the addition of the second ingot, which in effect would dilute the melt instead of increasing the amount of CaO inclusions within it.

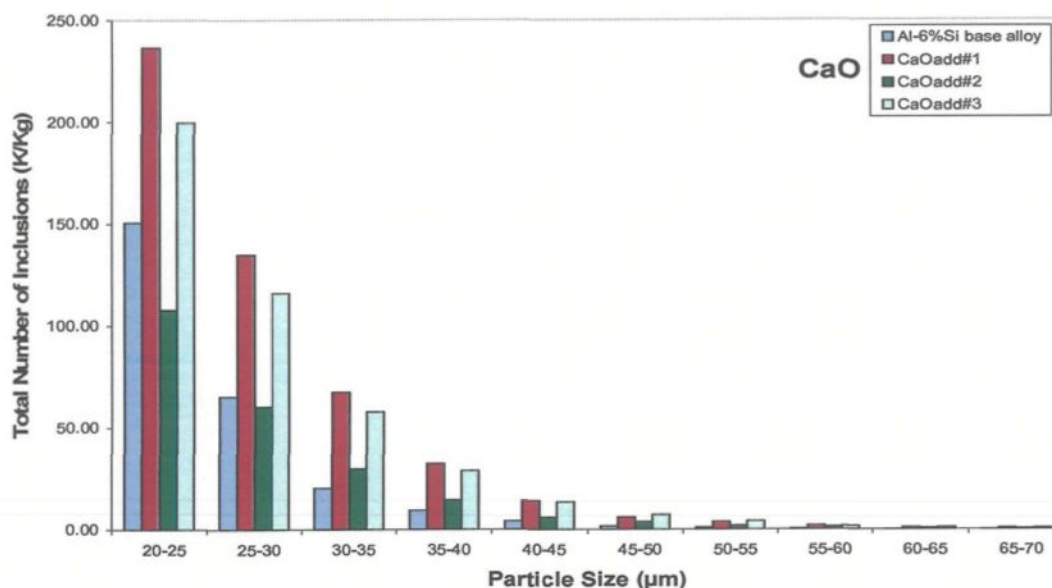


Figure 5.13 Total number of CaO inclusions in Al-6%Si alloy as a function of particle size.

C₂₀ Measurements: Volumic concentration of inclusions (inclusions > 20µm)

Figure 5.14 shows the volumic concentration of CaO inclusions over a 60 min period of LiMCA sampling. The curves are seen to be very similar to those of the N₂₀ curves of Figure 5.12, reaching the steady state-low volumic concentration levels even before 30 min of sampling. The corresponding total volume vs. particle size plot of Figure 5.15, although similar to that of Figure 5.13, shows a much more gradual decrease in volume concentrations over the lower and medium particle size ranges. Even in the higher particle size ranges, definite volume concentrations can be observed. In comparison, the base alloy melt exhibits similar number and volumic concentration distributions over the entire particle size range. The high volumic concentrations of the CaO-containing Al-6%Si alloy melts would indicate that larger volumes are associated with these inclusions.

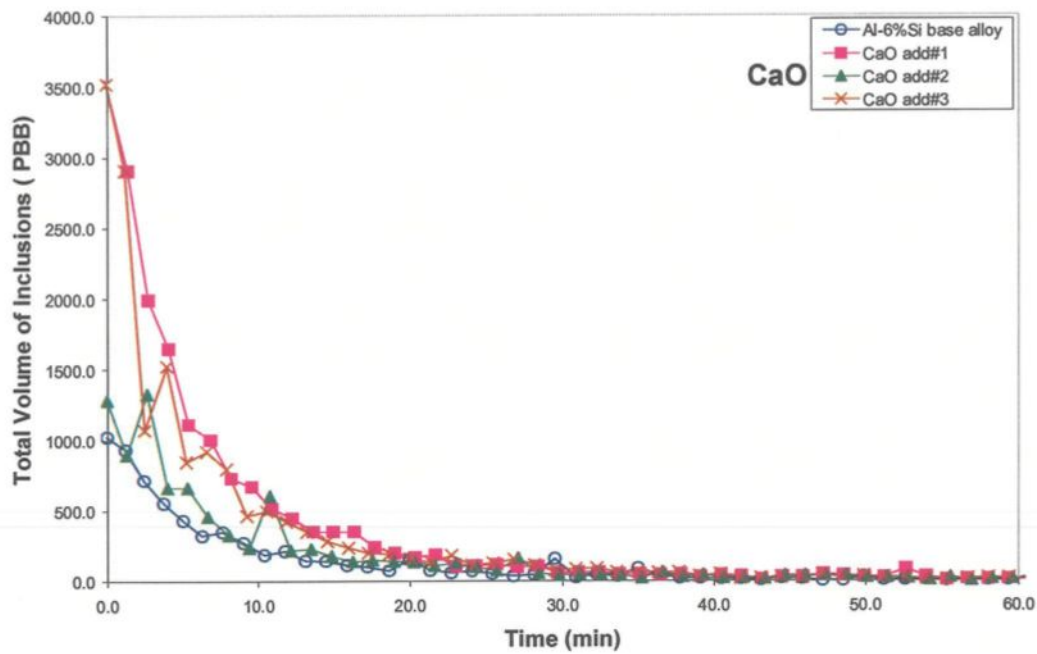


Figure 5.14 Volumic concentration of CaO inclusions in Al-6%Si alloy as a function of time.

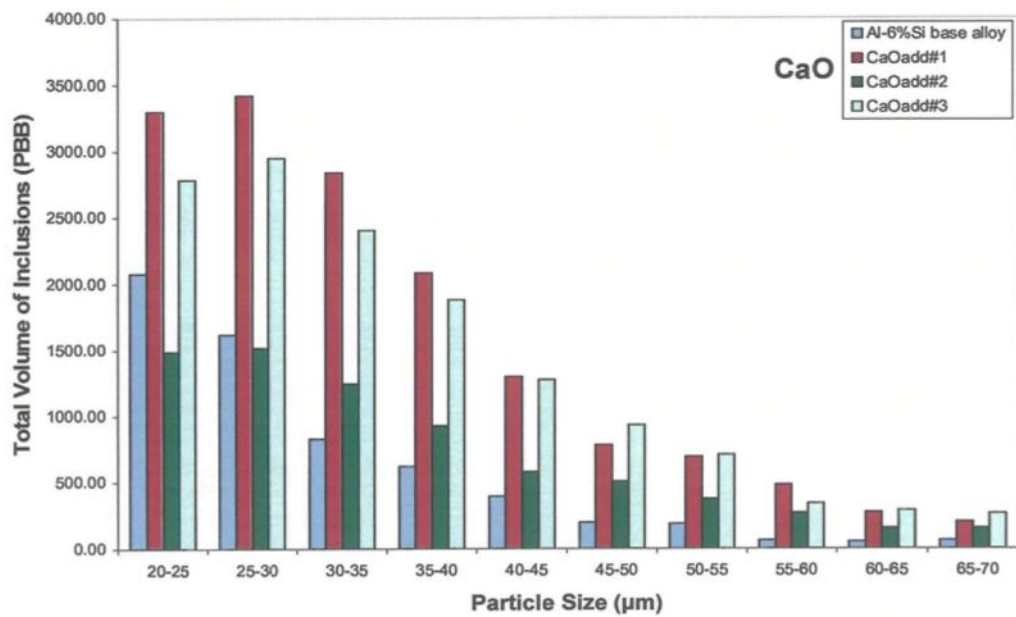


Figure 5.15 Total volume of CaO inclusions in Al-6%Si alloy as a function of particle size.

5.2.4 Evaluation of MgO Inclusions

The addition of MgO inclusions to the Al-6%Si alloy melt was carried out using the same procedures described in previous sections. The inclusion addition was carried out in three stages to an 8.5 Kg charge of Al-6%Si alloy melt, maintained at 750 °C. After each addition, the melt was stirred properly, followed by a LiMCA sampling over a period of 60 min. The primary size of the MgO powder particles before injection was less than 70 μm .

N₂₀ Measurements: Total concentration number of inclusions (inclusions > 20 μm)

Figure 5.16 is the modified N₂₀ plot showing the total number of inclusions over the 60 min period of LiMCA sampling. All curves show similar trends. The inclusions levels drop within 20 min of the testing period and then gradually reach low, steady state levels. Surprisingly, the Al-6%Si base alloy melt shows higher inclusion levels than those observed after the first MgO addition until they reach their steady state level after about 40 min of sampling.

The total distribution vs. particle size plot of Figure 5.17 reflects this trend nicely. Keeping in mind the comparatively large particle size of the MgO particles (70 μm vs. other inclusions will particle sizes, of < 10 μm), it is to be expected that the MgO-containing melts will exhibit much higher inclusion concentrations than the Al-6%Si base alloy melt in the larger particle size ranges.

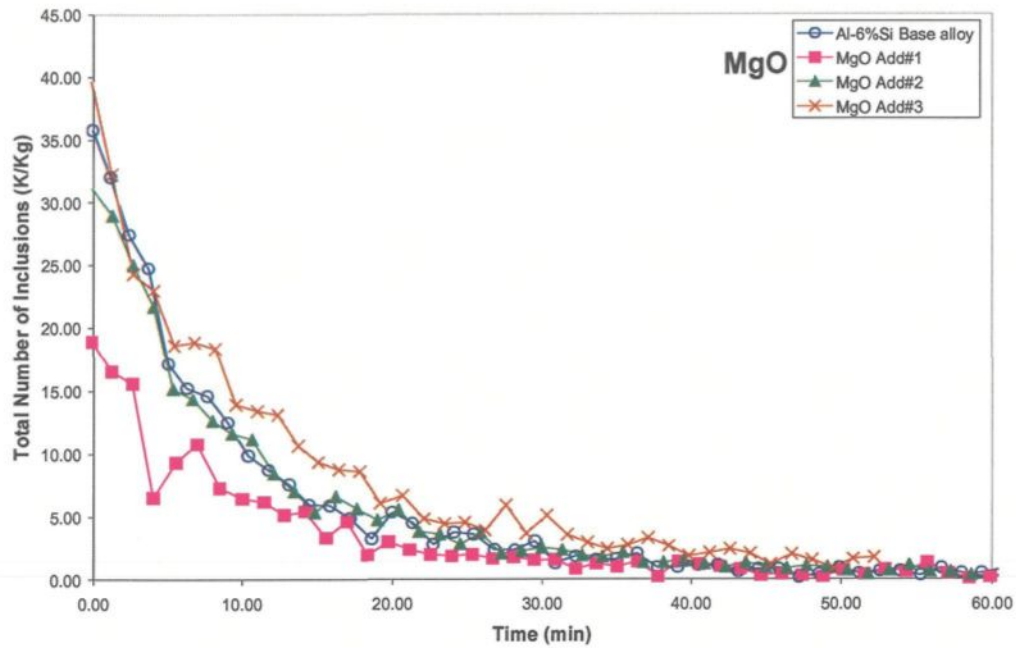


Figure 5.16 Concentration number of MgO inclusions in Al-6%Si alloy as a function of time.

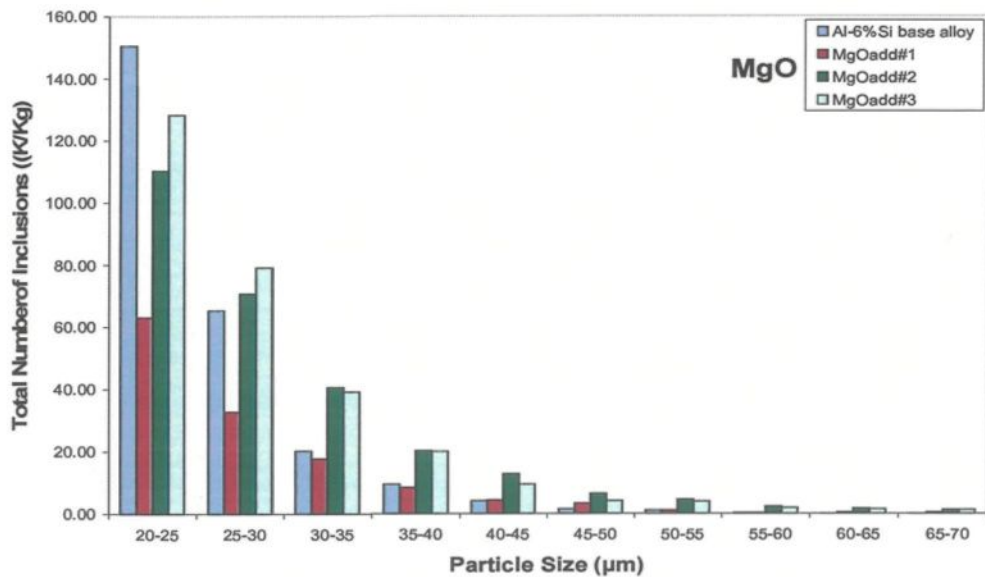


Figure 5.17 Total number of MgO inclusions in Al-6%Si alloy as a function of particle size.

C₂₀ Measurements: Volumic concentration of inclusions (inclusions >20 μ m)

The volumic concentration of inclusions for MgO inclusion additions to the Al-6%Si alloy melt is displayed in Figure 5.18. The inclusion levels drop swiftly within ten minutes of sampling, then decrease gradually till, at about 30 min, they attain minimum levels (almost nil) that are maintained until the end of the sampling period.

The total volume of inclusions plotted as a function of particle size range, Figure 5.19, reveals that, similar to the case of the CaO inclusions, the MgO inclusions are also associated with high volumic concentrations that decrease relatively slowly over the entire particle size range. Compared with the distribution obtained for the base Al-6%Si alloy melt, the MgO inclusion-containing alloy melts show larger volume concentrations on

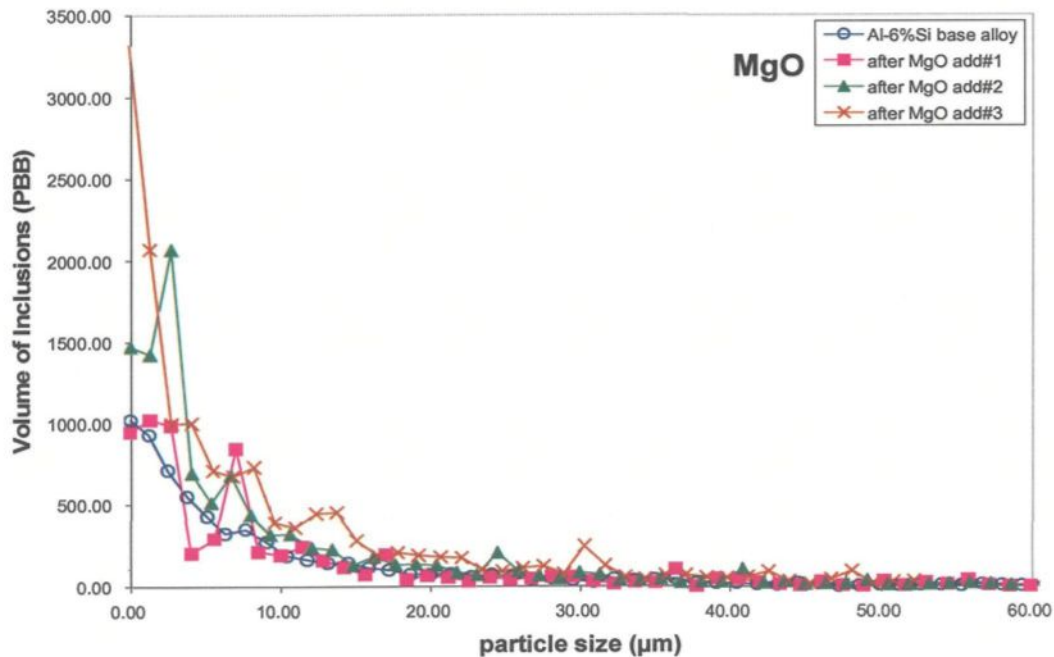


Figure 5.18 Volumic concentration of MgO inclusions in Al-6%Si alloy as a function of time.

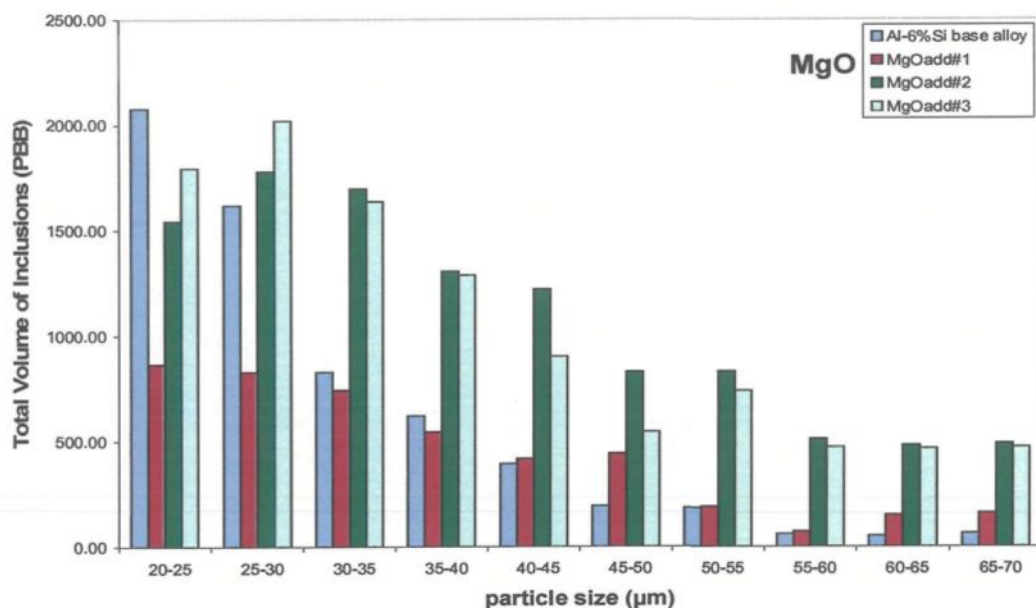


Figure 5.19 Total volume of MgO inclusions in Al-6%Si alloy as a function of particle size.

account of their large particle size. The low number and volumic concentrations observed in the case of the first addition should most likely be due to the lack of sufficient amount of MgO inclusions in the ingot used for the first addition.

5.2.5 Evaluation of TiB₂ Inclusions

The addition of TiB₂ inclusions to the Al-6%Si alloy melt was carried out following the same procedures described in Chapter 3, section 3.2.2. The inclusion additions were made in three stages to the Al-6%Si alloy melt (8.5 kg charge maintained at 750 °C temperature). After each addition, the melt was stirred properly, followed by a LiMCA sampling that was carried on for 60 min. The size of the TiB₂ powder particles used was less than 10 μm.

N₂₀ Measurements: Total concentration number of inclusions (inclusions > 20 μm)

This experiment provided the best results on inclusion measurements. Figure 5.20 shows the modified N_{20} plot of the total number of inclusions as a function of time (*i.e.*, after correcting for the time delay in reading for the base alloy and first addition). As can be seen, the inclusion concentration increases with addition of the TiB_2 inclusion-containing ingot. With further additions, the inclusion concentrations decrease somewhat. However, each curve follows the same decreasing trend, and stabilization is achieved after about 45 or 50 min of testing, due to settling of the TiB_2 inclusions (density of 4.5-4.6 g/cm³) to the crucible bottom.

The TiB_2 particles possess excellent wettability with respect to liquid aluminum facilitating their injection into the melt. This is reflected nicely by the similarity of the four curves seen in the plot where, with reference to the base alloy curve, the increase in inclusion levels with TiB_2 additions show corresponding displacements in the other three curves.

Figure 5.21 shows the plot of the total number of inclusions as a function of particle size. The primary size of the TiB_2 particles is less than 10 μm. Thus, with TiB_2 addition, a significant increase in the number of inclusions in the lowest particle size ranges is observed compared to both the base alloy and the larger particle ranges. The effects of particle agglomeration and sedimentation are also reflected by the particle size distribution characteristics.

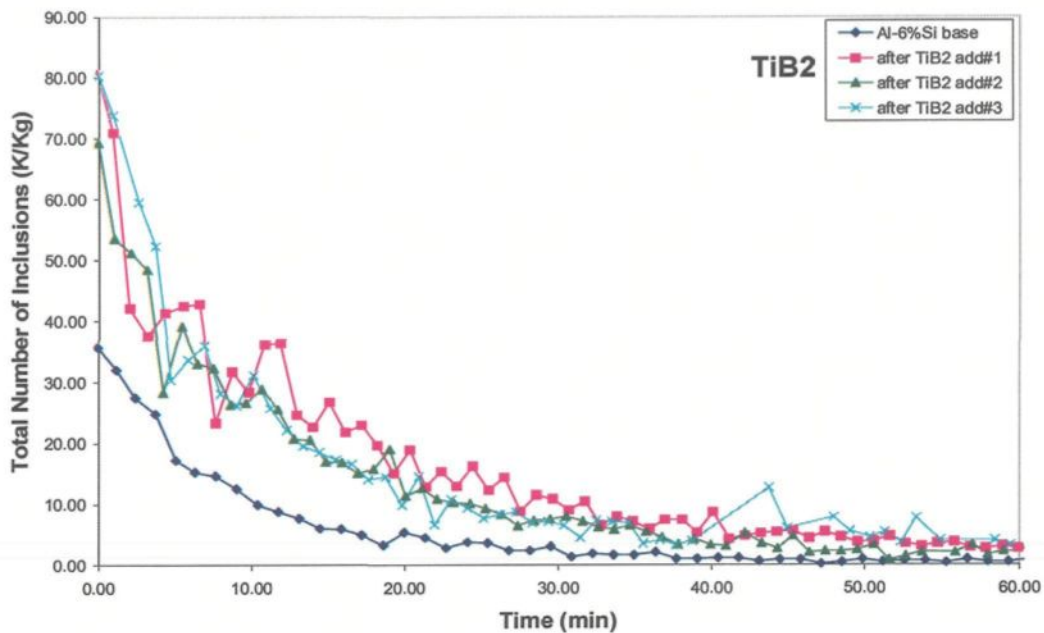


Figure 5.20 Concentration number of TiB₂ inclusions in Al-6%Si alloy as a function of time.

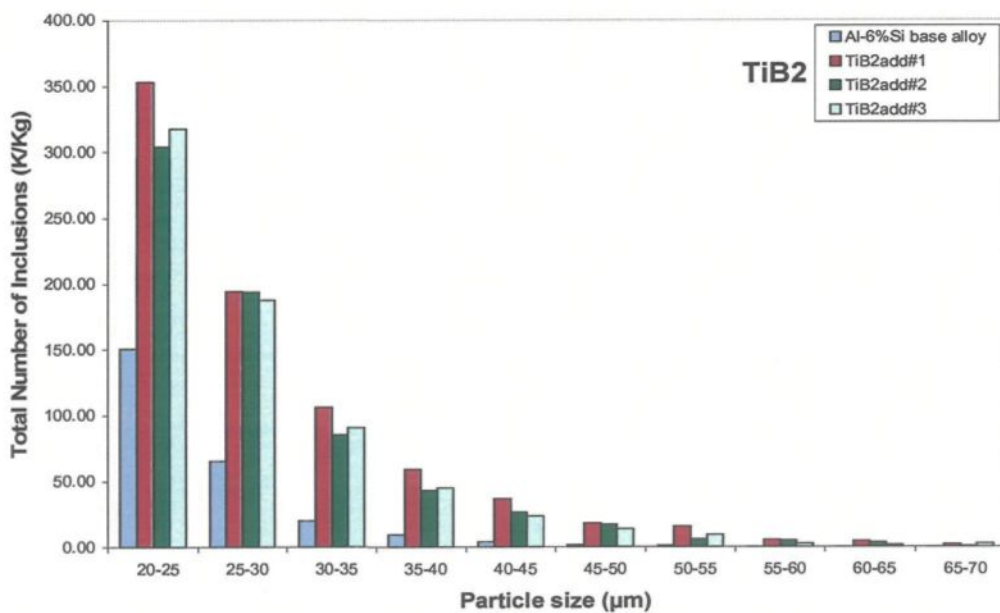


Figure 5.21 Total number of TiB₂ inclusions in Al-6%Si alloy as a function of time.

C₂₀ Measurements: Volumic concentration of inclusions (inclusions >20 μ m)

The volumic concentration plot for TiB₂ inclusion addition to the Al-6%Si alloy melt is shown in Figure 5.22. It is observed that the volume concentrations increase with TiB₂ addition, and fluctuations are observed even after 50 min of sampling time. In contrast, the base alloy curve shows a low volumic concentration (*cf.* 1000 with ~5500 ppb for a TiB₂ added alloy), which drops to negligible value almost after 20 min of testing, with no fluctuation over the 60 min period. Figure 5.23 displays the C₂₀ plot of volumic concentration of TiB₂ inclusions as a function of particle size in the Al-6%Si alloy at 750 °C. The figure clearly shows the high volume concentrations associated with TiB₂ inclusions, extending to the higher particle size ranges as well. Compared to other inclusion types studied, this appears to be a singular feature of TiB₂ powder inclusions.

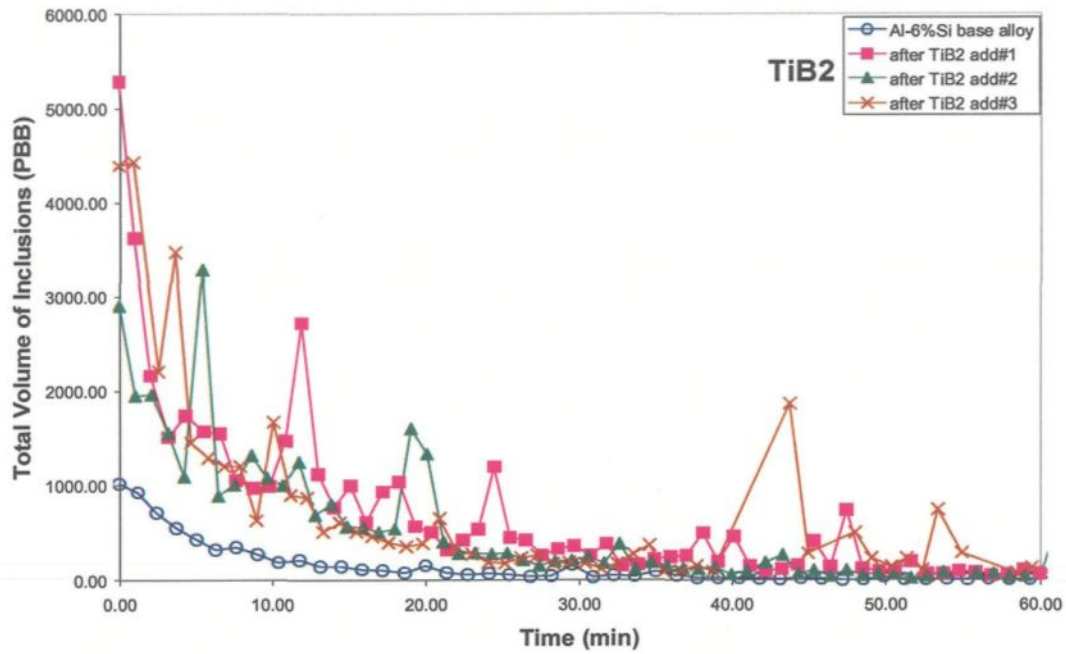


Figure 5.22 Volumic concentration of TiB₂ inclusions in Al-6%Si alloy as a function of time.

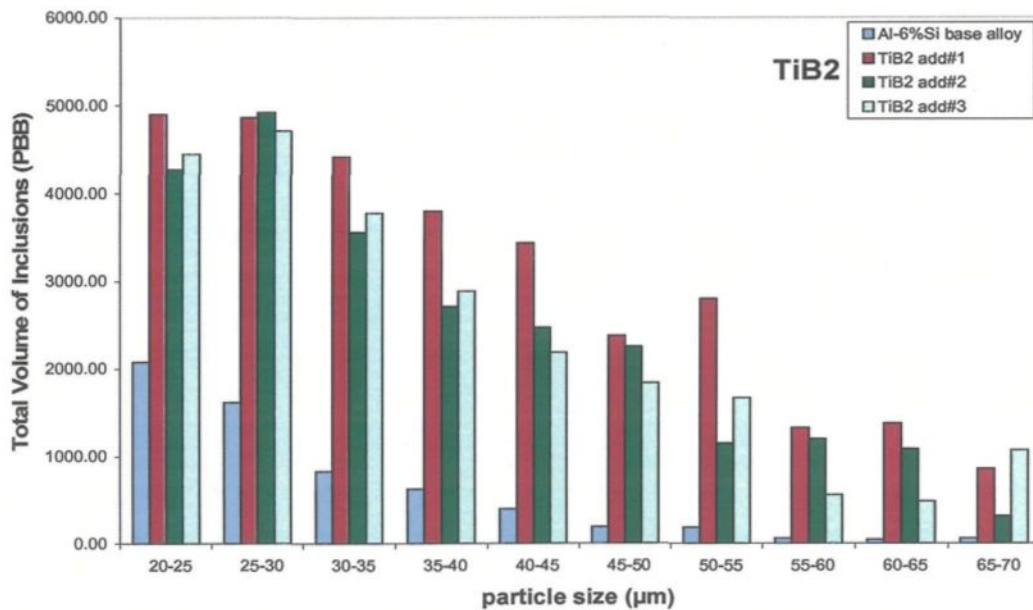


Figure 5.23 Total volume of TiB₂ inclusions in Al-6%Si alloy as a function of time.

5.3 COMPARISON OF DIFFERENT INCLUSION ADDITIONS

The total number of inclusions (N_{20} readings) as a function of particle size are compared in Figure 5.24 for the different inclusion types studied. It is interesting to find that the Al_2O_3 and TiB_2 inclusions display the highest concentrations in the lower particle size ranges, with TiB_2 displaying this tendency for almost all particle size ranges. The Al_4C_3 inclusions show concentrations close of those of Al_2O_3 , while CaO and MgO inclusions show the lowest concentrations, close to the base alloy levels at particle sizes greater than $35\ \mu m$.

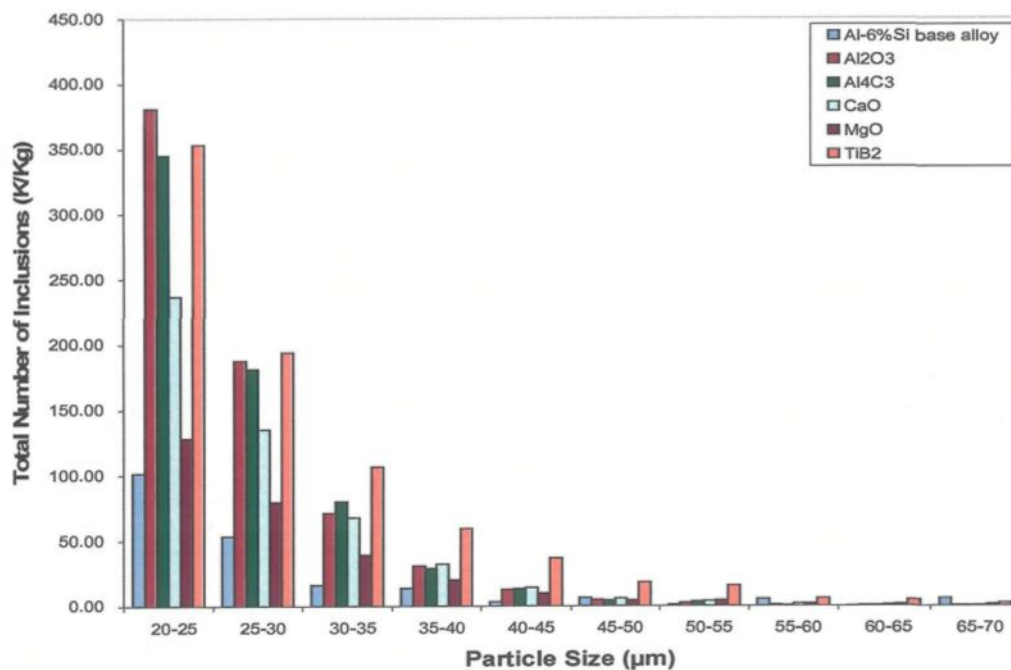


Figure 5.24 Comparison of concentration number of different inclusions in Al-6%Si alloy as a function of particle size.

CHAPTER 6

EVALUATION OF INCLUSIONS IN Al-6%Si ALLOY MEASURED

BY LiMCA AT 680 °C

CHAPTER 6

EVALUATION OF INCLUSIONS IN Al-6%Si ALLOY MEASURED

BY LiMCA AT 680 °C

6.1 INTRODUCTION

The evaluation of different inclusion types in Al-6%Si alloy melts using the LiMCA technique was also carried out at a lower melt temperature of ~680 °C. It was observed that measurements made at such temperatures (680° to 695°C) provided much better consistency and repeatability of results than those obtained at 750°C melt temperature (Chapter 5).

As mentioned previously, the two temperatures were selected to represent conditions of low and high melt superheat with the aim of assessing the capability of the LiMCA machine for measuring inclusions under these conditions.

This chapter presents a detailed analysis of the measurement data obtained for the various inclusion types studied, where both (a) a comparison of these results with the results presented in Chapter 5, and (b) comparison of the sources of inclusion addition in those cases where the inclusions were added in more than one form (*viz.*, powder, master alloy, metal or MMC alloy) will be made.

6.2 EVALUATION OF INCLUSIONS IN Al-6%Si ALLOY AT 680 °C

A charge of 8.5 Kg of Al-6%Si alloy was melted in a SiC crucible using an electric resistance furnace. The melt temperature was kept at 680 °C. Degassing was carried out for 15 min using a rotary impeller and pure, dry argon.

In these experiments the inclusion addition was carried out in one step. A measured amount of the specified inclusion type was added to the melt, and the melt stirred to achieve a homogeneous dispersion of the inclusions. Following this, several LiMCA samplings were taken from the same melt (four to five tests).

The LiMCA data obtained from these tests were plotted in the form of graphs showing (i) the total number of inclusions, and (ii) the volume concentration of inclusions as a function of time (*viz.*, N_{20} and C_{20} plots, respectively). It is to be mentioned here that each LiMCA sampling was done over a period of 30 minutes, and readings were taken at every 1-2 min intervals. In this regard, it should be noted that a sampling time of 30 min was sufficient to reach stable concentration values, as extensions in sampling time to 40 min showed no changes in the concentrations (see, for example, Figure 6.10 in section 6.2.2)

A schematic diagram of the inclusion addition and LiMCA sampling procedure is presented in Figure 6.1.

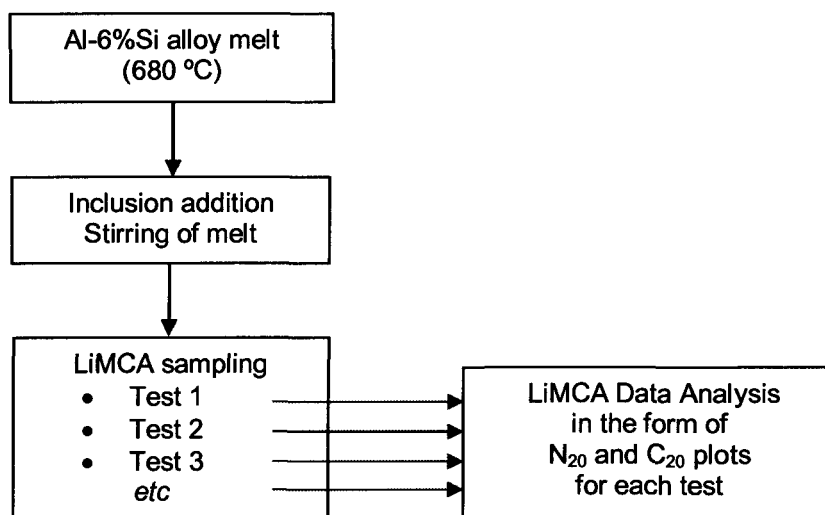


Figure 6.1 Schematic of inclusion addition to the Al-6%Si alloy melt at 680 °C.

6.2.1 Evaluation of TiB₂ Inclusions (added as powder)

In this case, the TiB₂ inclusions were added to the Al-6%Si alloy melt in the form of prefabricated TiB₂ powder-containing Al-6%Si alloy ingot. Only one addition was made. The LiMCA samplings were carried out five times. Although the melt temperature was preset to 680 °C, depending on the amount of melt, some amount of deviation in temperatures was observed from sampling to sampling. For example, for the five LiMCA samplings of the TiB₂ inclusion-containing melt, the temperatures varied as follows:

Test 1: 698 °C, Test 2: 693 °C, Test 3: 689 °C

Test 4: 680 °C, Test 5: 685 °C

N₂₀ Measurements: Total concentration number of inclusions (inclusions > 20 μ m)

Figure 6.2 shows the N_{20} plot of the total number of inclusions as a function of time, while Figure 6.3 depicts the total number of TiB_2 inclusions as a function of particle size over the 30 min period of sampling.

It is interesting to note that a decrease in the melt temperature from 689 °C in Test 1 to 680 °C in Test 4 increased the number of inclusions that were detected, particularly in the 20-35 μ m size range. The decrease in temperature resulted in an increase in the electrical resistance values, corresponding to the higher inclusion numbers observed in Figure 6.3. Also, Tests 1 and 2 with the higher melt temperatures (683 °C and above) provided lower inclusion concentrations. Thirdly, at particle sizes of 50 μ m or more, the melt temperature did not appear to affect the inclusion concentrations, which remained stable for all five tests.

From Figure 6.3 it can be judged that the LiMCA is sensitive to both inclusion size and inclusion concentration from test to test, and can distinguish between ‘clean’ (Al-6%Si base alloy) and ‘dirty’ (inclusion-containing) melts. However, as the results show, the sensitivity of the LiMCA is found to increase with a decrease in the melt temperature.

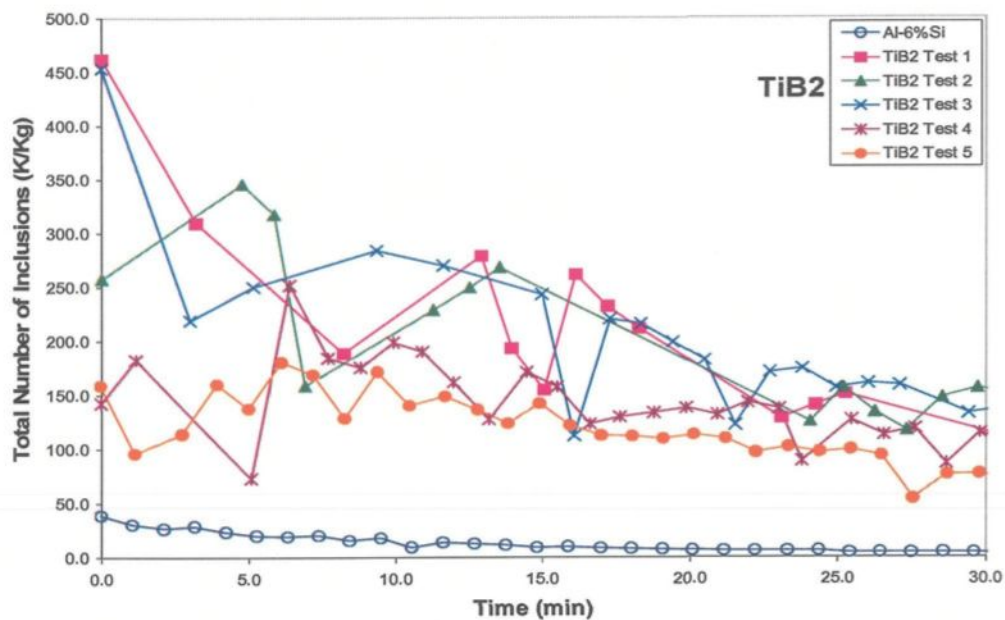


Figure 6.2 Concentration number of TiB_2 inclusions (powder source) in Al-6%Si alloy as a function of time.

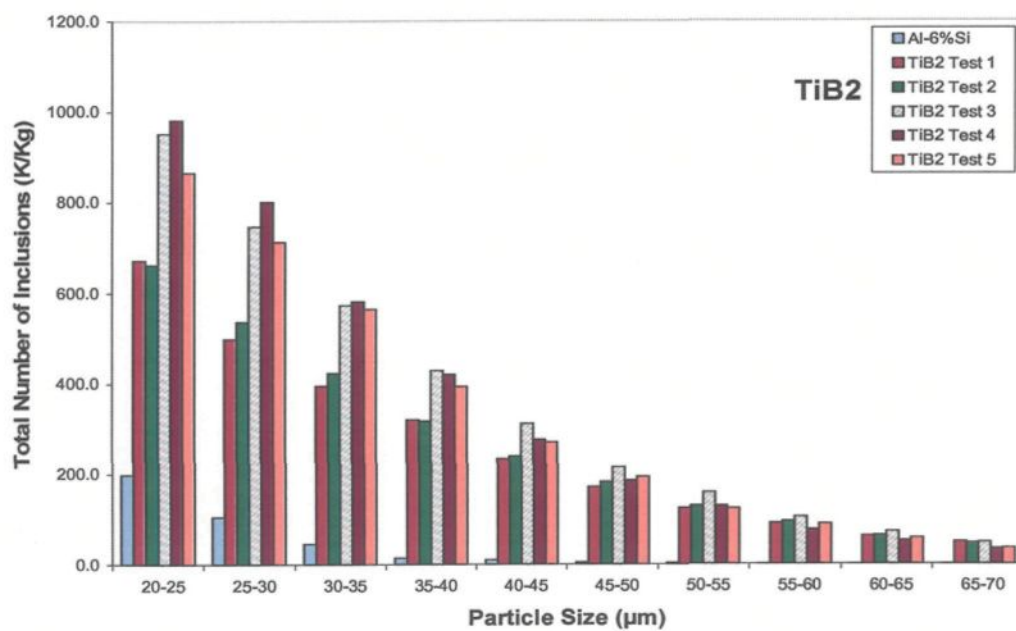


Figure 6.3 Total number of TiB_2 inclusions (powder source) in Al-6%Si alloy as a function of particle size.

Table 6.1 shows the actual inclusion concentrations (in K/Kg) that were obtained for the six samplings (base Al-6%Si alloy and five alloy + TiB₂ tests), corresponding to the different particle sizes.

Table 6.1 Inclusion concentration vs. particle size in base and TiB₂-containing Al-6%Si alloy melts (powder addition)

Alloy Melt/ Test (Temp)	Inclusion Concentration (K/Kg) vs. Particle Size (μm)									
	20-25	25-30	30-35	35-40	40-45	45-50	50-55	55-60	60-65	65-70
Al-6%Si base (680 °C)	199.1	105.1	45.5	14.8	10.3	5.1	2.6	1.0	0.5	0.5
Al-6%Si+TiB ₂ Test 1 (698 °C)	672.1	499.2	395.1	320.3	234.6	171.2	125.2	90.9	62.5	50.6
Al-6%Si+TiB ₂ Test 2 (693 °C)	663.2	536.4	423.7	317.9	240.0	183.6	129.3	95.7	64.2	46.5
Al-6%Si+ TiB ₂ Test 3 (689 °C)	951.7	747.6	573.2	428.7	311.7	215.4	159.5	105.1	72.2	48.8
Al-6%Si+ TiB ₂ Test 4 (680 °C)	980.8	801.3	581.6	420.9	275.9	186.5	129.2	76.8	53.1	34.3
Al-6%Si+ TiB ₂ Test 5 (685 °C)	864.9	713.1	565.1	394.4	270.9	194.1	123.0	89.0	58.9	35.6

A comparison of Test 3 and the base alloy inclusion readings is shown in Table 6.2 in ratio form. The increase in ratio with the increase in particle size range gives an indication of the large amount of TiB₂ inclusions present throughout the melt so that clustering and agglomeration are easily facilitated, resulting the increased concentrations observed for the higher particle size ranges.

Table 6.2 Comparison of inclusion readings of TiB₂-inclusion-containing (Test 3) and base Al-6%Si alloy melts reported in Table 6.1

Melt A: Melt B	Ratio of Inclusion Concentrations									
	Particle Size Range (μm)									
	20-25	25-30	30-35	35-40	40-45	45-50	50-55	55-60	60-65	65-70
Al-6%Si+ TiB ₂ (Test 3): Al-6%Si	4.78	7.11	12.68	28.96	30.26	42.23	61.34	108.1	144.4	97.6

C₂₀ Measurements: Volumic concentration of inclusions (inclusions > 20 μm)

Figures 6.4 and 6.5 show, respectively, the C₂₀ volumic concentration plot and the total volume of inclusions as a function of particle size over the 30 min period of LiMCA sampling. Compared to the base alloy, there is a substantial increase in volumic inclusion concentration with the addition of the TiB₂ powder inclusions, which persists over the entire range of particle sizes. Maximum volumes are observed in the 35-55-μm range of particle sizes. Test 3 (at 689°C melt temperature) displays the highest inclusion concentrations, while those of the other tests (at temperatures higher than 689°C) show relatively lower concentrations.

Microstructures obtained from castings of the melt taken just before the start of the LiMCA test (Figure 6.6) and at the end of the 30 min sampling period (Figure 6.7) show the large amount of TiB₂ inclusions in the former case, and their agglomeration with the passage of sampling time in the latter. Compared to all other inclusion types, the TiB₂ powder inclusions were observed to be present in significant amount in the melt.

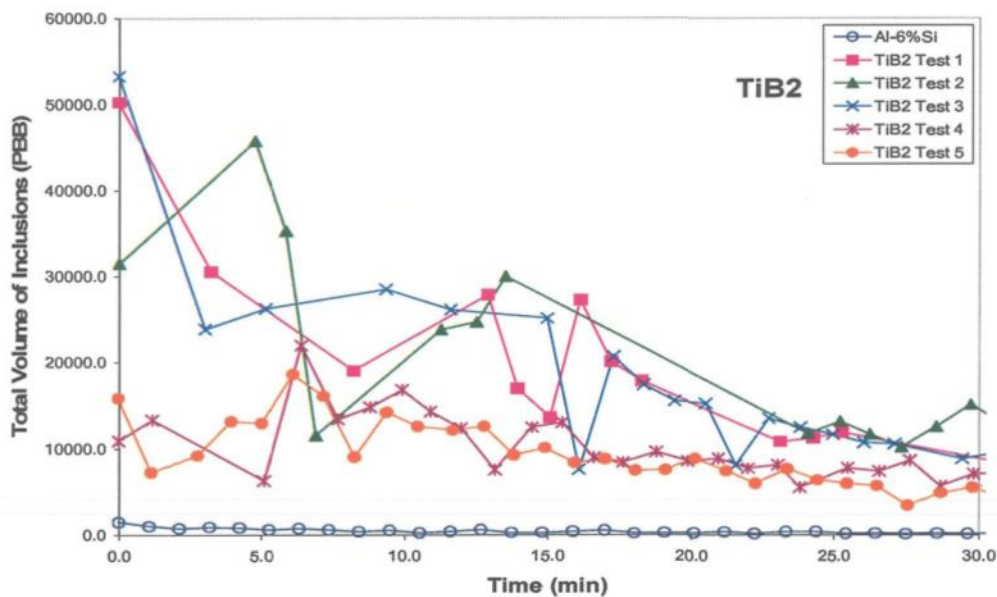


Figure 6.4 Volumic concentration of TiB_2 inclusions (powder source) in Al-6%Si alloy as a function of time.

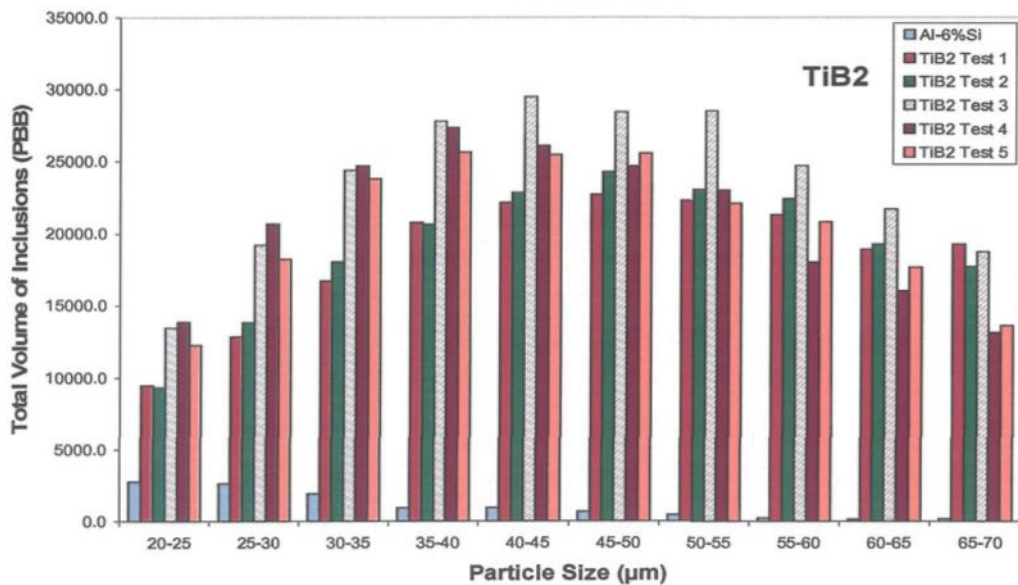


Figure 6.5 Total volume of TiB_2 inclusions (powder source) in Al-6%Si alloy as a function of particle size.

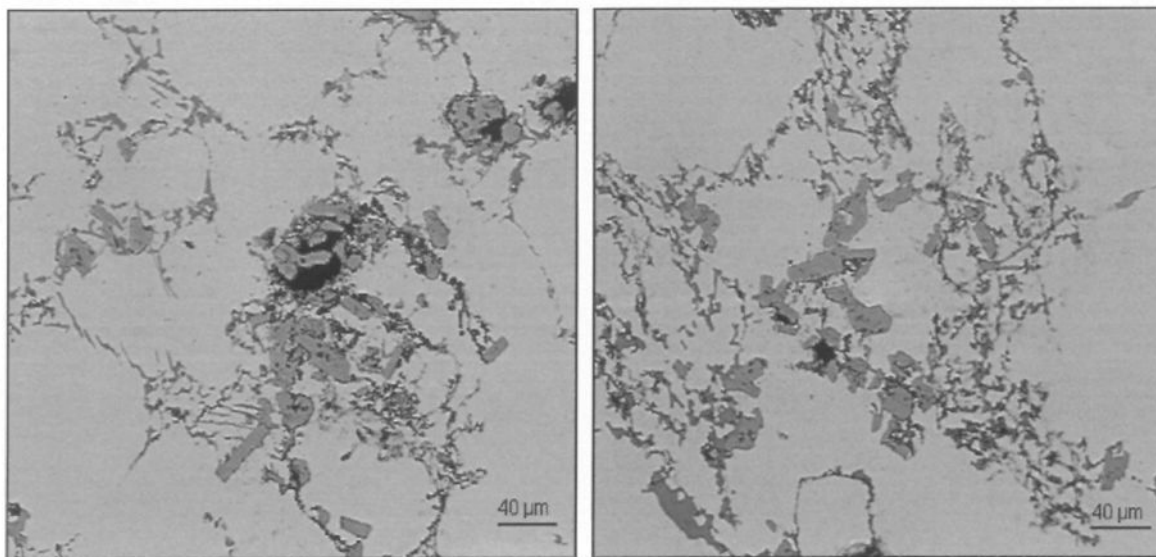


Figure 6.6 Microstructures of Al-6%Si alloy after addition of TiB₂ (powder source) before the start of the LiMCA test.

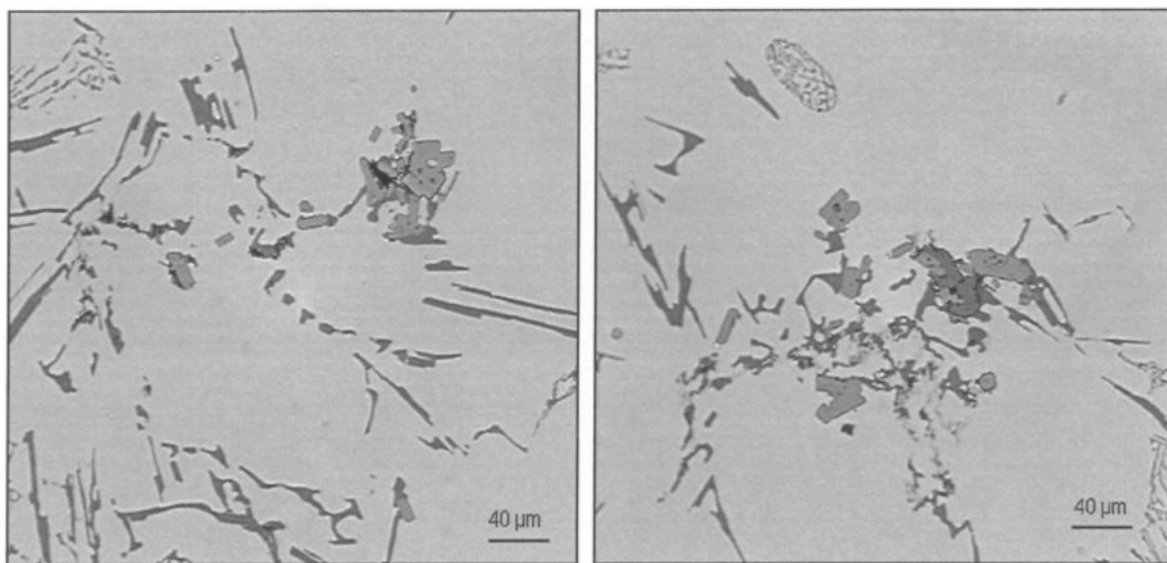


Figure 6.7 Microstructures of Al-6%Si alloy after addition of TiB₂ (powder source) at the end of the LiMCA test.

6.2.2 Evaluation of TiB₂ Inclusions (added as Al-5%Ti-1%B master alloy)

In this case, the TiB₂ inclusions were introduced into the melt through the addition of Al-5%Ti-1%B master alloy. An 8.5 kg charge of Al-5%Si alloy was melted. The melt temperature was kept at 680°C. Degassing was carried out for 15 min. Following this, 150g of Al-5%Ti-1%B master alloy was added to the melt. The melt was stirred properly to ensure dispersion of the master alloy throughout the melt. LiMCA samplings of the TiB₂-containing alloy melt were taken (four tests), each for a period of 30 min. Although the melt temperature was set to 680°C, the temperature varied somewhat from test to test as follows:

Test 1: 674°C, Test 2: 693 °C

Test 3: 683 °C, Test 4: 681°C

N₂₀ Measurements: Total concentration number of inclusions (inclusions > 20µm)

The N₂₀ plot for the above case is shown in Figure 6.8, while Figure 6.9 shows the distribution of the total number of inclusions as a function of particle size over the 30 min period of sampling. As in the case of TiB₂ power inclusion addition, the third and fourth tests show the highest concentration of inclusions. However, the inclusion counts are almost half those of the former. In addition, for the third and fourth tests, the concentration levels drop rapidly after about 10-12 min of sampling. This tendency is clearly reflected in Figure 6.9. It is also seen that in the master alloy addition, inclusion particle sizes are mainly concentrated in the 20-35 µm range.

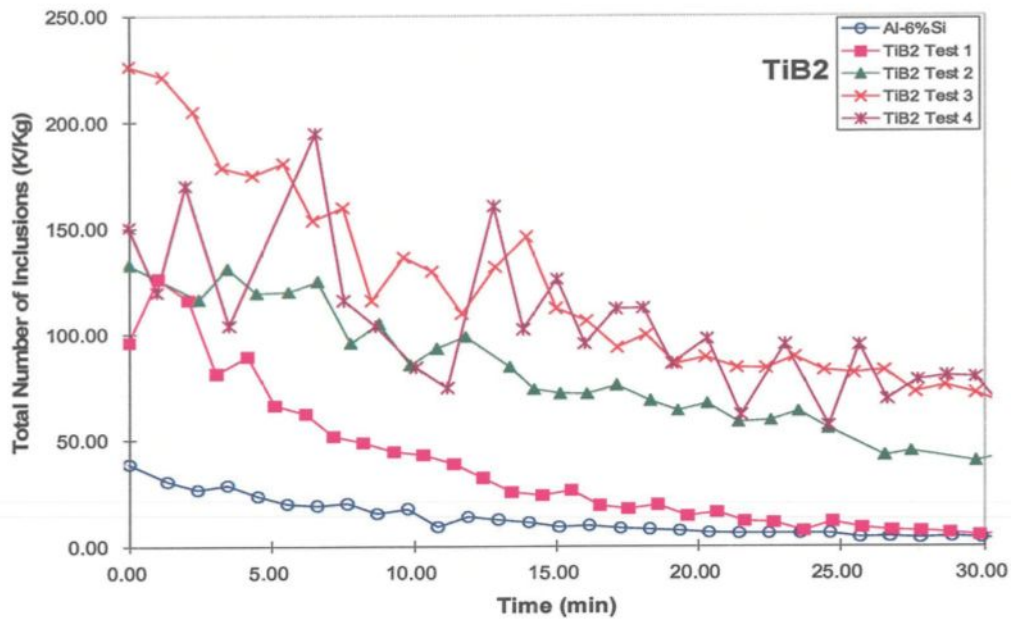


Figure 6.8 Concentration number of TiB_2 inclusions (master alloy source) in Al-6%Si alloy as a function of time.

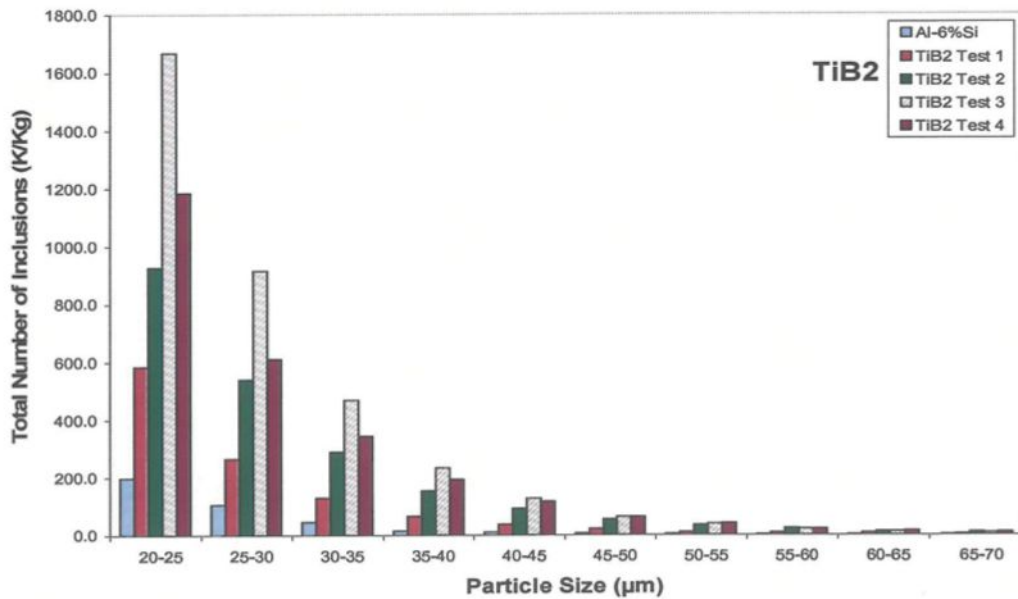


Figure 6.9 Total number of TiB_2 inclusions (master alloy source) in Al-6%Si alloy as a function of particle size.

It should be mentioned that in Test 3, the melt was held at 683 °C temperature for a long time (overnight) before the sampling was done the next day, providing ample time for the master alloy to react with the melt. This is reflected in the highest concentration levels obtained for Test 3 amongst the others. In this context, in their studies on the sedimentation and agglomeration behaviour of Al-Ti-B and Al-Ti-C grain refiners, Gazanion *et al.*⁶² have reported that the sedimentation behaviour of TiB₂ particles remains the same over holding periods of up to 24 hours. The TiB₂ particles and clusters (20-25 µm) tend to agglomerate together to reduce the surface energy during sedimentation and further holding. However, these particles are very stable in the melt during holding. In a way, the high concentrations of TiB₂ in Test 3 reflect these findings. Table 6.3 lists the actual concentrations that were obtained for the various tests.

Table 6.3 Inclusion concentration vs. particle size in base and TiB₂-containing Al-6%Si alloy melts (master alloy addition)

Alloy Melt/ Test (Temp)	Inclusion Concentration (K/Kg) vs. Particle Size (µm)									
	20-25	25-30	30-35	35-40	40-45	45-50	50-55	55-60	60-65	65-70
Al-6%Si base (680 °C)	199.1	105.1	45.5	14.8	10.3	5.1	2.6	1.0	0.5	0.5
Al-6%Si+TiB ₂ Test 1 (674 °C)	584.6	265.9	129.7	64.9	36.2	20.7	9.8	7.2	6.9	2.9
Al6%Si+TiB ₂ Test 2 (693 °C)	927.1	540.0	290.3	153.5	93.1	55.1	35.3	22.2	13.2	10.3
Al-6%Si+ TiB ₂ Test 3 (683 °C)	1667.6	917.6	469.6	232.8	127.6	64.4	39.0	21.3	13.1	7.2
Al-6%Si+ TiB ₂ Test 4 (681 °C)	1184.8	610.7	344.7	194.7	117.1	63.7	41.5	21.9	15.1	9.4

A comparison of Test 3 and the base alloy inclusion readings is shown in Table 6.4 in ratio form.

Table 6.4 Comparison of inclusion readings of TiB₂-inclusion-containing (Test 3) and base Al-6%Si alloy melts reported in Table 6.3

Melt A: Melt B	Ratio of Inclusion Concentrations									
	Particle Size Range (μm)									
	20-25	25-30	30-35	35-40	40-45	45-50	50-55	55-60	60-65	65-70
Al-6%Si+ TiB ₂ (Test 3): Al-6%Si	8.37	8.73	10.32	15.72	12.38	12.62	15.0	21.3	26.2	14.4

As Table 6.4 shows, in the case of master alloy addition, a comparison of Test 3 and the base alloy inclusion readings provides much smaller ratios than those seen in Table 6.2 for the powder addition of TiB₂, for particle sizes of 30 μm and above, whereas much higher ratios are observed for particle sizes below 30 μm (*i.e.*, in the 20-25 μm range).

C₂₀ Measurements: Volumic concentration of inclusions (inclusions > 20μm)

Figure 6.10 shows the C₂₀ plot for the volumic concentration of TiB₂ inclusions over 40 min of sampling. The volumic concentrations follow the same tendency as the N₂₀ curves of Figure 6.8. The extension in sampling time to 40 min showed that after 30 min, the concentration values remained stable. In other words, a sampling time of 30 min is sufficient to obtain a good estimation of the inclusion behavior.

The plot of volumic concentration vs. particle size, Figure 6.11, shows not only high volume concentrations in the lower particle size ranges (20-40 μm), but also relatively significant amounts over all the particle size ranges when compared to Figure 6.9. This is one of the noticeable features associated with TiB₂ inclusions.

Figure 6.12 and 6.13 show microstructures corresponding to melts containing Al-5%Ti-1%B master alloy before and after a LiMCA sampling. The difference in the inclusion concentrations can be clearly observed. It is also interesting to compare the morphologies of the TiB_2 inclusions in Figure 6.12 with those shown in Figure 6.6, coming from the two sources of TiB_2 addition (*viz.*, powder *vs.* master alloy).

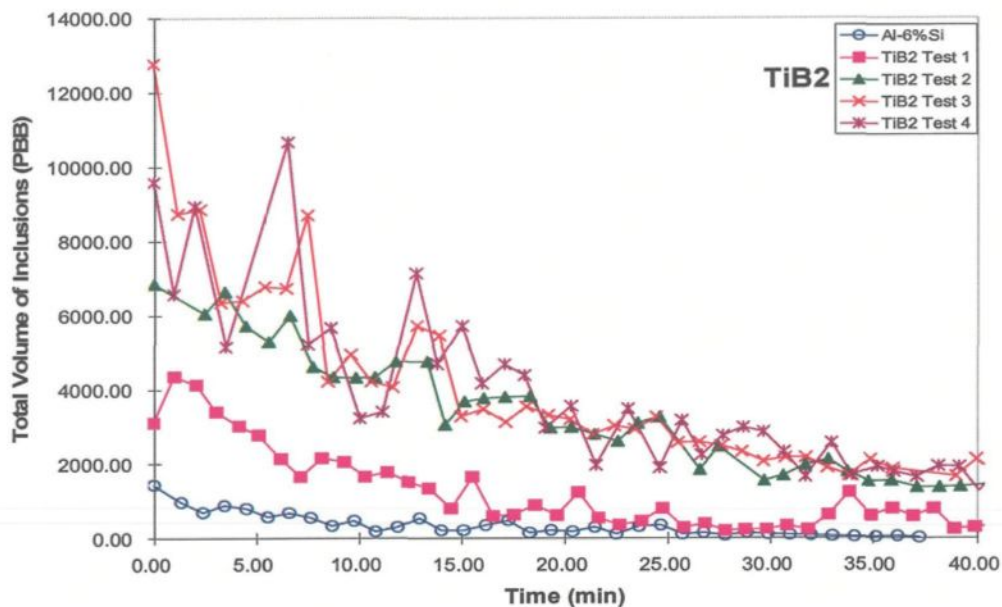


Figure 6.10 Volumic concentration of TiB_2 inclusions (master alloy source) in Al-6%Si alloy as a function of time.

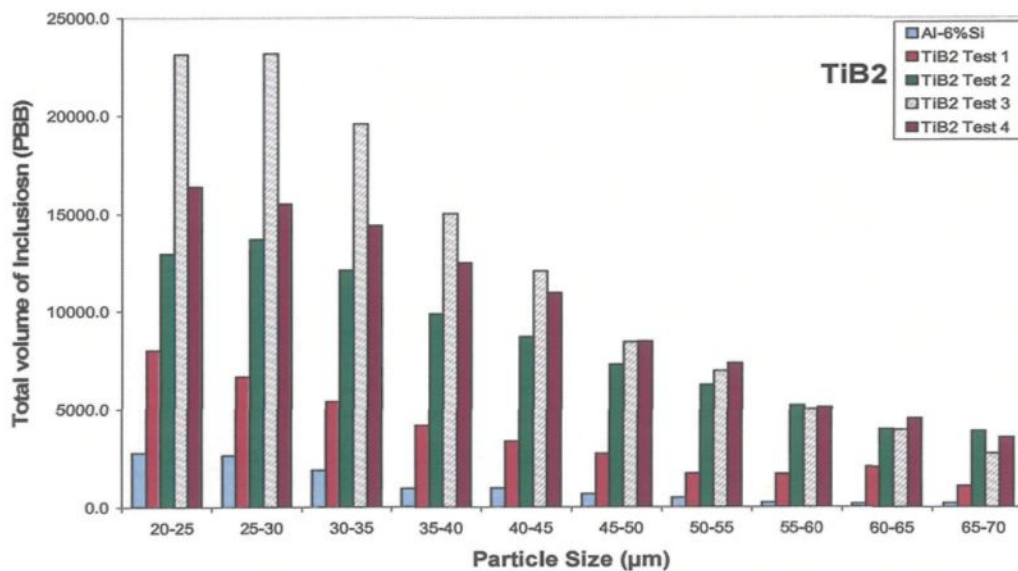


Figure 6.11 Total volume of TiB_2 inclusions (master alloy source) in Al-6%Si alloy as a function of particle size.

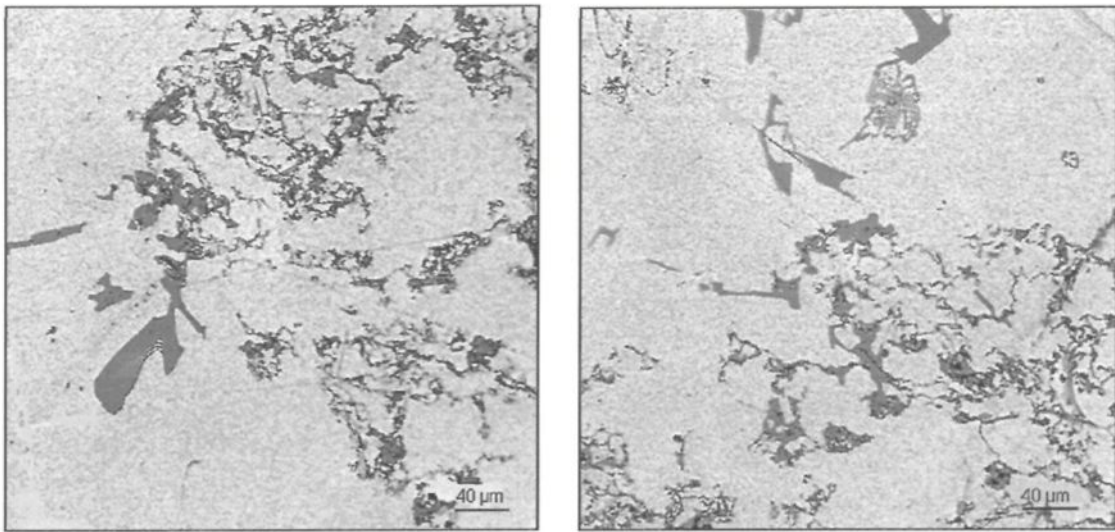


Figure 6.12 Microstructures of Al-6%Si alloy after addition of TiB₂ (as Al-5%Ti-1%B master alloy) before the start of the LiMCA test.

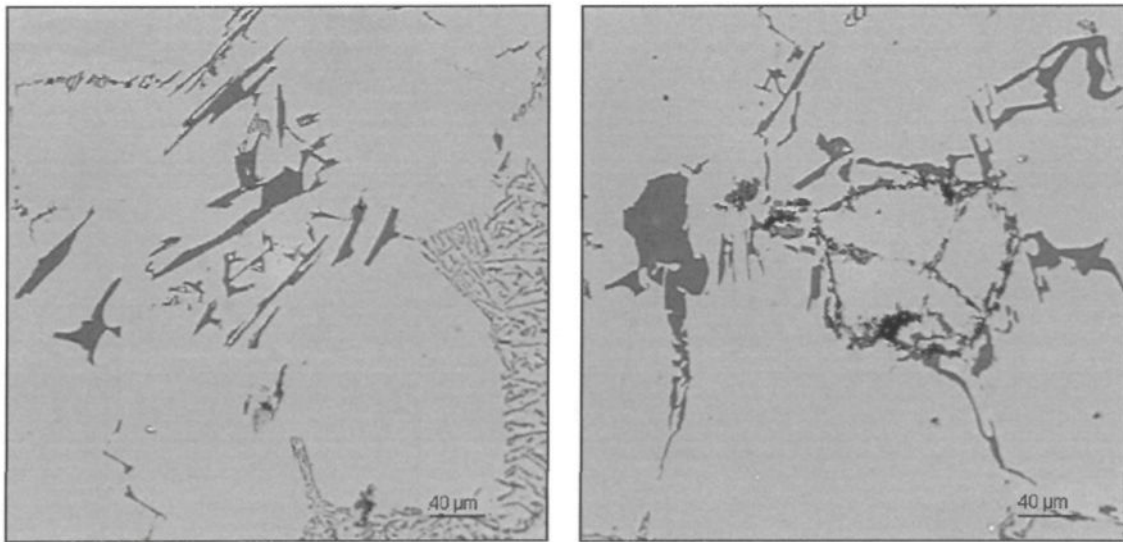


Figure 6.13 Microstructures of Al-6%Si alloy after addition of TiB₂ (as Al-5%Ti-1%B master alloy) at the end of the LiMCA test.

6.2.3 Evaluation of Al_4C_3 Inclusions (added as powder)

The Al_4C_3 inclusions were added to the Al-6%Si alloy melt following the same procedure as that described in section 6.2, with the melt temperature maintained at 680 °C. Five LiMCA tests were conducted. Again, although the melt furnace temperature was preset to 680 °C, the temperature varied somewhat from test to test as follows.

Test 1: 694 °C, Test 2: 685 °C, Test 3: 680 °C

Test 4: 687 °C, Test 5: 680 °C

N_{20} Measurements: Total concentration number of inclusions (inclusions > 20 μm)

Figure 6.14 shows the N_{20} plots for the LiMCA samplings corresponding to the Al_4C_3 inclusion addition. Test 1 shows the highest concentration of inclusions. In general, the concentrations drop relatively rapidly over the first ten minutes of sampling, then decrease gradually and remain stable after about 25 min. Figure 6.15 reflects this tendency and also shows that in the case of the Al_4C_3 inclusions, the dominant particle size ranges from 20 to 30 μm . Not many particles with sizes > 45 μm are observed.

C_{20} Measurements: Volumic concentration of inclusions (inclusions > 20 μm)

Figure 6.16 shows the total volumic concentration of Al_4C_3 inclusions over the 30 min period of LiMCA sampling, while Figure 6.17 shows the corresponding volume concentrations as a function of particle size. The volume concentrations are observed to spread over a larger range of particle sizes (from 20 to 50 μm), with limited concentration value also observed in the largest particle size range.

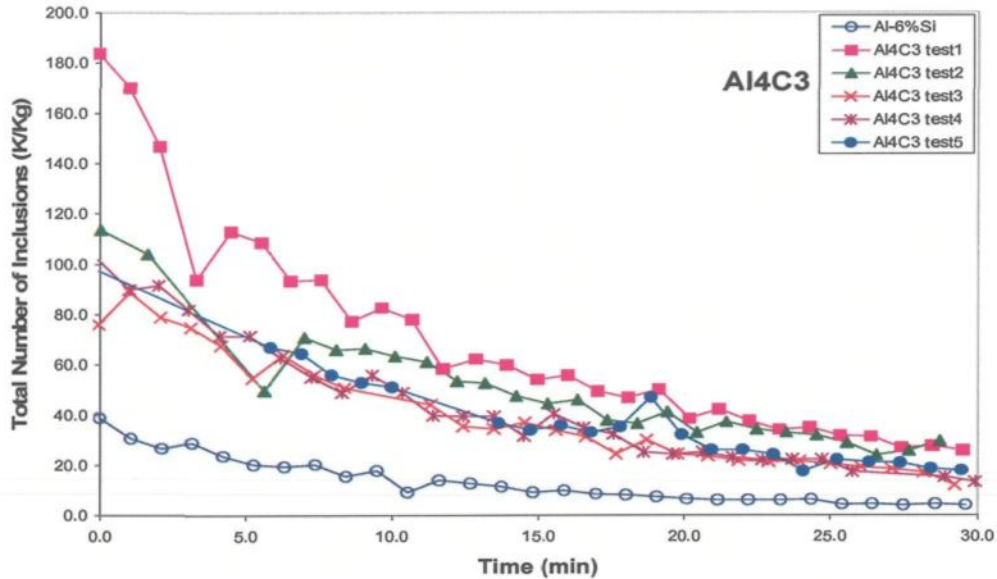


Figure 6.14 Concentration number of Al_4C_3 inclusions (powder source) in Al-6%Si alloy as a function of time.

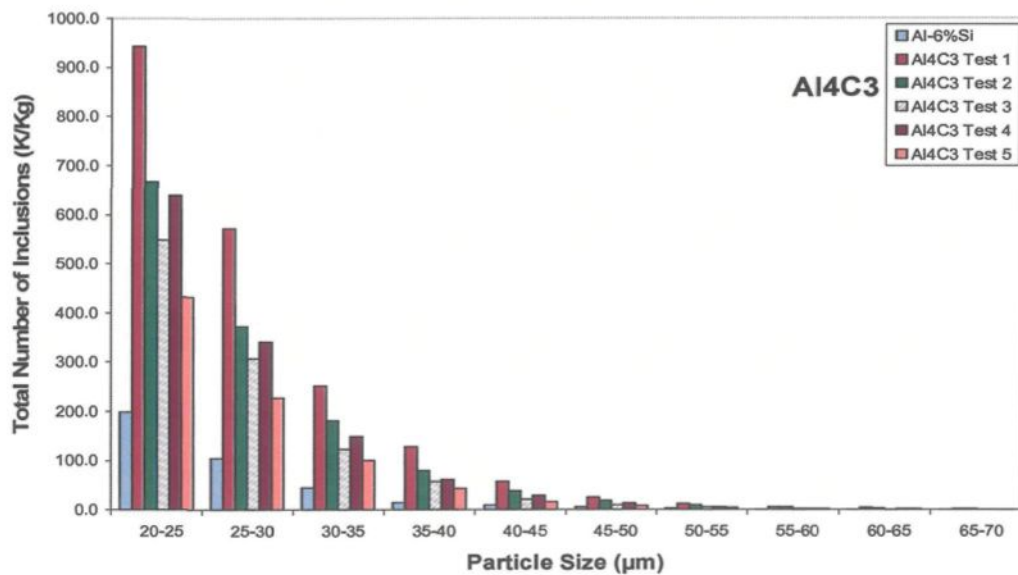


Figure 6.15 Total number of Al_4C_3 inclusions (powder source) in Al-6%Si alloy as a function of particle size.

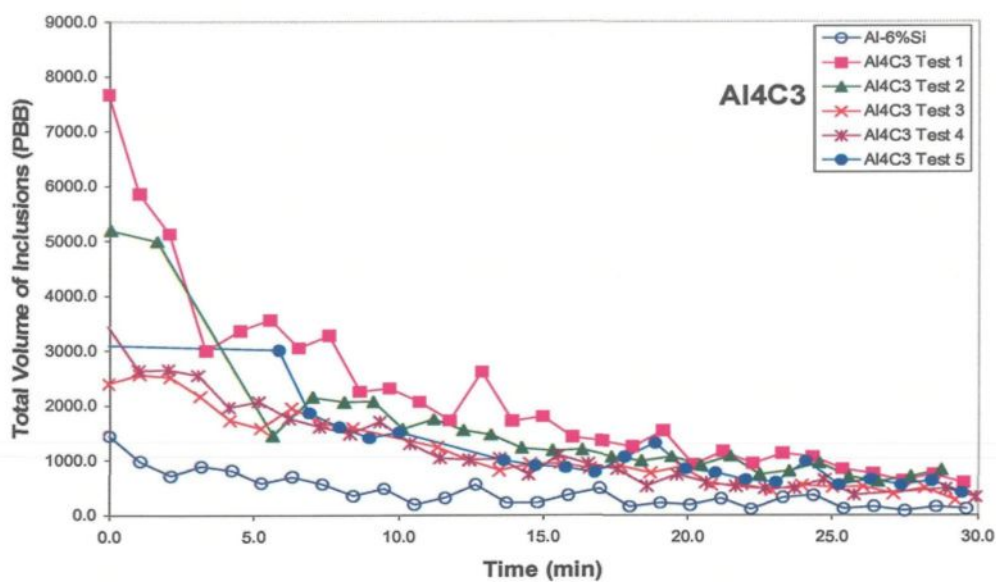


Figure 6.16 Volumic concentration of Al_4C_3 inclusions (powder source) in Al-6%Si alloy as a function of time.

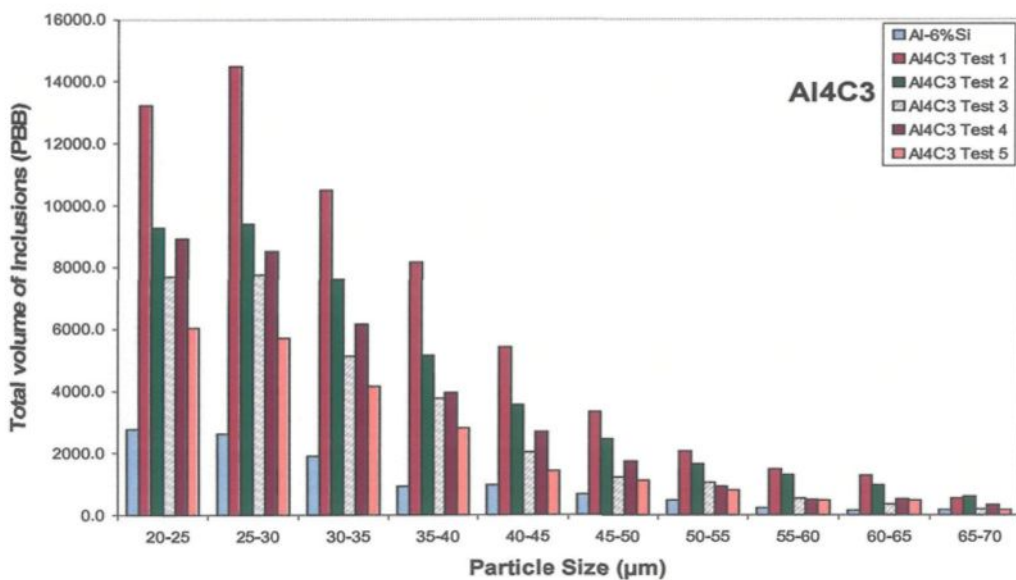


Figure 6.17 Total volume of Al_4C_3 inclusions (powder source) in Al-6%Si alloy as a function of particle size.

As in the case of the TiB_2 inclusions, the Al_4C_3 inclusions are also associated with comparatively significant volumes, particularly for particles in the 25-30 μm range.

6.2.4 Evaluation of Al_2O_3 Inclusions (added as MMC)

The Al_2O_3 inclusions were added to the Al-6%Si alloy melt following the same procedure as that described in section 6.2, with the melt temperature maintained at 680 °C. The source of Al_2O_3 inclusions was in form of an Al_2O_3 particulate reinforced aluminum metal matrix composite alloy (MMC), rather than the power injected Al-6%Si alloy ingots used for other inclusion additions. For this, 684g of composite alloy were added to the 8.5 Kg melt of Al-6%Si base alloy. The melt temperature was kept at 680 °C. Five LiMCA samplings were carried out. In this case, also, although the melt furnace temperature was preset to 680 °C, the temperature varied somewhat from test to test as follows.

Test 1: 692 °C, Test 2: 680 °C, Test 3: 682 °C

Test 4: 675 °C, Test 5: 693 °C

N₂₀ Measurements: Total concentration number of inclusions (inclusions > 20 μm)

Figure 6.18 shows the N_{20} plots for the LiMCA samplings corresponding to the Al_2O_3 inclusion addition. Test 2 shows the highest concentration of inclusions. In general, due to the density difference between the Al_2O_3 inclusions and the melt, the inclusion concentrations drop considerably after 10-15 minutes of sampling, then decrease gradually and remain stable after about 25 min.

Figure 6.19 reflects this tendency and also shows that in the case of the Al_2O_3 inclusions, the dominant particle size ranges from 20 to 25 μm . For particle sizes greater

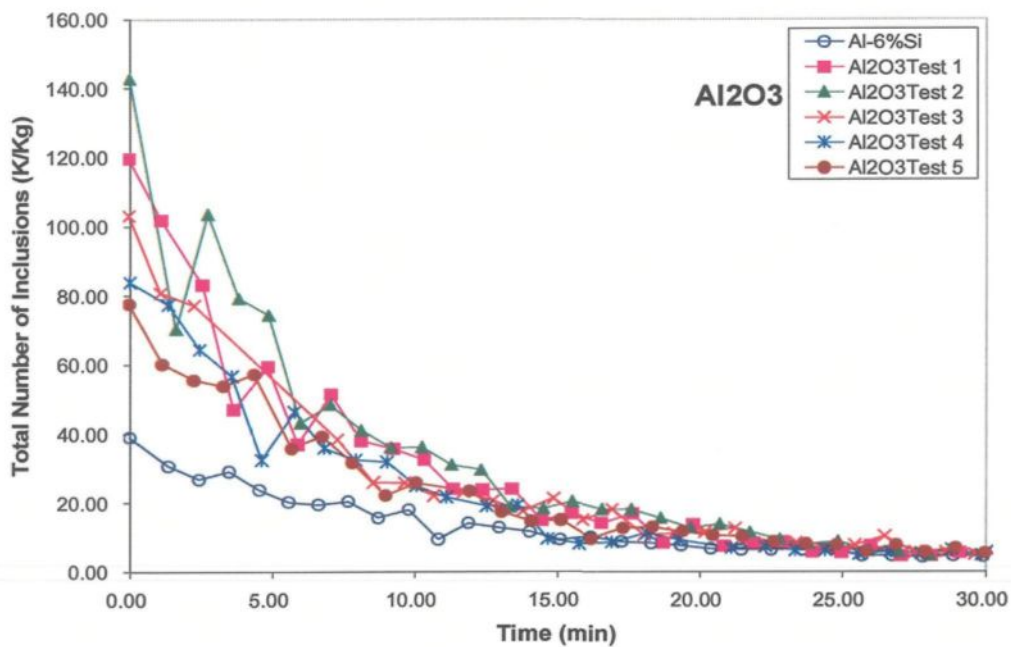


Figure 6.18 Concentration number of Al_2O_3 inclusions (MMC source) in Al-6%Si alloy as a function of time.

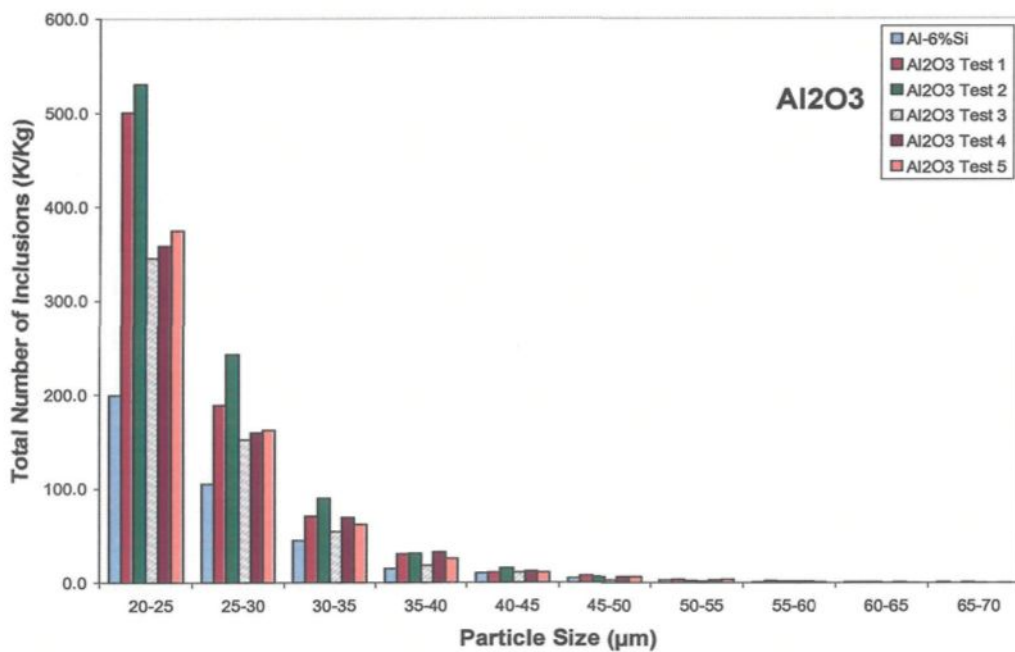


Figure 6.19 Total number of Al_2O_3 inclusions (MMC source) in Al-6%Si alloy as a function of particle size.

than 50 μm , hardly any inclusions are recorded. The average particle size of the Al_2O_3 inclusions was $\sim 23 \mu\text{m}$.⁶¹ As seen in Figure 6.18, the curves for the different LiMCA tests are alike. This indicates that the LiMCA is reliable over different tests without change in test condition (*i.e.*, for the same melt). As to why the amount of inclusions decreases from Test 1 to Test 5, this is explained by the fact that the melt is both stirred and its surface skimmed to remove surface oxides and dross before a LiMCA sampling is taken. A certain number of inclusions will definitely be removed on account of both these processes. In addition, samplings for microstructural analysis taken before and after a LiMCA sampling in some cases would further decrease the inclusion concentration levels in the melt.

C₂₀ Measurements: Volumic concentration of inclusions (inclusions >20 μm)

Figure 6.20 shows the total volumic concentration of Al_2O_3 inclusions over the 30 min period of LiMCA sampling, while Figure 6.21 shows the corresponding volume concentrations as a function of particle size. The volumic concentrations are observed to spread over a larger range of particle sizes (from 20 to 50 μm), with a limited concentration value also observed in the largest particle size range. Test 2 shows the highest concentrations of Al_2O_3 inclusions amongst the other tests. Comparison of Test 2 with Al-6%Si base alloy (before addition of inclusions) for different particle sizes in terms of volume of inclusions shows that the 20-25 μm sized particles show highest volume of Al_2O_3 inclusions with respect to the base alloy. After one minute of testing, the total volume of Al_2O_3 inclusions with 3529.6 ppb decreased to 139 ppb in 30th minute of the test during this time the number of inclusions in Al-6%Si base alloy without addition changed

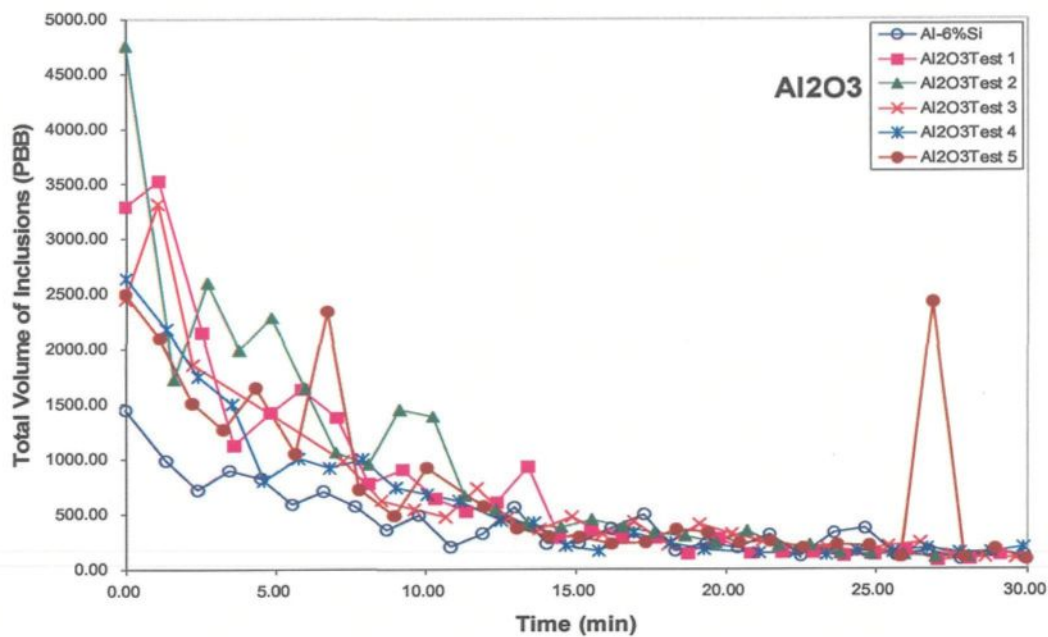


Figure 6.20 Volumic concentration of Al₂O₃ inclusions (MMC source) in Al-6%Si alloy as a function of time.

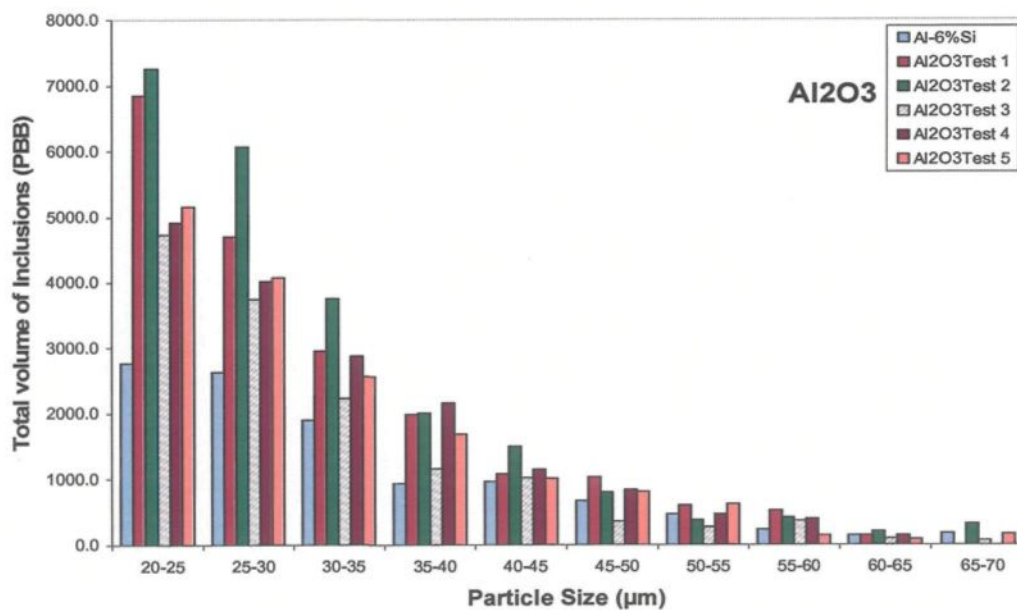


Figure 6.21 Total volume of Al₂O₃ inclusions (MMC source) in Al-6%Si alloy as a function of particle size.

from 987.3 to 123.8 ppb after 30 minute of test with LiMCA. In extending the measurement time to 40 min, it was observed that the curve remained stable. The number and volume of inclusion particles as a function of particle size showed the same decreasing trend with increase in particle size.

6.2.5 Evaluation of CaO Inclusions (added as powder)

The CaO inclusions were added to the Al-6%Si alloy melt following the same procedure as that described in section 6.2, with the melt temperature kept at 680 °C. Five LiMCA samplings were taken. In this case also, the melt temperature varied from test to test as follows.

Test 1: 694 °C, Test 2: 682 °C, Test 3: 680 °C
Test 4: 683 °C, Test 5: 680 °C

N₂₀ Measurements: Total concentration number of inclusions (inclusions > 20µm)

Figure 6.22 shows the N₂₀ plots for the LiMCA samplings corresponding to the CaO inclusion addition to the Al-6%Si alloy melt, over the 30 min period of sampling. The highest inclusion concentrations are observed for Test 1 and Test 4 and, after about 20 min, the readings stabilize in each case. Figure 6.23 shows the corresponding distribution of inclusions as a function of particle size.

Compared to other inclusion additions, the concentration of CaO inclusions is much less, as expected, due to the problems associated with the low wettability of the CaO inclusions and hence their incorporation into the melt.

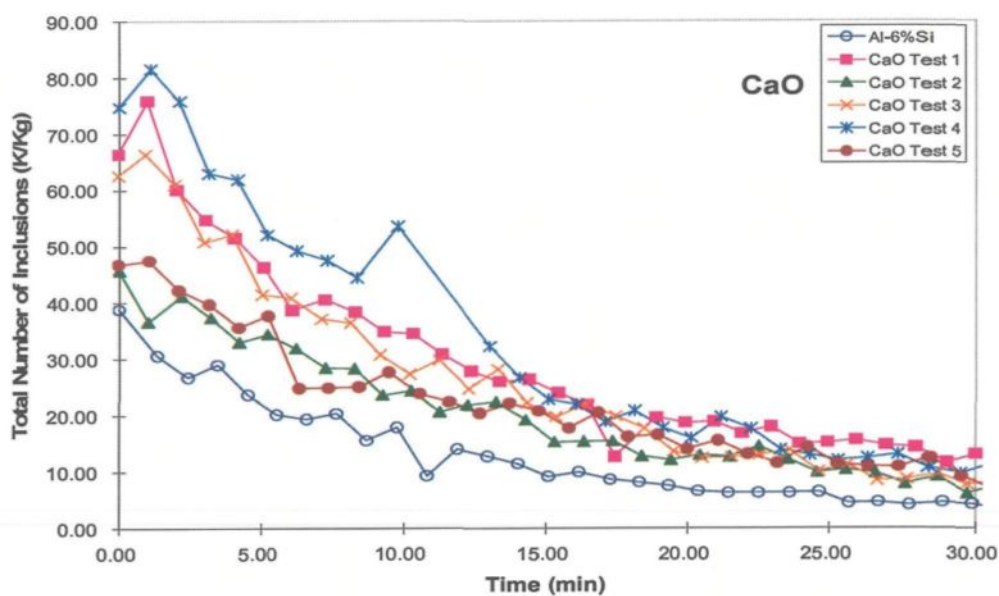


Figure 6.22 Concentration number of CaO inclusions (powder source) in Al-6%Si alloy as a function of time.

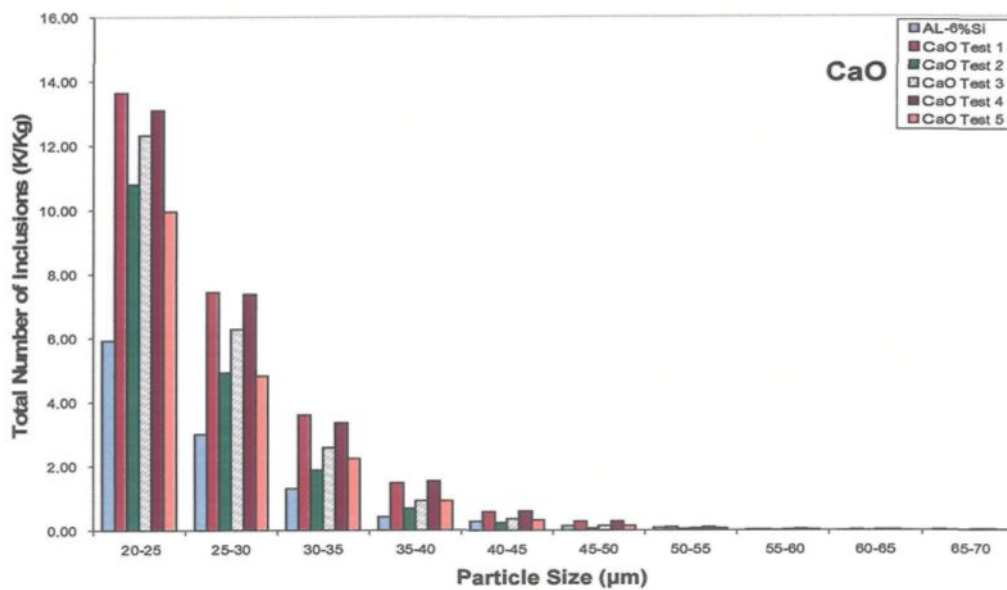


Figure 6.23 Total number of CaO inclusions (powder source) in Al-6%Si alloy as a function of particle size.

Table 6.5 shows the actual inclusion concentrations (in K/Kg) that were obtained for the samplings in this case, corresponding to the different particle sizes. A comparison of Test 1 and the base alloy inclusion readings in Table 6.6 shows ratios that are very much smaller than those observed in the case of other inclusions (see, for example, Table 6.2).

Table 6.5 Inclusion concentration vs. particle size in base and CaO-containing Al-6%Si alloy melts (master alloy addition)

Alloy Melt/ Test (Temp)	Inclusion Concentration (K/Kg) vs. Particle Size (μm)									
	20-25	25-30	30-35	35-40	40-45	45-50	50-55	55-60	60-65	65-70
Al-6%Si base (680 °C)	199.1	105.1	45.5	14.8	10.3	5.1	2.6	1.0	0.5	0.5
Al-6%Si+CaO Test 1 (694 °C)	450.5	246.8	120.2	50.1	19.4	10.2	3.2	1.0	1.0	0.1
Al6%Si+ CaO Test 2 (682 °C)	358.8	165.7	64.1	22.9	8.3	2.1	1.3	0.3	0.2	0.3
Al-6%Si+ CaO Test 3 (680 °C)	434.8	228.3	94.7	33.7	12.2	4.3	2.1	0.7	0.3	0.1
Al-6%Si+ CaO Test 4 (683 °C)	434.6	255.4	118.0	55.5	21.7	10.2	4.2	1.6	1.0	0.6
Al-6%Si+ CaO Test 5 (680 °C)	345.4	173.0	80.8	34.5	11.7	5.8	2.1	1.1	0.2	0.3

Table 6.6 Comparison of inclusion readings of CaO-inclusion-containing (Test 1) and base Al-6%Si alloy melts reported in Table 6.5

Melt A: Melt B	Ratio of Inclusion Concentrations									
	Particle Size Range (μm)									
	20-25	25-30	30-35	35-40	40-45	45-50	50-55	55-60	60-65	65-70
Al-6%Si+ CaO Test 1: Al-6%Si	2.26	2.35	2.64	3.38	1.88	2.00	1.23	1.00	2.00	0.20

C₂₀ Measurements: Volumic concentration of inclusions (inclusions > 20 μ m)

Figure 6.24 shows the C₂₀ volumic concentration plots over the 30 min period of LiMCA sampling. The highest volume concentrations are observed for Test 4 and Test 1. After 15 min of sampling, the volume concentrations (for all tests) drop down to a minimum and remain stable until the end of the sampling period.

The high volume concentrations in the case of Test 4 and Test 1 can be understood by looking at the data provided in Table 6.5. In both tests, inclusions in the 30-35 μ m and 35-40 μ m size ranges are much higher than those noted in the other tests. These will naturally be associated with larger volumes. Thus, other inclusion size ranges being similar for all tests, Tests 4 and 1 will exhibit the highest volume concentrations. Compared to the base alloy, as well, inclusions in the 30-40 μ m range are higher in the case of the CaO-containing melt (Table 6.6).

Figure 6.24 also shows that the more the inclusions detected in a test early on during the sampling period, the more inclusions with larger particle sizes that will be present in the melt. These will settle down with time, so that towards the end of the sampling, the volume concentrations (as detected by LiMCA) will reach their stable, minimum value.

Figure 6.25 shows the distribution of the volume concentration of inclusions as a function of particle size, where Tests 4 and 1 show the highest volume concentrations as well as relatively high concentrations in the 30-40 μ m particle size range.

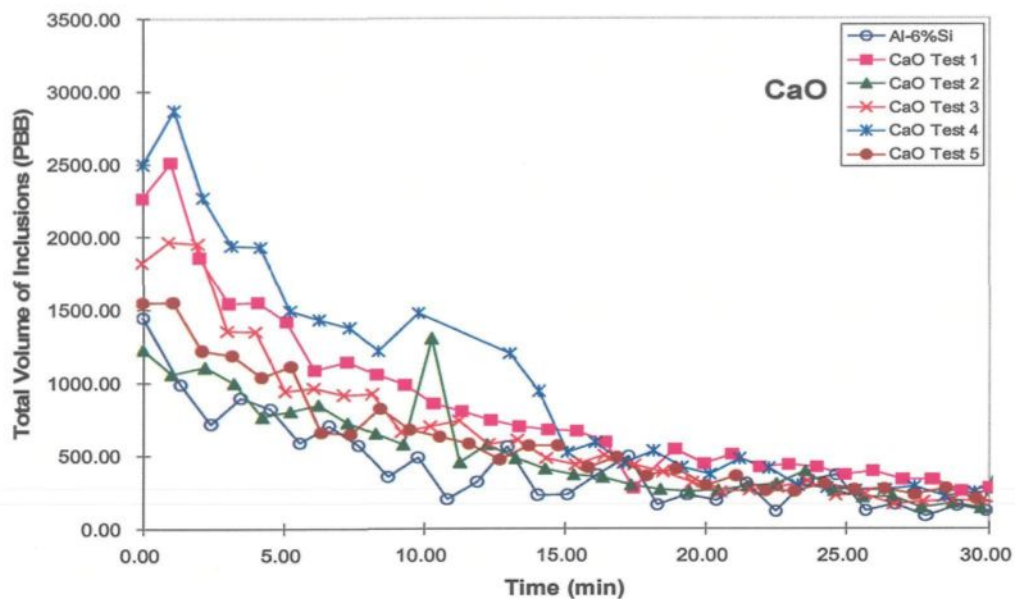


Figure 6.24 Vulomic concentration of CaO inclusions (powder source) in Al-6%Si alloy as a function of time.

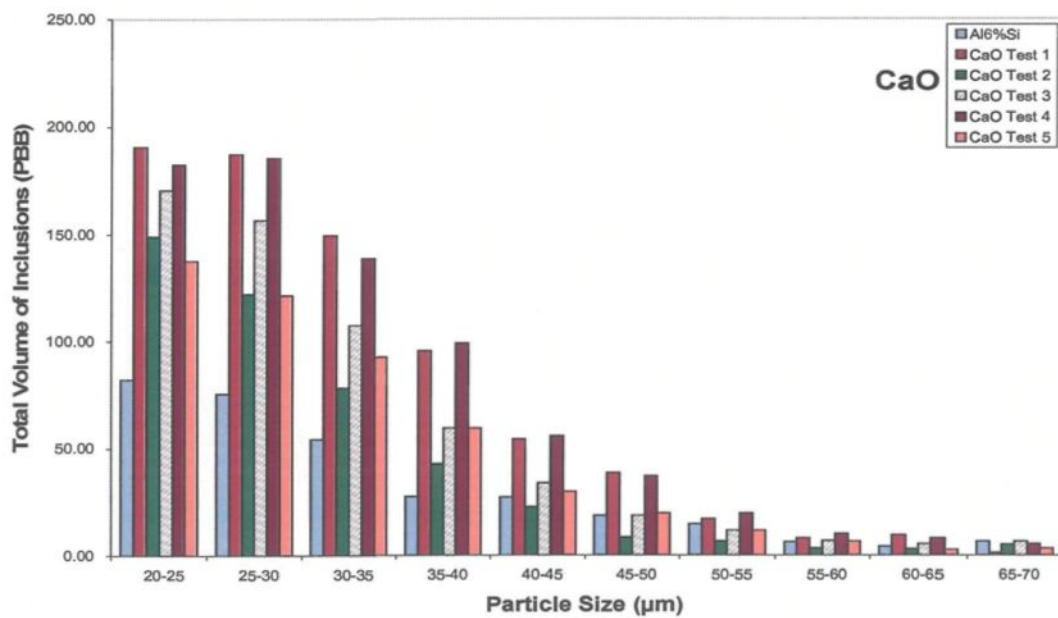


Figure 6.25 Total volume of CaO inclusions (powder source) in Al-6%Si alloy as a function of particle size.

6.2.6 Evaluation of MgO Inclusions (added as powder and Mg metal)

The MgO inclusions were added to the Al-6%Si alloy melt following the same method as that described in section 6.2, with the melt temperature kept at 680 °C. Four LiMCA samplings were taken. Following that, 200 g of Mg in the form of metal was directly added to the remaining Al-6%Si alloy melt containing the MgO powder inclusions. The melt was superheated at 800 °C to generate MgO oxide formation. The melt temperature was brought down to 680 °C before the LiMCA sampling was done. This step was taken to increase the amount of MgO inclusions in the melt, given that the previous LiMCA samplings showed very low concentrations of MgO. Direct addition of Mg metal to the melt and its oxidation under the superheated melt conditions was expected to considerably increase the MgO inclusion level. This was actually found to be the case, as the corresponding LiMCA sampling showed. The samplings were done with the melt temperature kept at 680 °C. Temperature variations from sampling to sampling were as follows.

Test 1: 700 °C, Test 2: 680 °C, Test 3: 680 °C
Test 4: 682 °C, Test 5 (Mg addition): 680 °C

N₂₀ Measurements: Total concentration number of inclusions (inclusions > 20µm)

Figure 6.26 shows the N₂₀ plots for the four LiMCA samplings for the MgO inclusion addition to the Al-6%Si alloy melt and a last sampling with Mg metal added to the melt. The sampling was carried out for 40 min. While Test 4 shows the highest number of MgO inclusions amongst the four tests, after about 25 min, the inclusion levels drop to a

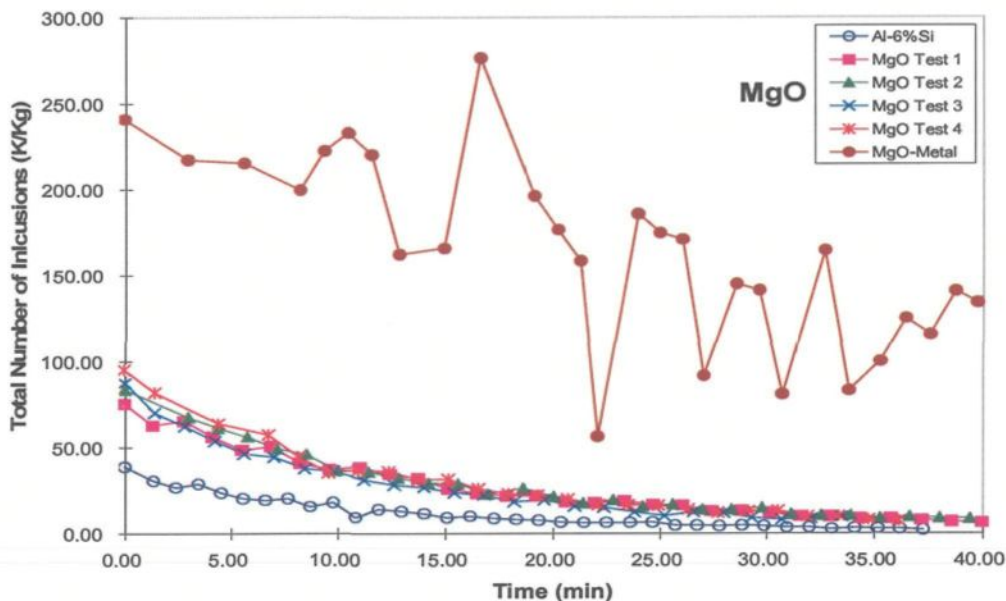


Figure 6.26 Concentration number of MgO inclusions (powder + metal source) in Al-6%Si alloy as a function of time.

minimum level that remains stable until the end of the sampling. In comparison, addition of Mg metal to the melt increased the inclusion concentration remarkably: two to two-and-a-half times greater than that observed for Test 4, with the concentration remaining consistent overall over the entire sampling period. This result reveals the high oxidation potential of Mg. Apparently, direct addition of the metal is a much better source of MgO inclusions than using MgO powder itself.

Figure 6.27 shows the corresponding distribution of inclusions as a function of particle size. Clearly, the MgO inclusion levels for the Mg metal addition stand out from the others.

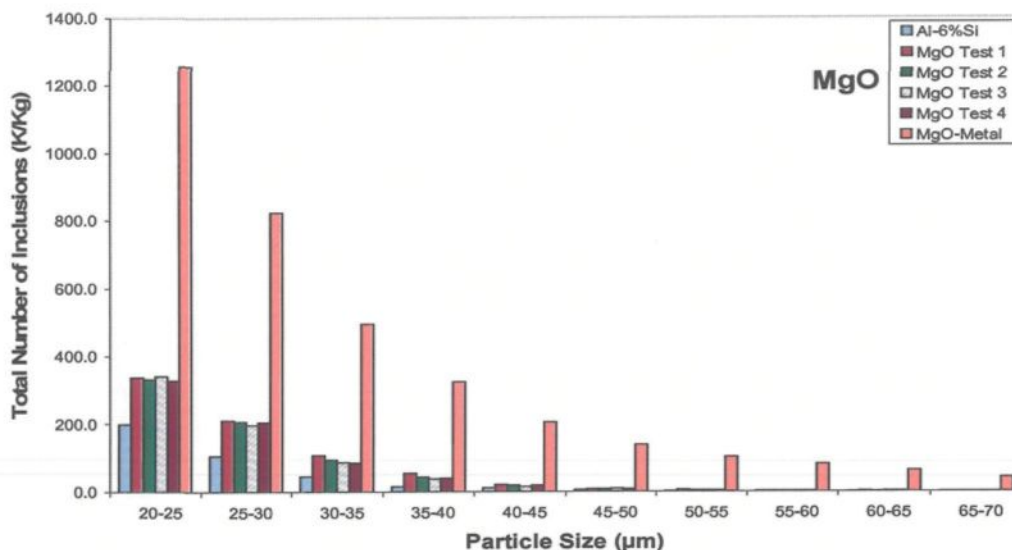


Figure 6.27 Total number of MgO inclusions (powder + metal source) in Al-6%Si alloy as a function of particle size.

C₂₀ Measurements: Volumic concentration of inclusions (inclusions > 20 µm)

Figure 6.28(a) shows the C₂₀ plots for the volumic concentrations for the four LiMCA tests carried out after MgO powder addition to the Al-6%Si alloy melt (maintained at 680 °C). More or less consistent volume concentrations are obtained for all the samplings. The values decrease rapidly within 15 min of sampling, then more gradually until, at about 30 min, the values are stable and at their minimum concentrations (~300 ppb).

Compared to the maximum volumic concentrations of 3200 ± 300 ppb for the powder addition, Figure 6.28(b), the Mg metal addition produces MgO inclusion volume concentrations that range on average from about 20,000 to 10,000 ppb over the entire sampling period (the high concentration value at ~18 min is erroneous and thus not taken into account).

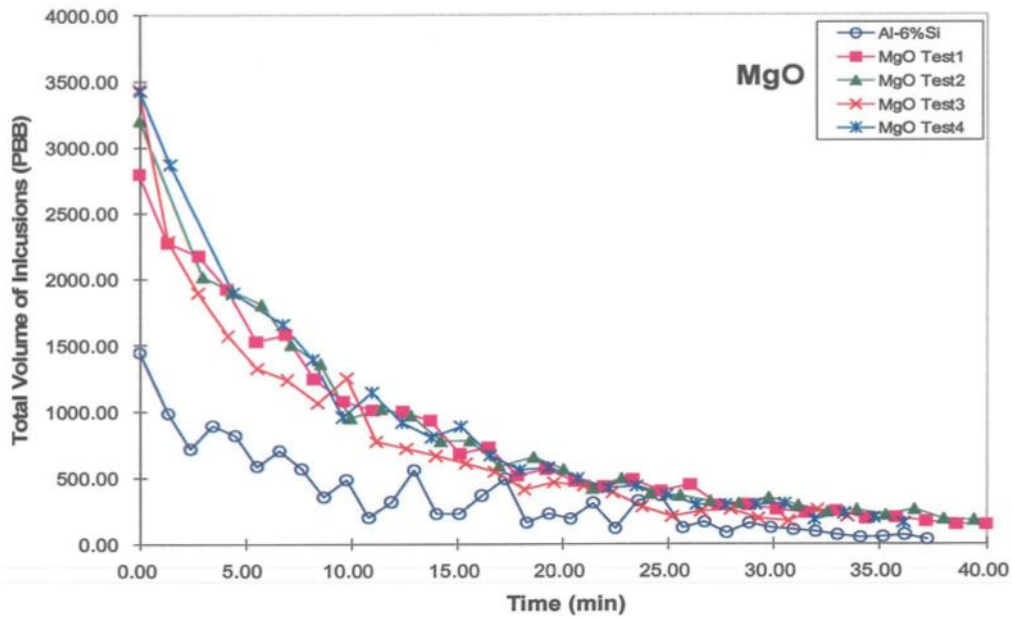


Figure 6.28(a) Volumic concentration of MgO inclusions in Al-6%Si alloy as a function of time (MgO powder addition).

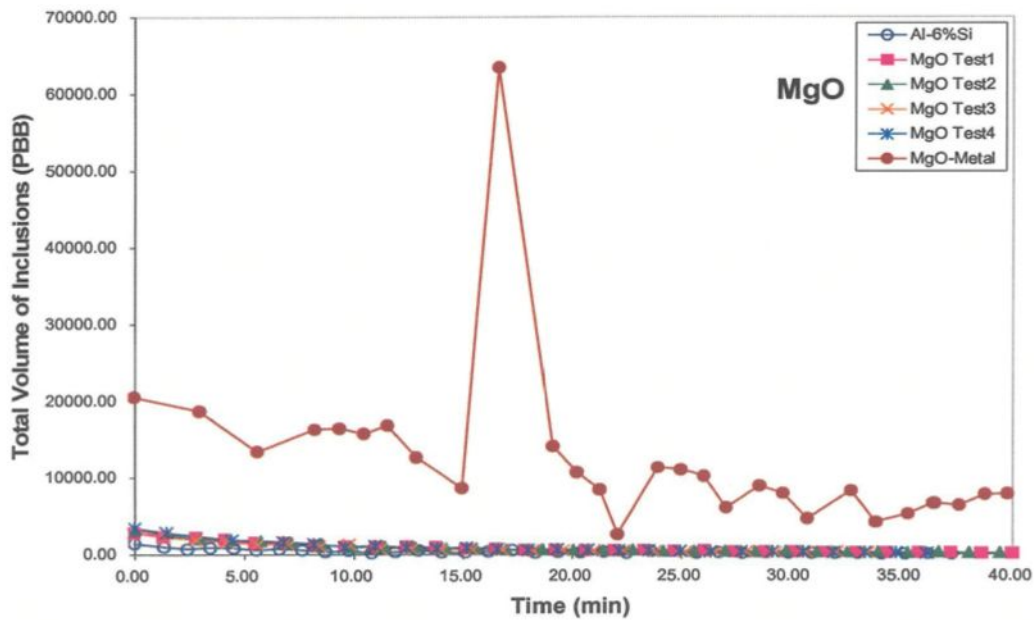


Figure 6.28(b) Comparison of volumic concentration of MgO inclusions in Al-6%Si alloy as a function of time: MgO powder vs. Mg metal addition.

Figure 6.29 shows the corresponding volume concentration of MgO inclusions as a function of the particle size. The Mg metal addition shows very high volumes of inclusions for all particle sizes. In comparison, the MgO powder addition shows significant concentrations only up to 40-45 μm particle sizes. Even so, these concentrations are four times smaller than those obtained with the Mg metal addition (*cf.* 5000 ppb and 20,000 ppb).

In a way, the results of Figure 6.29 demonstrate the sensitivity and reliability of the LiMCA technique to the presence of inclusions added to the melt and to the changes resulting from the change in source that provides these inclusions to the melt.

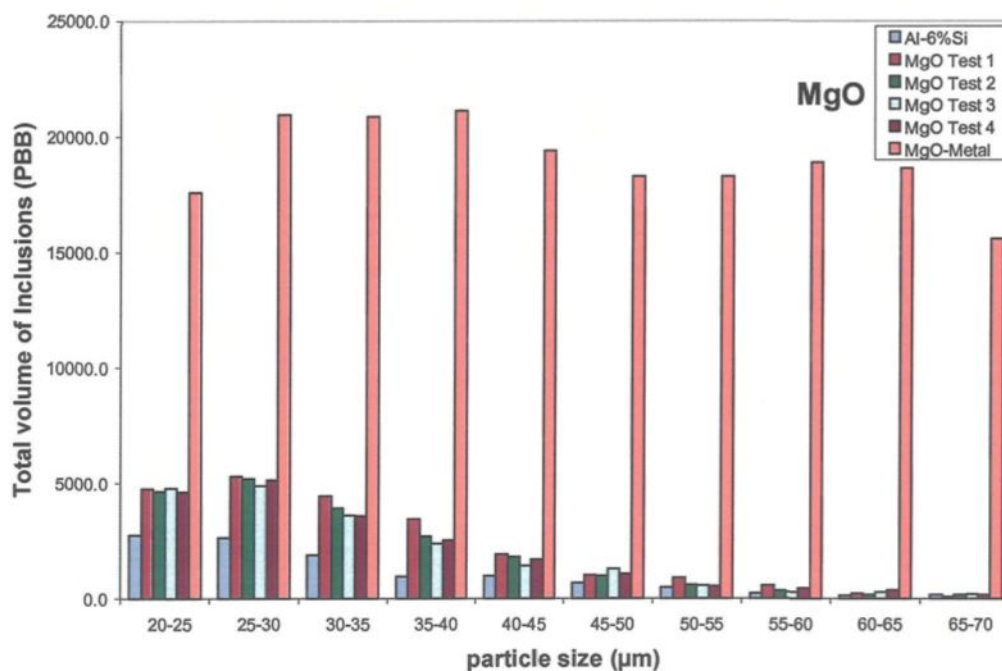


Figure 6.29 Total volume of MgO inclusions (powder + metal source) in Al-6%Si alloy as a function of particle size.

6.2.7 Evaluation of TiAl_3 Inclusions (added as Al-Ti 10% master alloy)

Following the same procedures outlined in section 6.2, the TiAl_3 inclusions were added to a 8.5 Kg melt of Al-6%Si alloy in the form of Al-10%Ti master alloy (250 gm). The melt temperature was kept at 680 °C. The melt was stirred properly to disperse the inclusion particles throughout the melt. Following this, a LiMCA sampling of the melt was taken.

N_{20} Measurements: Total concentration number of inclusions (inclusions > 20 μm)

Figure 6.30 shows the N_{20} plots of the total number of TiAl_3 inclusions as a function of time during the 30 min sampling period. The plots for the TiAl_3 inclusion-containing and base Al-6%Si alloy melts show similar trends, with the former showing elevated inclusion levels, roughly twice those observed in the base alloy. The slope of the curve is gradual and stabilizes after about 20 min of sampling time.

Figure 6.31 shows the plot of the total number of inclusions as a function particle size. Most of the TiAl_3 inclusions are found to lie the particle size range of 20-35 μm , although larger particle sizes are also present even if in much smaller amounts (compared to practically none in the base alloy).

It is interesting to compare Figures 6.30 and 6.31 with Figures 6.8 and 6.9 for the TiB_2 inclusions added to the melt in the form of Al-5%Ti-1%B master alloy. The concentration numbers are much higher in the latter case: the TiB_2 inclusion levels reach ~100K/Kg levels at the *end* of the sampling period, while this is the level obtained at the *start* of the LiMCA sampling for the TiAl_3 inclusions. The slopes of the N_{20} curves in both

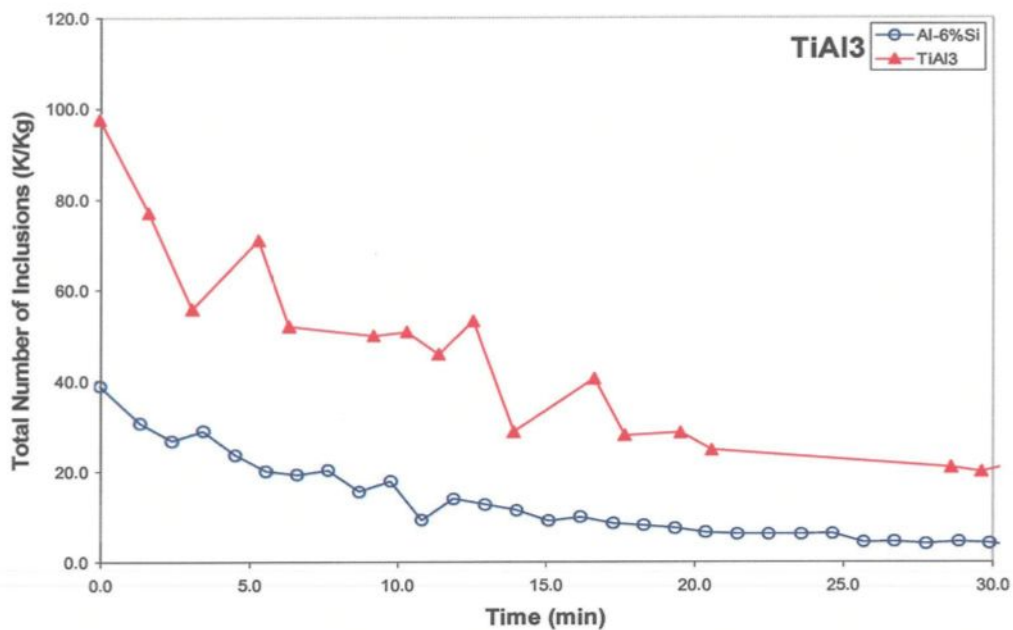


Figure 6.30 Concentration number of TiAl₃ inclusions (master alloy source) in Al-6%Si alloy as a function of time.

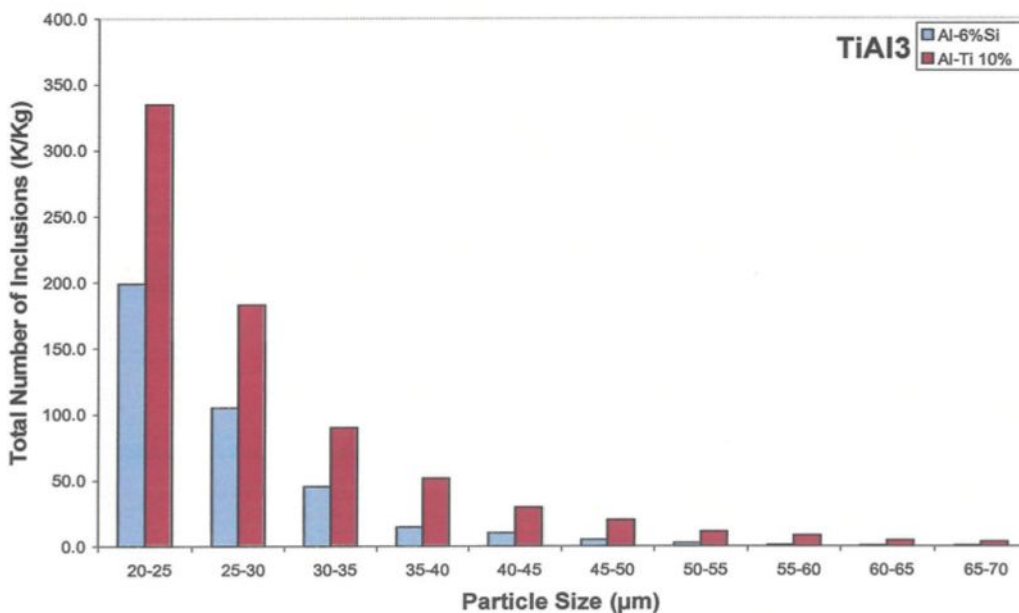


Figure 6.31 Total number of TiAl₃ inclusions (master alloy source) in Al-6%Si alloy as a function of particle size.

cases are similar in nature (gradual decrease in inclusion concentration over time). Comparison of Figure 6.31 and 6.9 also brings into sharp focus the extremely large number of TiB_2 inclusions present in the melt compared to the TiAl_3 inclusions. However, similar to the TiAl_3 inclusions, most of the TiB_2 inclusions are found in the 20-35 μm particle size range.

From the point of view of providing heterogeneous nuclei into the melt through the use of grain refining master alloys, apparently, Al-5%Ti-1%B is much more effective than Al-10%Ti, as the LiMCA measurements show in the present work.

C₂₀ Measurements: Volumic concentration of inclusions (inclusions >20 μm)

Figure 6.32 shows the C_{20} plots for the volumic concentrations of the TiAl_3 inclusions in Al-6%Si alloy over the 30 min period of sampling. This plot is similar to the N_{20} plot of Figure 6.30. Figure 6.33, which shows the corresponding volume distribution of the inclusions as a function of particle size, reveals the large volume concentrations associated with the TiAl_3 inclusions over all particle sizes in general, with the highest volumes obtained for the 20-40 μm sized inclusions. Comparing Figure 6.33 with Figure 6.11 for the TiB_2 inclusions, however, the volume concentrations are noted to be about four to five times smaller (*cf.* 4500 ppb for TiAl_3 with $\sim 23,000$ ppb for TiB_2).

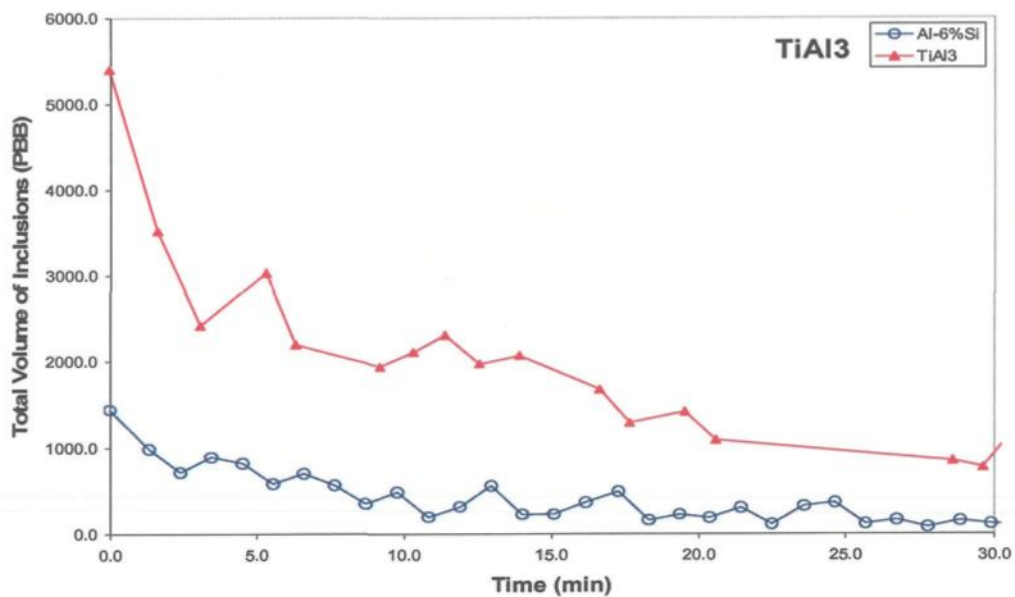


Figure 6.32 Volumic concentration of TiAl_3 inclusions (master alloy source) in Al-6%Si alloy as a function of time.

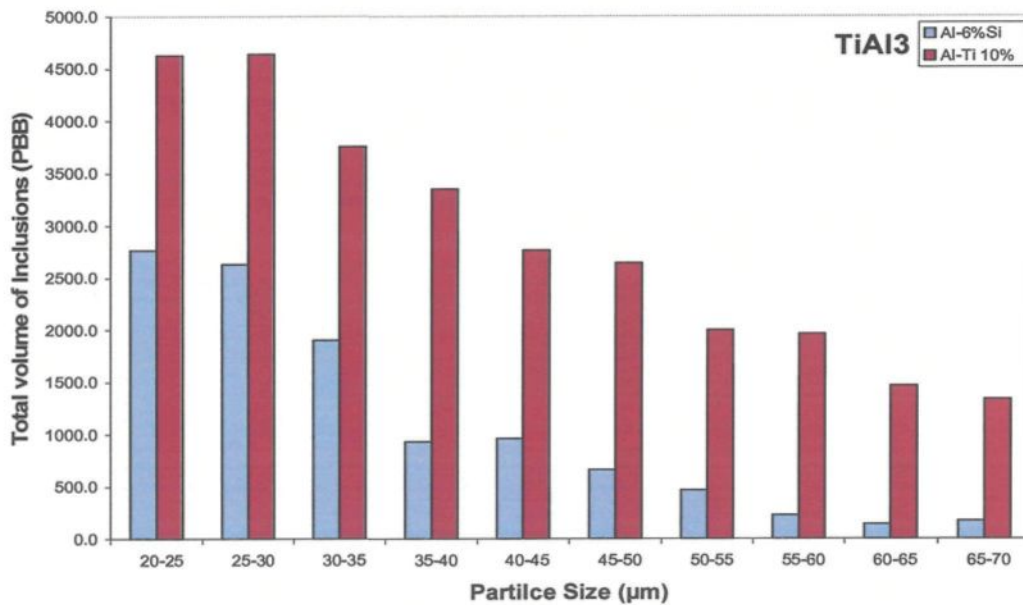


Figure 6.33 Total volume of TiAl_3 inclusions (master alloy source) in Al-6%Si alloy as a function of particle size.

6.3 COMPARISON OF DIFFERENT INCLUSION ADDITIONS

A summary of the N_{20} plots (total number of inclusions vs. time) obtained for various inclusion additions made to the Al-6%Si alloy melts at 680 °C melt temperature is provided in Figure 6.34. The N_{20} curves corresponding to the highest inclusion concentrations (*i.e.*, best test) in each case were selected as representative of that inclusion type. In the legend, P and M indicate powder and master alloy sources, respectively, while Mg and MMC represent the Mg metal and metal matrix composite sources for the MgO and Al_2O_3 inclusion additions in those cases.

As Figure 6.34 shows, the TiB_2 powder inclusion addition produces the highest concentrations, followed by the MgO inclusions resulting from the direct addition of Mg metal to the melt. The third highest inclusion levels correspond to the TiB_2 inclusions derived from the Al-5%Ti-1%B master alloy addition. In contrast, the CaO inclusions show the lowest concentrations, as expected, given the problems associated with their wettability and, hence, incorporation into the melt. Russel *et al.*⁶³ have reported that CaO particles have a high contact angle, a high interfacial energy and small work of adhesion, with respect to aluminum melts, which accounts for their poor wettability and interaction with the melt. Nevertheless, it is important to note that their presence is still differentiated by the LiMCA with respect to the base alloy inclusion levels (without any additions).

In Figure 6.34, the extension of sampling time from 30 to 40 min shown in some cases confirms that the readings are stabilized after about 25 min of sampling and thus a 30 min period is sufficient for conducting a LiMCA test.

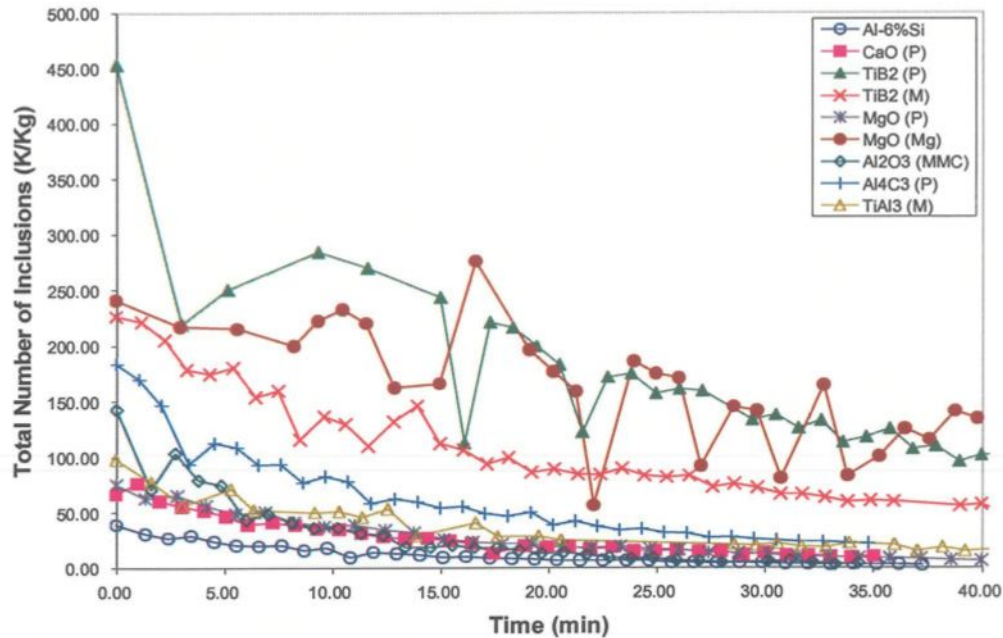


Figure 6.34 Comparison of different inclusions added to Al-6%Si alloy melts (at 680 °C) as a function of time.

Figure 6.35 shows a three-dimensional representation of the inclusion concentration distributions as a function of particle size for the various additions. Three salient features are noted: (i) all inclusion types show the highest concentrations in the 20-30 μm particle size range, (ii) the TiB_2 (master alloy), MgO (Mg metal), TiB_2 (powder) and Al_4C_3 (powder) inclusions show the maximum concentrations, in that order, and (iii) the MgO (Mg metal) and TiB_2 (powder) are the two inclusion types that show noticeable concentrations over all the particle size ranges. Table 6.7 lists the actual concentrations shown in Figure 6.35.

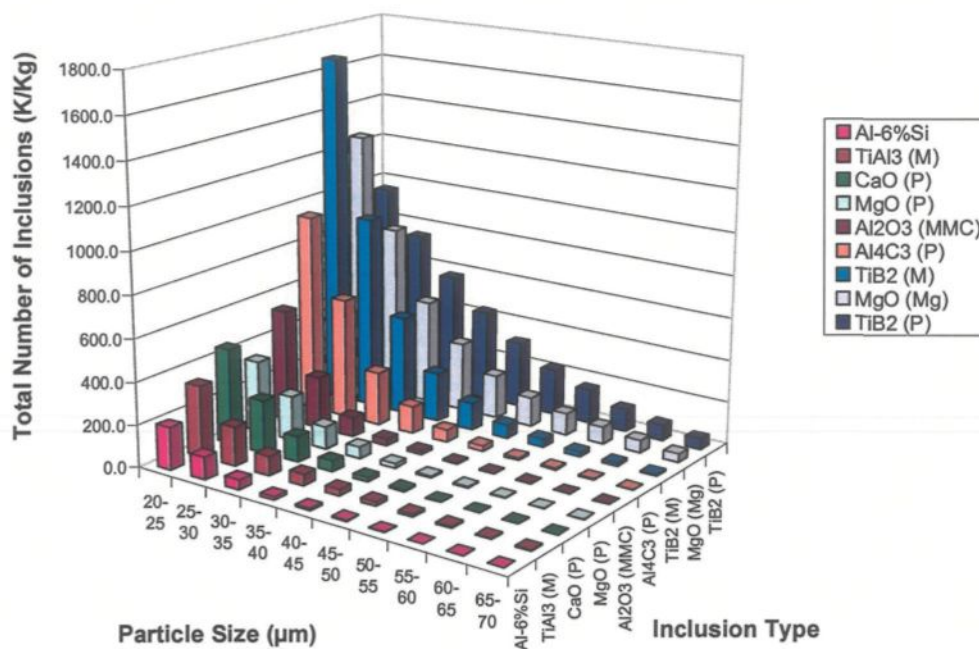


Figure 6.35 Comparison of concentration numbers of different inclusions in Al-6%Si alloy as a function of particle size.

Table 6.7 Comparison of concentrations of different inclusions in Al-6%Si alloy (at 680 °C) as a function of particle size.

Addition	Inclusion Concentration (K/Kg) vs. Particle Size (μm)									
	20-25	25-30	30-35	35-40	40-45	45-50	50-55	55-60	60-65	65-70
Al-6%Si base	199.1	105.1	45.5	14.8	10.3	5.1	2.6	1.0	0.5	0.5
TiB ₂ (M)	1667.6	917.6	469.6	232.8	127.6	64.4	39.0	21.3	13.1	7.2
MgO (Mg)	1255.0	823.8	495.4	324.3	204.1	138.4	101.9	80.5	61.7	40.8
TiB ₂ (P)	951.7	747.6	573.2	428.7	311.7	215.4	159.5	105.1	72.2	48.8
Al ₄ C ₃ (P)	943.2	571.7	252.9	128.2	58.0	25.5	11.9	6.5	4.3	1.4
Al ₂ O ₃ (MMC)	530.4	243.3	90.5	31.4	16.1	6.2	2.1	1.7	0.7	0.8
CaO (P)	450.5	246.8	120.2	50.1	19.4	10.2	3.2	1.0	1.0	0.1
MgO (P)	338.4	209.9	107.5	53.9	20.4	7.7	5.0	2.4	0.8	0.3
TiAl ₃ (M)	334.6	183.0	90.2	51.8	29.7	20.0	11.3	8.5	4.9	3.6

Figure 6.36 compares the corresponding C_{20} plots of volumic concentration for the different inclusion types shown in Figure 6.34. The TiB_2 (powder) and MgO (Mg metal) inclusion volume concentrations lie way above those of the other inclusions, and are still present in relatively significant amounts until the end of sampling period. In comparison, the other inclusion types show volumic concentrations that are half inclusions or even less at the start of sampling. These concentrations drop to their minimum values after about 15-18 min of sampling and remain stable thereafter.

Figure 6.37 provides a much clearer three-dimensional view of these volume concentrations. Taking into consideration the four main inclusions of interest, *viz.*, TiB_2 (powder), MgO (metal), TiB_2 (master alloy), and Al_4C_3 (powder) inclusions, and comparing this figure with the concentration numbers of Figure 6.35, one can see clearly that the TiB_2 (powder) and MgO (metal) inclusions are associated with high volumes over all the particle size ranges. In comparison, the volume concentrations of the TiB_2 (master alloy) and Al_4C_3 (powder) inclusions follow patterns that are similar to the concentration numbers, although volume concentrations in the larger particle size ranges are much more noticeable than the corresponding concentration numbers.

As for the other inclusions, the number and volume concentrations resemble each other, except for the $TiAl_3$ inclusions which, although possessing relatively low concentrations compared to the four showing maximum concentrations, nevertheless shows distinct volumic concentrations over all the particle size ranges.

Table 6.8 lists the actual volumic concentrations shown in Figure 6.37 as a function of particle size.

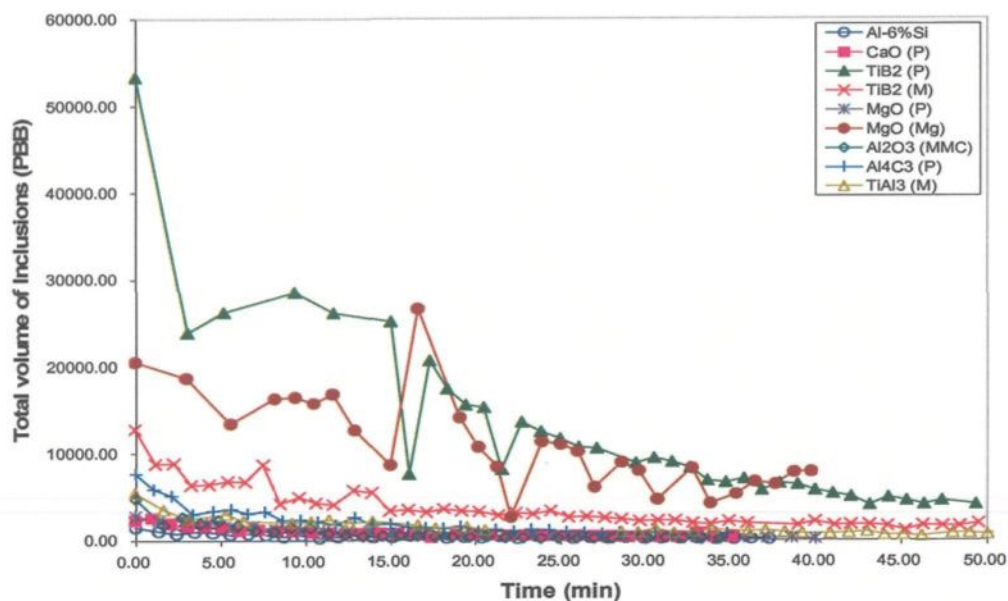


Figure 6.36 Comparison of volumic concentrations of different inclusions in Al-6%Si alloy (at 680 °C) as a function of time.

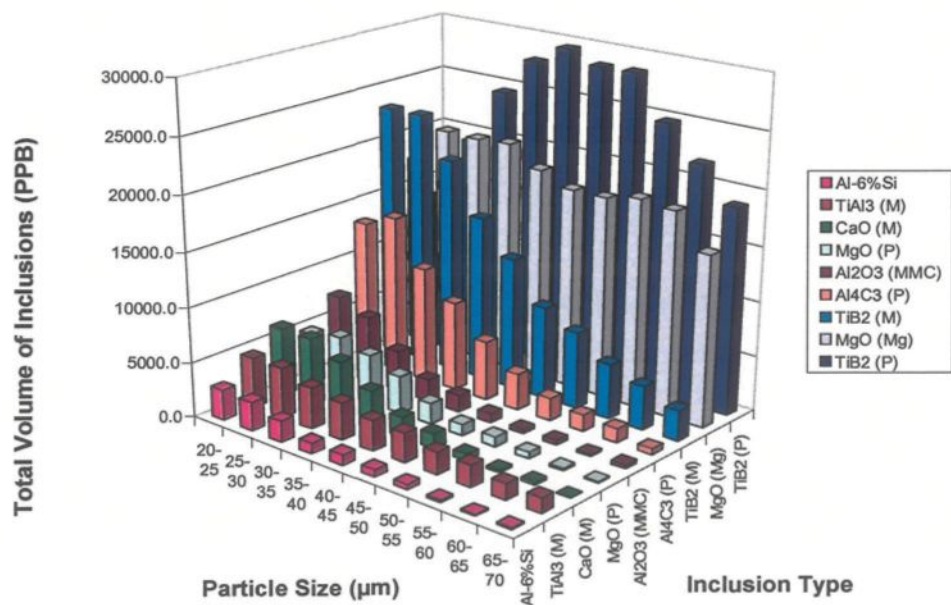


Figure 6.37 Comparison of volumic concentrations of different inclusions in Al-6%Si alloy as a function of particle size.

Table 6.8 Comparison of volumic concentrations of different inclusions in Al-6%Si alloy (at 680 °C) as a function of particle size.

Addition	Volumic Concentration (ppb) vs. Particle Size (μm)									
	20-25	25-30	30-35	35-40	40-45	45-50	50-55	55-60	60-65	65-70
Al-6%Si base	2767.5	2636.1	1903.3	938.4	964.2	668.4	469.8	227.9	145.4	176.4
TiB ₂ (M)	23152.2	23172.0	19581.6	15032.8	12064.9	8456.6	6984.8	4994.6	3956.9	2737.0
MgO (Mg)	17571.9	20930.9	20865.0	21097.2	19379.5	18281.7	18274.2	18891.4	18644.0	15589.6
TiB ₂ (P)	13449.6	19233.6	24379.7	27795.8	29452.4	28423.2	28483.0	24705.4	21736.1	18719.6
Al ₄ C ₃ (P)	13215.8	14481.6	10505.5	8165.3	5412.5	3325.8	2066.8	1490.5	1278.5	545.3
Al ₂ O ₃ (MMC)	7258.3	6067.1	3757.2	2006.3	1497.6	796.1	375.0	416.8	203.6	324.5
CaO (P)	6288.7	6218.2	4983.5	3210.2	1814.6	1332.3	581.5	228.7	298.7	44.6
MgO (P)	4749.6	5300.2	4461.5	3441.4	1907.6	1003.2	892.0	567.2	219.1	94.8
TiAl ₃ (M)	4630.9	4638.4	3757.8	3350.9	2768.9	2647.7	2000.9	1963.3	1470.6	1338.2

6.3.1 Effect of Melt Temperature on Inclusion Concentrations Recorded by LiMCA

To complete this chapter, a comparison of the inclusion concentrations for the different inclusion types in Al-6%Si alloy melts obtained at the 750°C and 680°C melt temperatures is made, as shown in Figure 6.38. As mentioned elsewhere, the best tests were selected in each case for presentation in Figure 6.38. The figure shows very clearly that the LiMCA records higher inclusion concentrations at the lower melt temperature for all the inclusion types studied. However, this effect is most pronounced for the TiB₂ and Al₄C₃ powder inclusions.

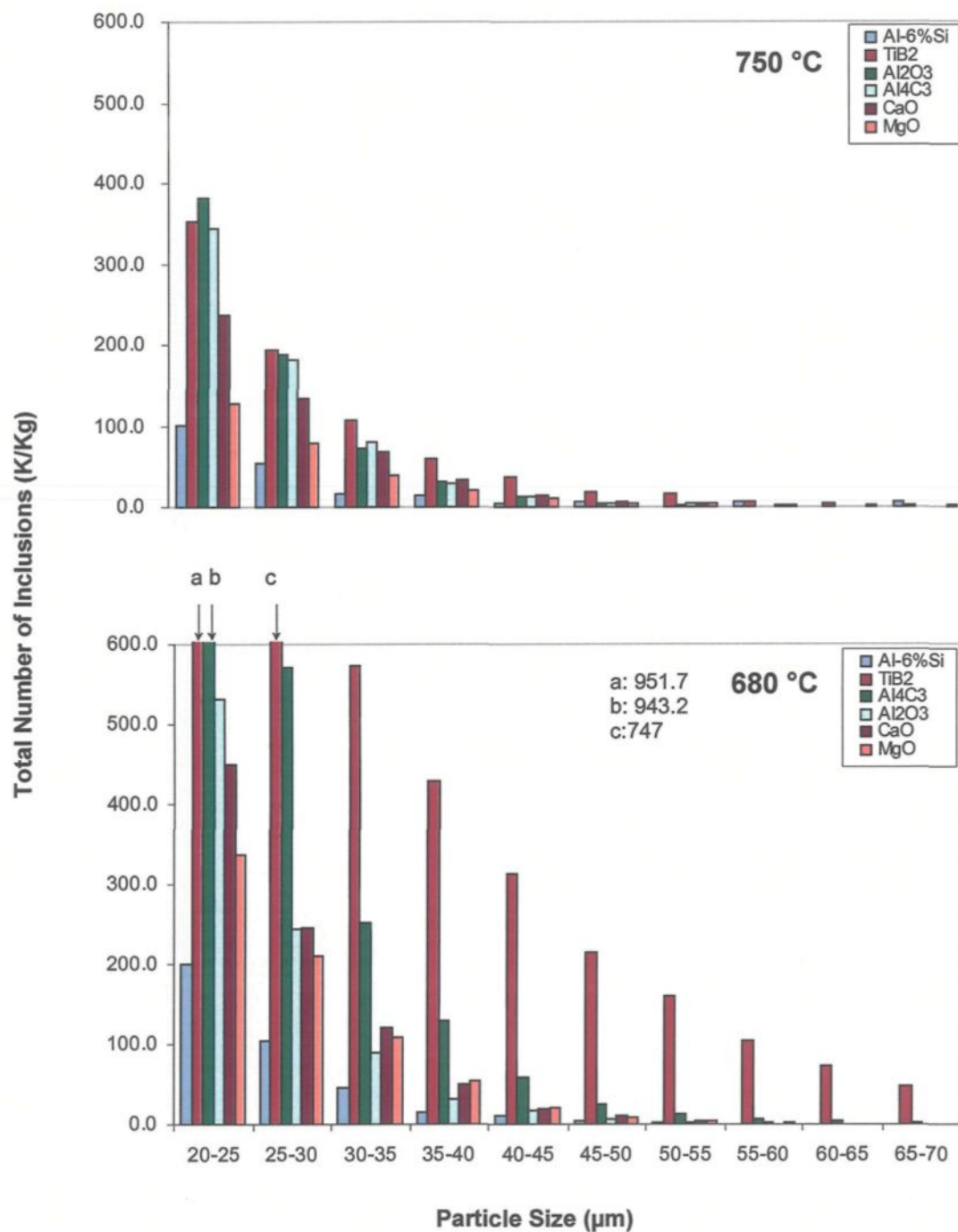


Figure 6.38 Comparison inclusion concentrations for different inclusion types in Al-6%Si alloy at 750 °C and 680 °C melt temperature.

CHAPTER 7

EXAMPLES OF INCLUSIONS IN PURE Al AND Al-6%Si ALLOY

CHAPTER 7

EXAMPLES OF INCLUSIONS IN PURE Al AND Al-6%Si ALLOY

7.1 INTRODUCTION

In order to obtain a qualitative understanding of the LiMCA data acquired for different inclusion additions to the pure aluminum and Al-6%Si alloy melts, metallography samples for microstructural analysis were prepared from the solidified metal in the LiMCA probe tube resulting after a particular LiMCA data acquisition. Figure 7.1(a) shows examples of LiMCA tubes before and after sampling, while Figure 7.1(b) shows a close-up of the actual solidified metal block obtained from within the probe tube. In this case, the sample was sectioned from the solidified block of metal, mounted in bakelite and polished to a fine finish (1 μ m diamond paste). Figure 7.1(c) shows clearly how the sectioning was done, and the mounted sample.

Besides the LiMCA probe tube samples, metallography samples were also prepared from samplings taken from the melts before and after the LiMCA test was carried out. These samplings were poured into a small metallic cup and allowed to solidify. In each case, a sample was then sectioned from the central part of the casting (20 x 20 mm in size, 5 mm thick). The sectioned piece was mounted in bakelite and polished to a fine finish, as before.

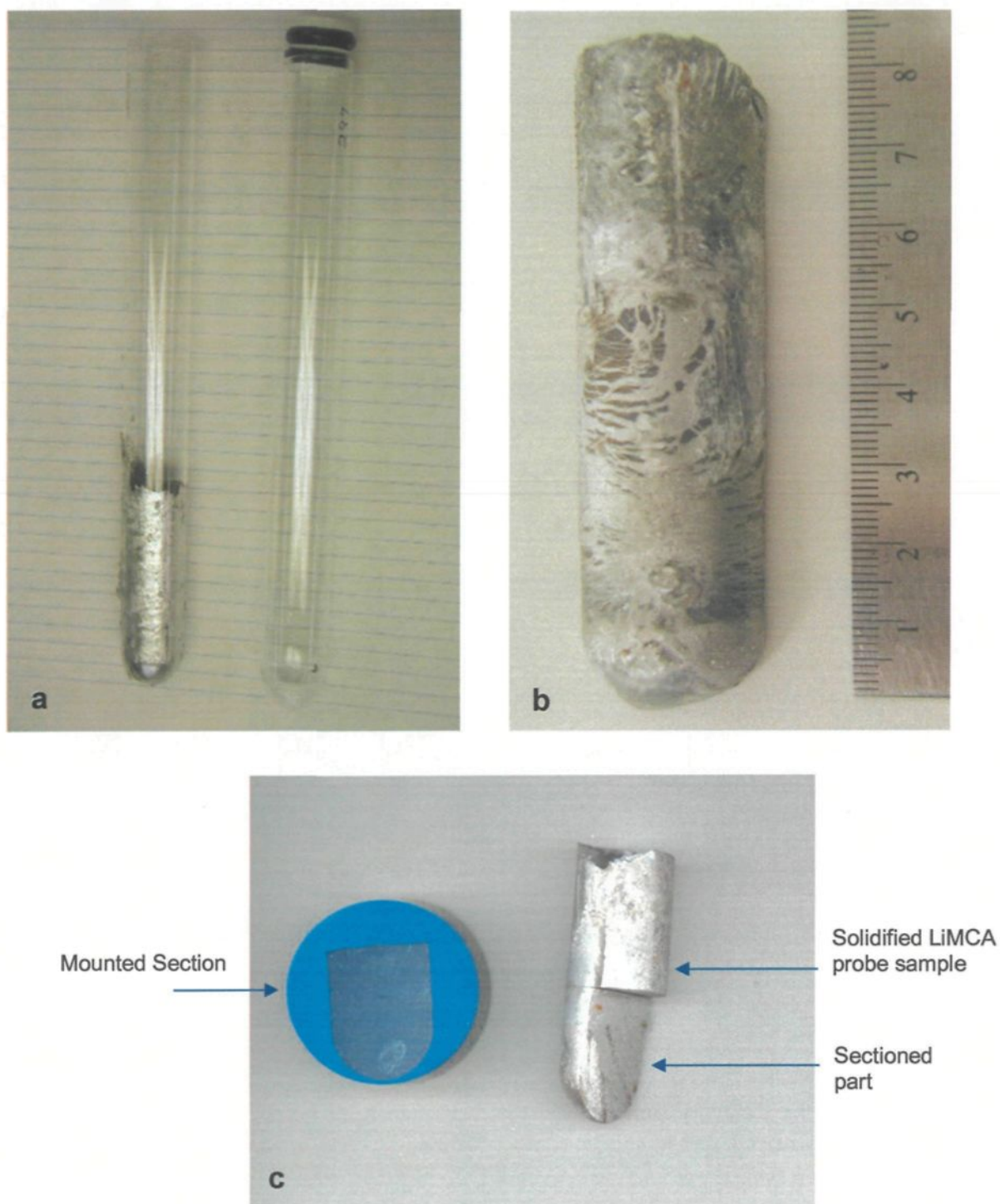


Figure 7.1 (a) LiMCA tube before and after sampling, (b) close-up of the actual solidified metal block obtained from probe tube, (c) the sectioned and mounted sample.

An Olympus optical microscope - Leco 2001 image analyzer system was employed to examine the different inclusion types observed in the various samples. In certain cases, electron probe microanalysis (EPMA) was also used to complement the analysis and obtain further information on any interesting features or characteristics observed during the optical microscopic examination, and to confirm the composition of inclusions observed in the microstructure, using wavelength dispersive spectroscopy (WDS) and energy dispersive X-ray (EDX) analysis.

This chapter highlights some of the more interesting microstructural data obtained from the various LiMCA samplings. It ought to be mentioned that most of the micrographs presented here were obtained from alloy melts at 680 °C melt temperature, as these provided better inclusion measurements than those obtained at 750 °C melt temperature.

7.2 MICROSTRUCTURES OF INCLUSIONS

Given that the emphasis of this study is more on inclusions in the Al-6%Si alloy, the microstructures shown in this section mainly cover the Al-6%Si alloy samples. Some examples of inclusions added to commercial pure aluminum have also been provided.

7.2.1 Microstructures of Inclusions Added to Pure Aluminum Melts

CaO

Figure 7.2 shows examples of the backscattered images of CaO inclusions observed in a commercial pure aluminum sample obtained from the LiMCA probe tube at the beginning of the LiMCA testing. Figure 7.2(a) shows a cluster of these inclusion particles. Note the black pores in the vicinity of the inclusions.

Figure 7.2(b) shows a spherical particle which could either be an agglomerate of smaller CaO inclusions, or a Ca-containing compound, resulting from the reaction of the CaO inclusions with the melt (this point will be elaborated upon further in section 7.2.3). The X-ray images provided in Figures 7.2(c) and (d) for the two cases show clearly that these particles contain calcium.

MgO

Figure 7.3(a) shows an example of two MgO inclusion particles in the aluminum matrix of a sample obtained from the LiMCA probe tube. In this case, the Mg, O and Al X-ray images of Figures 7.3(b), (c) and (d) confirm that these are MgO particles embedded in an aluminum matrix.

Compared to the MgO particles shown in Figure 7.3(a), Figures 7.4(a) and (b) show two examples of MgO inclusions occurring in the form of oxide films within shrinkage pores in the aluminum matrix, corresponding to the LiMCA probe tube sample taken at the beginning of the LiMCA test, after the addition of Mg metal to the MgO inclusion-containing Al melt and its subsequent oxidation. The black lace-like features observed in the region indicate that these are oxide films. As can be seen, the oxide films are associated with porosity. The corresponding oxygen images shown in Figures 7.4(c) and (d) confirmed that these were oxide films, as did the X-ray image for Mg (not shown here).

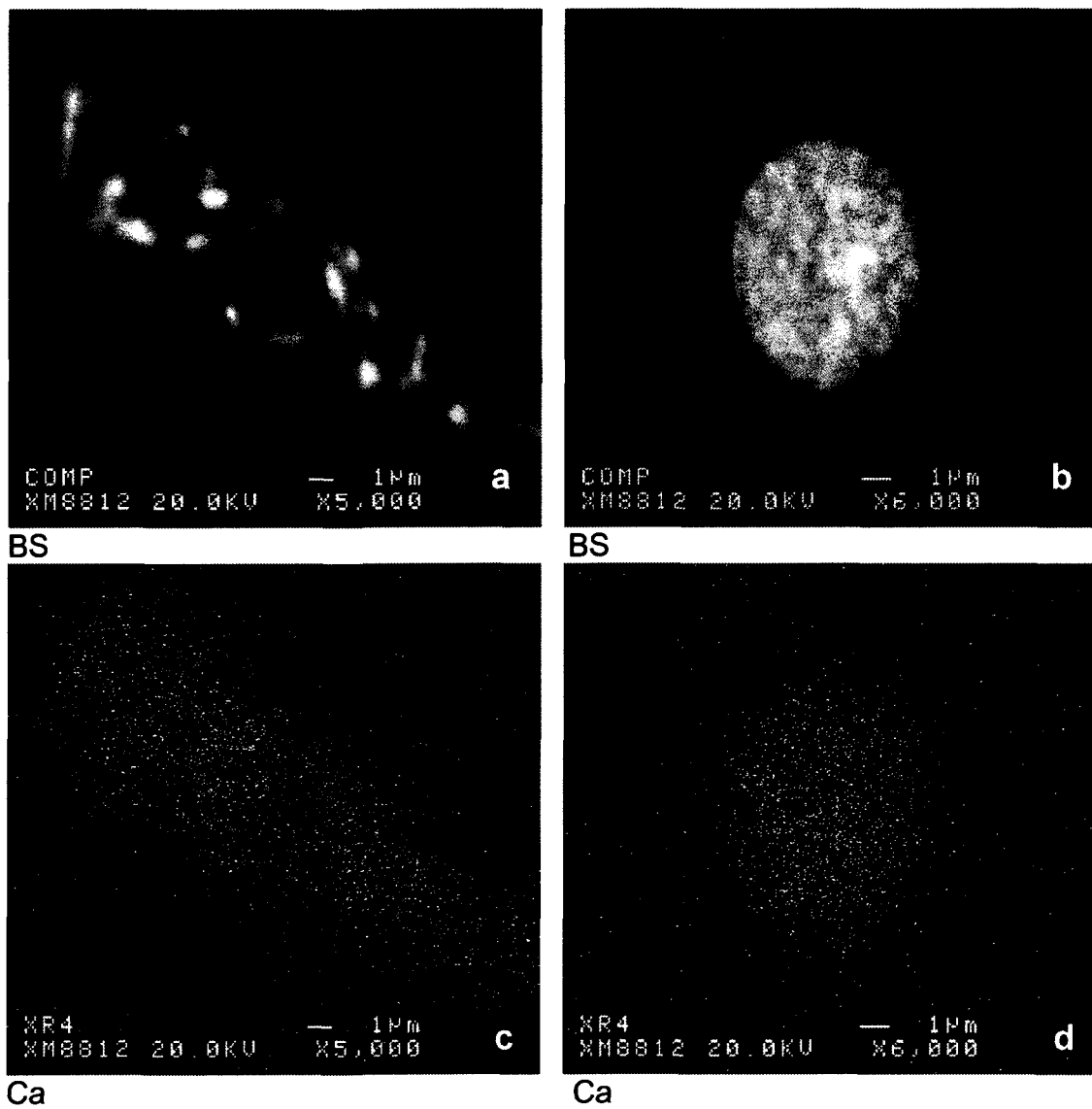


Figure 7.2 (a, b) Backscattered images of CaO inclusions and (c, d) corresponding X-ray images of Ca obtained from a LiMCA probe tube sample at the start of a LiMCA test.

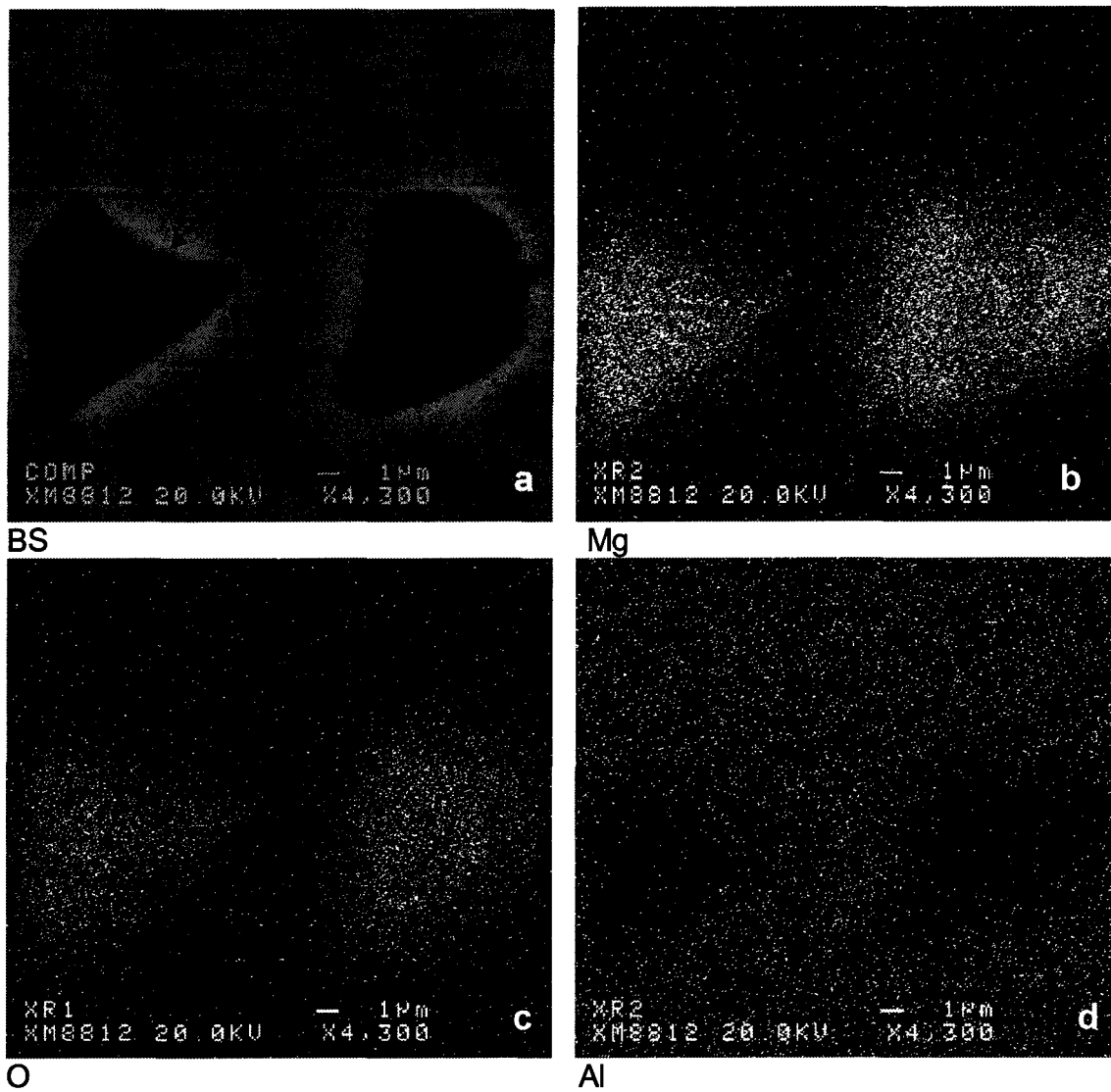


Figure 7.3 (a) Backscattered image of two MgO inclusions in a commercial pure Al matrix obtained from a LiMCA probe tube sample at the start of a LiMCA test, (b, c, d) corresponding X-ray images of Mg, O and Al.

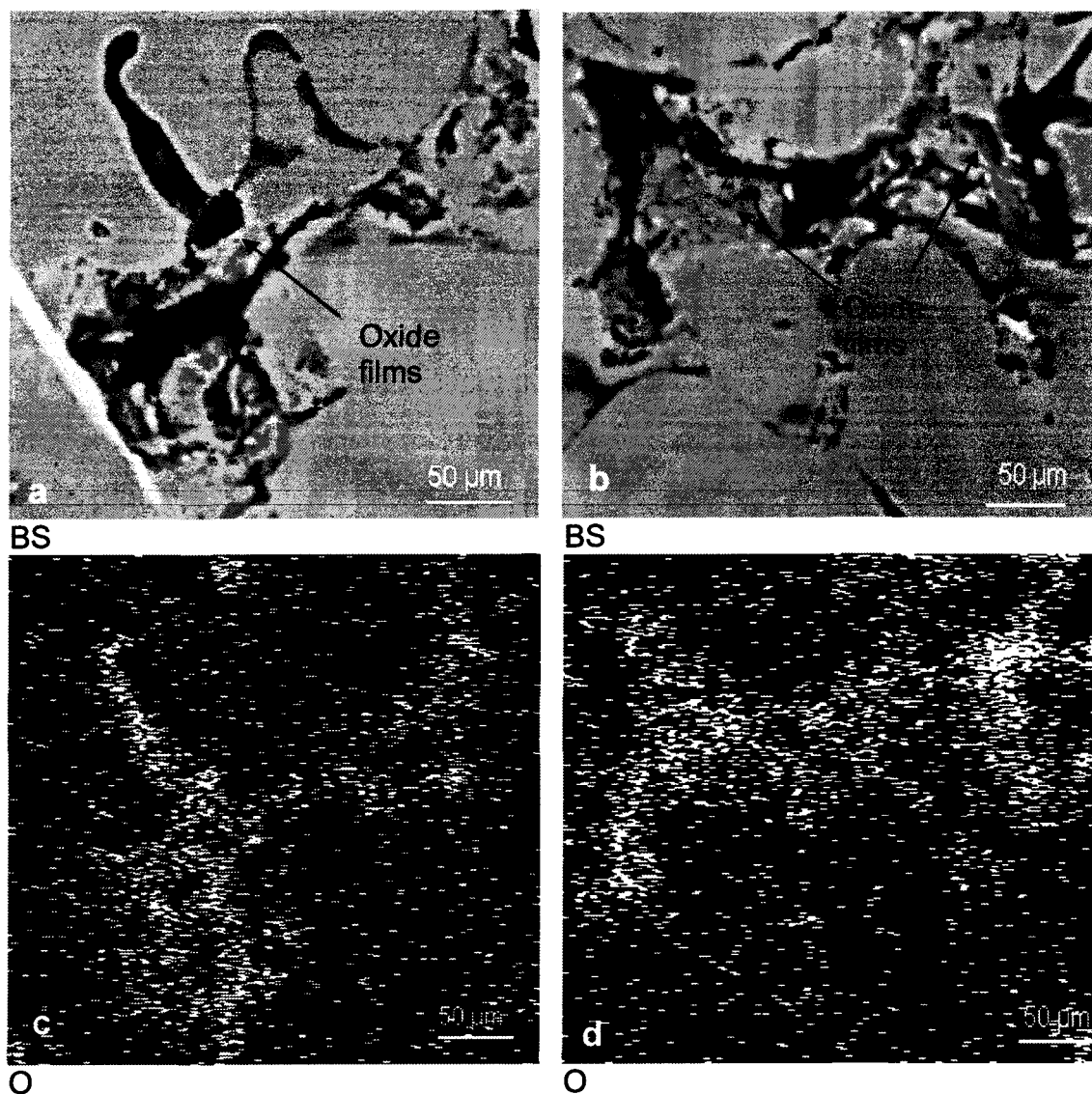


Figure 7.4 Backscattered images showing examples of MgO films in commercial pure Al, obtained from a LiMCA probe tube sample at the start of the LiMCA test; (c, d) corresponding X-ray images of oxygen.

TiAl₃

Figure 7.5(a, b) shows examples of backscattered images of $TiAl_3$ inclusions in commercial pure Al obtained from two different areas of a LiMCA probe tube sample taken at the start of the LiMCA test. The $TiAl_3$ inclusions were added to the pure Al melt in the form of Al-10%Ti master alloy. The inclusions are observed as bright white particles in the matrix, and the X-ray images of Ti confirm that they are $TiAl_3$ inclusions. Note, in particular, the fine size of these inclusions.

As has been found from another study in our group, it is believed that only such small inclusions are responsible for the grain refining properties of the Al-10%Ti master alloy.⁶⁴ However, the majority of $TiAl_3$ particles in the master alloy used appear in the form of plates of considerable lengths. These particles, being much larger than the grain sizes observed in the Al-Si alloy samples to which the Al-10%Ti master alloy was added, are obviously not expected to act as nucleants for the solidifying aluminum (and hence take part in the grain refining process).

The efficiency of the Al-Ti master alloy would thus vary, depending on the relative amounts of these long plates versus the very small particles of $TiAl_3$ present in the master alloy. This would explain the inconsistent behavior reported for Al-Ti master alloys and why they are less effective than Al-Ti-B master alloys.⁶⁵ Examples of the extent of these massive $TiAl_3$ plates are shown in Figures 7.9(c) and (d) in section 7.2.3 for an Al-6%Si alloy sample.

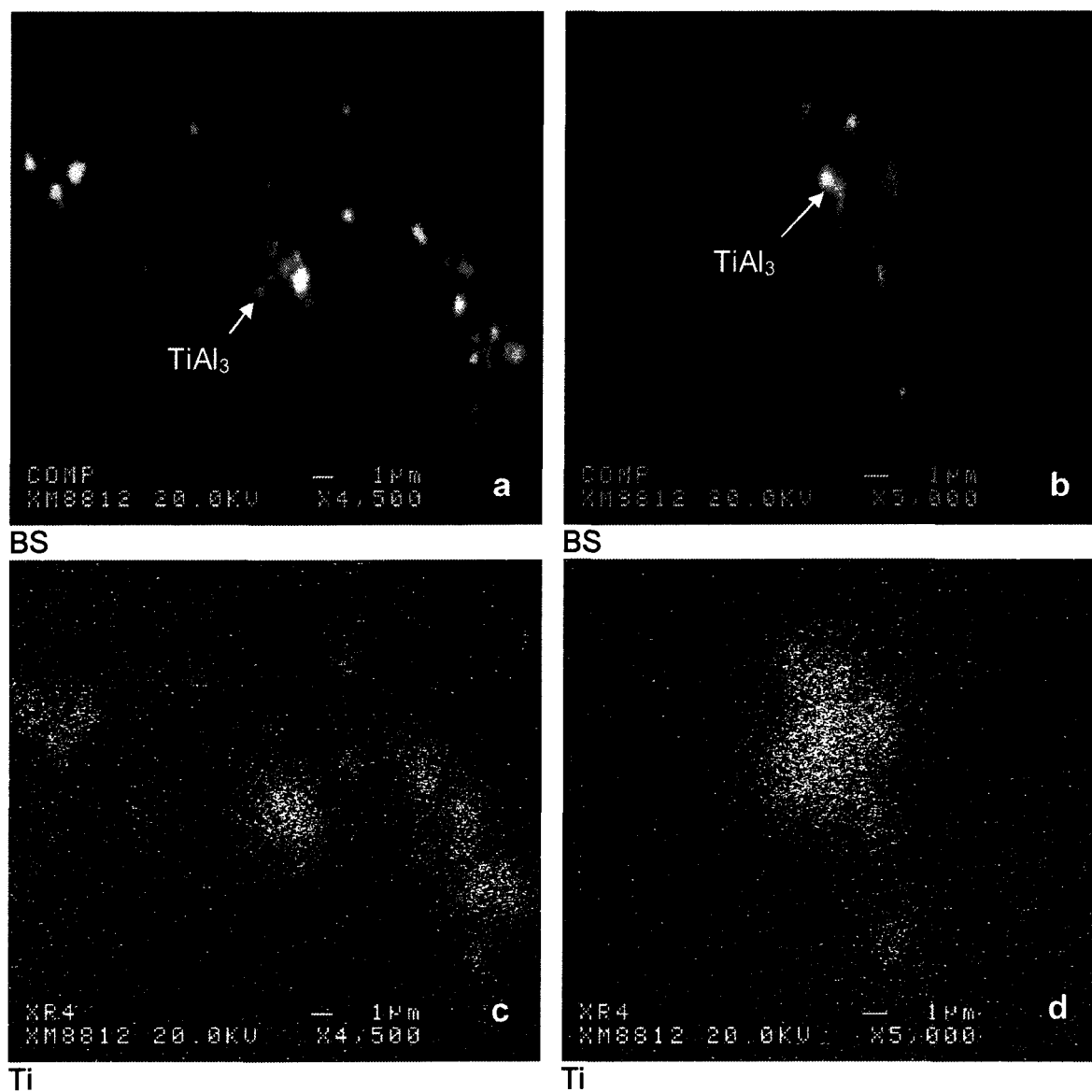


Figure 7.5 (a, b) Backscattered images of TiAl₃ inclusions, and (c, d) corresponding X-ray images of Ti obtained from a LiMCA probe tube sample at the start of a LiMCA test.

7.2.2 Microstructures of Inclusion-Containing Al-6%Si Alloy Ingots

Figure 7.6 shows examples of Al_4C_3 , CaO, MgO and TiB_2 inclusions observed in the optical micrographs of samples taken from the respective inclusion-containing Al-6%Si alloy ingots (which were used to add inclusions to Al-6%Si alloy melts to carry out the LiMCA tests). All micrographs are taken at the same magnification of 200X. One of the interesting features to note in these micrographs is that the inclusion particles are often associated with pores in their vicinity.

The Al_4C_3 inclusions in (a) are the small black particles scattered in the Al-Si eutectic regions. Similarly, the CaO inclusions in (b) appear as clusters (bumpy looking areas) in the Al-Si eutectic regions, with lighter grey polygonal particles (compared to the darker color of the Si particles) occurring close to them. The nature of these polygonal particles (Ca-containing compounds) will be discussed later in section 7.2.3. In comparison, the large agglomerate of MgO inclusions in (c) makes it difficult to pinpoint the matrix region.

However, the α -Al dendrite contours on the upper right side indicate that the inclusions are probably located within a pore in the matrix. The main point of interest to note is that the TiB_2 inclusions in (d) are present in very large amounts compared to the other inclusions. They also appear to be located over porous areas (dark regions interspersed between the TiB_2 particles), in the Al-Si interdendritic regions, and also within the α -Al dendrites to a small extent.

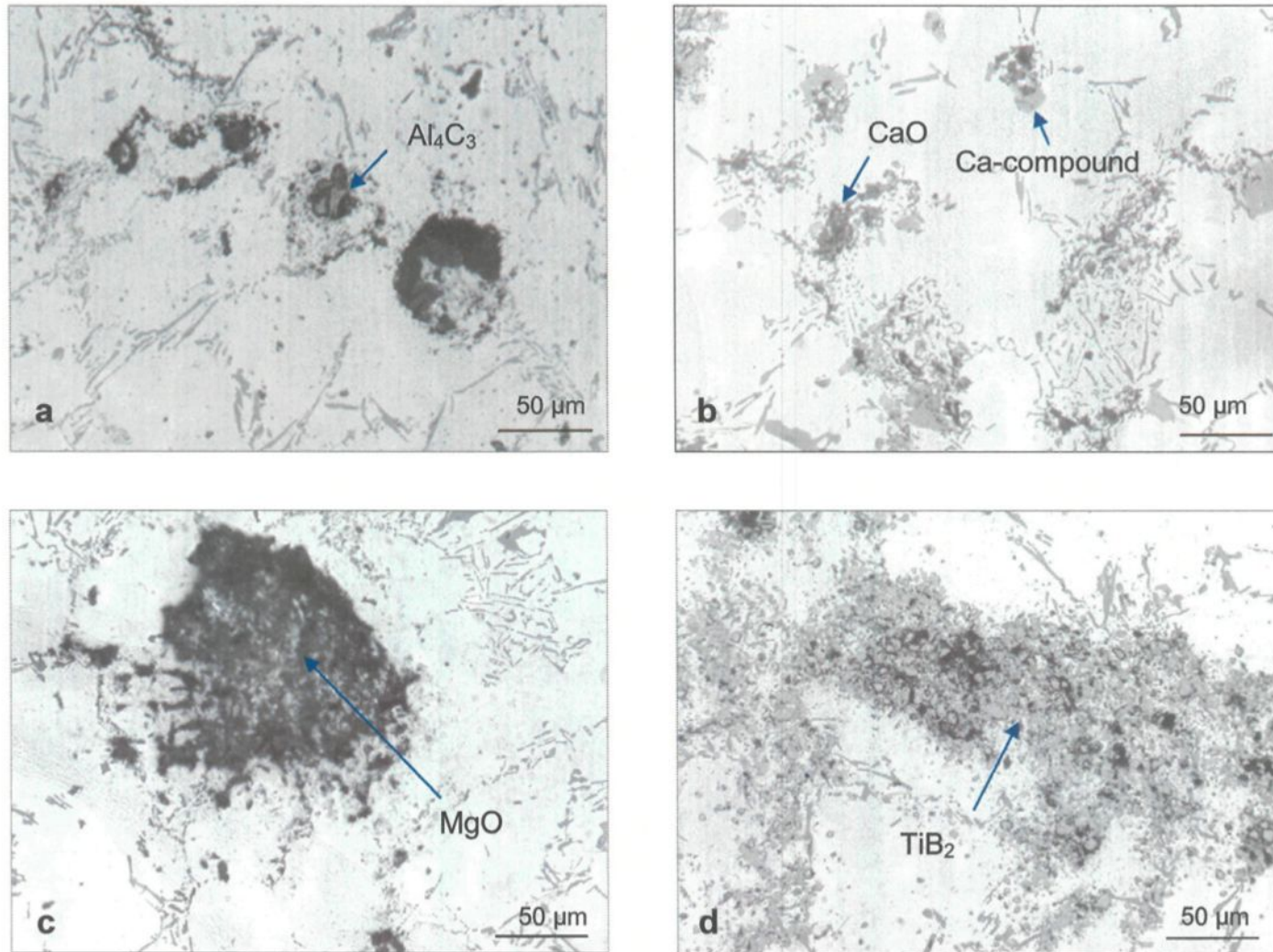


Figure 7.6 Optical micrographs showing inclusions observed in various inclusion-containing Al-6%Si alloy ingots: (a) Al_4C_3 , (b) CaO , (c) MgO , and (d) TiB_2 .

7.2.3 Microstructures of Inclusions Added to Al-6%Si Alloy Melts

TiAl₃

Figure 7.7 shows examples of $TiAl_3$ inclusions in Al-6%Si alloy samples obtained from the LiMCA probe tube at (a) the start, and (b) the end of a LiMCA test, and the corresponding X-ray images of Ti (c, d). It ought to be mentioned here that a LiMCA probe tube sample obtained “at the start” of a LiMCA test means that the probe tube was removed from the melt after about 2 min of the LiMCA sampling. The melt was stirred again to ensure homogeneous distribution of the inclusions, and a new LiMCA test started, using a fresh probe tube. The solidified metal in the first probe tube was sectioned to produce the metallography sample corresponding to the “start of LiMCA test” conditions. Obviously, a LiMCA probe tube sample corresponding to “the end” of a LiMCA test was the sample obtained from the probe tube that was removed after the LiMCA sampling was completed.

Figure 7.8 shows examples of $TiAl_3$ inclusions observed in the form of (a) long, and (d) short plates, taken, respectively, from LiMCA probe tube samples obtained at the start and end of a LiMCA test. The variation in length of the $TiAl_3$ particles is brought out clearly if we consider the magnifications at which these two backscattered images were taken (800X and 2500X, respectively). The X-ray images of Ti (b, e) for the two backscattered images confirms that these are Ti-containing particles.

The X-ray image of Si (c), corresponding to the BS image in (a) reveals the distribution of the silicon particles in the Al-Si eutectic regions, and which are observed as

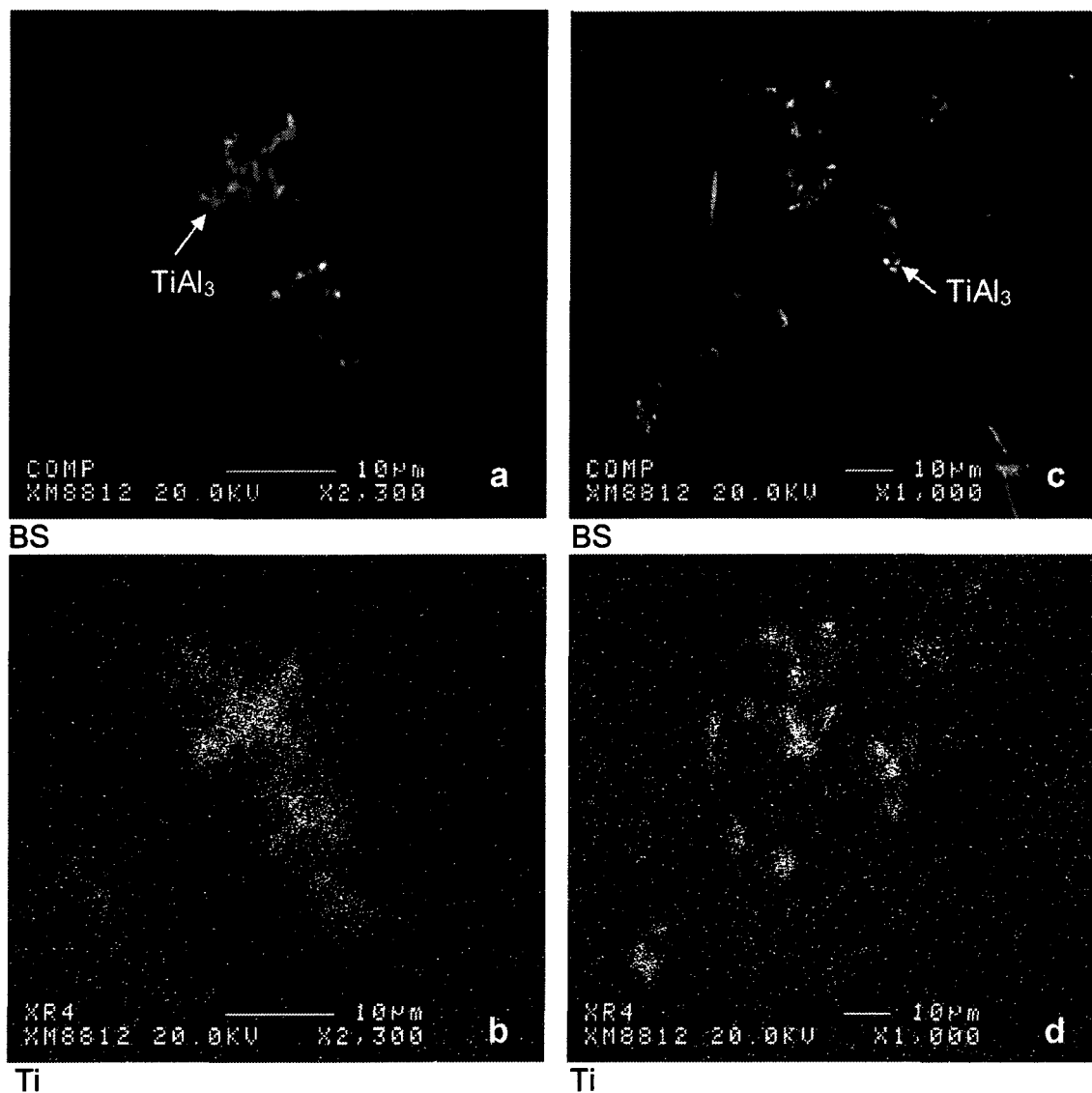


Figure 7.7 Backscattered images of TiAl_3 inclusions in Al-6%Si alloy, and corresponding X-ray images of Ti obtained from LiMCA probe tube samples: (a), (c) at the start, and (b), (d) at the end of the LiMCA test. (BS: backscattered image).

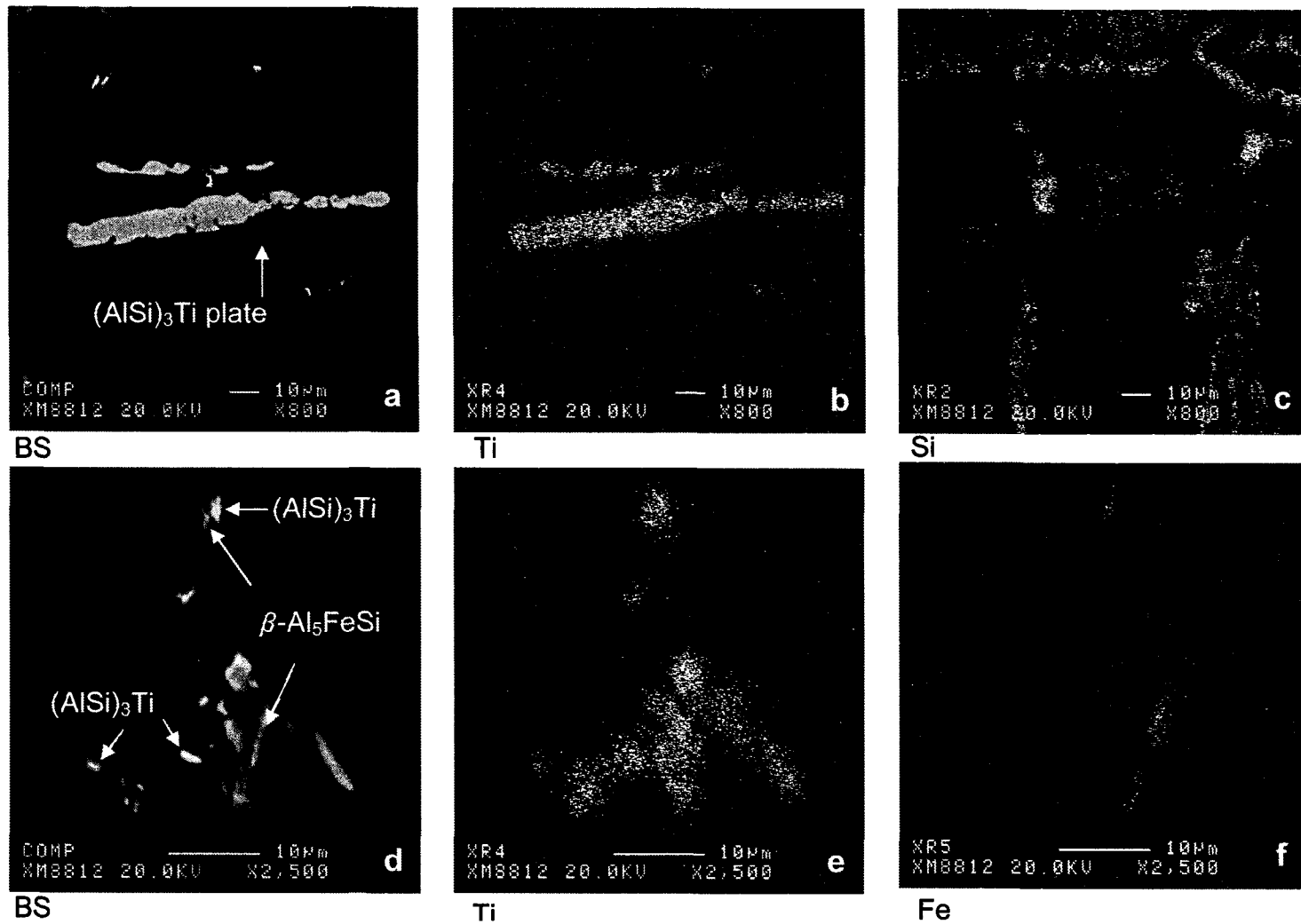


Figure 7.8 Backscattered images (a, d) showing long and short TiAl_3 plates and corresponding images of Ti (b, e), Si (c) and Fe (f). Samples obtained from LiMCA probe tube at the start (a, b, c) and end (d, e, f) of the LiMCA test.

pale grey constituents in (a).

In addition, it is also noticed that the TiAl_3 plates/particles contain some Si as well. Thus, these particles would correspond more correctly to $(\text{Al,Si})_3\text{Ti}$ rather than TiAl_3 . In fact, this observation was also noted in the other study⁶⁴ referred to in section 7.2.1.

In Figure 7.8(d), a couple of $\beta\text{-Al}_5\text{FeSi}$ iron intermetallic plate-like particles are also observed, associated with the TiAl_3 plates, and the corresponding X-ray image of Fe shown in (f) points clearly to their location in the matrix. As mentioned previously (in section 7.2.1) in the context of grain refining, it is the very small $(\text{Al,Si})_3\text{Ti}$ particles such as those shown in (d) that more likely act as nuclei for the nucleation and growth of the $\alpha\text{-Al}$ dendrites rather than the large $(\text{Al,Si})_3\text{Ti}$ plates of Figure 7.8(a).

The optical micrographs of Figure 7.9 show the acicular morphology of the TiAl_3 plates in Al-6%Si alloy, obtained from the addition of Al-10%Ti master alloy to the melt and taken from a LiMCA probe tube sample at the start of the LiMCA test. The large plates are the ones that act as deleterious inclusions and have little or no contribution towards grain refining. The presence of these hard, acicular plates is actually harmful to the casting, in terms of tool wear associated machining problems.

With reference to the LiMCA test, obviously, TiAl_3 plates of such large size will be inhibited from entering the probe tube orifice (of 300 μm diameter) and hence the ESZ region of measurement for them to be detected by the LiMCA.

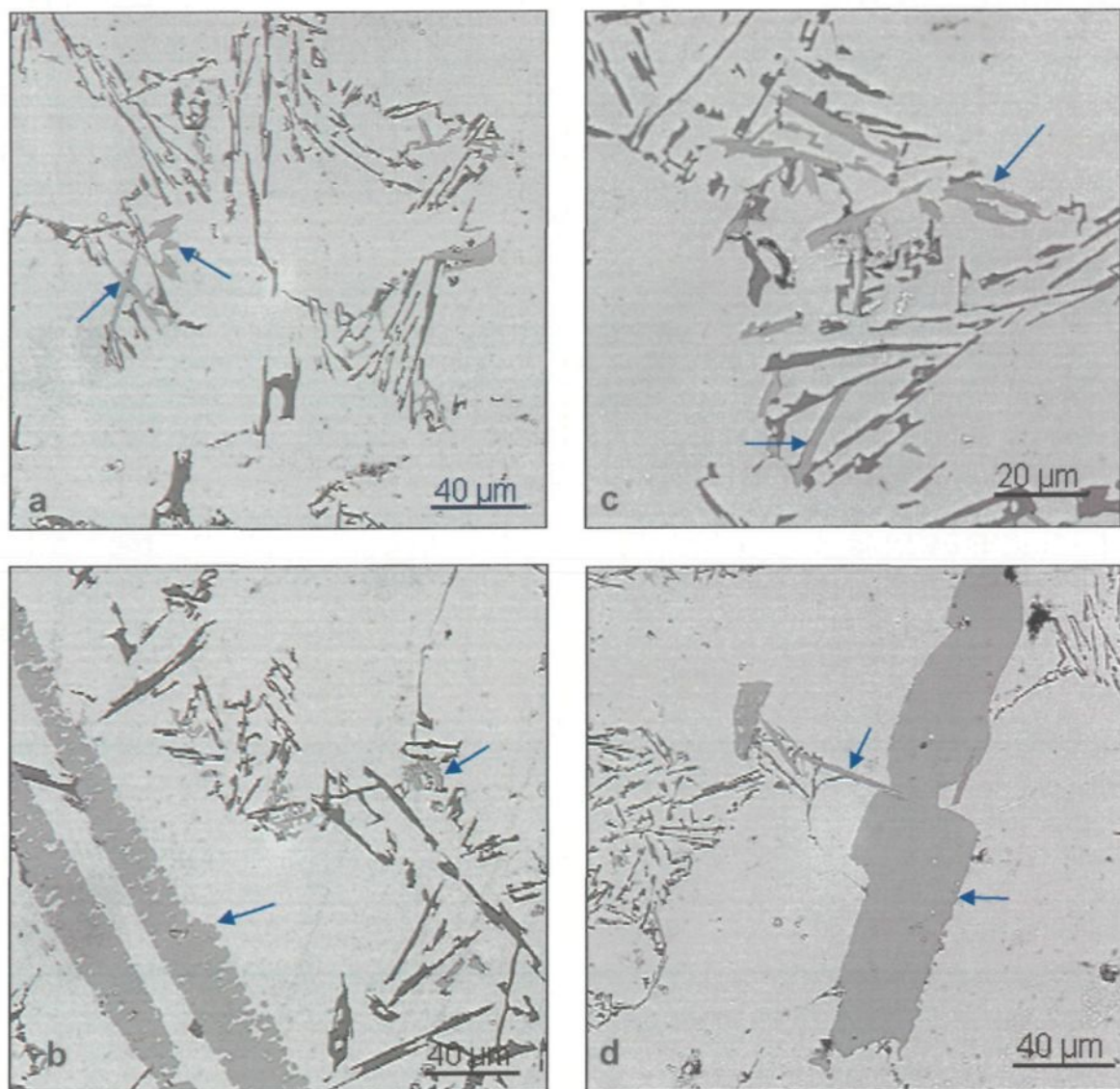


Figure 7.9 Optical micrographs showing the sizes and acicular nature of TiAl_3 inclusion particles (arrowed) in a LiMCA probe tube sample of Al-6%Si alloy melt to which Al-10%Ti master alloy was added. Note the massive size of the TiAl_3 plates in (c) and (d).

CaO

Figure 7.10 (a) shows a backscattered image taken from an Al-6%Si alloy melt to which CaO inclusions were added. The metallography sample in this case was obtained from the sampling cup casting taken from the melt before the LiMCA test was started. The microstructure reveals faint Al-Si eutectic regions towards the top left of the figure, bright irregular shaped particles, and black clusters associated with the latter. The corresponding X-ray images of Ca (b) reveals that both the bright particles and the black clusters contain calcium, whereas the X-ray image of O (c) shows that it is mainly the black clusters that are rich in oxygen and, hence, are CaO inclusions. From the EDX spectrum (d) of the bright particles, it would be reasonable to say that these particles are Ca-containing compounds that have formed as a result of the reaction between the CaO inclusions and the melt.

In a study on the role of inclusions in nucleating α -Al and Fe intermetallics in the Al-rich corner of the Al-Si-Fe ternary system, Khalifa *et al.*⁶⁶ reported that the CaO particles interact with the aluminum alloy melt to form Ca-compounds rich in silicon, due to the high chemical affinity of CaO to form intermetallic compounds with Al-Si melts. The present findings also confirm these results, as seen from the EDX spectrum of Figure 7.10(d), where peaks for Al, Si and Ca are clearly observed.

With respect to the X-ray image of oxygen shown in Figure 7.10(c), and comparing it with the BS image in (a), the bright patch on the upper right would most probably correspond to an oxide film within the black, elongated pore observed in the BS image. In

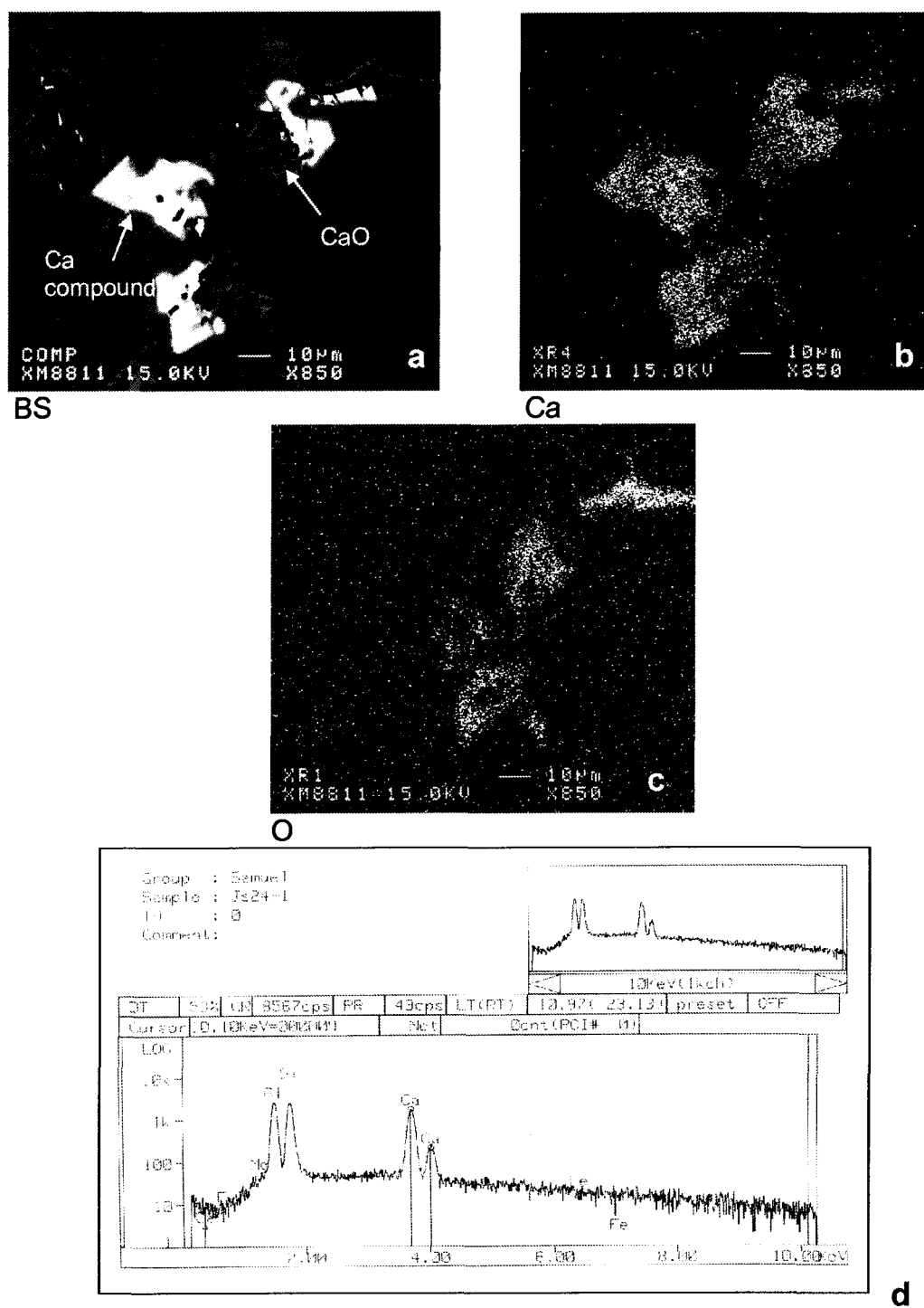


Figure 7.10 (a) Backscattered image of CaO inclusions and Ca-containing compounds in Al-6%Si alloy; (b, c) corresponding X-ray images of Ca and O; (d) EDX spectrum corresponding to the light gray large Ca-compound particle shown in (a).

comparison, the bright particles along the left bottom of the elongated pore in (a) are more likely Ca-containing compounds rather than CaO. The optical micrographs shown in Figure 7.11 provide a clear picture of the morphology of the CaO inclusions. Those on the left are taken from the casting obtained from the melt before the start of the LiMCA test, while those on the right correspond to the casting obtained at the end of the LiMCA test. The large and small black clusters of CaO inclusions are clearly observed in the micrographs in (a), while the microstructures on the right also show the presence of the black CaO inclusions, although in relatively smaller concentrations.

Al₄C₃

The backscattered image of Figure 7.12(a) reveals the presence of several particles within the matrix, taken from a sampling cup casting of the Al₄C₃ inclusion-containing Al-6%Si melt before starting the LiMCA test. The X-ray images (b, c) for O and C show that these constituents are, in fact, a mixture of oxides and carbides particles, where the carbide particles are those arrowed in the BS image.

The optical micrographs of Figure 7.13, obtained from the same sample as well as a casting sample obtained at the end of the LiMCA test, show how the Al₄C₃ inclusions actually appear in the matrix. Notice the much larger concentrations of Al₄C₃ in the samples at the start, compared to those obtained at the end of the test. Also, the inclusions appear to be generally associated with oxide films judging by the lace-like features of the regions in which they are found.

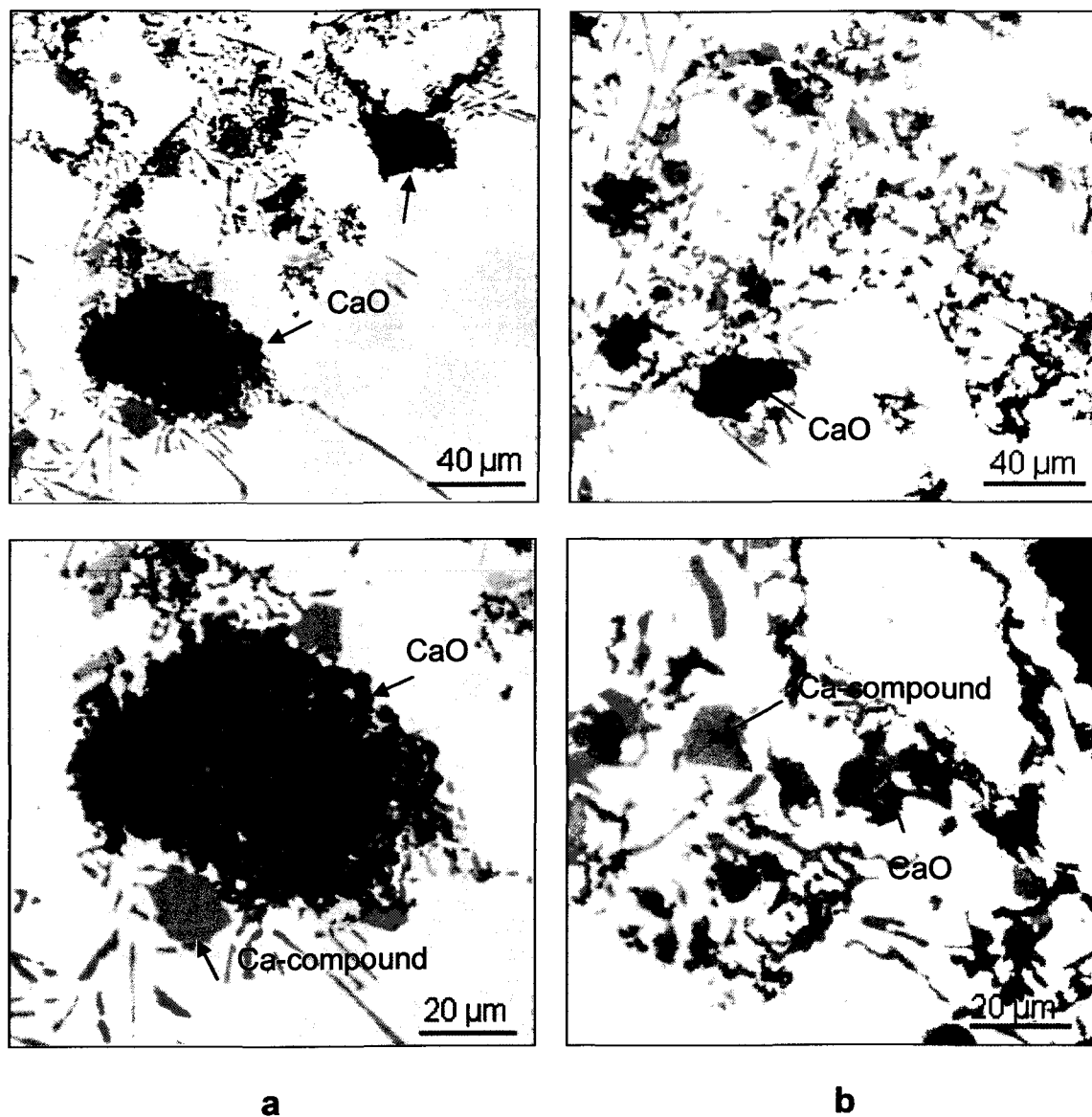


Figure 7.11 Optical micrographs showing CaO inclusions in Al-6%Si alloy; (a) at the start, and (b) end of the LiMCA test.

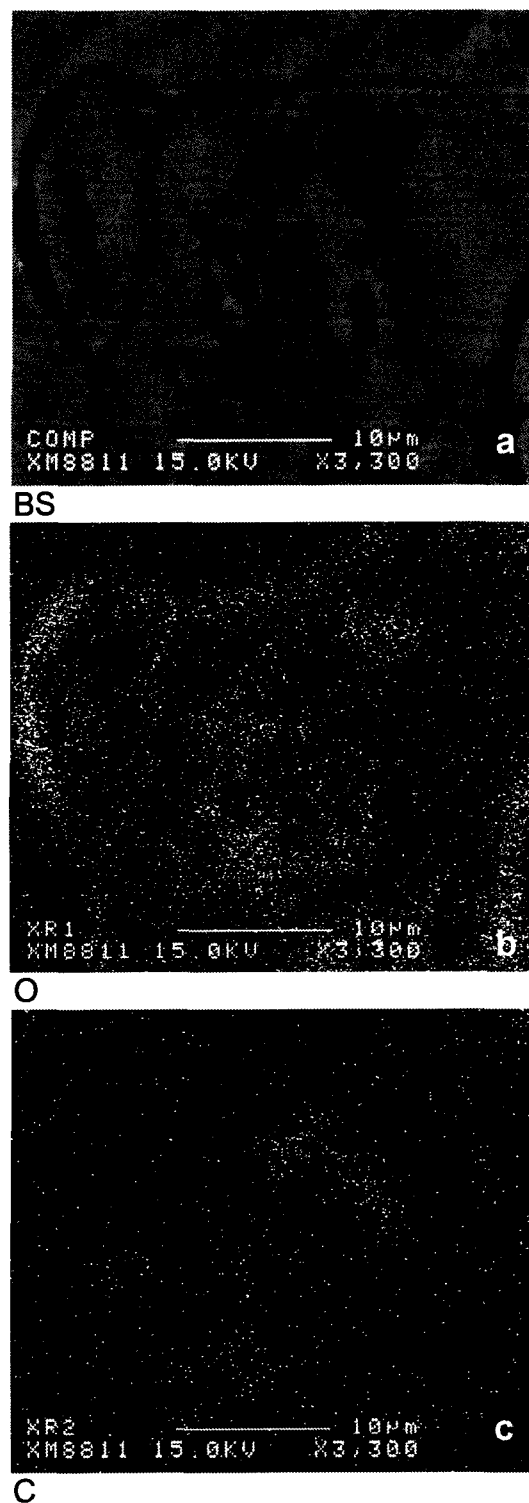


Figure 7.12 (a) Backscattered image of Al_4C_3 inclusions (arrowed) in Al-6%Si alloy, and, (b, c) corresponding X-ray images of O and C taken from a sampling cup casting before the start of the LiMCA test.

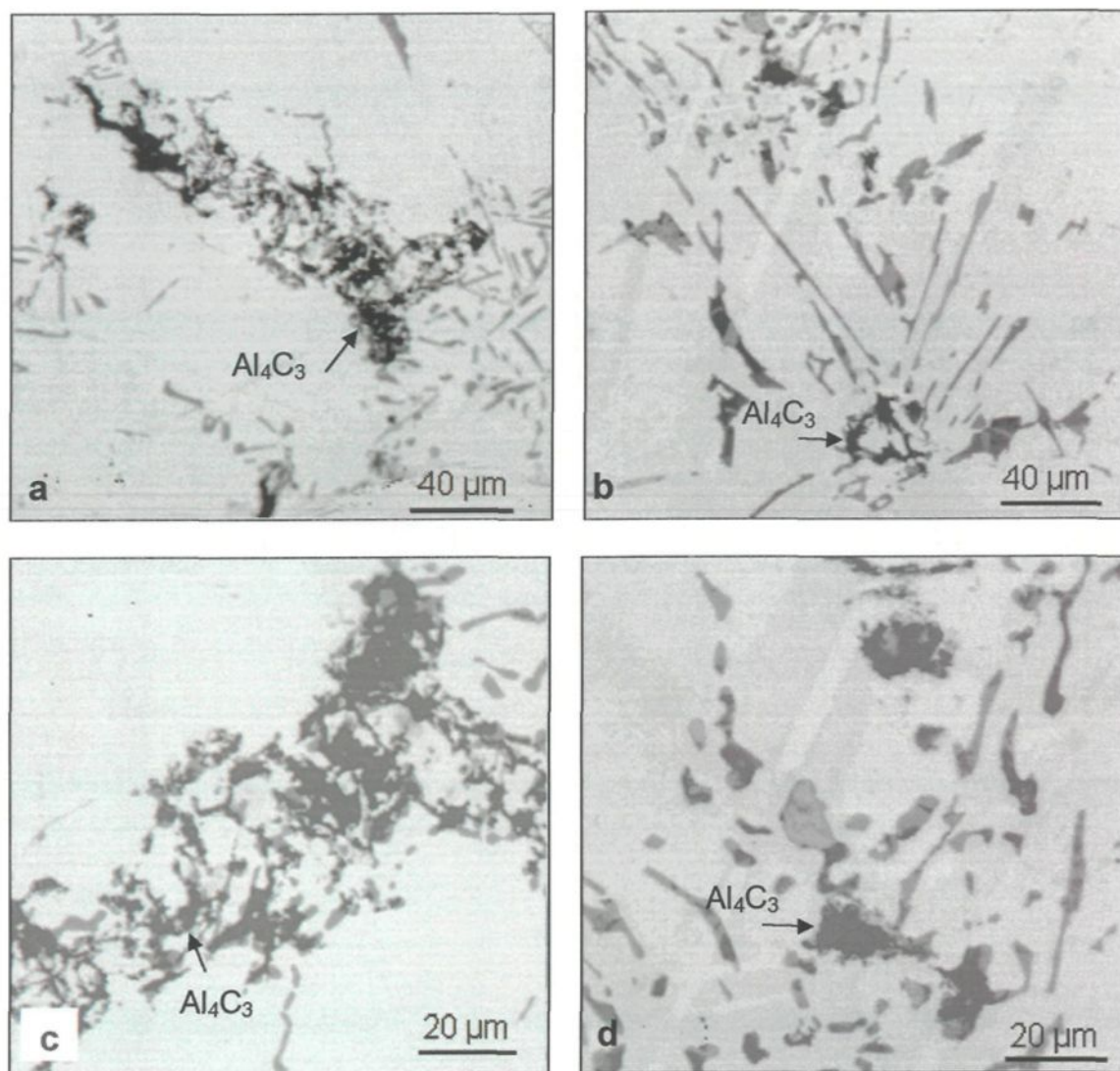


Figure 7.13 Optical micrographs showing Al_4C_3 inclusions in Al-6%Si alloy samples before the start (a, c) and at the end (b, d) of a LiMCA test.

MgO

The optical micrographs of Figure 7.14 provide examples of MgO inclusions (powder addition) in Al-6%Si alloy, taken from a sample obtained from the corresponding melt before the start of the LiMCA test (a, b), and after the LiMCA test (c, d). In (d) one is able to distinguish the MgO inclusions at the bottom right and right half of the micrograph, whereas the dark black fine particles in (a) probably correspond to Mg₂Si. One can also estimate the range of particle sizes of the MgO inclusions, from a comparison of (b) and (d).

Figure 7.15 shows optical micrographs obtained from the MgO inclusion-containing Al-6%Si alloy melt after pure Mg metal was also added (followed by superheating of the melt, then returning the melt temperature to 680 °C). These micrographs were taken from a sampling cup casting of the melt before conducting the LiMCA test. Figure 7.15(a) shows a lumpy area containing the MgO inclusions at the top centre, while beautiful examples of script-like black Mg₂Si particles are observed within the α -Al dendritic regions at the bottom. The higher magnification micrograph of Figure 7.15(b) shows the MgO inclusion clusters very clearly.

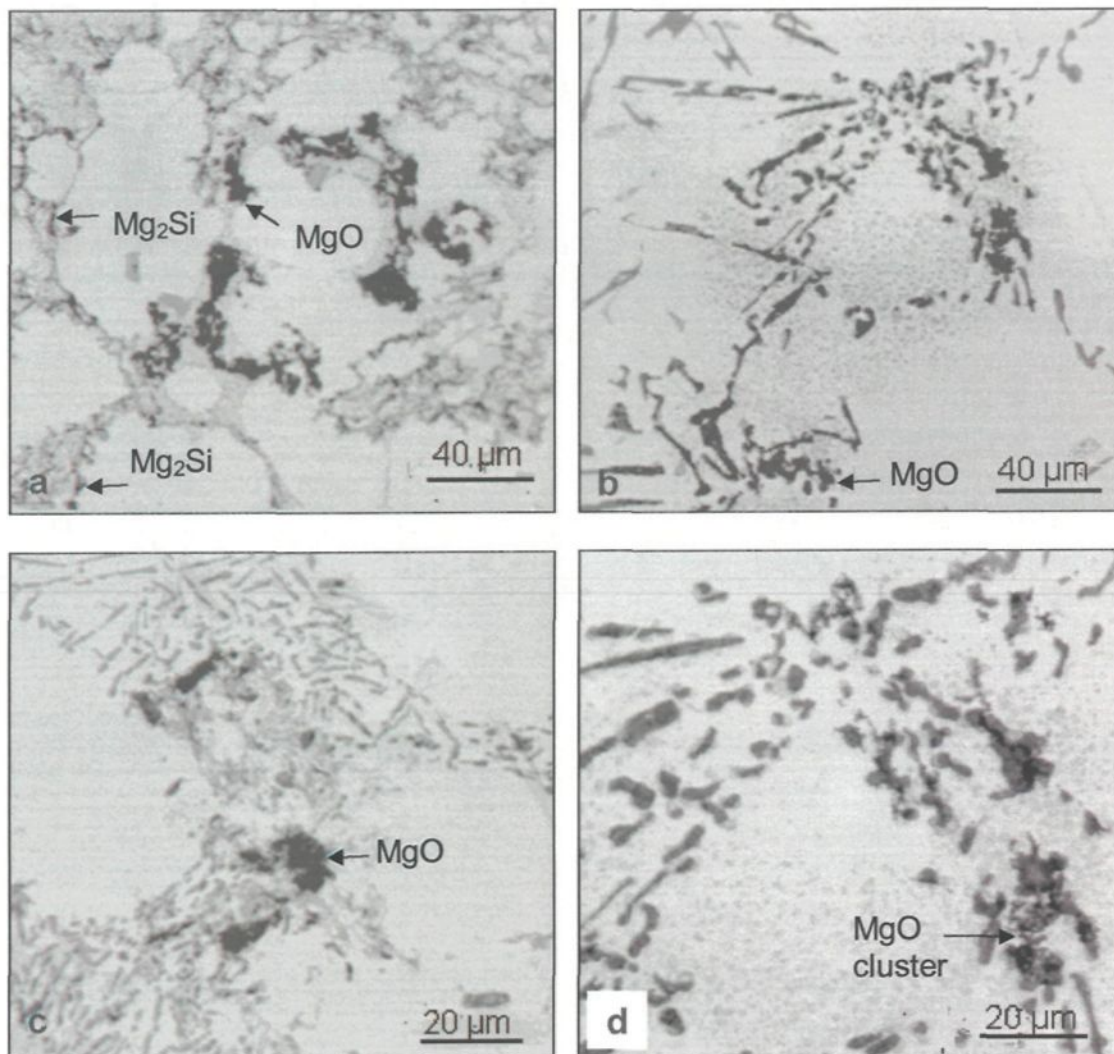


Figure 7.14 Optical micrographs showing MgO inclusions in Al-6%Si alloy samples before the start (a, c) and at the end (b, d) of a LiMCA test.

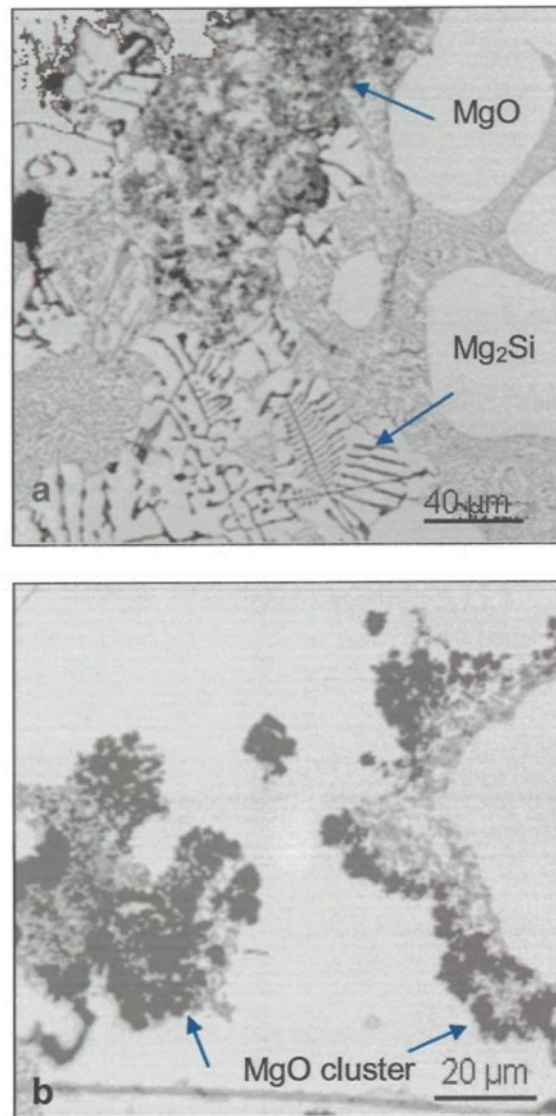


Figure 7.15 Optical micrographs showing MgO inclusions (Mg metal source) in Al-6%Si alloy samples.

Al₂O₃

Examples of Al₂O₃ inclusions observed in Al-6%Si alloy melts are shown in Figure 7.16. The Al₂O₃ inclusions were added in the form of an Al-Si-Mg/Al₂O₃/10p metal matrix composite. As reported previously, these inclusions have particle sizes ranging from 4 to 60 μm, the average particle size being ~23 μm. The rough contours of the particles indicate that these particles reacted with the melt. Probably on account of their size and morphology, the Al₂O₃ inclusions appear in loosely grouped entities within the matrix, in the Al-Si eutectic regions.

TiB₂

Figure 7.17(a) shows the backscattered image of TiB₂ inclusion particles in Al-6%Si alloy, where the inclusions were added in the form of TiB₂ powder. The corresponding X-ray images (b, c) of Ti and B confirm that these are TiB₂ inclusions. Optical micrographs of the powder inclusions taken from casting samples obtained at the start and end of the LiMCA test are shown in Figures 7.18(a) and 7.18(b), respectively. As in the case of Figure 7.17(a), the TiB₂ inclusions appear in loose clusters in the matrix, in the Al-Si eutectic regions. In Figure 7.18(a) some pores are also observed, associated with the TiB₂ particles.

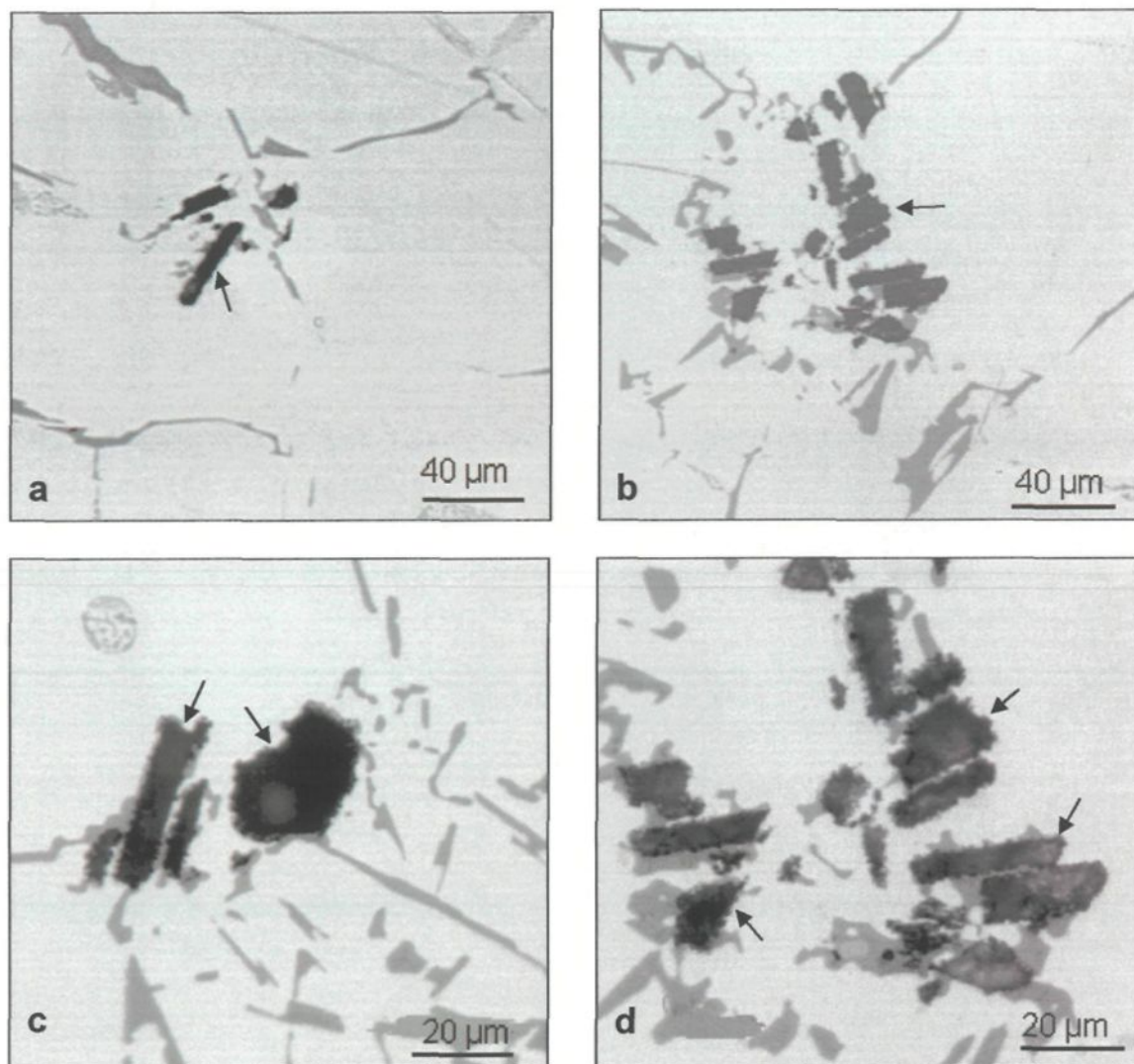


Figure 7.16 Optical micrographs showing Al_2O_3 inclusions (arrowed) in Al-6%Si base alloy, obtained from casting samples taken at the start (a, c), and end (b, d) of the LiMCA measurement.

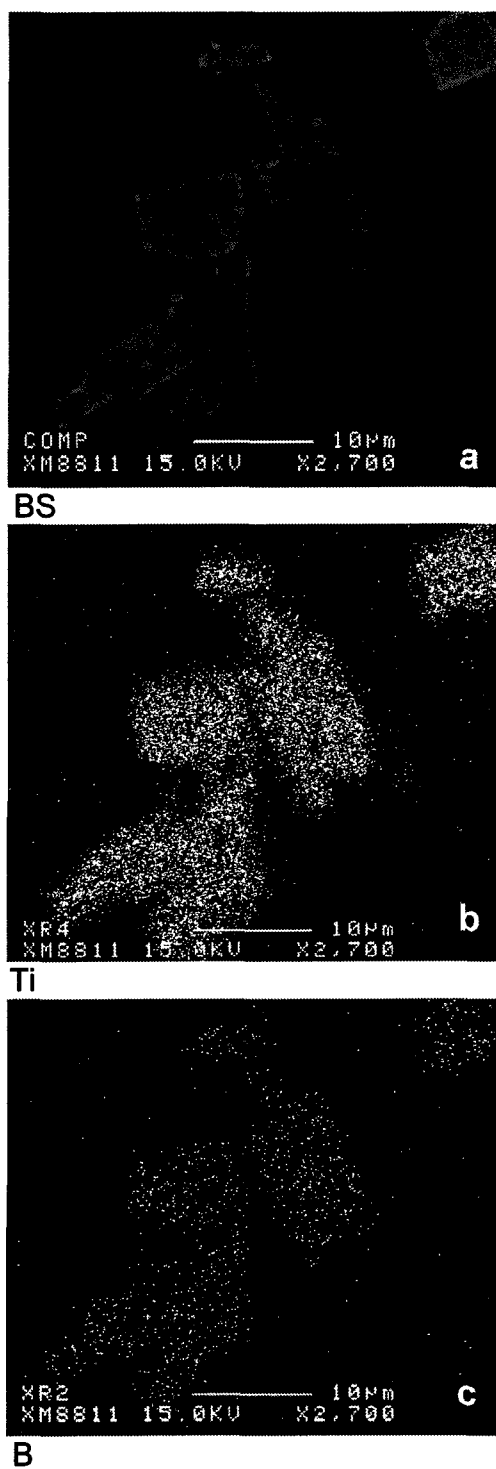


Figure 7.17 (a) Backscattered image of TiB_2 powder inclusion particles in Al-6%Si alloy taken from a casting sample obtained before the start of the LiMCA test; (b, c) corresponding X-ray images of Ti and B.

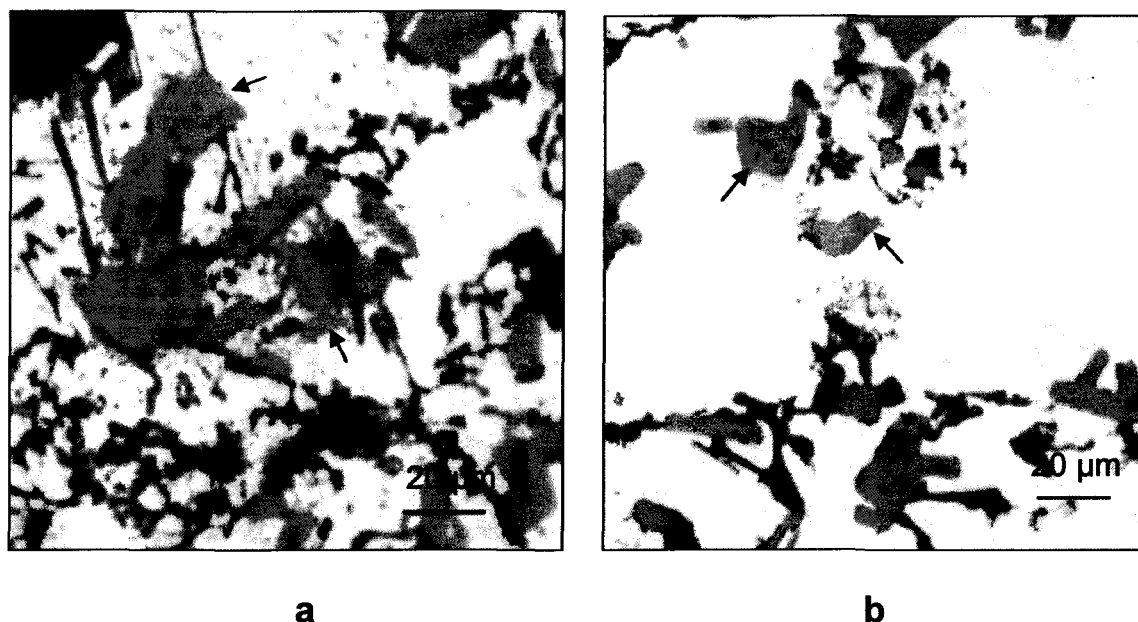


Figure 7.18 Optical micrographs showing TiB_2 powder inclusion particles (arrowed) in Al-6%Si alloy in samples obtained at the start (a) and end (b) of the LiMCA test.

Figure 7.19(a) shows the backscattered image of TiB_2 particles in Al-6%Si alloy where, in this case, the TiB_2 inclusions were added in the form of Al-5%Ti-1%B master alloy. The matrix exhibits TiB_2 particle clusters in the centre and upper half of the image, along with large dark grey particles of undecomposed master alloy. Some oxide films are also observed. The corresponding X-ray images (b, c) of Ti and B distinguish the locations of the TiB_2 inclusions from the oxide films.

The optical micrographs of Figure 7.20, taken from the same sample, provide a much clearer view of these constituents. The metallography sample corresponding to these micrographs was prepared from a sampling cup casting taken from the melt just before starting the LiMCA test.

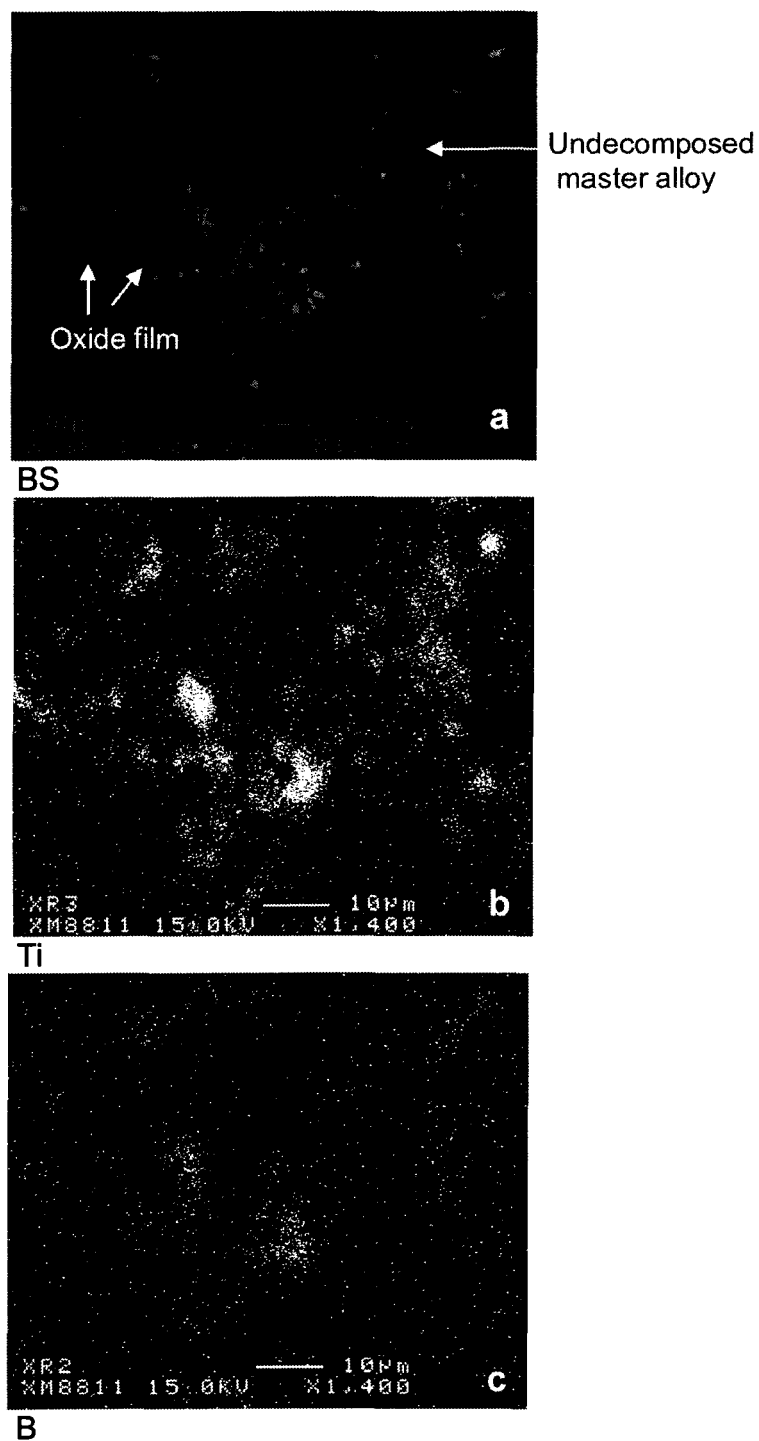


Figure 7.19 (a) Backscattered image showing TiB_2 inclusions resulting from Al-5%Ti-1%B master alloy addition to Al-6%Si alloy; (b, c) corresponding X-ray images of Ti and B.

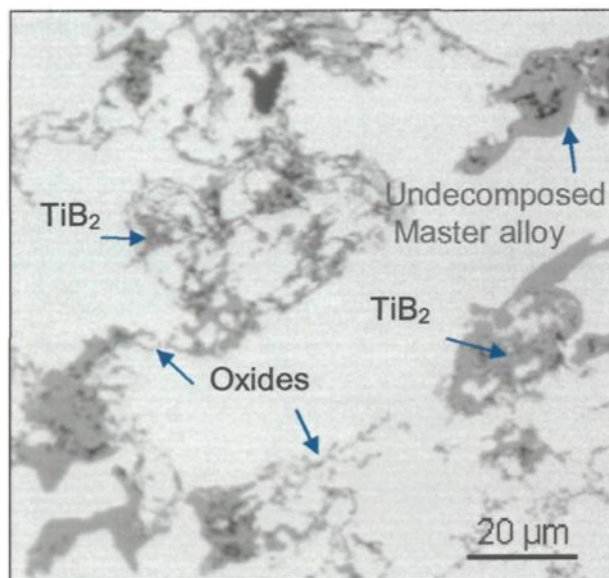
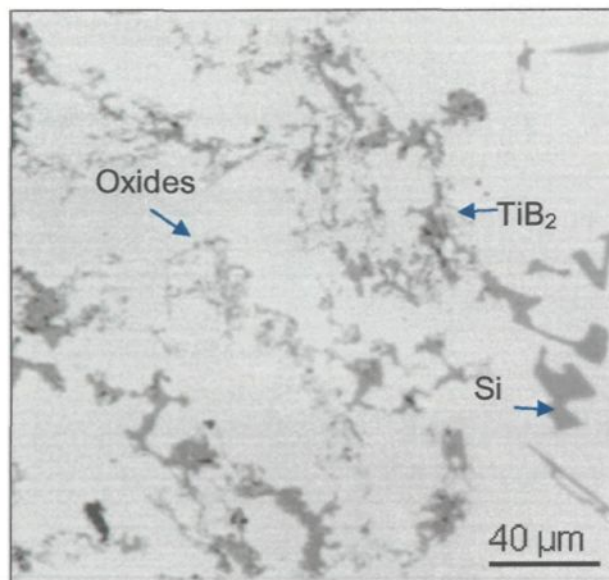


Figure 7.20 Optical micrographs taken from the same sample shown in Figure 7.19, showing TiB₂ inclusions, oxides and undecomposed master alloy particles in the Al-6%Si alloy matrix.

An excellent example of the agglomeration of TiB_2 inclusions as captured by the LiMCA probe tube is shown in Figure 7.21(a). Note the vast amount of TiB_2 particles that constitute the agglomerate. The corresponding X-ray images of Ti and B in (b) and (c) confirm that these are TiB_2 inclusions. It should be noted that, due to the difficulty associated with mapping boron, the X-ray map for B is rather faint compared to that of Ti. Nevertheless, the contour of the agglomerate can still be distinguished in (c).

The results presented in Figure 7.21 constitute a very important aspect of the LiMCA. Other melt cleanliness techniques such as Prefil and PoDFA cannot measure such clusters or agglomerates of TiB_2 inclusions, as the filters in these systems invariably become blocked, interrupting/stopping the measurements. The LiMCA, on the other hand, is able to capture these clusters without any problem. The only limitation for the LiMCA would be that posed by the size of the probe tube orifice.

Thus, it appears that the LiMCA technique is the only means to measure TiB_2 clusters in Al-Si alloys. Given the fact that Al-Ti-B master alloys are regularly employed in foundries for refining aluminum alloys, the significance of this finding is evident.

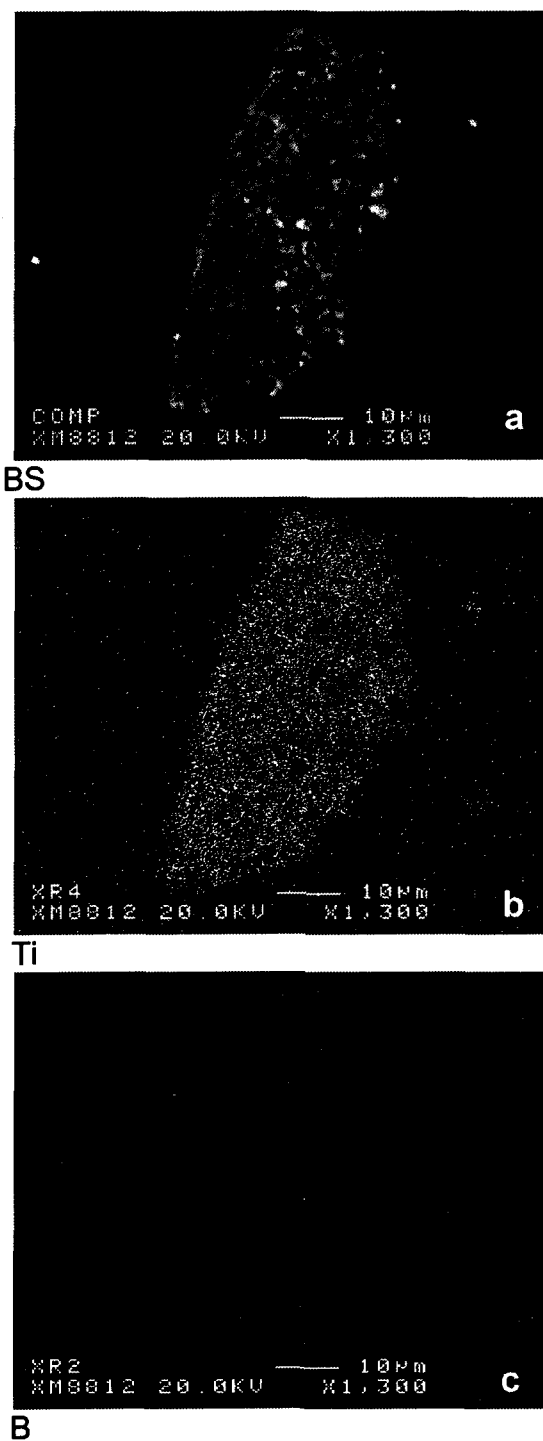


Figure 7.21 (a) Backscattered image showing a large agglomerate of TiB_2 inclusions resulting from Al-5%Ti-1%B master alloy addition to Al-6% alloy, obtained from a sample taken from the LiMCA sampling probe at the start of the LiMCA test; (b, c) corresponding X-ray images of Ti and B.

CHAPTER 8
CONCLUSIONS

CHAPTER 8

CONCLUSIONS

The present study was conducted to investigate the capability of the LiMCA II technique for measuring different types of inclusions in commercial pure aluminum and Al-6%Si casting alloys under low (680 °C) and high (750 °C) melt temperature conditions. The inclusion types studied included Al_2O_3 , Al_4C_3 , MgO, CaO, TiB_2 and TiAl_3 , representing inclusions typically found in aluminum casting alloys. The latter two types, *viz.* TiB_2 and TiAl_3 are important from the point of view of the grain refining treatments normally applied to these alloys, using Al-Ti-B and Al-Ti type master alloys.

The LiMCA data was obtained in the form of N_{20} and C_{20} plots which provided the total concentration number and volume concentration of inclusions, respectively, as a function of time and also of particle size. Microstructural examination of solidified samples obtained from the LiMCA probe tube used for the measurements and from samplings of the melt was also carried out.

From an analysis of the LiMCA data obtained and the corresponding microstructures, the following may be concluded.

Commercial Pure Al Melt

1. Following similar inclusion addition procedures, the maximum number of inclusions in commercial pure aluminum melts at 750 °C is observed in the case of Al_2O_3 inclusions, followed by Al_4C_3 inclusions. Other inclusions show concentration levels close to the base levels observed in pure aluminum without any additions. The lowest concentrations are exhibited by CaO.
2. Most of the inclusions are detected in the 20-25 μm size range. The almost negligible concentrations in the larger particle size ranges (50 μm and above) can be explained by the effects of particle agglomeration and settling, due to the difference in densities between the inclusions and the pure Al melt.
3. In the case of MgO inclusions, however, the more inclusions added to the melt, the more the inclusions distributed in the upper particle size ranges, showing a clear tendency for MgO inclusions to agglomerate. This observation is confirmed by microstructural analysis. The similar nature/slopes of the curves for MgO inclusion concentrations obtained from successive tests carried out at 680°C melt temperature indicate the repeatability of LiMCA samplings taken from the same melt.
4. A comparison of the average and total number of TiB_2 inclusions with those of pure Al indicates that the TiB_2 inclusions disperse in the melt and have less tendency to agglomerate. However, some amount of settling due to the density of the TiB_2 inclusions (*cf.* 4.5-5.6 g/cm^3 vs. 2.71 g/cm^3 for Al) can take place. Even with an increased addition of TiB_2 inclusions to the melt, the LiMCA can properly

detect the corresponding increase in the number of inclusions observed in the 20-25 μm particle size range.

5. The volume concentrations of TiAl_3 inclusions in pure Al melts at 680 °C remain high for all particle size ranges, whereas for other inclusions, the higher particle size ranges show low volumes.

Al-6%Si Alloy Melt

6. For the Al-6%Si alloy melt at 750 °C, there is an initial period of about 15-20 min before the inclusion readings begin to be detected properly by the LiMCA machine.
7. The Al_2O_3 and TiB_2 inclusions display the highest concentrations in the lower particle size ranges, where TiB_2 displays this tendency for almost all particle size ranges. The Al_4C_3 inclusions show concentrations close to Al_2O_3 , while CaO and MgO show the lowest concentrations, close to the base alloy levels for particle sizes $> 35 \mu\text{m}$. The effects of particle agglomeration and sedimentation are also reflected by the particle size distribution characteristics.
8. Although the CaO inclusions show the lowest concentrations on account of their low wettability, their presence is still differentiated by the LiMCA with respect to the base alloy inclusion levels (without any additions). The high volumic concentrations of CaO-containing melts indicate that large volumes are associated with these inclusions. These high volumic concentrations reflect the relative deleterious effects of different inclusions sizes and their presence in the melt. This is important in the context of monitoring in-line treatment efficiency for inclusion

removal during a casting process. On account of their large particle size, MgO inclusions also show large volume concentrations.

9. High volumic concentrations are also associated with TiB_2 inclusions, which extend over the higher particle size ranges, as well. The LiMCA is sensitive to both inclusion size and concentration from test to test, and can distinguish between “clean” (base Al-6%Si alloy) and “dirty” (inclusion-containing Al-6%Si) melts.
10. The sensitivity of the LiMCA II is found to increase as the melt temperature decreases. The LiMCA II records higher inclusion concentrations at the lower melt temperature for all the inclusion types studied. This effect is most pronounced for the TiB_2 and Al_4C_3 powder inclusions. LiMCA tests conducted at ~ 680 °C melt temperatures provide far better results than those obtained at 750 °C melt temperature with respect to both repeatability and consistency of results.
11. In the case of MgO inclusions, the jump in inclusion levels after addition of Mg metal and superheating the melt shows that direct addition of metal is a much better source of MgO inclusions than using MgO powder itself. Mg metal addition shows very high volumes of inclusions for all particle sizes. These concentrations are four times larger than those obtained with MgO powder addition which shows significant concentrations only up to 40-45 μm particle sizes (*cf.* 20,000 vs. 5000 ppb). The importance of this data is that it demonstrates the sensitivity and reliability of the LiMCA technique to the presence of inclusions added to the melt and to the changes resulting from the change in source that provides these inclusions to the melt.

12. In terms of inclusion concentrations, the following inclusion types show the highest concentrations: TiB_2 (powder) > $\text{MgO}+\text{Mg}$ > TiB_2 (master alloy) > Al_4C_3 (powder), in that order. The TiB_2 (powder) and MgO (metal) inclusions are associated with high volumes over all the particle size ranges.
13. With respect to TiB_2 vs. TiAl_3 inclusion additions using master alloys, the concentration numbers are much higher in the case of the TiB_2 inclusions (inclusion concentration at the start of measurement for TiAl_3 compares with that observed at the end of measurement for TiB_2 inclusions, ~ 100 K/Kg). However, similar to the TiAl_3 inclusions, most of the TiB_2 inclusions are found in the 20-35 μm particle size range. From the point of view of providing heterogeneous nuclei to the melt through the use of grain refining master alloys, the LiMCA measurements clearly show that Al-5%Ti-1%B is much more effective than Al-10%Ti.
14. The most important result from the microstructural analysis corresponds to the evidence of the agglomeration of TiB_2 inclusions as captured by the LiMCA probe tube, where the agglomerate comprises a vast amount of TiB_2 particles. This evidence constitutes a very important aspect of the LiMCA. Other melt cleanliness techniques such as Prefil and PoDFA cannot measure such clusters or agglomerates of TiB_2 inclusions, as the filters in these systems invariably become blocked. The LiMCA is the only technique that is able to capture these clusters in-line, without any problem. This is also confirmed by the high volumic concentrations observed from the TiB_2 inclusions. Given the fact that Al-Ti-B master alloys are regularly employed for refining aluminum alloys, this is a significant finding.

Recommendations for Future Work

Recommendations for Future Work

The results obtained from the present study on commercial pure aluminum and Al-6%Si experimental alloy have shown that the LiMCA II can be used to measure inclusions in aluminum casting alloys. The results on volumic concentrations are useful in that they can be used to monitor the presence of larger sized inclusions in the melt and take the necessary steps to improve in-line treatment efficiency during the casting process.

It is therefore recommended that the LiMCA II be tested for commercial Al-Si casting alloys such as A356, 319, 380, *etc.* which are commonly employed in automotive and die casting applications, to control the molten metal cleanliness and hence, the casting quality.

REFERENCES

REFERENCES

1. J.E. Gruzleski and B.M. Closset, *The Treatment of Liquid Aluminium-Silicon Alloys*, American Foundrymen's Society, Inc., Des Plaines, IL, 1990, pp. 59-65; pp. 135-155.
2. D.P. Kanicki and W. M. Rasmussen, "Cleaning Up Your Metal", *Modern Casting*, February 1990, pp. 55-58.
3. J.R. Davis, *ASM Specialty Handbook: Aluminum and Aluminum Alloys*, ASM International, The Materials Information Society, Materials park, OH, 1994, pp. 1-30.
4. D. Altenpohl, *Aluminum Viewed From Within*, Aluminum-verlag, Dussldorf, 1982, pp. 1-20.
5. H. Cong and X. Bian, "The relationship of the inclusions and hydrogen content in the molten alumium alloys", *Materials Science Forum*, Vols/ 331-337, 2000, pp. 325-330.
6. A. Shivkumar, D. Apelian and H. Brucher, "Melt Cleanliness in Die Cast Aluminum Alloys", *Driving Die Casting into the 21st Century*, NADCA, Detroit, 1991, pp. 143-151.
7. D. Apelian and S. Shivkumar, "Molten Metal Filtration: Past, Present and Future Trends", *Proc. 2nd AFS International Conference on Molten Metal Processing*, American Foundrymen's Society, Inc, Des Plaines, IL 1989, pp. 14-1 to 14-36.
8. M.J. Lessiter and W.M. Rasmussen, "To Pour or Not to Pour: The Dilemma of Assessing Your Aluminum Melt's Cleanliness", *Modern Casting*, March 1996, pp. 45-48.
9. M.J. Lessiter, "Understanding Inclusions in Aluminum Castings", *Modern Casting*, January 1993, pp. 29-31.

10. S. Viswanathan, A.J. Duncan, A.J. Duncan, Q. Han, W. D. Porter, and B.V. Rimers, "Modeling of Solidification and Porosity in Aluminum Alloy Castings", *AFS Transactions*, Vol. 106, 1998, pp. 411-417.
11. C.J. Simensen and G. Berg, "A survey of inclusions in aluminum", *Aluminium*, Vol. 56, 1980, pp. 335-340.
12. S. Makarov, D. Apelian and R. Ludwig, "Inclusion Removal and Detection in Molten Aluminum: Mechanical, Electromagnetic, and Acoustic Techniques", *AFS Transactions*, Vol. 107, 1999, pp. 725-735.
13. C.E. Eckert, "Inclusions in Aluminum Foundry Alloys", *Modern Casting*, April 1991, pp. 28-30.
14. J. Langerweger, "Non-Metallic Particles as the Cause of Structural Porosity, Heterogeneous Cell Structure and Surface Cracks in DC Cast Al Products", *Swiss Aluminum Ltd. J.* Vol. 4, 1980, pp. 685-705.
15. D.K. Lewis, "Control of Hardspot Inclusions In Aluminum Die Casting", *Die Casting Engineer*, 1991, pp.18-22.
16. G. Sauthoff, *Intermetallics*, VCH Verlagsgesellschaft, Weinheim, 1995, pp. 2-18.
17. C.R. Loper, Jr. and J.-I. Cho, "Influence of trace amounts of calcium in aluminium casting alloys: Review of Literature", *AFS Transactions*, Vol. 108, 2000, pp. 585-592.
18. B.T. Lee, S.Z. Lu and A. Hellawell, *Solidification Processing*, Sheffield, UK, 1997, pp. 243-247.
19. S. Shivkumar, L. Wang and R. Lavigne, "Qualitative Evaluation of Pore Characteristics in Cast Aluminum Alloys", *Light Metals 1993*, S.K. Das (Ed.), The Minerals, Metals & Materials Society, Warrendale, PA, 1993, pp. 829-833.
20. D.V. Neff and P.V. Cooper, "Clean Metal for Aluminum Foundries: New Technology", *AFS Transactions*, Vol. 98, 1990, pp. 579-584.

21. H. Zhao, I. Ohnada, Y. Sako, H. Onada, J. Zhu and H. Yasuda, "Estimation of Porosity Defects with Consideration of Oxide Entrapment", *Proceedings of the 65th World Foundry Congress*, Gyeongju, Korea, 2002, pp. 749-754.
22. C. Tian, J. Law, J. van der Touw, M. Murray, J.Y. Tao., D. Graham and D. St. John, "Effect of melt cleanliness on the formation of porosity defects in automotive aluminum high pressure die castings", *Journal of Materials Processing Technology*, Vol. 122, 2002, pp. 82-93.
23. D. Doutre, B. Gariepy, J.P. Martin and G. Dube, "Application in progress development and quality control", *Light Metals*, 1985, H. O. Bohner (Ed.), pp. 1179-1195.
24. X.G. Chen, R.I.L. Guthrie and J.E. Gruzleski, "Quantitative measurements of melt cleanliness in aluminum-silicon casting alloys, *Proc. 4th International AFS Conference on Molten Metal Processing*, American Foundry Society, Des Plaines, IL, 1996, pp.15-28.
25. X. Guang Chen and J. E. Gruzleski, "Influence of melt cleanliness on pore formation in aluminium-silicon alloys", *Int. Journal of Cast Metals Research*, 1996, Vol. 9, pp. 17-26.
26. C. Sztur, F. Balestreri, J.L. Meyer, B. Hannart, "Settling of inclusions in holding furnaces", *Light Metals 1990*, C.M. Bickert (Ed.), The Minerals, Metals & Materials Society, Warrendale, PA,1990, pp. 709-716.
27. J.P. Martin, G. Dube, D. Frayce and R. Guthrie, "Settling Phenomena in Casting Furnaces: A Fundamental and Experimental Investigation", *Light Metals 1988*, L.G. Boxall (Ed.), 1988, pp. 445-455.
28. M. Maniruzzaman and M. Makhlof, "Removal of Solid Inclusions from Aluminum Alloy Melts by Flotation - A Mathematical Model", *Proc. 5th AFS International Conference on Molten Aluminum Processing*, American Foundry Society, Inc., Des Plaines, 1998, pp. 63-66.
29. L. C. B. Martins and G. K. Sigworth, "Inclusion removal by flotation and stirring", *Proc. 2nd AFS International Conference on Molten Aluminum*

- Processing*, Nov 6-7, 1989, American Foundrymen's Society, Inc., Des Plaines, IL, pp. 16-1 to 16-2.
30. D. Apelian, "Metal Filtration: A Critical Review and Update", *48th Electric Furnace Conference Proceedings*, Pittsburgh, PA Dec 6-9, 1988, pp. 375-389.
31. D.H. DeYoung, "Metal Filtration Performance: Removal of Molten Salt Inclusions", *Aluminum Cast House Technology*, The Minerals, Metals & Materials Society, Warrendale, PA, 1999, pp. 121-132.
32. C. Conti, P. Netter, "Deep filtration of liquid metals: Application of a simplified model based on the limiting trajectory method", *Separation Technology*, Vol. 2, January 1992, pp. 46-48.
33. A.H. Castillejos E., F.A. Acosta G., J.M. Almanza R., "Metal filtration with a new ceramic porous medium: CEFLIPB", *Light Metals 1992*, E. R. Cutshall (Ed.), The Minerals, Metals & Materials Society, Warrendale, PA, 1992, pp. 1113-1122.
34. G. Clement, "The Pechiney Deep Bed Filter: Technology and Performance", *Light Metals 1995*, J. Evans (Ed.), The Minerals, Metals & Materials Society, W 1995, pp. 1253-1262.
35. D.E. Grotke, "The reduction of inclusions in aluminum by filtration", *Modern Casting*, April 1983, pp. 25-28.
36. J.F. Meredith, "Metal Treatment of Aluminum Alloys", *Metal Asia*, Dec. 1999, pp. 28-29.
37. S. King III and J. Reynolds: "Flux Injection/Rotary Degassing Process Provides Cleaner Aluminum", *Modern Casting*, April 1995, pp. 37-40.
38. S. Shivkumar, L. Wang and D. Apelian, "Molten Metal Processing of Advanced Cast Aluminum Alloys", *JOM*, January 1991, pp. 26-32.
39. P.G. Enright and I.R. Hughes, "A shop floor technique for quantitative measurement of molten metal cleanliness of aluminum alloys", *Foundryman*, Vol. 39, Part 11, November 1996, pp. 390-395.

40. F.H. Samuel, P. Ouellet and A. Simard, "Assesment of melt cleanliness and analysis of inclusions in Al-Si alloys using the Prerfil pressure filtration technique", *Int. Journal of Cast Metals Research*, Vol. 12, 1999, pp. 17-33.
41. P. Bakke and D.O. Karlsen, "Inclusion Assessment in Magnesium and Magnesium Base Alloys", *Characteristics and Applications of Magensium in Automotive Design (sp-1250)*, SAE Technical Paper No. 970330, 1997, pp. 61-73.
42. P. Bakke, J.A. Laurin, A. Provost and D.O. Karlsen, "Consistency of inclusions in pure magnesium", *Light Metals 1997*, R. Huglen (Ed.), The Minerals, Metals & Materials Society, Warrendale, PA, 1997, pp. 1019-1026.
43. D.D. Smith, L.S. Aubery, W.C. Miller, "LiMCA II Evaluation of the Performance Characteristics of Single Element and Staged Ceramic Foam Filtration", *Light Metals 1998*, B. Welch (Ed.), The Minerals, Metals & Materials Society, Warrendale, PA, 1998, pp. 893-915.
44. L.C. Lynnworth, *Ultrasonic Measurements for Process Control*, Academic Press, New York, 1989, pp. 513-515.
45. H. Hu and A. Luo, "Inclusion in molten magnesium and potential assessment techniques", *JOM*, Vol. 48, October 1996, pp. 47-51.
46. A.M. Samuel and F.H. Samuel, "The Reduced Pressure Test as a Measuring Tool in the Evaluation of Porosity/Hydrogen Content in Al-7 wt Pct Si-10 Vol pct SiC(p) Metal Matrix Composites", *Metallurgical Transactions A*, Vol. 24A, 1993, pp. 1857-1868.
47. M. Iwatasuki, S. Nishida and T. Kitamura, "Determination of Inclusions in Molten Alumium Alloy by X-Ray Diffractometry after Selective Dissolution", *Analytical Science*, Vol. 14, June 1998, pp. 617-619.
48. J.P. Martin and F. Painchaud, "On-line metal cleanliness determination in molten aluminum alloys using the LiMCA analyzer", *Light Metals 1994*, U. Mannweiler (Ed.), The Minerals, Metals & Materials Society, Warrendale, PA, 1994, pp. 915-920.

49. LiMCA II Operation and Maintenance Guide, Version 2-0, Bomem Inc., Quebec, 1995.
50. E.U. Comerford, L.G. Hudson and G. Beland, "Extended user's experience with the LiMCA technology to continuously monitor and improve can body stock quality", *Light Metals 1994*, U. Mannweiler (Ed.), The Minerals, Metals & Materials Society, Warrendale, PA, 1994, pp. 1083-1091.
51. M. Li, C. Carozza and R.I.L. Guthrie, "Particle discrimination in water-based LiMCA", *Canadian Metallurgical Quarterly*, Vol. 39, No. 3, 2000, pp. 325-338.
52. M. Li and R.I. L. Guthrie, "Liquid Metal Cleanliness Analyzer (LiMCA) in Molten Aluminum", *ISIJ International*, Vol. 41, No. 2, 2001, pp. 101-110.
53. R.I.L. Guthrie and M. Li, "*In situ* detection of inclusions in liquid metals: Part II-Metallurgical applications of LiMCA systems", *Metallurgical and Materials Transactions B*, Vol. 32B, No. 6, December 2001, pp. 1081-1093.
54. R.I.L. Guthrie and M. Li, "*In situ* detection of inclusions in liquid metals: Part I-Mathematical modeling of the behavior of particles traversing the electric sensing zone", *Metallurgical and Materials Transactions B*, Vol. 32B, December. 2001, pp. 1067-1079.
55. M. Li and R.I.L. Guthrie, "On the Detection and Selective Separation of Inclusions in Liquid Metal Cleanliness Analyzer (LiMCA) Systems", *Metallurgical and Materials Transactions B*, Vol. 31B, August 2000, pp. 767-777.
56. M. Syvertsen and T. Abel Engh, "Error analysis of LiMCA II data", *Light Metals*, 2001, J.L. Anjier (Ed.), The Minerals, Metals & Materials Society, Warrendale, PA, 2001, pp. 957-963.
57. M. Cooksey, T. Ware and M.J. Couper, "Effect of pressure cycles and extension probe on LiMCA measurement of inclusions", *Light Metals 2001*, J.L. Anjier (Ed.), The Minerals, Metals & Materials Society, Warrendale, PA, 2001, pp. 965-971.

58. *Handbook of Aluminum, Vol.1: Physical Metallurgy and Process*, G.E. Totten and D. Mackenzie (Eds.), Marcel Dekker, Inc., New York, 2003, pp. 170.
59. P.S. Mohanty, F.H. Samuel and J.E. Gruzleki, "Studies on Addition of Inclusions to Molten Aluminum Using a Novel Technique", *Metallurgical and Materials Transactions B*, 1995, Vol. 26B, pp. 103-109.
60. W. Khalifa, Role of Inclusions in the Nucleation of α -Aluminum and Fe-Intermetallics in Aluminum Rich Corner of the Al-Si-Fe Ternary System, Ph. D. Thesis, UQAC, 2004.
61. A.M. Samuel, A. Gotmare and F.H. Samuel, "Effect of Solidification Rate and Metal Feasibility on Porosity and SiC/Al₂O₃ Particle Distribution in an Al-Si-Mg (359) Alloy", *Composites Science and Technology*, Vol. 53, 1995, pp. 301-315.
62. F. Gazanion, X.G. Chen and C. Dupuis, "Studies on the Sedimentation and Agglomeration Behavior of Al-Ti-B and Al-Ti-C Grain Refiners", *Materials Science Forum*, Vols 396-402, 2002, pp. 45-52.
63. K. Russell, J. Cornie and S.Y. Oh, "Particulate Wetting and Particle/Solid Interface Phenomena in Casting Metal Matrix Composites", *Interfaces in Metal Matrix Composites*, A. Dhingra (Ed.), The Minerals, Metals & Materials Society, Warrendale, PA, 1986, pp. 61-91.
64. F.H. Samuel, Unpublished work.
65. E.J. Asbornsson, T.I. Sigfusson, D.G. McCartney, T. Gudmundsson and D. Bristow, "Studies on the Dissolution of Al-Ti-C Master Alloy Using LiMCA II", *Light Metals*, C.E. Eckert (Ed.), The Minerals, Metals & Materials Society, Warrandale, PA, 1999, pp. 705-710.
66. W. Khalifa, F.H. Samuel, and J.E. Gruzleski, "Nucleation of Solid Aluminum on Inclusion Particles Injected into Al-Si-Fe Alloys", *Metallurgical and Materials Transactions A*, Vol 35A, 2004, pp. 3233-3250.